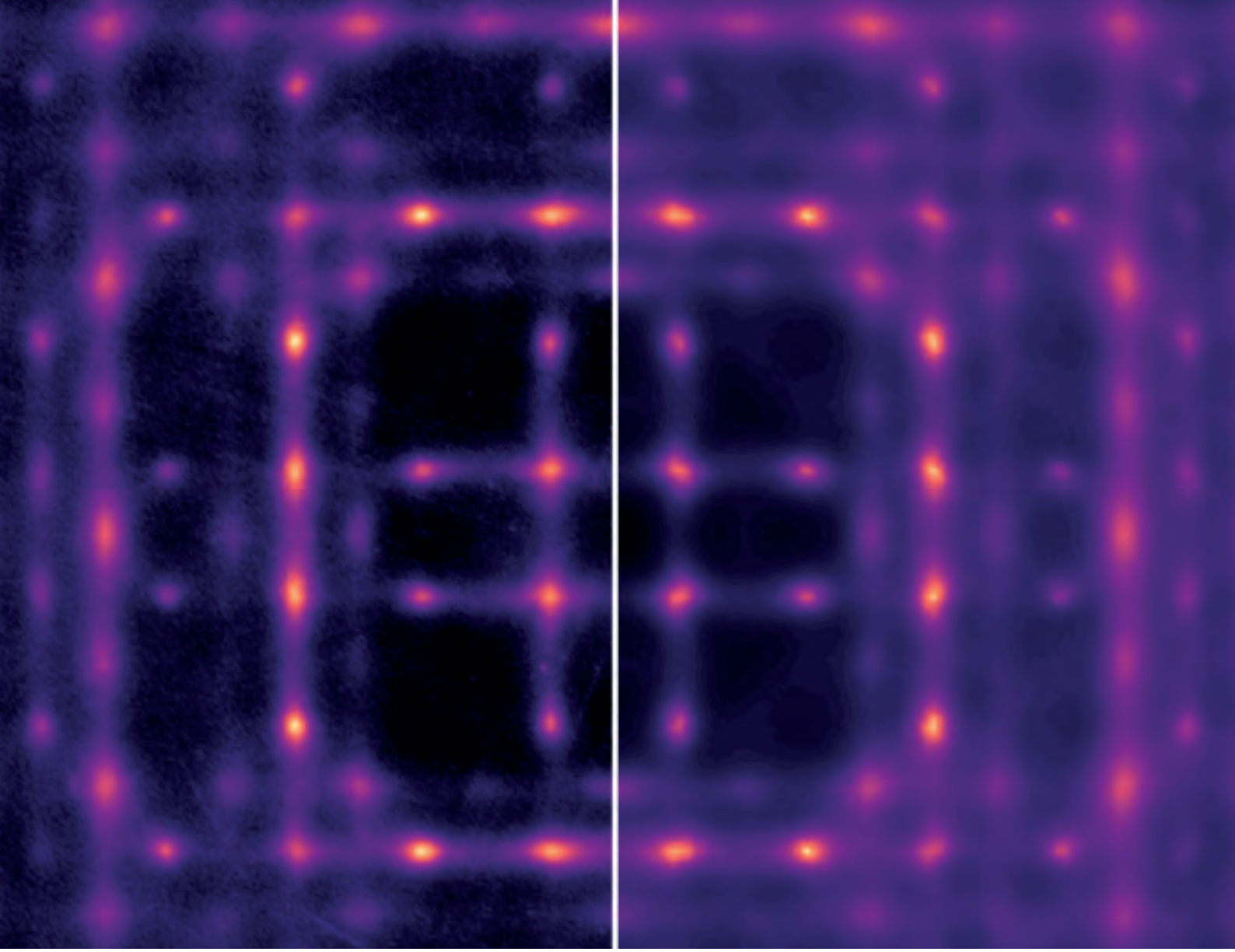

PHOTON SCIENCE 2025.

Highlights and Annual Report

Deutsches Elektronen-Synchrotron DESY
A Research Centre of the Helmholtz Association

PHOTON SCIENCE 2025.

Highlights and Annual Report

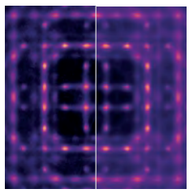

Cover

The cover image shows single-crystal X-ray diffraction measurements and molecular dynamics (MD) calculations of the dynamic nanodomains in lead halide perovskites. Slices of the X-ray scattering function for methylammonium lead bromide ($MAPbBr_3$) are displayed on the left side, while the corresponding MD simulations can be seen on the right side. They shows remarkable agreement with the experimental data. The overall measured results reveal that the local atomic structure comprises low-symmetry tetragonal nanodomains with lifetimes on the picosecond timescale. Their highly dynamic lattice makes perovskites ideal semiconductors for high-performance photovoltaics.

(Details see page 54)

(Measurements at the PETRA III beamline P21.1)

Contents

Publications

The list of publications based on work done at DESY Photon Science is accessible online:
http://photon-science.desy.de/research/publications/list_of_publications/index_eng.html

DESY tries to keep this list complete and up-to-date and relies on the support by all users who are kindly requested to register their publications in our database (login via door.desy.de).

The year 2025 at DESY

Chairman's foreword

Dear Colleagues and Friends of DESY

As I reflect on the year 2025, I am proud to present this annual report of DESY. For me it is the first time that I have the honour to do this having started as Chair of the DESY Directorate on 1 April. I have very much enjoyed this first half year in my new job, most of all as every day I learn something new about DESY and I get to work with so many talented and committed people.

In 2025, there were many changes in the directorate: Britta Redlich started on 1 January as the new Director of Photon Science, taking over from Franz X. Kärtner who had filled this role at interim for a year after Edgar Weckert's term finished at the end of 2023. On 1 April, Iris Wilhelm started as Administrative Director. And, on 1 November, Ulrich Husemann started as new Director of Particle Physics. My deep gratitude goes to the former and interim directors, namely Christian Harringa, Edgar Weckert, Arik Willner and Ties Behnke, and in particular Helmut Dosch, for their tireless commitment to advance DESY. Together with the experienced directors, Wim Leemans and Christian Stegmann, we are forming a team that is now steering DESY – together with the deputy directors, group and team leaders, all emplo-yees as well as the members of our advisory boards and the funding agencies – through these somewhat turbulent times.

Science faces profound challenges in today's world. The pace of technological and geopolitical change has blurred the lines between open knowledge and strategic competition. Global crises such as pandemics, climate change, conflicts and wars underscore the need for international collaboration, and simultaneously trust and cooperation across borders are eroding. At the same time, the spread of misinformation and the politicisation of scientific facts threaten public confidence in evidence-based decision and policy making. Researchers must balance openness with responsibility – safeguarding integrity, transparency, and security while ensuring that science continues to serve humanity as a shared, global endeavour.

DESY as a premier research institution plays an important role in the national and international science landscape. Each year thousands of scientists from around the World come to us to perform measurements, attend workshops or conferences or to collaborate with colleagues on our sites in Zeuthen or Hamburg. We have collaborations with institutions across Europe and the entire World, and our scientists travel across the globe to advance their research.

The success of DESY is founded on the design, construction and operation of fantastic research infrastructures, contributions to science, the thriving of many scientists at all career levels who pursue their ideas and engage in collaborations world-wide, and – above all – on the skilled and dedicated employees of DESY who enable all this at a technical and administrative level.

This year, DESY has once again demonstrated its scientific excellence. In February 2025, a panel of international scientists appointed by the Helmholtz Association visited and reviewed DESY. All areas of our research and of the

The Board of Directors with newly appointed members in November 2025 (from left to right): Dr. Miriam Hufnagl (Delegate of the Directorate for Innovation, CTO (interim)), Iris Wilhelm (Director of Administration), Prof. Christian Stegman (Director in Charge of Astroparticle Physics), Prof. Wim Leemans (Director in Charge of the Accelerator Division), Prof. Britta Redlich (Director in Charge of Photon Science), Prof. Beate Heinemann (Chair of DESY's Board of Directors, Prof. Ulrich Husemann (Director in charge of Particle Physics (Photo: DESY, Marta Mayer)

Ceremonial transition at DESY on 31 March 2025: Outgoing Chair of DESY's Board of Directors Helmut Dosch (right) transfers leadership to Beate Heinemann (left), with Manja Schüle (Minister of Science, Brandenburg) and Katharina Fegebank (Senator and Second Mayor of Hamburg) in attendance. (Photo: DESY, Daniel Reinhardt)

operation of the facilities were rated with the highest marks, and many useful recommendations were given for the next funding period of the 'Programme-Oriented Funding' (POF V). The panel was also impressed by our activities in the areas of diversity, international cooperation, sustaina-bility, innovation and talent development. Later during the year, we were thrilled that six 'Clusters of Excellence' with DESY contributions were selected for funding by the German Research Foundation (DFG), and at the European level one European Research Council (ERC) Starting Grant and two Synergy Grants were awarded.

A major achievement this year has been the completion of the upgrade project FLASH2020+. The implementation of external seeding and the newly installed variable-gap undulators will significantly enhance the capabilities of the free-electron laser facility FLASH so that it remains at the forefront of the extreme ultraviolet (EUV) and soft X-ray (XUV) science. In Zeuthen, a major accomplishment has been the completion of the construction of new sensor models (mDOMs) for the IceCube Upgrade: 201 mDOMs have been shipped to Antarctica to be installed there during the Antarctic summer. During the 2nd half of 2025, the European XFEL accelerator was warmed up for the first time since its start-up in 2017 to allow the mandatory inspection of helium valves, perform maintenance tasks and to install a completely newly developed electron source at the beginning of the accelerator. That source was developed at DESY's Photo Injector Test Facility (PITZ) in Zeuthen.

2025 has also seen DESY at the forefront of critical political and strategic initiatives. The selection of our two future projects, IceCube Gen-2 and PETRA IV, for the national 'Roadmap for Research Infrastructures' (FIS), which includes a total of nine large research infrastructures in Germany, underscores our important role in shaping the national and European research agendas. In 2026, we expect to get the final go-ahead of the PETRA IV project, and continue to advance the detailed planning with the goal of delivering the project on time and on budget.

It is particularly important to attract young talents to DESY. At any time, we have about 130 apprentices, 250 doctoral students and 250 postdoctoral researchers at DESY. Among the PhD students and postdoctoral researchers about two thirds are not from Germany, and our international office plays a key role to ensure that these young people are supported during the first weeks to quickly feel at home. This year, we also welcomed three new lead scientists, who bring fresh perspectives and expertise to DESY: Elina Fuchs in theoretical particle physics, Samaya Nissanke in gravitational and multi-messenger astrophysics, and Nønne Prisle in physical chemistry and aerosol research.

Innovation is also a very important part of DESY's mission. We want to contribute to ensuring that science also results in making life better for society at large. The successful participation in the Startup-Factory competition, which resulted in the 'Impossible Founders' that strengthens the innovation ecosystem in Hamburg, as well as the strategic cooperation with the Fraunhofer-Gesellschaft exemplify our commitment to translating research into practical applications. These collaborations, along with our many regional, national and global partnerships with industry partners and academic institutions, position DESY as a leader in both scientific and industrial innovation.

The campuses in Hamburg and Zeuthen continue to evolve. We had three topping-out ceremonies this year, celebrating the structural completion of the 'Centre for Accelerator Science and Technology' (CAST) building, and the two DESY Innovation Factory buildings. The new visitor centre DESYUM in Hamburg will open in spring 2026. Together with our campus partners, we are striving to make our campuses more sustainable and greener, and have been awarded prizes this year: The roof terrace of the Max-Planck-Institute for the Structure and Dynamics of Matter and the DESY building 36, a big hall from 1977 on the Hamburg campus.

In an increasingly interconnected world, international collaboration is more important than ever. The partnerships with institutions like the synchrotron light source SESAME in Jordan and our engagement in science diplomacy reflect our belief in the power of global cooperation. As we navigate geopolitical challenges, DESY remains committed to fostering transparency, exchange, and collaboration on both local and international levels.

In closing, I would like to express my gratitude to the entire DESY community – our experienced and early-career scientists, engineers, technicians, administrators, users and partners – for their dedication and hard work. My special thanks go to the funding agencies – the Federal Ministry of Research, Technology and Space (BMFTR) and the Science Ministries in Hamburg and Brandenburg (BWFG and BMWK) – who have been supporting DESY for many decades. I would also like to extend my heartfelt thanks to Helmut Dosch for his outstanding leadership and long-standing commitment to DESY, which have laid the foundations for much of what we are building on today. Together, we continue to push the boundaries of knowledge and innovation, ensuring that DESY remains at the forefront of global research.

Warm regards,

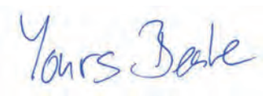

Beate Heinemann
Chairperson of the DESY Board of Directors

Celebrating a milestone for German science: On 8 July, DESY employees gathered in the auditorium to mark the BMFTR's decision to prioritize IceCube-Gen2 and PETRA IV as key research infrastructures. In the front row (from left): New directors Iris Wilhelm and Britta Redlich. (Photo: DESY, Daniel Reinhardt)

An impression of the roof of DESY's award-winning Hall 36. (Photo: DESY, Elisabeth Fröhlich)

Photon Science at DESY

Introduction

Dear Colleagues and Friends of DESY

It is a great pleasure and honor for me to address you for the first time as Director in charge of DESY Photon Science. When I took on this role at the beginning of 2025, I joined a vibrant, talented and deeply committed community that drives science with X-rays forward with great creativity, resilience and collaboration. This spirit has shaped an impressive year of achievements—a year which in many ways has prepared us for the next era of discovery.

The outstanding results of the evaluation by the Helmholtz Association have provided valuable confirmation of our strategic direction and highlighted the strong scientific and technological foundation across Photon Science and with PETRA III and FLASH in the Helmholtz research field 'Matter'. We are now preparing thoroughly for the upcoming strategic evaluation to ensure that our priorities, technologies and scientific vision are clearly aligned with long-term goals of the Helmholtz Centers in 'Matter'.

Britta Redlich, Director in charge of DESY Photon Science.
(Credit: Jörg Müller, DESY)

2025 was a decisive year for DESY's lighthouse project PETRA IV, culminating in its formal prioritisation as a national research infrastructure of highest importance announced by the Federal Minister of Research, Technology and Space (BMFTR) Dorothee Bär on 8 July. With the completion of the Engineering Design Report including the Conceptual Design Report (CDRs) for the 31 beamlines in phase I and II and deepened project plans, our teams at DESY have demonstrated their extraordinary commitment and the project readiness during a PETRA IV on-site evaluation by a committee appointed by the German 'Wissenschaftsrat' in December. This momentum carries into all preparations and prototype developments that will shape the next phase of PETRA IV, the world's best 4D X-ray microscope.

Another major highlight was the outstanding success in the national Excellence Strategy, where four Hamburg Clusters of Excellence involving DESY were selected for funding. This achievement underscores our pivotal role as a provider of world-leading infrastructures and reflects the strength of our partnerships across disciplines—from quantum physics and materials science to cultural heritage and sustainable technologies. Together, these clusters reinforce Hamburg's position as an internationally visible hub of cutting-edge research and demonstrate how DESY contributes to catalyse innovation and shape future scientific directions.

This year also marked 25 years since the first lasing at the TTF VUV-FEL (now FLASH), a milestone that celebrates DESY's pioneering role in free-electron laser science. Since that first Self-Amplified Spontaneous Emission (SASE) light in February 2000, FLASH has evolved into the world's first operational SASE FEL user facility. Continuous upgrades, advances in diagnostics and breakthrough experiments have been seen during two decades of user operation, and the FLASH2020+ upgrade project reaffirms the facility's strength and resilience. The achievement of first successful seeding of photons at FLASH1 in December marked the entry into a new regime of FEL operation and paves the way towards fully coherent soft X-ray pulses that will open new possibilities for demanding ultrafast science.

Meanwhile at PETRA III, user operation continued at a high level of excellence thanks to our truly dedicated teams even under strained circumstances, and with two new beamlines P25 and P63 soon expanding our scientific capacities for academia and industry. Progress in AI-assisted data handling workflows and rolling access models strengthen the current operation and initiate the transition to the novel level of service envisioned for the future.

Across our interdisciplinary research centers and our facilities, 2025 brought remarkable scientific highlights—from breakthroughs in high-pressure physics to following catalytic reactions in operando and insights into dynamic biological processes (for further examples see Highlights Section of this report). The discoveries demonstrate how light from our accelerators continues to reveal the invisible. Beyond the large-scale projects, DESY Photon Science thrives through strong collaborations, exceptional talents and an international outlook. Successes in the ERC Starting as well as Synergy Grants, in BMFTR, German Research Foundation (DFG) and EU funded projects, long-standing partnerships in LEAPS (League of European Accelerator-based Photon Sources) and with the SESAME synchrotron in Jordan, the inauguration of the Center for Molecular Water Science CMWS: all reflect a vibrant, outward-looking community committed to global scientific progress. This spirit of collaboration also defines our new strategic partnership with the Fraunhofer-Gesellschaft, which creates a powerful bridge between fundamental discovery and application-oriented innovation.

This year also marked important transitions. With the retirement of Helmut Dosch in March 2025, we bid farewell to a director whose vision and leadership shaped DESY for more than a decade. Thanks to Helmut, we enter a new chapter with vision, ambition and international visibility. I would also like to express my sincere thanks to Edgar Weckert for his many years of leadership of Photon Science and to Franz Kärtner for ensuring continuity as interim director in 2024 until my start on 1 January 2025. From my very first days in this role, I have experienced exceptionally constructive, open and forward-looking discussions within the DESY directorate. In April 2025,

An innovative experimental hall with a length of 600 metres is being designed for PETRA IV. Presenting the model of the hall (from left to right): Britta Redlich, Director of the Photon Science division, Chairwoman of the DESY Directorate Beate Heinemann and Wim Leemans, DESY Director for the Accelerator division.
(Credit: Daniel Reinhardt, DESY)

Beate Heinemann took over as chair of the board of directors, and while we have been working together in changing compositions over the year, the directorate has become more diverse but kept the contagious and convincing team spirit.

Stepping into this new and demanding role has been both an exciting and deeply rewarding experience. I am truly grateful for the warm welcome, great support, open exchange and constructive spirit I have encountered across Photon Science and the wider DESY community, our international user community and all strategic partners. These interactions have made the transition not only smoother, but also inspiring and rewarding, and they reinforce my enthusiasm for shaping the next chapter together.

With warm regards,

Yours Britta

Britta Redlich
Director in charge of DESY Photon Science

News and Events

News and Events

A busy year 2025

January

Since October 2024:
Chemistry triggered by light: Felix Allum takes up Humboldt fellowship at FLASH

Spectroscopy expert Felix Allum from Stanford University will use DESY's free-electron laser FLASH for time-resolved X-ray spectroscopic investigations of the dynamics of organic photochemical reactions with potential synthetic applications.

He comes to Hamburg through a two year's 'Humboldt Research Fellowship', a funding programme offered by the Alexander von Humboldt Foundation for international researchers to conduct long-term research projects in Germany.

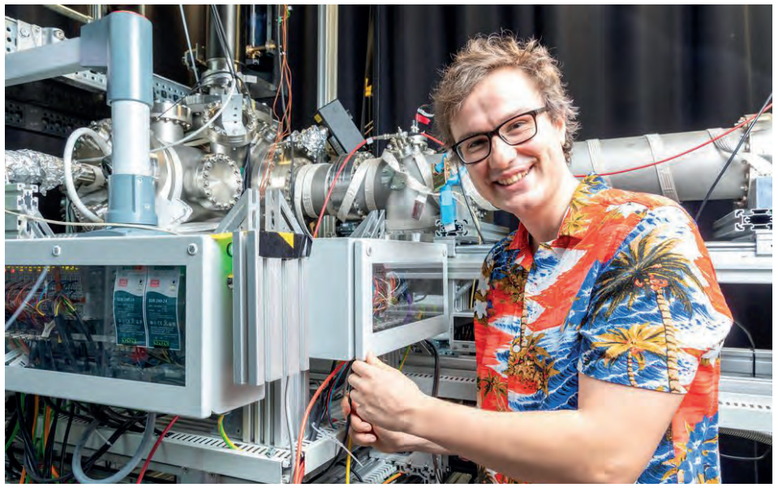

24 January:
Lower Saxony Impulse Professorship for Andrea Trabattoni

Andrea Trabattoni, a scientist at CFEL, DESY and W2 professor for Ultrafast

Photoelectron Research at Leibniz University Hannover (LUH), was awarded a 'Niedersachsen–Impuls–Professur'. This prestigious funding aims at advancing the awardees' careers by expanding expertise, refining the professional profile and preparing for future leadership roles in science. Additionally, the grant is set to strengthen the already close collaboration between DESY and LUH, enhancing their joint research efforts and fostering new synergies in the field of ultrafast electron dynamics.

25 January:
Over 1100 participants registered for the joint Users' Meeting of DESY Photon Science and European XFEL

High level of participation once again at the Users' Meeting 2025 in Hamburg. More than 1100 scientists registered to discuss the latest research performed at DESY's X-ray light sources PETRA III and free-electron laser FLASH as well as at the X-ray laser European XFEL. Participants informed themselves about new developments and prospects over the course of the three-day event. This jointly organised users' meeting is the largest gathering of this kind worldwide. At the meeting, Yongjae Lee was honoured with the 'DESY Photon Science User Award'. This award is given to a user or group of users of FLASH and/or PETRA III and acknowledges singular and exceptional contributions to the general advancement of science using DESY's large-scale photon science facilities.

February

24 February:
Technology and technology transfer in focus: Hamburg's Senator for Economic Affairs Melanie Leonhard visits DESY

Hamburg's Senator for Economic Affairs Melanie Leonhard visited DESY to learn about innovation activities at DESY and in the 'Science City Hamburg Bahrenfeld', which will be a centre for scientific research and technology transfer in future. Of particular interest were examples of collaboration with industry and DESY's support for start-ups.

25 February:
Fraunhofer and DESY launch strategic collaboration to promote innovation and research

Germany has an excellent research and innovation system with a clear division of labour. Each institution makes its own important contribution to the innovation chain. Fraunhofer stands for applied research and the transfer of technology, while DESY develops and operates leading infrastructures that serve as catalysts for technology developments and innovation processes. To address economic and social challenges and ensure Germany's and Europe's technological sovereignty, it is crucial to pool expertise, infrastructure and knowledge across the boundaries of research institutions and to translate this into targeted innovations

28 February:
Centre for Molecular Water Science inaugurated in Hamburg

With an inaugural ceremony on the DESY Campus, the DESY-initiated 'Centre for Molecular Water Science' (CMWS) consortium was formed. The CMWS is a Europe-wide research network in the field of molecular water research, encompassing crossing subjects, disciplines and methods. Forty-seven founding members from twelve countries – including fourteen German universities and eight Helmholtz Centres – signed the CMWS declaration. As strategically important partners, they complement the pan-European excellence network for molecular water science with the unique analytical possibilities on the Hamburg-Bahrenfeld campus.

April

1 April:
Beate Heinemann to lead DESY's Board of Directors

Professor Beate Heinemann became the new head of the research centre DESY. She took over as the chairperson of DESY's Board of Directors to which she already belonged in her role as director for Particle Physics. Beate Heinemann took over from Helmut Dosch, who has presided over the centre for more than 16 years. He was also professor of experimental physics with a focus on research with photons. With this change, she is the first woman to head the research centre.

May

22 May:
Four 'Clusters of Excellence' with DESY involvement in Hamburg

As part of Germany's Excellence Strategy, the University of Hamburg was awarded four Clusters of Excellence, while Hamburg University of Technology received one. DESY is involved in all four of these Hamburg-based Clusters of Excellence which will receive funding from 2026 onwards.

June

13 June:
DESY scientist wins the young scientist contest 'Talents for Fusion'

Marcus Seidel, team leader at DESY Photon Science and the Helmholtz Institute Jena, is one of six winners of the 'Fusion Talents' competition for young researchers announced by the German Federal Ministry of Education and Research in 2024. His proposed project 'Incoherent-drive Gas Nonlinear Optics with Yb:YLF Lasers at Cryogenic Temperatures' IGNYTe impressed the jury of internationally renowned scientists in the field of nuclear fusion research. As a result, the Federal Ministry will fund IGNYTe over the next five years, enabling Marcus Seidel to build a scientific team and conduct fundamental research in the field of laser technology which is expected to pave the way for the development of inertial fusion power plants.

July

8 July:
PETRA IV: Acceleration for Europe from Hamburg

The 'Prioritisation procedure for extensive research infrastructures' of the German Federal Ministry of Research, Technology and Space ended with a bang: Federal Research Minister Dorothee Bär announced that both projects submitted by DESY were classified as research infrastructures of national importance. The X-ray light source PETRA IV and the neutrino telescope IceCube-Gen2 were thus attested to have high scientific excellence, innovation and transfer potential as well as well thought-out planning.

30 July:
DESY welcomes 100 summer students from all over the world

A total of 100 summer students from 33 different countries participated in DESY's summer programme in Hamburg and Zeuthen. Students from Ukraine, Spain and Italy were particularly well represented. The students spent their time working on research projects, attending lectures, touring the campus and enjoying cultural exchange – and of course doing some sightseeing.

August

3 August:
FLASH restarts after extensive upgrade

Following a comprehensive 14-month upgrade from June 2024 to August 2025, the FLASH tunnel was closed again on 3 August to start with the commissioning of the machine. As part of the FLASH2020+ project, DESY's free-electron laser FLASH started operation again – now offering new, unique capabilities for research on its FLASH1 branch for users. This makes tailor-made, extremely stable and spectrally narrow X-ray pulses available for experiments. Combined with FLASH's high repetition rate, this opens up entirely new opportunities for precise studies in biology, chemistry and materials science, with exceptionally high temporal resolution in the femtosecond range.

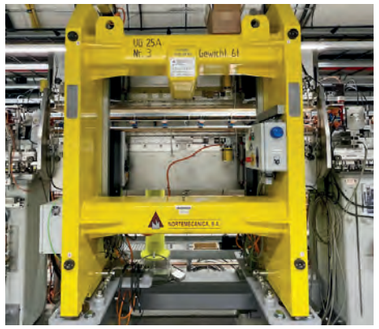

29 August:
Fernando Garcia-Martinez received 'Best Oral Presentation Award' at the ECOSS 38 conference

Fernando Garcia-Martinez, DESY researcher at the HAXPES beamline P22 at PETRA III, won the 'Best Oral Presentation Award' at the 38th European Conference on Surface Science ECOSS 38 held in Braga, Portugal, from 24-29 August 2025. In his talk on 'Structure and pressure gap in the NO reduction reaction on Rh model catalysts studied by operando HAXPES and SXRD', Fernando showcased how advanced X-ray techniques are crucial for understanding catalytic reactions at industrially relevant conditions.

September

2 September:
Polish Bronze Cross of Merit for Beata Ziaja-Motyka

Prof. Beata Ziaja-Motyka, group leader at the Center for Free-Electron Laser Science at DESY and full professor at the Institute of Nuclear Physics, Polish Academy of Sciences (IFJ PAN), was awarded the prestigious Bronze Cross of Merit during the official ceremony marking IFJ PAN's 70th anni-versary at the Auditorium Maximum of the Jagiellonian University in Krakow on 2 September. The Bronze Cross of Merit is a state honour re-cognising outstanding public and scientific contributions in Poland. Ziaja-Motyka was nominated by the President of the Polish Academy of Sciences and decorated by Vice-President Natalia Sobczak, on behalf of the President of the Republic of Poland. The ceremony was attended by distinguished guests from the scientific community and the leadership of Poland's academic institutions.

4 September:
ERC Starting Grant for DESY researcher Vincent Wanie: providing new insights into how molecules recognise chirality

With his ERC Starting Grant, DESY physicist Vincent Wanie wants to develop a new experimental setup based on a special laser system to investigate the interactions between chiral molecules. This is made possible by state-of-the-art ultra-fast light sources combined with experimental methods that are particularly sensitive to the structure of molecules. The setup has a great importance as its functionality is relevant in chemistry, pharmacy and materials research. Already earlier this year, Vincent Wanie was awarded the 'JPhys Photonics Early Career Award 2024'. Every year, the Journal of Physics: *Photonics* brings together the best early-career researchers in photonics and publishes their exceptional work in an annual collection dedicated to 'Emerging leaders'.

November

4 November:
FLASH welcomes its first user groups after shutdown

A new round of user experiments started at DESY's free-electron laser (FEL) FLASH. During the long FLASH2020+ shutdown, the FLASH1 FEL branch was completely replaced and converted into an externally seeded FEL, which is now gradually put into operation. The practically unchanged FLASH2 FEL branch already started operation successfully. Just three weeks after the FLASH accelerator restarted, FLASH2 achieved its usual excellent beam parameters.

6 November:
DESY Photon Science scientists receive prestigious ERC Synergy Grants

Synergies abound: Scientists from DESY were awarded highly competitive European Research Council (ERC) Synergy Grants for two ambitious research programmes. These grants are among the most prestigious offered in the European Union, recognising outstanding scientific excellence and unique collaboration. The team from DESY Photon Science, comprising Saša Bajt, Francesca Calegari, Henry Chapman and Nina Rohringer, was awarded 14 million Euro and will combine atomic-scale imaging with the Nobel Prize-winning field of attosecond science, the most advanced ultrafast imaging of matter in science.

17 November:
25th anniversary of the first lasing at the TESLA Test Facility (TTF) – today known as FLASH

More than 200 scientists from across the world gathered on 17 and 18 November 2025 where it all started: The first X-ray free-electron laser in the world, FLASH, turned 25 this year. The scientists came to discuss FLASH's legacy, its contributions to current research and the ambitious future of the 300-metre-long facility situated on the DESY campus in Hamburg. There were talks on the new frontiers of experiments in X-ray free-electron laser science as well as updates from the facilities across the world that have taken FLASH's blueprint and are making outstanding contributions in medicine, materials science, astrochemistry, photochemistry and much more.

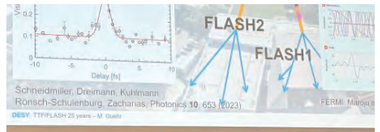

17 November:
Workshop on soft X-ray science at PETRA III

The scientific insights achieved with soft X-rays from the PETRA III storage ring were discussed in an international workshop at DESY on 17 and 18 November 2025. Over 80 participants from three continents discussed results and developments in 26 talks and 25 posters. The workshop was conducted by the consortium of scientists interested in the use of soft X-rays. Soft X-rays are generated and delivered to users at the P04 beamline. This range of the X-ray spectrum enables detailed studies of the interaction between radiation and matter.

26 November:
Workshop 'Theory meets XFELs' – from extreme conditions to attosecond physics

Around 80 scientists discussed the latest theoretical developments and their experimental application to X-ray lasers at EuXFEL and DESY during the workshop 'Theory meets XFELs' from 26 to 28 November 2025. The aim of the workshop series Theory meets XFELs, jointly organised by EuXFEL, the University of Hamburg and DESY Photon Science, was to foster collaborations between theoreticians and experimentalists engaged in XFEL research. Topics ranging from experiments under extreme conditions to attosecond physics were covered.

25 November:
PIER Day 2025: advancing collaboration in AI, data science & beyond

The PIER DAY 2025 was held at CFEL, bringing together researchers and management from DESY and the University of Hamburg to discuss the latest developments and collaboration opportunities arising from PIER-supported research at Bahrenfeld campus. A special focus of this year's PIER Day was on AI and data science, organised in collaboration with PIER PLUS.

Dezember

5 December:
Kick-off workshop for HICAPE

The kick-off workshop for HICAPE – 'Hamburg International Center for Accelerators, Photonics and Entrepreneurship' (formerly known as HIPACE) took place on 5 December 2025 at DESY. The HICAPE initiative aims to establish Hamburg as a world-class hub for photonics and accelerator research by bringing together the cutting-edge photonic and accelerator technologies, expertise and infrastructures available in the city. The objective was to attract the world's most talented and innovative minds to Hamburg in order to address pressing societal challenges through technological advancements and innovation.

Science Highlights

Complex S(IV) equilibria at the liquid-vapor interface

Detection of solvated SO_2

Sulfur dioxide (SO_2) plays a central role in the atmospheric sulfur cycle, acting both as a precursor of sulfate aerosols that affect air quality and climate and as a source of radicals through multiphase chemistry [1,2]. So far, climate models mainly rely on gas-phase and bulk-liquid composition measurements, with direct investigations of the interface chemistry under reaction conditions still largely missing. Consequently, predictions of aerosol chemistry still carry large uncertainties. In this study, scientists directly observed the complex acid–base equilibria of S(IV) species at the liquid–vapor interface. A detailed description of the interfacial composition will help to improve the accuracy of predictions of the role of aerosols for, e.g. urban air quality and cloud albedo.

The S(IV) acid–base equilibrium is particularly intricate because multiple tautomeric forms coexist (Fig. 1). In the present measurements the concentrations of the tautomers sulfonate (HSO_3^-), bisulfite (SO_3H^-), sulfite (SO_3^{2-}) as well as those of dissolved and gaseous SO_2 at the liquid–vapor interface were determined for a wide range of pH values, from strongly basic to strongly acidic. This was achieved by using the powerful combination of liquid microjets and X-ray photoelectron spectroscopy (XPS) at beamline P04 at PETRA III with the EASI end station [3]. In addition, the equilibria of these S(IV) species in the bulk of the solution were monitored by Raman spectroscopy.

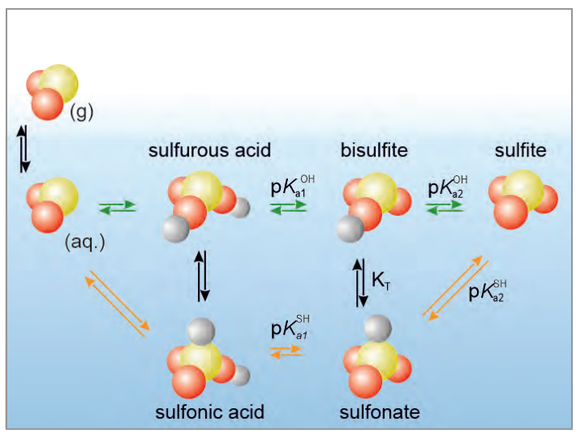

Figure 1
Acid-base equilibria of S(IV) species at the liquid-vapor interface. (Figure adapted from original publication)

Sulfur 2p photoelectron spectra recorded across various pH values revealed distinct peaks corresponding to sulfite, bisulfite, sulfonate and SO_2 (Fig. 2). Remarkably, a spectral signature of dissolved SO_2 was detected for the first time by suppressing gas-phase signals through the application of a negative bias voltage to the liquid jet [4]. The concentration of dissolved SO_2 was determined to be approximately 1 mM, thus demonstrating the exceptional sensitivity of beamline P04, capable of detecting roughly one SO_2 molecule among 55000 water molecules.

The detailed analysis of photoelectron spectra such as the ones shown in Fig. 2 enabled the determination of individual pK_a values for the different interface acid–base equilibria. While acid–base equilibria in the bulk (Raman) and at the surface (XPS) are broadly similar across a wide pH range, their comparison revealed a striking contrast: The interfacial layer becomes enriched in sulfonate and depleted in bisulfite as the acidity increases. In the bulk, the bisulfite-to-sulfonate tautomer ratio remains constant at approximately 3:1 over the entire pH range (0.3–13) investigated here, while at the interface sulfonate becomes the dominant tautomer.

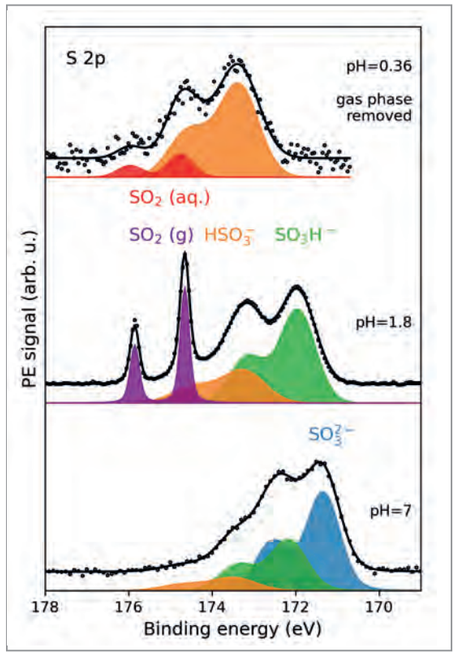

Figure 2
S 2p spectra of S(IV) solutions at various pH values. (Figure adapted from original publication)

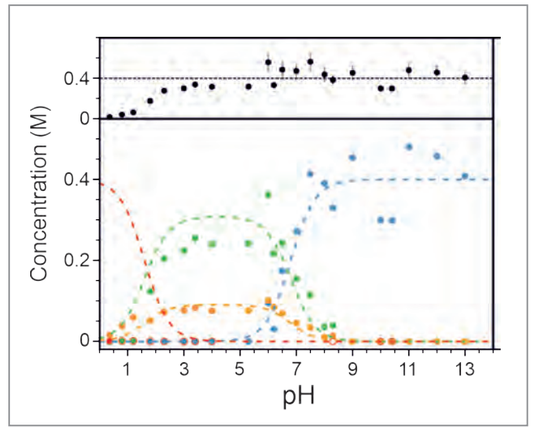

Figure 3
Experimentally determined acid-base equilibria of S(IV) species at the liquid-vapor interface. (Figure adapted from original publication)

To rationalise these findings, molecular dynamics simulations and free-energy calculations were performed. As expected, the doubly charged sulfite ion is more strongly repelled from the interface than the singly charged bisulfite and sulfonate ions. Although bisulfite and sulfonate show similar interfacial probability distributions, two additional effects explain the preferential stabilisation of sulfonate at the surface: (1) Sulfonate anions form transient contact ion pairs with hydronium ions near the interface, lowering their free energy relative to bisulfite, and (2) sulfurous acid, the protonated form of bisulfite, can dehydrate more readily to release SO_2 than sulfonic acid.

The quantitative speciation of S(IV) species at the liquid–vapor interface as a function of pH is summarised in Fig. 3. The upper trace illustrates the decrease of total S(IV) in solution due to volatilisation into the vapor phase under acidic conditions. This investigation provides direct experimental access to the interfacial S(IV) composition across a broad pH range. Notably, the observed depletion of bisulfite at low pH should be accounted for in future studies of multiphase S(IV) chemistry and in refined atmospheric and climate models. Beyond its atmospheric significance, the study also demonstrates the unique capability of beamline P04 for investigating dilute aqueous solutions and interfacial processes.

Author contact: Tillmann Buttersack, buttersack@fhi.mpg.de

References

1. J. H. Seinfeld and S. N. Pandis, 'Atmospheric chemistry and physics: from air pollution to climate change', John Wiley & Sons (2016).
2. T. Buttersack, 'The composition of aqueous interfaces as foundation for multiphase chemistry', Bunsen-Magazin 4, 155–159 (2025).
3. S. Malerz et al., 'A setup for studies of photoelectron circular dichroism from chiral molecules in aqueous solution', Rev. Sci. Instrum. 93, 015101 (2022).
4. S. Thürmer et al., 'Accurate vertical ionization energy and work function determinations of liquid water and aqueous solutions', Chem. Sci. 12, 10558–10582 (2021).

Original publication

'Direct observation of the complex S(IV) equilibria at the liquid-vapor interface', Nature Communications 15, 8987 (2024).
DOI: 10.1038/s41467-024-53186-5

Tillmann Buttersack[1], Ivan Gladich[2], Shirin Gholami[1], Clemens Richter[1], Rémi Dupuy[3], Christophe Nicolas[4], Florian Trinter[1], Annette Trunschke[1], Daniel Delgado[1], Pablo Corral Arroyo[5], Evelyne A. Parmentier[5], Bernd Winter[1], Lucia Lezzi[6], Antoine Roose[6], Anthony Boucly[6], Luca Artiglia[6], Markus Ammann[6], Ruth Signorell[5] and Hendrik Bluhm[1]

1. Fritz Haber Institute of the Max Planck Society, Berlin, Germany
2. Hamad Bin Khalifa University, Doha, Qatar
3. Sorbonne Université, CNRS, Paris, France
4. Synchrotron SOLEIL, Gif-sur-Yvette, France
5. ETH Zürich, Zürich, Switzerland
6. Paul Scherrer Institute, Villigen, Switzerland

Linking electronic and structural dynamics in photoexcited 2-thiouracil

Tracking both structure and charge flow during ultrafast relaxation of a nucleobase analogue

The absorption of UV light results in a concerted interplay of electronic excitation and structural deformation of a molecule [1]. Understanding this coupled behaviour is crucial for explaining photochemical reactivity in complex organic molecules such as nucleobases. Using two complementary time-resolved X-ray techniques — Near Edge X-ray Absorption Fine Structure Spectroscopy (NEXAFS) at FLASH and Coulomb Explosion Imaging (CEI) at the European XFEL — researchers have captured both the electronic and structural evolution of the noncanonical nucleobase 2-thiouracil, revealing how the breaking of planar symmetry drives its ultrafast internal conversion.

The photochemistry of heterocyclic molecules forms the basis of processes ranging from DNA photostability to photocatalysis. Ultraviolet absorption in nucleobases promotes electrons to excited states, thereby triggering ultrafast relaxation dynamics that determine whether the absorbed energy is harmlessly dissipated or leads to photochemical reactions. Canonical nucleobases proceed along the former route through rapid, radiationless decay, thereby preventing photodamage. In contrast, sulfur-substituted nucleobases promote photodamage by relaxing into triplet states. The exact mechanisms by which these electronically excited states couple to specific channels have remained elusive [2,3]. The sulfur-substituted nucleobase analogue 2-thiouracil (2-tUra) is an ideal system for corresponding studies: Its electronic structure enables strong UV absorption and the molecule has well-defined relaxation channels involving a ππ* → nπ* internal conversion.

To capture the intertwined dynamics occurring upon UV-absorption, two synergistic experiments were performed at Hamburg's highly complementary X-ray facilities. At the Small Quantum Systems (SQS) instrument of the EuXFEL, researchers used time-resolved Coulomb Explosion Imaging (CEI) [4] to directly observe how the molecular structure deforms after photoexcitation. Here, single intense X-ray pulses were used to ionise and fragment photoexcited 2-tUra molecules. From the fragmentation pattern, researchers extracted information on molecular geometries, using the emitted hydrogen ions as sensitive messengers for out-of-plane distortions. Fig. 1 shows the measured molecular-frame momentum space results, directly resembling the molecular structure in position space. A key step that breaks the molecule's initial planarity and enables a change of its electronic state occurs almost immediately after absorbing UV light (indicated by the decrease in Fig. 1b). Only after some time, the sulfur atom moves out of the molecular plane, driving the ππ* to nπ* internal conversion (Fig. 1c).

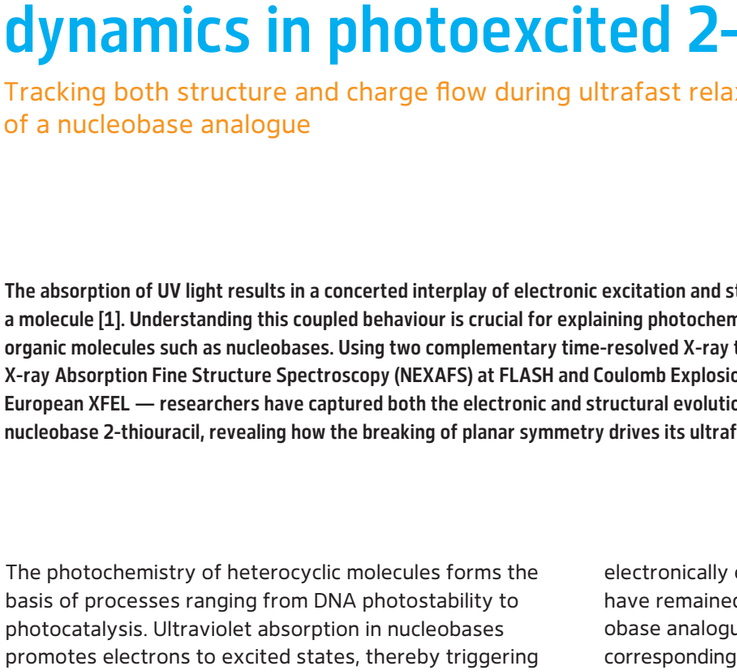

Figure 1

a) Molecular frame momenta of the protons and oxygen ions of 2-thiouracil recorded after rapid and extreme charge up using X-rays from the European-XFEL (atomising the molecule), directly resembling the geometry of the molecule. b,c) Time dependence of the intensity located in different parts of the measured proton momentum space. b) The decrease indicates the rapid out-of-plane movement of the H9 hydrogen. c) The delayed onset of the decrease of the H_{11} in-plane contribution and the increase of general out-of-plane contribution of the hydrogens is caused by the heavy sulfur moving slowly out of the molecular plane. (Adapted from original publication Jahnke et al.)

At FLASH, the longer wavelength radiation provides a direct view into the electronic processes of organic molecules via soft X-ray spectroscopy. While CEI exposes how the nuclei move, time-resolved Near-Edge X-ray Absorption Fine Structure (NEXAFS) spectroscopy [5] at DESY's FLASH facility provides a complementary window into the electronic side of the process. By probing the sulphur 2s and 2p absorption edges after UV excitation, the team followed the changing occupancy of molecular orbitals localised at the sulphur atom. The resulting transient spectra, shown in Fig. 2, revealed distinct signatures of the excited $S_2(\pi\pi^*)$ and $S_1(n\pi^*)$ states, the delayed rise of the nπ*-related features by 102 ± 11 fs relative to the ππ* population pinpointed the timescale of the internal conversion. Moreover, oscillations in the transient absorption signal indicated that the nuclear wave packet continues to vibrate coherently after the transition, in agreement with oscillatory features previously observed in time-resolved X-ray photoelectron spectra.

Together, these two studies provide a comprehensive picture of coupled electronic and nuclear motion in a prototypical heterocyclic molecule. This combined view bridges structural and electronic observables, offering an unprecedented insight into the non-Born–Oppenheimer dynamics that govern photochemistry in biologically and technologically relevant systems.

The analysis developed in the time-resolved CEI study demonstrates how ion-coincidence detection can capture key structural information, making future studies of larger systems feasible. Similarly, resonant X-ray absorption at free-electron lasers opens new possibilities for site-selective probing of excited-state populations with femtosecond resolution. Together, they showcase how different X-ray sources can unravel and ultimately help control the molecular processes that underlie photostability and light-driven chemistry.

Author contact: Fabiano Lever, fabiano.lever@desy.de
Till Jahnke, till.jahnke@xfel.eu
Markus Gühr, markus.guehr@desy.de

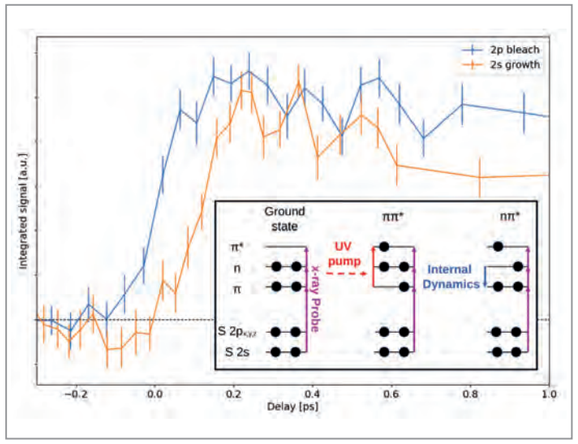

Figure 2

Comparison of the time-resolved differences in absorption signal from the ππ* (blue line, inverted) and nπ* (orange line) features in 2-thiouracil. We identify approx. 100 fs delay between the light-induced excitation of the $S_2(\pi\pi^*)$ and the internal conversion to the $S_1(n\pi^*)$. Different X-ray photon energies probe the occupation state of various orbitals in the molecule. UV-light is used to induce the molecular dynamic. (Adapted from original publication Lever et al.)

References

1. D.R. Yarkony, 'Diabolical conical intersections', Rev. Mod. Phys. 68, 985 (1996).
2. D. Mayer, F. Lever and M. Gühr, 'Time-resolved X-ray spectroscopy of nucleobases and their thionated analogs', J. Photochem. Photobiol. 100(2), 275-290 (2024).
3. S. Arslancan, L. Martínez-Fernández and I. Corral, 'Photophysics and Photochemistry of Canonical Nucleobases' Thioanalogs: From Quantum Mechanical Studies to Time Resolved Experiments', Molecules 22, 998 (2017).
4. B. Richard et al., 'Imaging collective quantum fluctuations of the structure of a complex molecule', Science 389, 650–654 (2025).
5. T.J.A. Wolf et al., 'Probing ultrafast ππ*/nπ* internal conversion in organic chromophores via Kedge resonant absorption', Nat. Comm. 8, 29 (2017).

Original publications

'Direct observation of ultrafast symmetry reduction during internal conversion of 2-thiouracil using Coulomb explosion imaging'. Nature Communications 16, 2074 (2025).
DOI: 10.1038/s41467-025-57083-3

Till Jahnke, Sebastian Mai, Surjendu Bhattacharyya, Keyu Chen, Rebecca Boll, Maria Elena Castellani, Simon Dold, Ulrike Frühling, Alice E. Green, Markus Ilchen, Rebecca Ingle, Gregor Kastirke, Huynh Van Sa Lam, Fabiano Lever, Dennis Mayer, Tommaso Mazza, Terence Mullins, Yevheniy Ovcharenko, Björn Senfftleben, Florian Trinter, Atia-Tul-Noor, Sergey Usenko, Anbu Selvam Venkatachalam, Artem Rudenko, Daniel Rolles, Michael Meyer, Heide Ibrahim and Markus Gühr

'Direct Observation of the ππ* to nπ* Transition in 2-Thiouracil via Time-Resolved NEXAFS Spectroscopy', The Journal of Physical Chemistry Letters 16 (16), 4038-4046 (2025).
DOI: 10.1021/acs.jpclett.5c00544

Fabiano Lever, David Picconi, Dennis Mayer, Skirmantas Ališauskas, Francesca Calegari, Stefan Düsterer, Raimund Feifel, Marion Kuhlmann, Tommaso Mazza, Jan Metje, Matthew S. Robinson, Richard J. Squibb, Andrea Trabattoni, Matthew Ware, Peter Saalfrank, Thomas J. A. Wolf and Markus Gühr

For affiliations, please refer to original publications.

Atomic nuclei in interaction

Coupling nuclei via X-ray waveguides

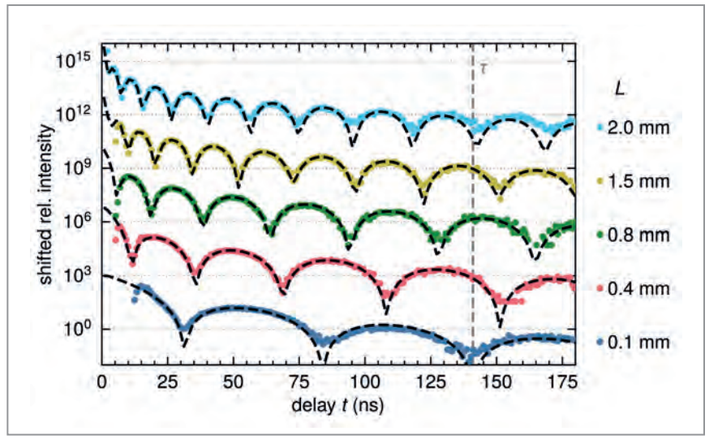

Figure 2

Experimentally observed photon counts as a function of delay t after excitation for different waveguide lengths L. The photons are emitted into the waveguide mode and measured in the far field. The beating pattern not only depends on the number of nuclei but also on their coupling strength to the waveguide mode.

'The whole is more than the sum of its parts' – even in quantum physics. Quantum objects, even simple ones such as atoms with only two possible energy states, can behave completely differently in a group than they do on their own. The behaviour of a whole depends on how the individual parts are arranged and connected. Waveguides can be used to realise such connections in a controlled way. We now have coupled a large ensemble of atomic nuclei of the iron isotope ^{57}Fe via an X-ray waveguide for the first time.

Waveguides confine waves such as radio waves, microwaves or visible light and guide them in a controlled direction. Even for X-rays, special X-ray waveguides can be designed and built [1] to confine X-rays down to about 10 nm. In the laboratory, waveguides are used, for example, to bring individual atoms into interaction in a controlled way—a field of research that was termed 'waveguide quantum electrodynamics' (waveguide QED) [2]. In this setting, photons are forced to propagate through a single or a few well-defined channels which alters light–matter coupling. This enables to realise phenomena that are absent in free space such as long-range interactions mediated by the waveguide mode, directional emission and even strong photon–photon correlations. It provides a powerful platform for studying fundamental aspects of quantum optics and for developing building blocks of quantum technologies.

Until now, waveguide QED was restricted to the 'other end' of the spectrum with long-wave radiation such as microwaves or visible light. In experiments at the High Resolution Dynamics Beamline Beamline P01 at PETRA III, we have now demonstrated how to couple a large number of atomic nuclei using X-ray waveguides. We have employed the Mössbauer isotope ^{57}Fe with its sharp 5 neV wide resonance at the hard X-ray energy of 14.4 keV. A visualisation of the experiment is shown in Fig. 1. We have first irradiated the ^{57}Fe nuclei with short flashes of X-ray light, thereby weakly exciting them. Exciting such a transition between energy states, of the nuclear spin in this case, requires that the energy of the radiation matches the energy difference exactly. Each X-ray pulse, consisting of around 1000 photons, contained on average less than one energy-matching photon due to the extremely sharp resonance.

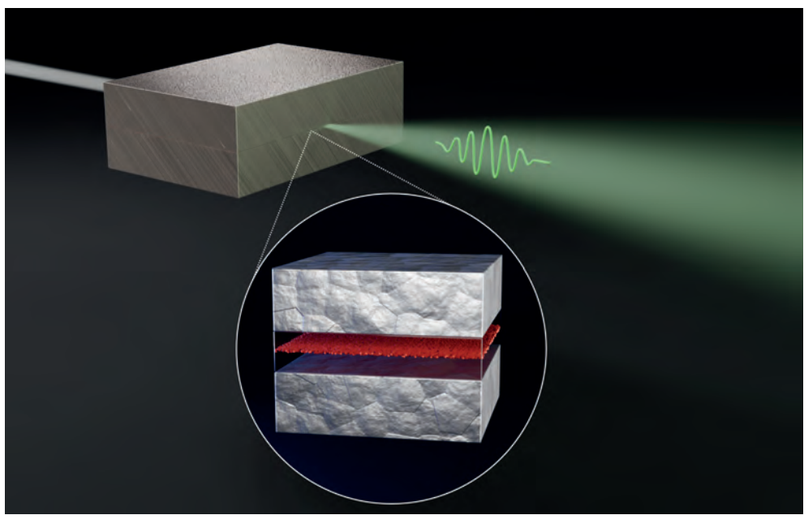

Figure 1

3D visualisation of the experiment. Inset: The X-ray waveguide consists of two 30-nm-thick molybdenum layers as cladding (grey) with a 20 nm boron carbide guiding core (opaque). Two atomic layers of ^{57}Fe (red) are arranged in the centre of the X-ray waveguide. The X-ray pulse (white) comes from the rear left, whereupon the atomic nuclei collectively emit a photon (green waveform).

When atoms, or nuclei in this case, are excited together, they influence each other and do not fall back to their ground state independently but collectively. We have measured this collective decay in which the nuclear ensemble emits a photon back into the waveguide mode. Depending on the arrangement of the atomic nuclei, characteristic temporal signals—beat patterns—emerged (Fig. 2) that could be analysed in detail. The measurements agree with a new theoretical model that we have developed with colleagues from the Universities of Erlangen-Nürnberg and Würzburg. It is shown that the excitation dynamics is sensitively influenced by a coupling strength parameter between nuclei and the waveguide mode—which can be engineered by the sample design.

A major technical challenge of the experiment was the preparation of X-ray waveguides which enabled both good coupling of the nuclei over large distances and allowed the strong X-ray pulses to be guided with low loss—without overloading the sensitive measurement electronics. To that end, the waveguides were designed based on a recently developed nano-optical theory and simulation software for X-ray waveguides [3]. The thin layers were then precisely grown by sputter deposition onto polished Germanium wafers, capped by an identical Germanium wafer to block the tails of the X-ray focal spot and cut to shape.

These initial experiments light the way to new possibilities, combining classical nuclear resonance experiments with modern quantum optics and waveguide technologies or X-ray nanophotonics [4]. The main obstacle is the still relatively low spectral flux density, in particular in combination with nanometre focusing. With PETRA IV, we expect to be able to feed a thousand times more photons into the waveguides. This would make much more complex experiments possible which require the interconnection of different nuclear ensembles via several waveguides.

Author contact: Leon M. Lohse, leon.merten.lohse@desy.de

References

1. T. Salditt, S. Hoffmann, M. Vassholz, J. Haber, M. Osterhoff and J. Hilhorst, 'X-Ray Optics on a Chip: Guiding X Rays in Curved Channels', Phys. Rev. Lett. 115, 203902 (2015).
2. A. S. Sheremet, M. I. Petrov, I. V. Iorsh, A. V. Poshakinskiy and A. N. Poddubny, 'Waveguide quantum electrodynamics: Collective radiance and photon-photon correlations', Rev. Mod. Phys. 95, 15002 (2023).
3. L. M. Lohse and P. Andrejić, 'Nano-optical theory of planar x-ray waveguides', Opt. Express 32, 9518 (2024).
4. X. Shi et al., 'Quantum nanophotonics with energetic particles: X-rays and free electrons', Prog. Quantum Electron. 102, 100577 (2025).

Original publication

'Collective Nuclear Excitation and Pulse Propagation in Single-Mode X-Ray Waveguides', Physical Review Letters 135, 053601 (2025). DOI: 10.1103/r2hf-9qn9

Leon M. Lohse[1,2,3], Petar Andrejić[4], Sven Velten[2,3], Malte Vassholz[1], Charlotte Neuhaus[1], Ankita Negi[2,3], Anjali Panchwanee[3], Ilya Sergeev[3], Adriana Pálffy[5], Tim Salditt[1] and Ralf Röhlsberger[6,7,8,2,3]

1. Georg-August-Universität Göttingen, Göttingen, Germany
2. The Hamburg Centre for Ultrafast Imaging, University of Hamburg, Hamburg, Germany
3. Deutsches Elektronen-Synchrotron DESY, Hamburg, Germany
4. Friedrich-Alexander-Universität Erlangen-Nürnberg, Erlangen, Germany
5. Julius-Maximilians-Universität Würzburg, Würzburg, Germany
6. Friedrich-Schiller-Universität Jena, Jena, Germany
7. Helmholtz-Institut Jena, Jena, Germany
8. GSI Helmholtzzentrum für Schwerionenforschung GmbH, Darmstadt, Germany

Heavy chalcogens as vibronic dampers

Element-targeted nuclear resonance vibrational spectroscopy identifies the vibrational mode driving spin control

Iron-sulphur clusters, nature's wiring for electron transfer in enzymes, play crucial roles in life-sustaining chemical reactions like photosynthesis, cellular respiration and nitrogen fixation. Understanding the fundamental electronic structure of these inorganic clusters is essential for the design of future catalysts. By linking specific vibrational motions to electronic structure, our results provide a mechanistic handle for targeting spin configuration in iron-chalcogenide motifs. The approach offers a general strategy for predicting and controlling reactivity in larger biological clusters and synthetic catalysts.

Iron-sulphur clusters consist of iron ions in different oxidation states, usually Fe^{2+} or Fe^{3+}. When these mixed-valent clusters form, the sharing of unpaired electrons is controlled by various interactions, determining the observed spin state [1]. The simplest building block for modelling interactions in very large clusters is the mixed-valent $[Fe_2S_2]^+$ subunit. This core usually settles into a low-spin (S = 1/2) ground state due to antiferromagnetic coupling of the two iron ions: [S = 5/2 Fe^{3+}] – [S = 2 Fe^{2+}] = 1/2. If they interact ferromagnetically, the S = 9/2 ground spin state is observed (Fig. 1).

A previously synthesised series of mixed-valent di-iron dichalcogenide dimers, $[L_2Fe_2Q_2]^+$ (Q = S, Se, Te), supported by a bulky isopropyl-substituted β-diketiminate ligand (L), was characterised by various spectroscopic methods [2]. As expected, the sulphur-bridged complex exhibited the typical S = 1/2 ground state. More interestingly, replacement of the S with Se showed signatures of both an S = 1/2 and 3/2 ground spin state. Going one step further, the Te-bridged dimer cleanly adopted the S = 3/2 state. This was the first observation of a stabilised intermediate spin state in a mixed-valent dimer. The Heisenberg double exchange explains the observed S = 3/2 intermediate spin state, but it overlooks molecular vibrations that localise electrons and destabilise such states.

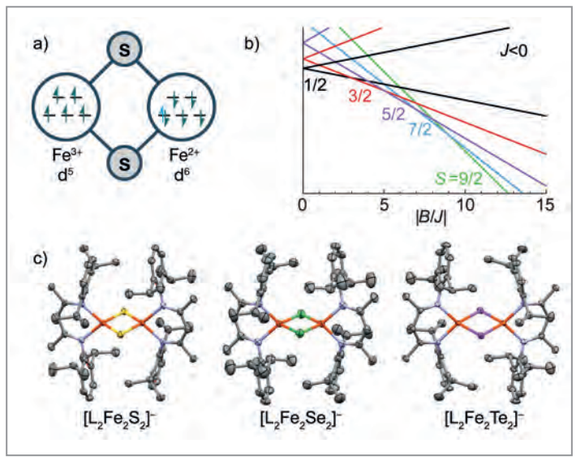

Figure 1

a) Antiferromagnetic Heisenberg exchange coupling (J) in a mixed-valent Fe^{3+}-Fe^{2+} pair results in a single unpaired electron, leading to a ground state with S = 1/2. b) In the Heisenberg double exchange interaction, the ground state spin increases from S = 1/2 to S = 9/2 as the double exchange interaction (B) becomes much larger than J. c) X-ray diffraction (XRD) patterns of $[L_2Fe_2Q_2]^-$ complexes, showing Fe (red), S (yellow), Se (green), Te (purple), N (blue) and C (grey) atoms, excluding hydrogen for clarity. (Figure adapted from Henthorn et al. [2] under a CC BY 4.0 license.)

In a new study published in *Nature Communications*, we employed ^{125}Te and ^{57}Fe nuclear-resonance vibrational spectroscopy (NRVS) alongside density-functional theory computations to investigate key vibration modes essential to the stabilisation of intermediate spin states [3]. The results reveal that swapping sulphur for heavier chalcogens like selenium or tellurium can essentially quiet or dampen the vibrations that usually localise electrons. The so-called "PKS" vibration, identified by Piepho, Krausz and Schatz (PKS)[4], was expected to be present at relatively low energies, presenting a challenge for most lab-based spectroscopies but was well-suited for NRVS spectroscopic characterisation (Fig. 2). The experimental observation, paired with density functional theory (DFT) analysis, suggests that minimising this vibration is crucial to stabilising unusual intermediate spin states in mixed-valent dimers.

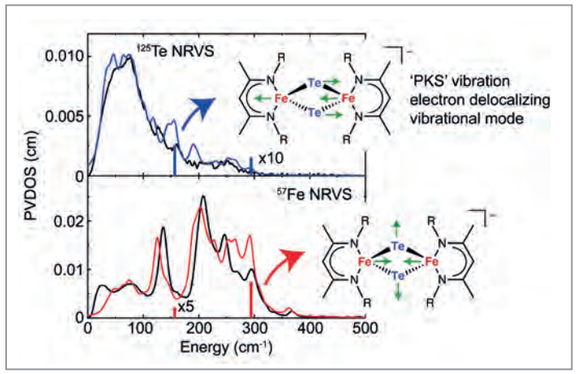

Figure 2

^{125}Te and ^{57}Fe nuclear resonance vibrational spectroscopies of a [2Fe-2Te]$^+$ cluster with key vibrations highlighted. The so-called 'PKS' vibration is typically responsible for electron localisation and delocalisation of intermediate spin-states. It is best observed via ^{125}Te NRVS due to the larger Te atomic displacement compared to the Fe atoms and associated ^{57}Fe NRVS.

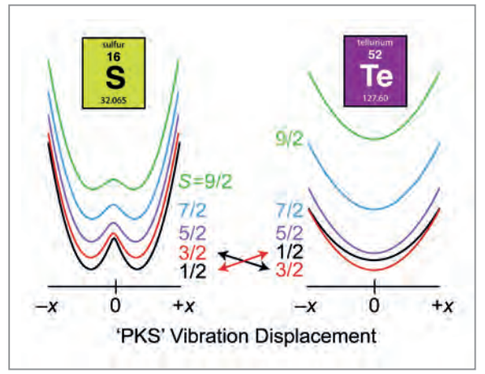

Figure 3

Ground and excited spin states in the PKS coordinate for the $[Fe_2S_2]^+$ and $[Fe_2Te_2]^+$ complexes. The $[Fe_2S_2]^+$ exhibits a localised electronic structure, a barrier of electron transfer between the two ions and an S = 1/2 ground-state. The $[Fe_2Te_2]^+$ complex exhibits fully electron delocalisation (equal sharing of the unpaired electron) and a S = 3/2 intermediate spin ground-state.

NRVS proved to be a uniquely powerful tool for this problem, as it is an element-selective technique. With different high-resolution monochromators, one can tune the X-ray beam to the ^{57}Fe or ^{125}Te Mössbauer nuclear excitation energies (approximately 14.4 keV and 35.5 keV, respectively) and ultimately measure the inelastic vibrational sidebands with meV resolution. That site selectivity allowed us to separately measure the $[Fe_2Q_2]^+$ core's vibrations that were coupled to the iron ions, or more specifically, to the heavy bridging tellurium ions. These ultra-sensitive measurements relied on intense, highly monochromatic synchrotron radiation at the PETRA III beamline P01. This beamline is well-positioned to measure the ^{125}Te NRVS due to its high-energy requirements, and a single-crystal back-scattering sapphire monochromator developed there enabled high-resolution ^{125}Te NRVS studies.

Why does this matter? The [2Fe–2S] unit is the module from which biology constructs larger catalysts, such as the [4Fe–4S] clusters and the complex cofactors of nitrogenase. Establishing how specific vibrations influence electron localisation versus delocalisation at the dimer level provides a template for understanding and, hopefully, predicting the spin states in larger clusters and synthetic analogues. In practical terms, controlling vibronic coupling via targeted atom substitution (Fig. 3) offers a rational lever for designing catalysts and molecular materials where spin configuration governs reactivity or information flow.

Author contact: George Cutsail, george.cutsail@cup.lmu.de

References

1. D. C. Johnson, D. R. Dean, A. D. Smith and M. K. Johnson, 'Structure, Function and Formation OF Biological Iron-Sulfur Clusters,' Annu. Rev. Biochem. 74, 247–281 (2005).
2. J. T. Henthorn, G. E. Cutsail III, T. Weyhermüller and S. DeBeer, 'Stabilization of intermediate spin states in mixed-valent diiron dichalcogenide complexes,' Nat. Chem. 14, 328–333 (2022).
3. A. Radović, J.T. Henthorn, H. Wang, D. Prajapat, I. Sergeev, N. Nagasawa, Y. Yoda, S. P. Cramer and G. E. Cutsail III, '125Te and 57Fe nuclear resonance vibrational spectroscopic characterization of intermediate spin state mixed-valent dimers, ' Nat. Com. 16, 6843 (2025).
4. S. B. Piepho, E. R. Krausz and P. N. Schatz, 'Vibronic coupling model for calculation of mixed valence absorption profiles', J. Am. Chem. Soc. 100, 2996–3005 (1978).

Original publication

^{125}Te and ^{57}Fe Nuclear Resonance Vibrational Spectroscopic Characterization of Intermediate Spin State Mixed-Valent Dimers', Nature Communications 16, 6843 (2025).
DOI: 10.1038/s41467-025-62118-w

Aleksa Radović[1], Justin T. Henthorn[1], Hongxin Wang[2], Deepak Prajapat[3], Ilya Sergeev[3], Nobumoto Nagasawa[4], Yoshitaka Yoda[4], Stephen P. Cramer[2] and George E. Cutsail III[1,5,6]

1. Max Planck Institute for Chemical Energy Conversion, Mülheim an der Ruhr, Germany
2. SETI Institute, Mountain View, CA, USA.
3. Deutsches Elektronen-Synchrotron DESY, Hamburg, Germany
4. Spring-8, Precision Spectroscopy Division, Sayo, Hyogo, Japan
5. Institute of Inorganic Chemistry, University of Duisburg-Essen, Essen, Germany
6. Department of Chemistry, Ludwig-Maximilians-Universität München, Munich, Germany

Laser-assisted photoemission reveals surface screening

Unveiling dynamic dielectric responses using time-resolved XPS

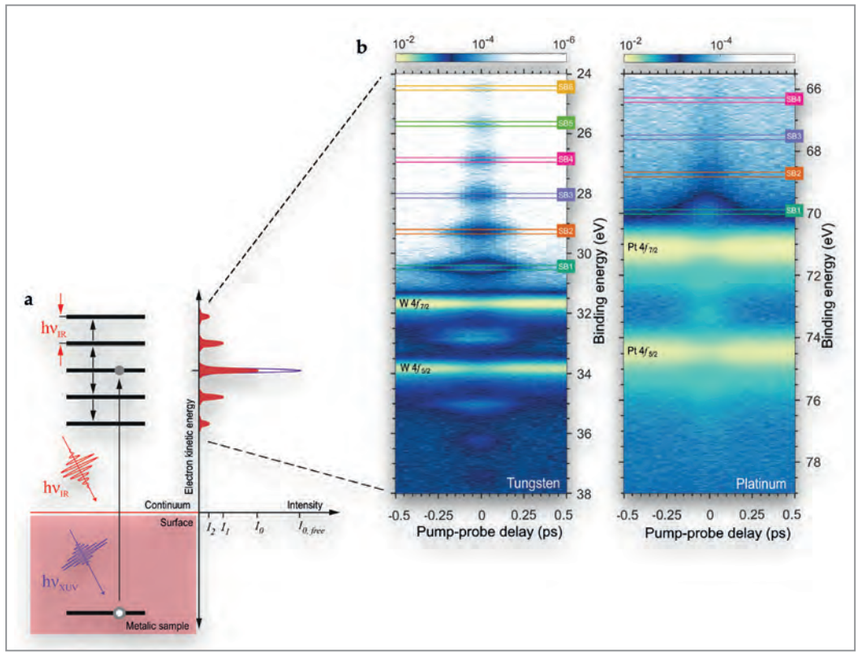

Figure 1

a) Fundamental principle of the laser-assisted photoemission effect (LAPE). The simultaneous exposure of a sample to both an X-ray field and an optical laser field leads to a multiplet of photoemission lines. This structure originates from the absorption or stimulated emission of a number of optical laser photons by the electrons excited into the continuum after XUV absorption. b) 2D false-colour plot of the measured time-dependent 4f core-level photoemission spectra of tungsten and platinum as a function of pump–probe delay and binding energy.

When light interacts with matter, electrons can be released in a process known as photoelectric effect which was first explained by Einstein over a century ago. Over the past century this effect has become a cornerstone of modern science and technology, forming the basis for photoelectron spectroscopy—one of the most powerful methods for studying the electronic structure of materials. Today, ultrafast X-ray sources such as free-electron lasers enable scientists to revisit this century-old effect in a completely new way by observing how electrons respond to light on their femtosecond timescales, revealing previously inaccessible information about the interactions of photons with surfaces.

Recent advances in ultrafast X-ray science have paved the way for a new era of time-resolved pump–probe experiments that uncover how photons interact with surfaces and drive electronic motion. When coherent X-ray and optical laser pulses overlap in time and space, their fields can interfere, creating a 'two-colour' excitation scheme. Under these conditions, photoelectrons emitted by the X-rays can absorb or emit additional laser photons as they leave the solid (see Fig. 1a). This process, known as the laser-assisted photoelectric effect (LAPE), leaves a characteristic fingerprint in the photoelectron spectrum in the form of a series of sidebands of the intrinsic photoemission line, spaced by the photon energy of the optical laser [1,2]. Although this effect has long been studied in gases, its behaviour at solid surfaces, where electrons are subject to complex screening effects and local field variations, remains much less well understood. The appearance of sidebands in X-ray photoelectron spectroscopy (XPS) spectra from solids has previously been used to determine the temporal overlap of X-ray and optical lasers in time-resolved photoemission experiments [3,4]. However, until now, a fundamental understanding of the two-photon processes that could be exploited, for example, for a new class of attosecond photoemission experiments on solid surfaces has been lacking. This new work represents a scientific and technical breakthrough in enabling a deeper understanding of ultrafast pump–probe photoemission experiments with X-rays.

The research team, composed of scientists from DESY, TU Bergakademie Freiberg, the European XFEL, University of Hamburg and Lawrence Berkeley National Laboratory, conducted a detailed investigation of LAPE from two model metal surfaces, tungsten (W) and platinum (Pt). The experiments were conducted at the FLASH free-electron laser in Hamburg, employing femtosecond time-resolved XPS using the WESPE end station at the PG2 beamline. By synchronising ultrafast X-ray pulses and infrared laser pulses, the team was able to study the emission of core-level electrons from W(110) and Pt(111) surfaces in real time and under the influence of the laser field. Remarkably, the number of generated sidebands differed significantly for the two metals, with tungsten producing a greater number of photoelectron sidebands under identical measurement conditions (see Fig. 1b).

These observations can be explained on a semi-quantitative level by analysing the dynamic dielectric responses of the two metals. In the vicinity of a metal surface, the infrared field undergoes modifications due to the effects of reflection, refraction and electronic screening. Consequently, the field experienced by electrons leaving the surface differs from the initial laser intensity. Utilising the strong-field approximation [5], the researchers demonstrate that the effective near-surface IR laser field strength at the tungsten surface is almost four times higher than at platinum. This discrepancy directly accounts for the enhanced LAPE response exhibited by tungsten. The discovery of this effect provides novel insight into the actual, time-dependent IR field strength in the surface region of the metals and the dynamics of the light–matter interaction which is governed not only by the laser parameters and measurement geometry, but also by the local dynamic dielectric properties of the surface.

Based on these findings, a new standard could be established for the quality and detail with which LAPE spectra from solid-state materials can be recorded with state-of-the-art ultrashort X-ray light sources. Furthermore, the experiment demonstrates that LAPE is not merely a diagnostic for the temporal overlap of light pulses in pump–probe experiments but a sensitive probe of how materials screen electromagnetic fields on ultrafast timescales and nanometer length scales. The development of new techniques for monitoring electronic and lattice dynamics in this surface region is important and may contribute to a deeper understanding of surface electromagnetic fields, including local fields at a chemisorbed atom or molecule. Furthermore, a detailed understanding of LAPE contributions in high-resolution pump–probe photoemission spectroscopy is a prerequisite for correctly interpreting a growing number of time-resolved experiments at next-generation, high repetition-rate light sources.

This work not only advances fundamental knowledge of light–matter interactions but also provides new tools for monitoring ultrafast processes in building blocks for next-generation technologies such as photocatalysis, optoelectronics and quantum materials. It sets the stage for high-precision diagnostics in complex systems and provides key benchmarks for future studies of electron dynamics at surfaces. By combining experimental excellence and theoretical innovation, this research delivers key insights into how intense laser fields influence electron behaviour at the femtosecond scale.

Author contact: Lukas Wenthaus, lukas.wenthaus@desy.de
Friedrich Roth, friedrich.roth@physik.tu-freiberg.de

References

1. J. M. Schins, P. Breger, P. Agostini, R. C. Constantinescu, H. G. Muller, G. Grillon, A. Antonetti and A. Mysyrowicz, 'Observation of laser-assisted auger decay in argon', Phys. Rev. Lett. 73, 2180–2183 (1994).
2. T. E. Glover, R. W. Schoenlein, A. H. Chin and C. V. Shank, 'Observation of laser assisted photoelectric effect and femtosecond high order harmonic radiation', Phys. Rev. Lett. 76, 2468–2471 (1996).
3. F. Roth, M. Borgwardt, L. Wenthaus, J. Mahl, S. Palutke, G. Brenner, G. Mercurio, S. Molodtsov, W. Wurth, O. Gessner and W. Eberhardt, 'Direct observation of charge separation in an organic light harvesting system by femtosecond time-resolved XPS', Nat. Comm. 12, 1196 (2021).
4. A. Pietzsch, A. Föhlisch, M. Beye, M. Deppe, F. Hennies, M. Nagasono, E. Suljoti, W. Wurth, C. Gahl, K. Döbrich and A. Melnikov, 'Towards time resolved core level photoelectron spectroscopy with femtosecond x-ray free-electron lasers', New J. Phys. 10, 033004 (2008).
5. L.V. Keldysh, 'Ionization in the field of a strong electromagnetic wave', Sov. Phys. JETP 20, 1307 (1965).

Original publication

'Insights into the laser-assisted photoelectric effect from solid state surfaces', Physical Review B 110, 235406 (2024).
DOI: 10.1103/PhysRevB.110.235406

Lukas Wenthaus[1], Nikolay M. Kabachnik[2,3], Mario Borgwardt[4], Steffen Palutke[1], Dmytro Kutnyakhov[1], Federico Pressacco[1], Markus Scholz[1], Dmitrii Potorochin[5,6], Nils Wind[7], Stefan Düsterer[1], Günter Brenner[1], Oliver Gessner[4], Serguei Molodtsov[2,5,6], Wolfgang Eberhardt[1] and Friedrich Roth[5,6]

1. Deutsches Elektronen Synchrotron DESY, Hamburg, Germany
2. European XFEL GmbH, Schenefeld, Germany
3. Donostia International Physics Center (DIPC), San Sebastian/Donostia, Spain
4. Chemical Science Division, Lawrence Berkeley National Laboratory, Berkeley, USA
5. Institute of Experimental Physics, TU Bergakademie Freiberg, Freiberg, Germany
6. Center for Efficient High Temperature Processes and Materials Conversion (ZeHS), TU Bergakademie Freiberg, Freiberg, Germany
7. Universität of Hamburg, Hamburg, Germany

Quantum fluctuations as never seen before

Ground-state fluctuations of a complex molecule imaged using Coulomb explosion

Molecules are restless. Even in their lowest energy state, the Heisenberg uncertainty principle prevents them from reaching absolute stillness. Instead, they twitch and tremble, combining various specific movements into their ground-state fluctuations. These fluctuations are a fundamental quantum effect and, for the first time, we performed their direct imaging in a large molecule.

Imaging of ground-state fluctuations was now achieved for 2-iodopyridine (C_5H_4IN), a molecule consisting of 11 atoms (Fig. 1). The molecules were exposed to intense X-ray pulses at the European X-ray Free-Electron Laser (EuXFEL). The X-ray pulse stripped numerous core electrons off the molecule which led to an ultrafast cascade of atomic events that resulted in cutting the chemical bonds and producing large positive charges on all of the atoms. Then, the atomic cores violently repelled each other. This is known as a Coulomb explosion, in which the molecule breaks into atomic fragments. These fragments and their momenta were measured using the COLTRIMS reaction microscope [1] installed at the SQS instrument. As a result of the ultrafast explosion, the ion momenta directly reflected the structure of the molecule.

Although the overall qualitative shape of the ion momenta was already well understood in our earlier manuscript [2], the *quantitative* understanding of details in the data turned out to be more involved. Even when employing the state-of-the-art simulation, implemented in our XMDYN software [3], some features of the experimental Coulomb explosion were initially mysterious: Since it is a planar molecule, all fragments of the 2-iodopyridine molecule may be expected to fly off exactly within its molecular plane. Instead, the experimental data show (Fig. 2a) significant out-of-plane momenta, in strong disagreement with the simulations performed on a classical molecule in its equilibrium geometry (Fig. 2b). The missing ingredient in the simulation was the ground-state quantum fluctuations of the molecule. By including them, we can model the correct dispersion of the momenta (Fig. 2c) and show how they are influenced by the shape of the ground-state fluctuations before the explosion.

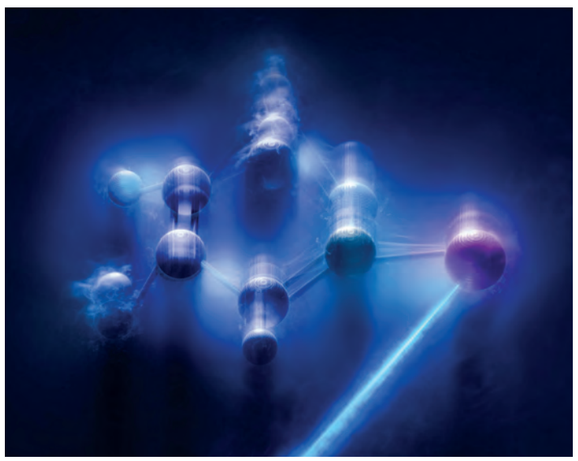

Figure 1
Artist view of the 2-iodopyridine molecule undergoing quantum fluctuations. (Credit: EuXFEL, T. Wüstefeld).

These quantum fluctuations are collective in nature and follow well-defined patterns, rather than erratic manifestations of noise. Our simulations reveal how these structural normal-mode patterns (Fig. 3a) translate into corresponding correlations in the fragment momenta produced in the Coulomb explosion, which we identify using principal component analysis (Fig. 3b). In order to identify these patterns as fingerprints of fluctuation modes in the experimental data, a number of challenges had to be met. The main hurdle was that only 60% of the fragments are detected for each explosion triggered by an X-ray pulse. We overcame this obstacle by developing a new machine-learning method that can reconstruct the complete momentum distribution of the molecule even from such incomplete datasets.

The good agreement between simulation and experiment (Fig. 3c) confirms the predictive power of the refined simulation method. In particular, the experimental data reveal some of the correlated momentum patterns predicted by the XMDYN simulation and thereby image the collective fluctuation patterns of the atoms in the ground-state molecule.

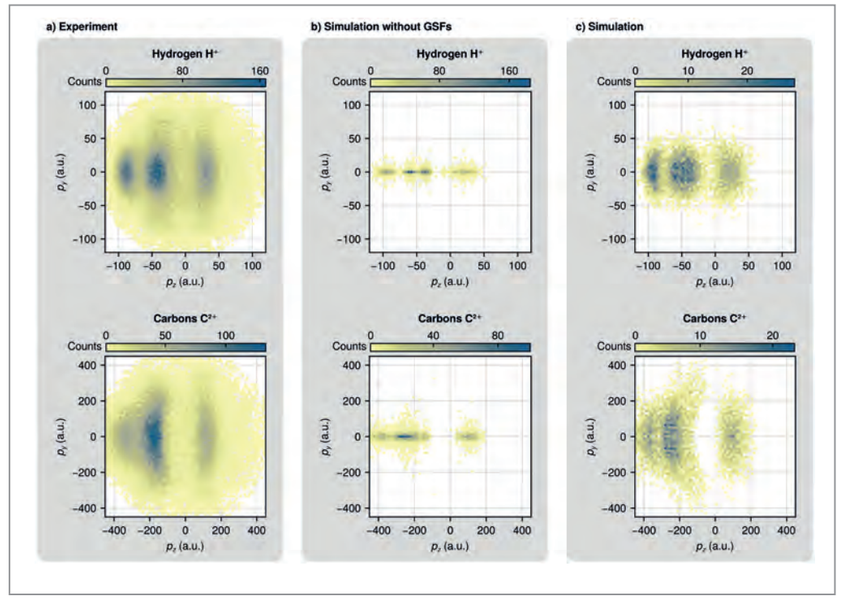

Figure 2
Distribution of the momenta of the hydrogen and carbon ions from the Coulomb explosion of 2-iodopyridine. p_z is defined as the emission direction of the iodine ion, and p_y as the direction perpendicular to the molecular plane. The data is given in atomic units (a.u.). a) Experimental data. b) Simulation, neglecting the ground-state fluctuations (GSFs). c) Simulation, including the GSFs.

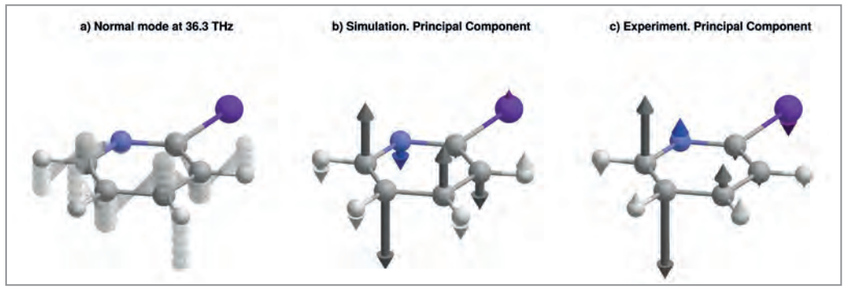

Figure 3
Chosen example of normal mode and principal component.
a) Normal mode of the molecule before its explosion. b) One of the corresponding principal components according to the simulation.
c) Independently identified principal component in the experimental data.

The ability to perform X-ray-induced Coulomb explosion imaging at high-repetition rate free-electron lasers, such as the EuXFEL, opens up new opportunities to explore complex quantum mechanical systems. A unique feature of the method is that it does not merely provide average values for an ensemble of molecules, as for example in X-ray crystallography. Instead, it is based on individual-molecule measurements, which are necessary to see collective behaviour such as ground-state quantum fluctuations. In the future, this technique could be used to study even larger molecules. At the same time, the method is inherently ultrafast, which makes it well-suited for producing time-resolved movies of molecules in a way that is unique compared to other methods.

Author contact: Benoît Richard, benoit.richard@desy.de
Rebecca Boll, rebecca.boll@xfel.eu
Robin Santra, robin.santra@desy.de
Ludger Inhester, ludger.inhester@desy.de
Till Jahnke, till.jahnke@xfel.eu

References

1. J. Ullrich, R. Moshammer, A. Dorn, R. Dörner, L. Ph. H. Schmidt and H. Schmidt-Böcking, 'Recoil-ion and electron momentum spectroscopy: reaction-microscopes', Rep. Prog. Phys. 66, 1463–1545 (2003).
2. R. Boll et al., 'X-ray multiphoton-induced Coulomb explosion images complex single molecules', Nat. Phys. 18, 423–428 (2022).
3. Z. Jurek, S.-K. Son, B. Ziaja and R. Santra, 'XMDYN and XATOM: versatile simulation tools for quantitative modeling of X-ray free-electron laser induced dynamics of matter', J. Appl. Cryst. 49, 1048–1056 (2016).

Original publication

'Imaging collective quantum fluctuations of the structure of a complex molecule', Science 389, 650–654 (2025).
DOI: 10.1126/science.adu2637

Benoît Richard, Rebecca Boll, Sourav Banerjee, Julia M. Schäfer, Zoltan Jurek, Gregor Kastirke, Kilian Fehre, Markus S. Schöffler, Nils Anders, Thomas M. Baumann, Sebastian Eckart, Benjamin Erk, Alberto De Fanis, Reinhard Dörner, Sven Grundmann, Patrik Grychtol, Max Hofmann, Markus Ilchen, Max Kircher, Katharina Kubicek, Maksim Kunitski, Xiang Li, Tommaso Mazza, Severin Meister, Niklas Melzer, Jacobo Montano, Valerija Music, Yevheniy Ovcharenko, Christopher Passow, Andreas Pier, Nils Rennhack, Jonas Rist, Daniel E. Rivas, Daniel Rolles, Ilme Schlichting, Lothar Ph. H. Schmidt, Philipp Schmidt, Daniel Trabert, Florian Trinter, Rene Wagner, Peter Walter, Pawel Ziolkowski, Artem Rudenko, Michael Meyer, Robin Santra, Ludger Inhester and Till Jahnke

For affiliation details refer to original publication.

Phase transition towards metallic hydrogen

Studying the complex crystal structure of solid hydrogen under ultrahigh pressure

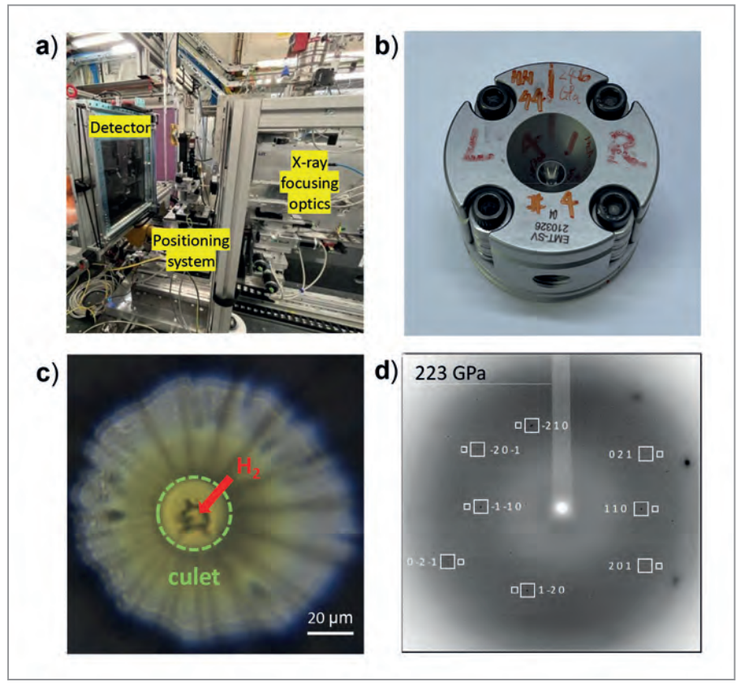

Figure 2
a) Experimental setup of the nanoprobe table in P02.2 high pressure beamline. b) Diamond anvil cell. c) Photo of a hydrogen sample compressed above 220 GPa. Culet means the flat part of diamond anvil used to compress sample. d) An example of SCXRD data of hydrogen. Boxes mark the positions of X-ray diffraction signal with Miller indices.

Imagine the pressure generated on a sesame seed on top of which an Airbus A380 aircraft is placed. It will exceed 200 GPa, two millions of times atmospheric pressure. Under such extreme conditions, what happens to the simplest element: hydrogen? We have achieved the world's first observation of solid hydrogen's complex crystal structure at ultrahigh pressures, utilising advanced synchrotron X-ray techniques. This result disclosed that the atoms of hydrogen are stacked in a novel way which has not been observed before. Such phenomenon gives a hint that hydrogen molecules may go through a polymerisation process on its pathway towards metallic hydrogen under strong compression.

Hydrogen is not a stranger to us. Under normal conditions, it exists as a gas (Fig. 1a) everywhere in the atmosphere. But you may not be familiar with hydrogen under strong compression. When compressed, it would firstly turn into liquid like water and then solid (Fig. 1b) like ice. If hydrogen is further compressed, eventually it may turn into an exotic metal which is called metallic hydrogen. Metallic hydrogen should possess an extraordinary energy density, making it an ideal fuel for space travel. It has also been predicted to be a room temperature superconductor which is a dream for generations of scientists to pursue. The crystal structure of metallic hydrogen may play an important role in its amazing properties, as different crystal structures can introduce sharply distinct properties to materials composed of the same type of atoms, for example, diamond and graphite. Unfortunately, the pressure required to produce metallic hydrogen is daunting, which exceeds the highest pressure in the core of the earth (360 GPa). Thus, directly measuring the crystal structure of the metallic hydrogen is not yet practical.

There is some good news. We can study the evolution of the crystal structure of hydrogen on its passage to metallic hydrogen to learn indirectly what could be the possible format of hydrogen as a unique metal, since hydrogen goes through a series of phase transitions before it becomes a metal. The only technical barrier is to enable high precision measurements to identify subtle changes in the crystal structure of hydrogen at pressures above 200 GPa. Without such high precision techniques, hydrogen would look almost the same even after it goes through a critical phase change, revealed by our previous study [1].

We advanced this frontier with single crystal X-ray diffraction (SCXRD) measurements of hydrogen by using advanced nanoprobe at beamline P02.2 at PETRA III (Fig. 2a). In this study, we used a device called diamond anvil cell (DAC) to generate extreme pressure above 220 GPa (Fig. 2b). This device is portable (pocket-size) and capable of generating extreme pressures by squeezing hydrogen between the needle tips of two opposing diamonds (Fig. 2c). By pushing the two diamonds closer, extreme pressure is generated on a piece of hydrogen crystal smaller than 1 µm. With the help of the high precision positioning system, high quality SCXRD data was obtained from the high-pressure phase of hydrogen (Fig. 2d), suggesting a more complex crystal structure (Fig. 1c) compared to that adopted by the low-pressure phase. We performed DFT-based molecular dynamics simulations and found a structure model with lower symmetry containing graphene-like layers consistent with the experimental data.

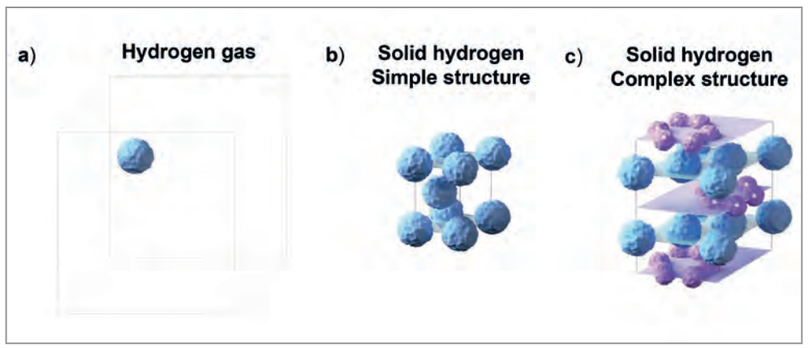

Figure 1
Different phases of molecular hydrogen H_2. Blue solid spheres represent freely rotating H_2 molecules. Pink dumbbells represent H_2 molecules with ordered orientations. a) Sparse hydrogen molecule in space (gas). b) Solid hydrogen in hexagonal close-packed structure. c) Complex crystal structure of hydrogen discovered in this work.

This finding has important implications for our understanding of metallic hydrogen. Metallic hydrogen was initially considered to adopt a crystal structure similar to alkali metals with a simple body centred cubic (bcc) structure. However, recent theoretical simulations suggested two other scenarios. Firstly, metallic hydrogen may possess a more complex structure with hydrogen atoms being 'polymerised' into networks [2]. Secondly, metallic hydrogen may be a complete liquid without a defined crystal structure [3]. Our new finding suggests that hydrogen is developing some 'polymerised' pattern along its metallisation pathway. Of course, directly measuring the SCXRD data of metallic hydrogen would give the final answer, which could be expected at upgraded PETRA IV in the future.

Author contact: Cheng Ji, cheng.ji@hpstar.ac.cn

References

1. C. Ji et al., 'Ultrahigh-pressure isostructural electronic transitions in hydrogen', Nature 573, 558–562 (2019).
2. J. M. McMahon, M. A. Morales, C. Pierleoni and D. M. Ceperley, 'The properties of hydrogen and helium under extreme conditions', Rev. Mod. Phys. 84, 1607–1653 (2012).
3. E. Babaev, A. Sudbø and N. W. Ashcroft, 'A superconductor to superfluid phase transition in liquid metallic hydrogen', Nature 431, 666–668 (2004).

Original publication

'Ultrahigh-pressure crystallographic passage towards metallic hydrogen', Nature 641, 904–909 (2025).
DOI: 10.1038/s41586-025-08936-w

Cheng Ji[1,2], Bing Li[1], Jie Luo[3,4], Yongsheng Zhao[5,1], Yuan Liu[3,4], Konstantin Glazyrin[5], Alexander Björling[6], Lucas A. B. Marçal[6,7], Maik Kahnt[6], Sebastian Kalbfleisch[6], Wenjun Liu[8], Yang Gao[1], Junyue Wang[1], Wendy L. Mao[9,10], Hanyu Liu[3,4,11], Yanming Ma[3,4,11], Yang Ding[1], Wenge Yang[1] and Ho-Kwang Mao[1,2]

1. Center for High Pressure Science and Technology Advanced Research, Beijing, China
2. Shanghai Key Laboratory of MFree, Shanghai Advanced Research in Physical Sciences, Shanghai, China
3. Key Laboratory of Material Simulation Methods and Software of Ministry of Education, College of Physics, Jilin University, Changchun, China
4. State Key Laboratory of Superhard Materials, College of Physics, Jilin University, Changchun, China
5. Deutsches Elektronen-Synchrotron DESY, Hamburg, Germany
6. MAX IV Laboratory, Lund University, Lund, Sweden
7. Brazilian Synchrotron Light Laboratory, Brazilian Center for Research in Energy and Materials, Campinas, Brazil
8. Advanced Photon Source, Argonne National Laboratory, Argonne, USA
9. Department of Earth and Planetary Sciences, Stanford University, Stanford, USA
10. Stanford Institute for Materials and Energy Sciences, SLAC National Accelerator Laboratory, Menlo Park, USA
11. International Center of Future Science, Jilin University, Changchun, China

Decoding structure-property in high-entropy oxides

Understanding magnetism in high-entropy oxides amid competing magnetic interactions

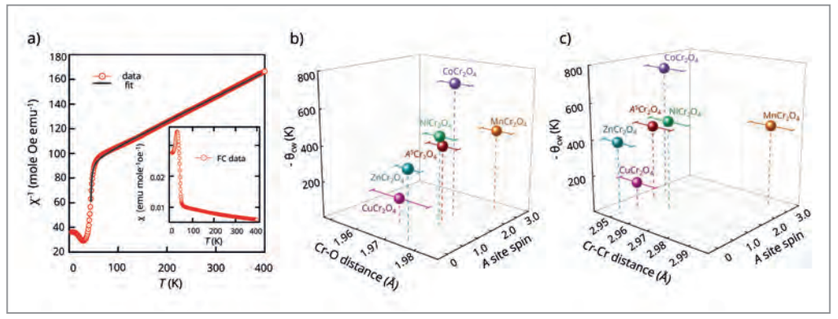

Figure 3

Mean field magnetism and its connection with local structure. a) Fitting of inverse magnetic dc susceptibility using Curie-Weiss equation above T_N at 5000 Oe in $A^5Cr_2O_4$. The Curie-Weiss temperature -θCW is plotted as a function of b) Cr-O bond, c) Cr-Cr distances and *A* site spins. Both plots include data for the parent spinels and the $A^5Cr_2O_4$.

Some of the world's most famous crown jewels belong to a mineral group called spinels. They are prized not only for their deep, vibrant colours but also for their remarkable electronic and magnetic properties. In our research, we explored high-entropy spinels, which are composed of five or more elements occupying the same atomic site, resulting in complex local environments. Using Extended X-ray Absorption Spectroscopy (EXAFS), we revealed how these materials maintain long-range structural order despite local distortions. This flexibility helps explain how consistent magnetic interactions emerge even with varied local atomic arrangements.

Extended X-ray Absorption Fine Structure (EXAFS) spectroscopy is an element-specific technique that probes the local atomic environment around selected atoms over short length scales (5–6 Å) [1]. It is highly sensitive to coordination numbers, bond distances, and neighbouring atomic species, providing a powerful means to study local structural distortions that remain invisible to conventional diffraction methods. In recent years, there has been a surge in interest in high-entropy oxides (HEOs), which are crystalline materials where multiple cations, typically five or more, share single lattice sites [2]. Many HEOs exhibit superior functionality compared to conventional materials and show considerable potential for electronic, magnetic and energy applications [3]. Probing their local structure is crucial to understanding how extreme chemical complexity gives rise to properties beyond those of their single-cation counterparts and how to further enhance their performance.

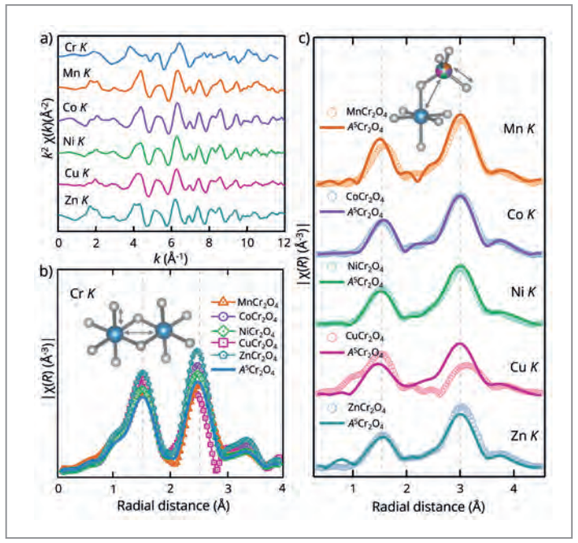

Figure 1

a) The *k*-weighted EXAFS spectra in $A^5Cr_2O_4$. The Fourier transform of the EXAFS spectra at b) Cr *K* edge and c) *A K* edges in the parent spinels and $A^5Cr_2O_4$. Inset panels show the first and second nearest neighbour distances b) for Cr, and c) for the *A* site.

To investigate this broad goal, we focused on a compositionally complex spinel oxide $[Mn_{0.2}Co_{0.2}Ni_{0.2}Cu_{0.2}Zn_{0.2}]Cr_2O_4$ $[A^5Cr_2O_4]$, and investigated its local atomic structure in comparison with its parent members $[ACr_2O_4$, *A* = Mn, Co, Ni, Cu, Zn] using EXAFS. This approach enabled us to understand how configurational disorder redistributes local bonding environments, including coordination geometry and bond distances, and how these local modifications affect macroscopic properties.

EXAFS measurements at all transition metal *K* edges were performed at the P65 beamline of PETRA III. $A^5Cr_2O_4$ adopts a normal cubic spinel structure, with Cr^{3+} sitting in the octahedral sites and the A^{2+} cations occupying the tetrahedral sublattice. Thus, in Fig. 1a, the EXAFS spectra of the Mn, Co, Ni, Cu and Zn *K* edges exhibit similar features among themselves but are distinct from the Cr *K* edge, indicating their different local environments.

Fourier transforms of $k^2\chi(k)$ for Cr and *A K* edges (Fig. 3b,c) reveal two peaks, corresponding to first-neighbour (Cr–O and *A*–O) and second-neighbour (Cr–Cr and *A*–Cr) interactions. The Cu *K* edge of $A^5Cr_2O_4$ differs considerably from that of its parent counterpart, $CuCr_2O_4$, reflecting a major change in the local structure around Cu. This is primarily because $CuCr_2O_4$ exhibits a tetragonal structure due to Jahn-Teller (J-T) distortion of Cu^{2+} cations.

The first and second neighbour bond distances as obtained from the analysis are shown in Fig. 2. For the octahedral environment, Cr–O (1.97 Å) and Cr–Cr (2.96 Å) bond lengths (Fig. 2b,c) in $A^5Cr_2O_4$ are similar to those in $CoCr_2O_4$, $ZnCr_2O_4$ and $NiCr_2O_4$, longer than in $CuCr_2O_4$, and shorter than in $MnCr_2O_4$. Within the tetrahedral environment (Fig. 2e,f), the variation in *A*–O bond lengths is seen depending on the specific cation, wherein all *A*–O bonds in $A^5Cr_2O_4$ are shorter than in their parent compounds. The distances at Co, Ni, and Cu sites are similar, while they differ at Mn and Zn sites. The *A*–Cr second-neighbour distances vary only marginally among cations, implying small local relaxations. Most importantly, the strong J-T distortion seen in $CuCr_2O_4$ is in $A^5Cr_2O_4$. Unlike earlier studies that focused only on the oxygen sublattice adapting to local distortions, our results show that the cationic sublattice also plays a flexible role in maintaining structural stability.

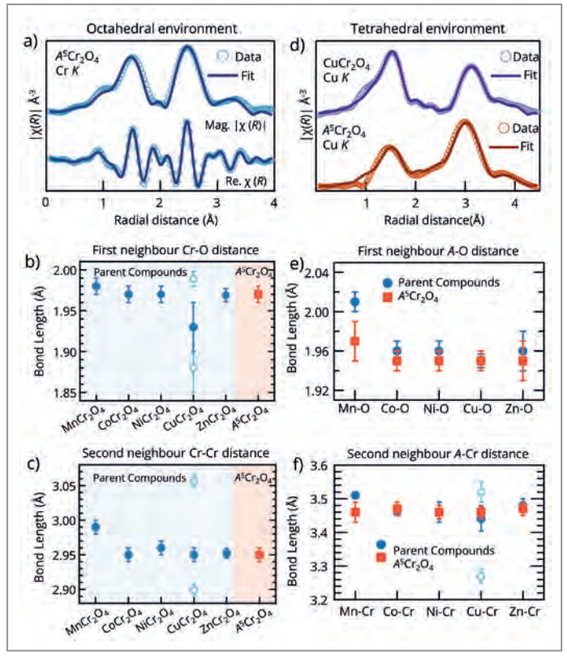

Figure 2

Analysis of local structure: a) and d) The Fourier transformed EXAFS spectra along with the fitted data (the magnitude $|\chi(R)|$ and the real part Re.$\chi(R)$) in $A^5Cr_2O_4$. b)-c) The first and second neighbour bond lengths from Cr site and e)-f) from every *A* site element in parent compounds and $A^5Cr_2O_4$.

Remarkably, despite the presence of multiple magnetic ions and varying bond lengths, $A^5Cr_2O_4$ undergoes a long-range magnetic ordering around 40 K (Fig. 3a). Moreover, the mean-field magnetic interactions of $A^5Cr_2O_4$ closely resemble those of $NiCr_2O_4$, as shown in Fig. 3b,c. This originates from the comparability of EXAFS-derived bond lengths Cr-O, Cr-Cr, and average A site magnetic moment in both materials. Thus, our study paves the way for a deeper understanding of the impact of local structural distortions on the physical properties of materials within the high-entropy framework.

Author contact: Rukma Nevgi: rukmagurudas@iisc.ac.in
Subha Dey: subhadey@iisc.ac.in
Srimanta Middey: smiddey@iisc.ac.in

References

1. M. Newville, 'Fundamentals of XAFS', Rev. Mineral. Geochem. 78, 33–74 (2014).
2. C. M. Rost, E. Sachet, T. Borman, A. Moballegh, E. C. Dickey, D. Hou, J. L.Jones, S. Curtarolo and J-P. Maria, 'Entropy-stabilized oxides', Nat. Commun. 6, 8485 (2015).
3. S. Schweidler, M. Botros, F. Strauss, Q. Wang, Y. Ma, L. Velasco, G. C. Marques, A. Sarkar, C. Kübel, H. Hahn, J. A. Hagmann, T. Brezesinski and B. Breitung, 'High-entropy materials for energy and electronic applications', Nat. Rev. Mater. 9, 266–281 (2024).

Original publications

'Local structural distortions drive magnetic molecular field in compositionally complex spinel oxide', Nature Communications 16, 7038 (2025). DOI:10.1038/s41467-025-62268-x

Rukma Nevgi[1], Subha Dey[1], Nandana Bhattacharya[1], Soheil Ershadrad[2], Tinku Dan[3], Sujay Chakravarty[4], S. D. Kaushik[5], Christoph Klewe[6], George E. Sterbinsky[7], Biplab Sanyal[2] and Srimanta Middey[1]

1. Department of Physics, Indian Institute of Science, Bengaluru, India
2. Department of Physics and Astronomy, Uppsala University, Uppsala, Sweden
3. Deutsches Elektronen-Synchrotron DESY, Hamburg, Germany
4. UGC-DAE Consortium for Scientific Research, Kalpakkam, India
5. UGC-DAE Consortium for Scientific Research, Mumbai, India
6. Advanced Light Source, Lawrence Berkeley National Laboratory, Berkeley, USA.
7. Advanced Photon Source, Argonne National Laboratory, Lemont, USA

Attosecond plasmonics in a single fullerene molecule

Tracking the ultrafast electron dynamics following the excitation of the giant surface plasmon in the C_{60} fullerene.

Plasmonic nanostructures can trap light in extremely small spaces, enabling advances in multiple disciplines, spanning from sensing to energy conversion, biology and quantum technologies. Fullerenes are a unique case: These carbon molecules are smaller than a nanometre, yet exhibit giant and ultrabroad plasmon resonances. However, how these plasmons form and evolve, is still unclear. Using attosecond chronoscopy, we measure the photoemission delay in C_{60} and reveal that electron correlations play a major role in the plasmon dynamics. This sheds light on ultrafast collective electron motion in these sub-nm systems and supports future nanoscale plasmonic applications.

Plasmonic excitations in nanostructures (1 nanometre = a billionth of a metre) enable extreme light confinement and are central to modern developments in nanoscale photonics, sensing, energy conversion and quantum technologies [1-3]. The position and width of a plasmon resonance are key properties as they define the frequency and lifetime of light confinement. These characteristics typically depend on the size, shape and material composition of the plasmonic nanostructure. For nanosystems with dimensions down to ~ 10 nm, semiclassical models accurately describe the plasmon characteristics. Below this length, our knowledge becomes more elusive [4]. For example, while certain aspects of plasmonic resonances, such as the peak energy, have been examined for ultra-small nanoparticles [4], the exact origin and detailed evolution of the linewidth have not been thoroughly investigated.

Fullerene molecules represent a limited case of nanoplasmonics [5]: These hollow carbon cages support giant plasmon resonances in the extreme-ultraviolet spectral range with an ultrabroad linewidth (>10 eV), indicating an ultrashort lifetime on the attosecond scale (1 as = a billionth of a billionth of a second) (Fig. 1a). In these extreme conditions it remains unresolved whether this plasmonic response arises purely from classical electron motion or whether quantum dynamics start playing a significant role, for instance through large-scale electron correlations.

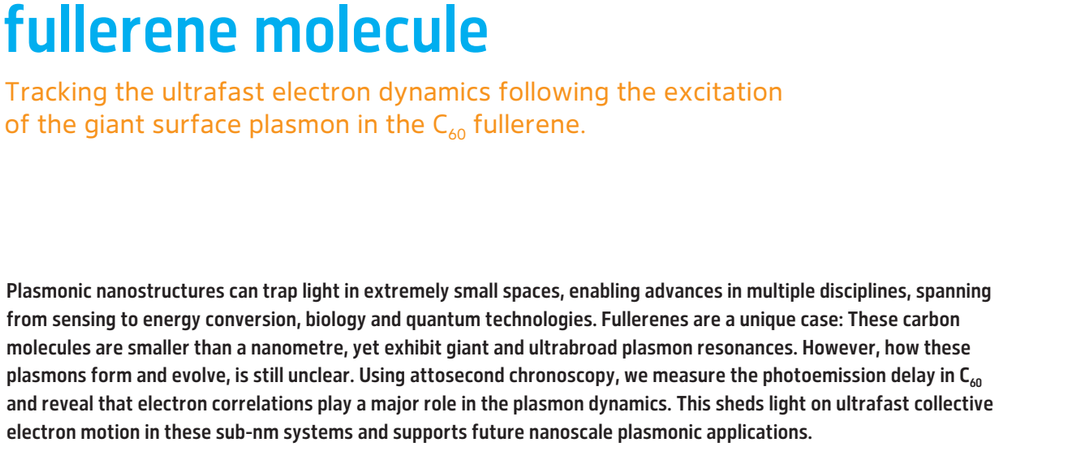

Figure 1

Attosecond chronoscopy of the giant plasmon resonance in C_{60}. a) Spherical shell-like distribution of delocalised electrons around C_{60} exhibits a collective giant plasmon excitation at around 20 eV. The jellium-based DFT potential depicted as a function of radial coordinate of C_{60} provides the energetics of the involved quantum states which can be classified into π and σ characters. The configuration interactions (schematically represented by the arrows) among the electrons occupying these states give rise to the GPR. b) Pictorial representation of the plasmon excitation in C_{60} in an attosecond streaking experiment. c) EWS delay contribution exclusively from the correlated excitation is extracted from the difference between the results of LR-TDDFT (correlated) and LR-DFT (mean-field) calculations. The inset represents the induced potential due to giant plasmon resonance.

Frequency-domain measurements (absorption and ionisation spectra) provide information on resonance energies and linewidths but cannot distinguish coherent quantum contributions from incoherent single-electron excitations. Time-resolved methods, instead, enable the direct measurement of the electron dynamics associated with the plasmonic excitation, thus probing possible quantum signatures in the plasmonic response. For fullerenes, the measurement of the photoemission delay is particularly suitable to probe the plasmon dynamics. Indeed, the excitation energy of the plasmon resonances in these molecules is typically larger than the ionisation potential, thus being embedded in the continuum, and the plasmonic response is thus imprinted in the time electrons take to escape the molecular potential during photoionisation.

In our work, we employed attosecond streaking spectroscopy [6] to measure the photoemission delay in isolated gas-phase C_{60} fullerene molecules and to disclose the key aspect of the plasmon response. In the experiment, a sub-300-attosecond extreme ultraviolet (XUV) excites the giant plasmon resonance at around 20 eV energy and triggers photoionisation. The produced photoelectron spectrum is then transiently modulated by a synchronised sub-5 fs near-infrared (NIR) field, giving rise to an XUV-NIR delay-dependent spectrogram (see Fig. 1b). In the framework of streaking spectroscopy, such a spectrogram contains a direct signature of the Eisenbud-Wigner-Smith (EWS) photoemission delay that is imprinted in the energy-dependent temporal shift of the photoelectron spectrum. As an absolute reference, we simultaneously performed the same experiment in Ne atoms and studied the photoemission delays in C_{60} relative to the simple atomic case.

As the main experimental result, the measured relative photoemission delays for C display a decaying, energy-dependent trend, ranging from approximately 300 as at low photoelectron energies (~8–10 eV) to ~50 as at higher energies (~20–24 eV). To interpret the data, *ab initio* simulations combining linear-response time-dependent density functional theory (LR-TDDFT) and classical trajectory Monte Carlo (CTMC) propagation are performed. LR-TDDFT incorporates many-body electron correlations. In addition, simulations based on linear-response DFT (LR-DFT) were also performed, in which correlation effects are omitted in the framework-independent particle dynamics. The experimental data exhibit excellent agreement with LR-TDDFT predictions but significantly deviate from LR-DFT results, suggesting that correlation-driven electron dynamics play a major role in C_{60}s' plasmonic response. Furthermore, the EWS delay, exclusively from the correlated excitation, can be extracted from the difference between the results of LR-TDDFT (correlated) and LR-DFT (non-correlated). We show that it is fully positive as a consequence of the trapping plasmon potential (Fig. 1c).

The findings demonstrate that the giant plasmon resonance in C_{60} cannot be interpreted as a simple sum of independent single-particle excitations. Instead, coherent, large-scale electron correlations play a significant role, shaping the scattering dynamics of the emitted electron.

This work provides the first direct time-domain observation of correlation-driven photoemission delays in a sub-nanometre plasmonic system. Given the broad significance of plasmonics across scientific fields, our study sheds light on the fundamental quantum mechanisms of plasmons under the extreme conditions of subnanometre systems. This insight could be crucial for the future development of quantum plasmonics technologies. While the ultrafast relaxation of ultra-small particles may pose practical challenges for applications like single-photon sources, it can also enhance the efficiency of plasmon-driven electronic processes, including catalytic reactions and controllable nanoscale slow-electron emission [7].

Author contact: Andrea Trabattoni, andrea.trabattoni@desy.de

References

1. A. F. Koenderink et al., nanophotonics: ´Shrinking light-based technology´. Science 348, 516–521 (2015).
2. M. I. Stockmanet et al., ´Roadmap on plasmonics´. J. Opt. 20, 043001 (2018).
3. K. D. Chapkin et al., ´Lifetime dynamics of plasmons in the few-atom limit´. Proc. Natl. Acad. Sci. U.S.A. 115, 9134–9139 (2018).
4. J. A. Scholl et al., ´Quantum plasmon resonances of individual metallic nanoparticles´. Nature 483, 421–427 (2012).
5. A. H. Kelkar et al., ´Angle-differential observation of plasmon electrons in the double-differential cross- section spectra of fast-ion-induced electron ejection from C60´. Phys. Rev. A 92, 052708 (2015).
6. R. Kienberger et al., ´Atomic transient recorder´. Nature 427, 817–821 (2004).
7. M. S. Tame et al., 'Quantum plasmonics', Nat. Phys. 9, 329–340 (2013).

Original publications

Correlation-driven attosecond photoemission delay in the plasmonic excitation of C_{60} fullerene, Science Advances 11, eads0494(2025). DOI:10.1126/sciadv.ads0494

Shubhadeep Biswas, Andrea Trabattoni, Philipp Rupp, Maia Magrakvelidze, Mohamed El-Amine Madjet, Umberto De Giovannini, Mattea C. Castrovilli, Mara Galli, Qingcao Liu, Erik P. Månsson, Johannes Schötz, Vincent Wanie, Pawel Wnuk, Lorenzo Colaizzi, Daniele Mocci, Maurizio Reduzzi, Matteo Lucchini, Mauro Nisoli, Angel Rubio, Himadri S. Chakraborty, Matthias F. Kling and Francesca Calegari

For affiliations, please refer to the original publication.

High-resolution stereo X-ray microscopy

Stereo X-ray ptychography delivers rapid 3D perception on the nanoscale

Understanding the internal structure of materials at the nanoscale is crucial in many fields of science and technology. Hard X-rays have the great advantage of penetrating deeply into matter, revealing fine details of a sample's inner structure. However, extracting 3D information through X-ray tomography requires recording many angular projections which can be very time-consuming. In addition, watching physical or chemical processes often relies on bulky sample environments in which the sample cannot be easily rotated. In these cases an experimental scheme is desired that can extract 3D information from 2D scans only. Inspired by human vision, we developed stereo hard X-ray ptychography.

Human vision perceives depth by collecting two perspectives of the surroundings, captured by our two eyes. Similarly, a stereoscopic X-ray image is created using two nanofocussed X-ray beams that illuminate a sample from two different angles. Combining these two perspectives creates a stereo image pair that can be viewed with special 3D viewers or on screen with 3D glasses, providing a direct impression of depth and shape.

The experiments were carried out at the P06 hard X-ray micro/nanoprobe beamline at PETRA III. The stereo ptychography setup was implemented in the Ptychographic Nano-Analytical Microscope (PtyNAMi) [1], a versatile instrument which can accommodate all the necessary optics. Three horizontally spaced X-ray beams were individually focused using a set of Fresnel zone plates, with the two outer beams additionally being deflected by multilayer mirrors as illustrated in Fig. 1. The sample was placed on a piezo scanner in the intersection of all three beams. The direct beam was primarily used to simplify the alignment procedure while the deflected beams created two perspectives with a stereo angle of 3°.

We demonstrated stereo hard X-ray ptychography using a microchip as a first example. These semiconductor devices are produced in layers using lithography techniques. To visualise the different layers separately, which are typically only a few hundred nanometres apart, the X-ray microscope would require a very small depth of focus. This, however, is difficult to achieve with hard X-rays, where X-ray microscopes with a high spatial resolution in the range of a few 10 nanometres still have a large depth of focus of several ten nanometres. In order to improve the depth perception, we scanned the logic structure of the microchip with all three mutually tilted beams at the same time. Each beam provided a separate ptychographic image from its perspective, and the two outermost perspectives were used to create a 3D image of the chip, shown as an anaglyph in Fig. 2 that can be viewed with 3D glasses. In this way, the microchip can be visually inspected in 3D, revealing the integrated circuit structure in several layers. The overall thickness of this layered structure is less than 4 µm, demonstrating the enhanced depth-sensitivity of the stereo X-ray microscope.

Another sample consisted of mainly two layers separated by less than 500 nm. Here, phase images of the individual layers could be extracted based on the measured stereo projections (see Fig. 3). One layer had the structure of a Fresnel zone plate, while the other one contained gold nanoparticles. This example shows that our new stereo X-ray microscope significantly improves the in-depth resolution by more than one order of magnitude as compared to most current X-ray microscopes based on single-beam optics. We believe that stereo X-ray microscopy will enable researchers to study nano-objects in various scientific fields ranging from electronics to biology in the future.

With the enhanced brightness of current and upcoming synchrotron radiation sources of the fourth generation, such as PETRA IV [2], it will be possible to acquire images significantly faster and with single-digit nanometre spatial resolution. For example, we expect that stereo X-ray ptychography will be able to efficiently provide 3D views of entire microchips. Although X-ray tomography will remain the primary method for fully visualising complex objects in 3D, stereo hard X-ray ptychography can be a fast and efficient alternative for objects made up of distinct, well-separated layers or features. This opens up the possibility of fast 3D imaging of physical and chemical processes at the nanoscale.

Author contact: Sina Röper, sina.roeper@xray-lens.de

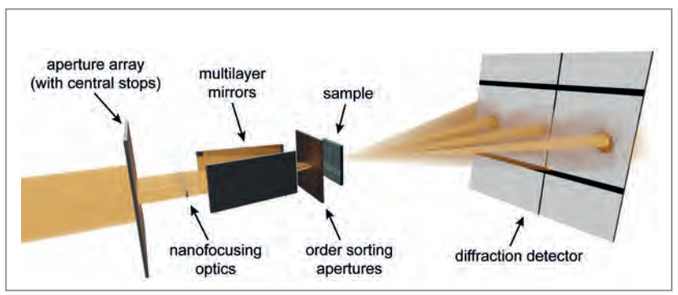

Figure 1
Three X-ray beams scan a sample, here a microchip, simultaneously. The X-ray beams are individually focused by Fresnel zone plates. In addition, the two outer beams get deflected by small multilayer mirrors. An order sorting aperture cleans the different nanofocussed X-ray beams from other focusing orders. The beams intersect in the sample plane and three individual far-field diffraction patterns get recorded by a detector. The two deflected beams provided the perspectives required for stereo X-ray microscopy. (Figure taken from original publication)

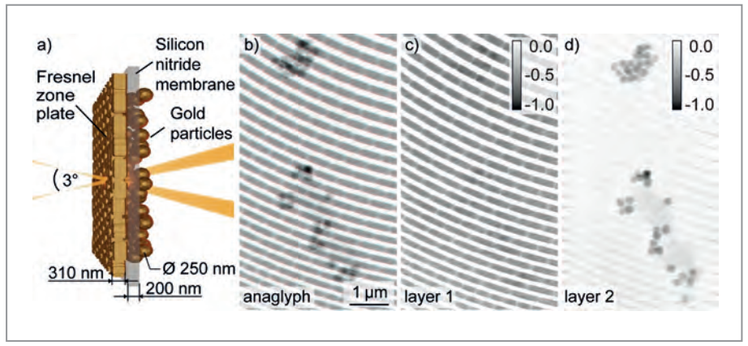

Figure 3
Layer recovery based on a stereo image pair. a) Schematic of the sample: a silicon nitride membrane with a brick-like structure of a Fresnel zone plate on one side and gold nanoparticles on its other side. b) Anaglyph of the two perspectives giving a qualitative depth impression. c) and d) Phase images of the recovered layers. Layer 1 exhibits the structure of the Fresnel zone plate and layer 2 the gold nanoparticles. (Figure adapted from original publication)

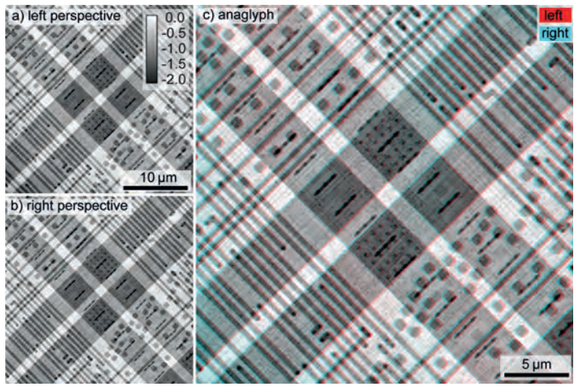

Figure 2
Reconstructions of a microchip scanned with the stereo ptychography setup. Reconstructed ptychograms recorded with the outermost two beams are shown in a) and b). The grey values depict the X-ray phase shift in radian. The two perspectives have a viewing angle of 3°. c) Falsely coloured overlay of both perspectives, a so-called anaglyph. When viewed with 3D glasses, the anaglyph provides a sense of depth of the microchip. (Figure adapted from original publication)

References

1. A. Schropp, R. Döhrmann, S. Botta et al., 'PtyNAMi: ptychographic nano-analytical microscope', J. Appl. Crystallogr. 53(4), 957–971 (2020).
2. C. G. Schroer, H.-C. Wille, O. H. Seeck et al., 'The synchrotron radiation source PETRA III and its future ultra-low-emittance upgrade PETRA IV', Euro. Phys. J. Plus. 137, 1312 (2022).

Original publications

'Stereo hard X-ray ptychography, Optics Express 33, 22755-22768 (2025). DOI: 10.1364/OE.559273

Sina Röper[1,2], Sarah-Alexandra Hussak[1,2], Karolina Stachnik[2], Dorota Koziej[2], Mattias Åstrand[3], Ulrich Vogt[3], Caterina Carus[1,4], Johannes Dora[1,5], Johannes Hagemann[1], Martin Seyrich[1], Christian G. Schroer[1,2,6] and Andreas Schropp[1,6]

1. Centre for X-ray and Nano Science CXNS, Deutsches Elektronen-Synchrotron DESY, Hamburg, Germany
2. Center for Hybrid Nanostructures, Institute for Nanostructure and Solid-State Physics, University of Hamburg, Hamburg, Germany
3. KTH Royal Institute of Technology, Department of Applied Physics, Biomedical and X-ray Physics, Stockholm, Sweden
4. Department Physik, Universität Hamburg, Hamburg, Germany
5. Institute for Biomedical Imaging, University of Technology Hamburg TUHH, Hamburg, Germany
6. Helmholtz Imaging, Deutsches Elektronen-Synchrotron DESY, Hamburg, Germany

Chiral quantum tunnelling under coherent control

Real-time insights from time-resolved pump–probe microwave spectroscopy

Chiral molecules undergoing quantum tunnelling continuously interconvert between their right- and left-handed forms by crossing the potential energy barrier between them, forming a 50:50 quantum racemic mixture. This behaviour reflects the wave–particle duality of matter, and the molecules exist in quantum superpositions arising from the symmetric and antisymmetric combinations of the chiral wavefunctions. As a result, the two-handed forms, called enantiomers, cannot be isolated with conventional chemical methods. In this study, we developed an advanced microwave spectroscopy approach that enables coherent manipulation of the tunnelling process and a time-resolved investigation of coherent tunnelling dynamics via pump–probe measurements.

Chiral molecules are prevalent in nature and everyday life, appearing as two non-superimposable mirror-image forms, termed enantiomers, analogous to left and right hands. Governed by their interconversion double-well potential, they can exist in stationary chiral states (|S⟩ and |R⟩), corresponding to being either of left- or right-hand character, or in quantum superpositions (|±⟩), as shown in Fig. 1a, being left- and right-handed simultaneously. In the latter case, the enantiomers interconvert between the potential wells via quantum tunnelling, forming a racemic mixture in which a single-handedness cannot be isolated with traditional purification methods.

Establishing precise quantum control to switch molecules between their localised chiral states and delocalised tunnelling states has long been a compelling goal in quantum physics. Such control could shed light on many longstanding chirality-related mysteries, such as the well-known Hund's paradox [1] and the origin of chirality in molecular physics and biology. Nevertheless, it remains a formidable challenge, and experimental progress has been limited. In theory, a coherent superposition of the delocalised tunnelling states can drive coherent tunnelling dynamics, causing molecules to relocalise into their chiral forms. These chiral states are inherently non-stationary, forming chiral wave packets that oscillate between the two potential wells at the tunnelling frequency under field-free conditions [2].

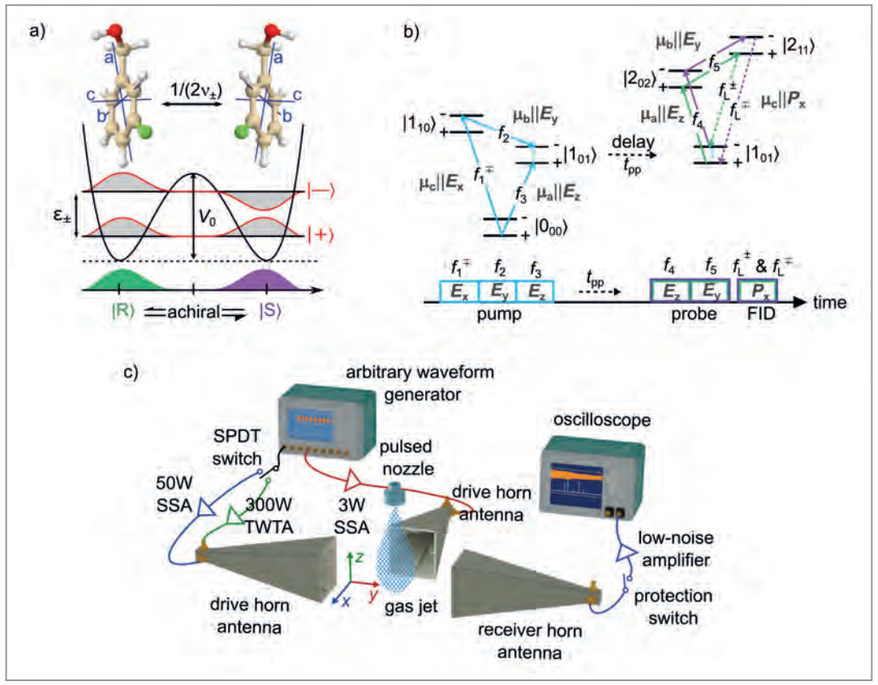

Figure 1

a) Double-well potential governing the chiral tunnelling in 3-fluorobenzyl alcohol. b) Rotational level scheme for the designed pump–probe microwave experiment, with the pulse sequence shown below, indicating the directions of the linearly polarised fields and the corresponding transitions. Transitions with solid arrows are directly driven by microwave fields in the designated polarisation directions, while those shown with dashed arrows represent the induced 'listen' transitions to be measured. c) Schematic of the custom-built Fourier transform microwave spectrometer.
FID: free induction decay;
SPDT: single-pole double-throw;
SSA: solid-state amplifier;
TWTA: traveling-wave tube amplifier.

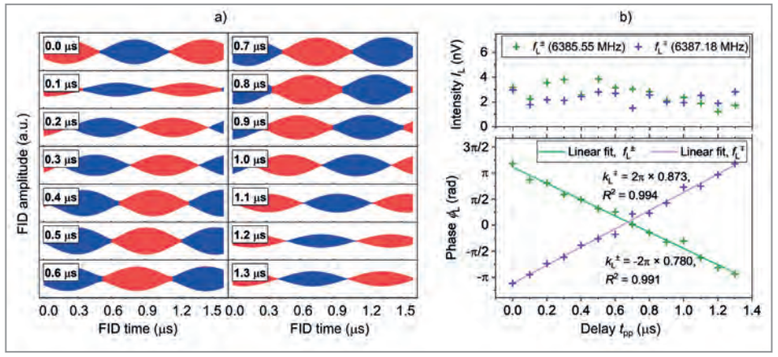

Figure 2

a) Time-domain experimental FID signals, showing frequency beats arising from the listen transitions $f_L^{\pm}$ (6385.55 MHz) and $f_L^{\mp}$ (6387.18 MHz), measured at different pump–probe delay times (t_{pp}). Neighbouring beats are highlighted in red and blue to indicate the sign change of the cosine-shaped beat envelopes. b) Intensities (I_L) and phases (ϕ_L) of the two listen transitions ($f_L^{\pm}$ and $f_L^{\mp}$), as a function of the pump–probe delay (t_{pp}). The scatter points represent experimental data, while the coloured lines show linear fits on the phase results.

Previously, we successfully prepared such chiral wave packets from a quantum racemic mixture of benzyl alcohol, selectively breaking the 50:50 enantiomeric ratio in a chosen rotational state using tailored microwave fields [3]. However, its key feature—the time-dependent dynamics—was not directly observed. In the present study, we developed an advanced pump–probe scheme in the microwave range (Fig. 1b), targeting specific rotational transitions in 3-fluorobenzyl alcohol. A pump cycle (blue) was exploited to generate a chiral wave packet in the rotational state of interest, while a coupled probe cycle captured its temporal evolution by inducing a chiral-sensitive signal at the listen transitions ($f_L^{\pm}$ and $f_L^{\mp}$). More elegantly, the probe cycle is divided into two subcycles, monitoring the chiral wave packet from opposite directions: The green subcycle tracks the rotational transition $|1_{01}^{+}\rangle \rightarrow |1_{01}^{-}\rangle$ while the purple subcycle follows $|1_{01}^{+}\rangle \rightarrow |1_{01}^{-}\rangle$.

The experiments were carried out with a custom-built broadband chirped-pulse Fourier transform microwave spectrometer (Fig. 1c), allowing excitations along mutually orthogonal polarisation directions (E_x, E_y, and E_z), as required for microwave three-wave mixing techniques [4]. By varying the delay between the pump and probe cycles, we successfully observed the time-dependent evolution of the chiral wave packet induced in the $|1_{01}\rangle$ rotational state (Fig. 2a), revealing an oscillation period of about 1.2 μs, consistent with the tunnelling period of 3-fluorobenzyl alcohol. Fast Fourier analysis of the two listen transitions ($f_L^{\pm}$ and $f_L^{\mp}$) in the probing subcycles showed a linear phase evolution with opposite slopes ($k_L^{\pm}$ and $k_L^{\mp}$), confirming the harmonic nature of the tunnelling oscillation from the respective observation directions (Fig. 2b).

Furthermore, we also achieved the phase control over the induced coherence, enabling precise positioning of the induced chiral wavepacket within the double-well potential. Our results provided important experimental evidence supporting the superposition principle in molecular chiral tunnelling, laying a foundation for future research in achieving complete quantum control of chiral tunnelling, resolving Hund's paradox and examining parity-violating effects.

Author contact: Wenhao Sun, wenhao.sun@desy.de
Melanie Schnell, melanie.schnell@desy.de

References

1. F. Hund, 'Zur Deutung der Molekelspektren. III. Bemerkungen über das Schwingungs- und Rotationsspektrum bei Molekeln mit mehr als zwei Kernen', Z. Phys. 43, 805 (1927).
2. C. Fábri, R. Marquardt, A. G. Császár and M. Quack, 'Controlling tunneling in ammonia isotopomers', J. Chem. Phys. 150, 014102 (2019).
3. W. Sun, D. S. Tikhonov, H. Singh, A. L. Steber, C. Pérez and M. Schnell, 'Inducing transient enantiomeric excess in a molecular quantum racemic mixture with microwave fields', Nat. Commun. 14, 934 (2023).
4. D. Patterson, M. Schnell and J. M. Doyle, 'Enantiomer-specific detection of chiral molecules via microwave spectroscopy', Nature 497, 475 (2013).

Original publications

'Direct observation of time-dependent coherent chiral tunneling dynamics', Physical Review Letters 134, 123403 (2025).
DOI: 10.1103/PhysRevLett.134.123403

Wenhao Sun[1], Denis S. Tikhonov[2] and Melanie Schnell[1,3]

1. Deutsches Elektronen-Synchrotron DESY, Hamburg, Germany
2. Center for Free-Electron Laser Science CFEL, DESY, Hamburg, Germany
3. Institute of Physical Chemistry, Christian-Albrechts-Universität zu Kiel, Kiel, Germany

Imaging a catalytic nanoburger at work

Using X-rays to learn how to design catalysts

Catalysts play a key role for the emission control by changing the path of a chemical reaction so that it proceeds faster and at lower temperatures. To design catalysts with high activity, selectivity and a long lifetime, it is crucial to understand the structure-activity relation in more detail. A powerful technique to measure the structure under *operando* conditions is Bragg coherent X-ray diffraction imaging (BCDI) which allows reconstruction the real-space electron density (so the shape) and the strain distribution in three-dimensions (3D) of a single nanoparticle.

We choose to investigate the nanoparticle under CO oxidation conditions because the reaction of CO and O_2 to CO_2 is relatively simple, thus it is a good model to investigate catalysts. Since CO is a toxic gas, this model reaction also has real-world application. For the material of the catalyst we picked alloyed PtRh nanoparticles on a $SrTiO_2$ support. Both Pt and Rh are active for CO oxidation and combining them is increasing their activity [1].

Investigating the pre-selected nanoparticle by BCDI on three different Bragg peaks revealed, to our great surprise, that the nanoparticle was twinned (Fig. 1). This means that the nanoparticle consisted of two parts, the bottom and the top part. The bottom part was rotated by 180° in respect to the top part, with a coherent Σ3 grain boundary. Such grain boundaries parallel to the support have so far only been reported for nanoparticles prepared by dewetting [2] and not for nanoparticles prepared by molecular beam epitaxy which we used for this sample.

Throughout the course of the experiment, after applying multiple cycles of CO and O_2, pure O_2 to oxidise and pure H_2 to reduce the nanoparticle, we observed the formation of two new facets (Fig. 2). These facets are of higher order than the initial {111} and {100} facets. This means that the new facets have more steps and, consequently, a higher number of undercoordinated surface atoms. These are promising adsorption sites for CO and O_2 molecules.

Taking a closer look at the reconstruction of the 111 Bragg peak data shows three dislocations (Fig. 3a), coloured in red, green and purple. A cut perpendicular to one of the dislocation lines and the substrate through the displacement reveals a sign change (Fig. 3b), and plotting the displacement around the dislocation line indicates that the dislocation is an edge dislocation (Fig. 3c). Such dislocations involve a missing plane of atoms, as illustrated in the schematic (Fig. 3d). Since the dislocations have a high strain and lower coordination number, they can serve as preferential adsorption sites.

This study demonstrates that BCDI is a powerful technique to image the shape, strain and the defect state of catalytic nanoparticles under *operando* conditions. The investigated nanoparticle showed several features which are expected to have a positive influence on the catalytic activity. Artificially introducing such features may allow to tune the activity of nanoparticles in industrial catalysts.

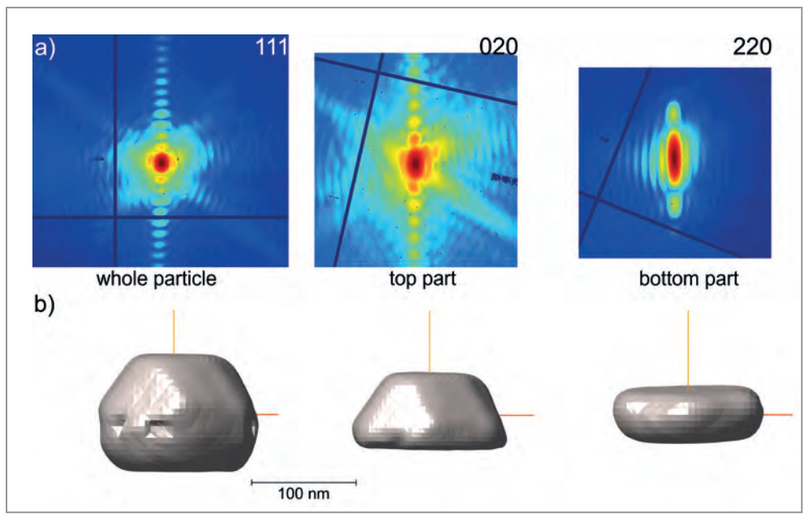

Figure 1

a) Stacked detector images of a BCDI measurement on the 111 Bragg peak, the 020 Bragg peak and 220 Bragg peak in a 180° rotated coordinate system compared to the measured 020 Bragg peak.
b) Reconstructed shape from the datasets shown in a). It is clear that the reconstructed shapes from the 020 and the 220 Bragg peaks only contain parts of the reconstructed shape from the 111 Bragg peak.

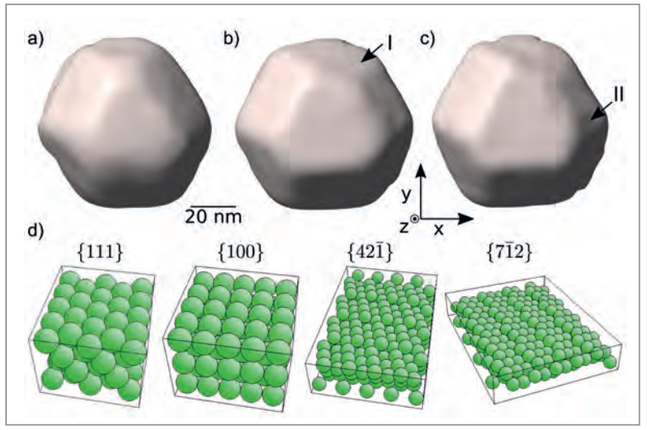

Figure 2

a) – b) Top view of the reconstructed shape of the nanoparticle. A new facet (I) with {42-1} orientation is visible in b) and a second new facet (II) with {7-12} orientation in c). d) Ball models of different surface orientations. As visible, the original {111} and {100} facets have less steps than the new {42-1} and {7-12} facets. Thus, the formation of the new facets is increasing the number of adsorption sites on the nanoparticle.

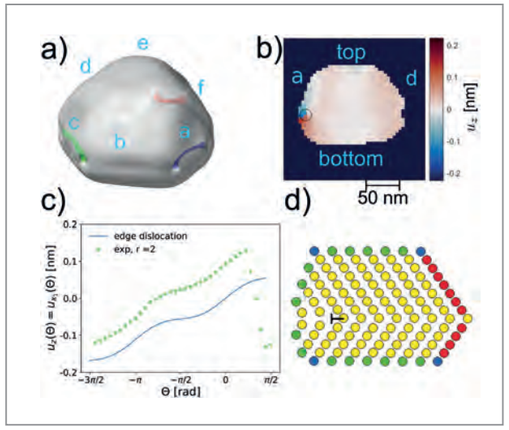

Figure 2

a) Reconstructed shape with coloured dislocations. b) Cut through the displacement, perpendicular to the substrate. c) Plot of the displacement along the circle indicated in b) together with the displacement of an edge dislocation, indicating the dislocation to be an edge dislocation. d) Sketch of such an edge dislocation: On the margin at the left side one part of the plane is missing (marked with T) and the atoms of the neighbouring planes are shifted accordingly.

Author contact:
Lydia J. Bachmann, lydia.bachmann@desy.de
Andreas Stierle, andreas.stierle@desy.de

References

1. J. Y. Park, Y. Zhang, M. Grass, T. Zhang and G.A. Somorjai, 'Tuning of Catalytic CO Oxidation by Changing Composition of Rh-Pt Bimetallic Nanoparticles', Nano Lett. 8, 673–677 (2008).
2. F. Lauraux, S. Labat, S. Yehya, M.I. Richard, S. J. Leake, T. Zhou, J.-S. Micha, O. Robach, O. Kovalenko, E. Rabkin, T. U. Schülli, O. Thomas and T. W. Cornelius, 'Simultaneous Multi-Bragg Peak Coherent X-ray Diffraction Imaging', Crystals 11, 312 (2021).

Original publication

'Coherent X-ray Diffraction Imaging of a Twinned PtRh Catalyst Nanoparticle under Operando Conditions', ACS Nano 19, 23552–23563 (2025). DOI: 10.1021/acsnano.4c15457

Lydia J. Bachmann[1,2], Dmitry Lapkin[3,4], Jan-Christian Schober[1,2], Daniel Silvan Dolling[1,2], Young Yong Kim[3,5], Dameli Assalauova[3,6], Nastasia Mukharamova[3], Jagrati Dwivedi[1], Tobias U. Schülli[7], Thomas F. Keller[1,2], Ivan A. Vartanyants[3], and Andreas Stierle[1,2]

1. Centre for X-ray and Nano Science CXNS, DESY, Hamburg, Germany
2. Department of Physics, University of Hamburg, Hamburg, Germany
3. Deutsches Elektronen-Synchrotron DESY, Hamburg, Germany
4. Present Adress: Insitute of Applied Physics, University of Tübingen, Tübingen, Germany
5. Present address: Pohang Accelerator Laboratory, POSTECH, Pohang, South Korea
6. Present address: Constructor University, Bremen, Germany
7. European Synchrotron Radiation Facility ESRF, Grenoble, France

Watching silver nanoparticles melting, bubbling and exploding

Following superheated particles to exotic regions of silver's phase diagram

Matter under extreme conditions, especially at extreme temperatures and pressures, plays an important role in many fields. These range from astrophysics and geology over inertial fusion reactor studies to applied research on material processing by laser ablation. Due to the complex behaviour of matter under such conditions, the underlying interactions are not yet fully understood. In our study, we applied time-resolved soft X-ray diffraction at FLASH to study the dynamics of superheated silver nanoparticles in a laser pump–FEL probe experiment. The experiments reveal a broad range of different particle responses that can be traced back to the stability limits of a metastable superheated liquid.

The silver nanoparticles were synthesised in a gas-aggregation source tailor-made for the experiment at the CAMP end station at beamline BL1 of FLASH. In the process, silver atoms are sputtered from bulk material into a cooled gas stream at such densities that nanosized solid crystals form.

We used a 400 nm laser which, in these particles, can resonantly excite a strong collective oscillation of the electrons, the plasmon resonance, thereby efficiently transferring energy into the electronic system of the particle. This energy initially leads to a heating just of the electrons, reaching temperatures of up to several 10000 K, before electron–ion interactions transfer it within several picoseconds to the nuclear degrees of freedom. Due to the larger heat capacity of vibrational excitations, this leads to overall temperatures of a few 1000 K, still far beyond the standard melting or boiling point of silver.

With the ultrashort FEL pulses, we took snapshots of the particles as their shape changed due to this strong and very rapid heating. Since these snapshots are produced by recording diffracted X-ray intensity, retrieving real-space images first requires reconstructing the phase of the diffraction amplitudes, as only intensities are measured in the experiment [1].

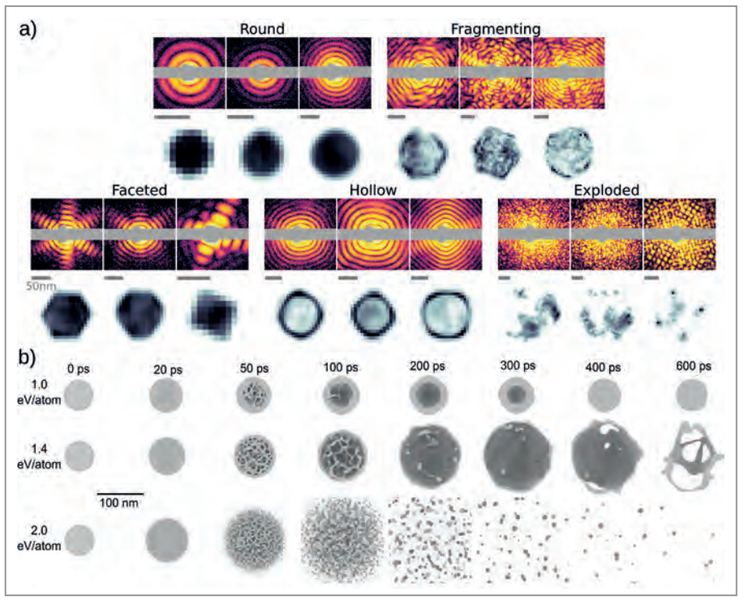

Figure 1

a) Three exemplary experimental diffraction patterns for each particle response (colour scale), along with the corresponding reconstructions in grey scale (object sizes indicated by 50 nm bars). b) Molecular dynamics simulations of strongly heated silver particles with 8 million atoms. The snapshots show sectional views for different times, for three different amounts of deposited energy. (Adapted from original publication Dold et al.)

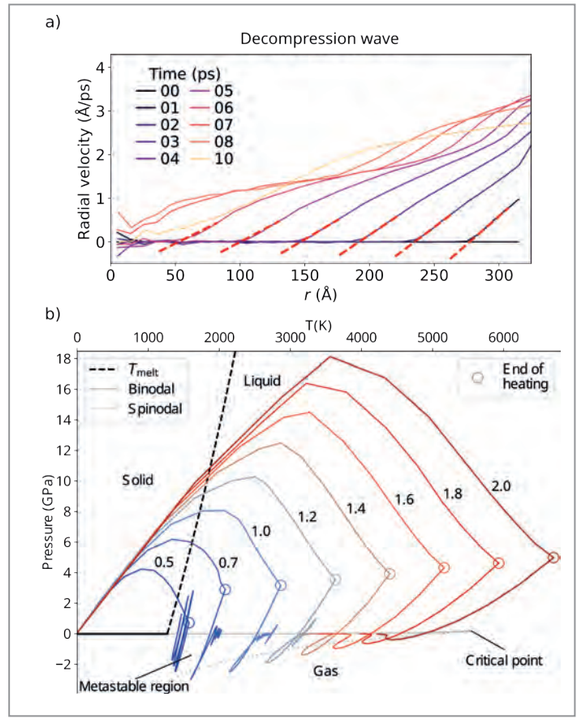

Figure 2

Decompression wave and trajectories in silver's phase diagram obtained from molecular dynamics simulations: a) Radial velocity distributions at different times of a spherical silver particle with 8×10^6 atoms that has been rapidly heated by 1.0 eV/atom. The zero-crossing of the linear fits shown as dashed red lines indicate the position of the boundary between moving and non-moving material layers, i.e. the front of the decompression wave. b) Evolution of the system within the phase diagram of silver; the circles indicate the end of the heating process at 10 ps. The numbers adjacent to trajectories indicate the deposited energy in eV/atom. (Adapted from original publication Dold et al.)

While melting of the particles and, at higher laser powers, disintegration was to be expected, to our surprise we also found droplets that were actually hollow, reminiscent of soap bubbles (Fig. 1). This unexpected result could only be fully understood with the help of atomistic simulations (Fig. 1b): Heating the particle to several thousand kelvins in a few picoseconds leads to almost instantaneous melting; furthermore, thermal expansion, hindered by inertia, causes a build-up of pressure of several gigapascals. Consequently, a rapid expansion sets in which starts at the surface and moves inwards in the form of a decompression front at the speed of sound (Fig. 2a). When it reaches the centre, the initially high positive pressure turns into a strongly negative pressure which renders the superheated liquid metastable.

If the pressure is negative enough, the system in the phase diagram crosses the so-called spinodal, the boundary at which the metastable superheated liquid becomes fully unstable (Fig. 2b), leading to a rapid liquid-gas transition. In this way, soap-bubble-like forms can appear, which, depending on deposited energy collapse again or expand until they rupture. For even higher energies, the full particle becomes unstable and undergoes a so-called phase explosion (Fig. 1b).

This, however, is not yet the full story: Not only does the ultimate fate of the particle depend on the total deposited energy but also on how fast the heat is transferred from the electrons to the atoms. The onset of melting, bubble formation and explosion as well as the expansion speed of the bubbles encode this coupling time. Thus, time-resolved real-space nanoparticle dynamics provide sensitive constraints on electron–phonon (electron–ion) coupling under extreme, non equilibrium conditions. Therefore, our results represent a novel pathway for investigating key coupling parameters of strongly heated metals. Future experiments with (chemically synthesised) particles of reproducible shapes will allow quantitative studies of electron-ion coupling strength for a large parameter space which could well contribute to the understanding of warm dense matter in general [2].

Author contact: Simon Dold, simon.dold@xfel.eu

References

1. A. Colombo et al., 'SPRING, an effective and reliable framework for image reconstruction in single-particle Coherent Diffraction Imaging', npj Comput. Mater. 11, 265 (2025).
2. A. Ng, 'Progress in the study of electron–ion coupling in nonequilibrium Warm Dense Au and Cu', Phys. Rep. 1089, 1-55 (2024).

Original publication

'Melting, Bubblelike Expansion, and Explosion of Superheated Plasmonic Nanoparticles', Physical Review Letters 134, 13610 1 (2025). DOI: 10.1103/PhysRevLett.134.136101

Simon Dold[1,2], Thomas Reichenbach[3], Alessandro Colombo[4*], Jakob Jordan[5], Ingo Barke[6,7], Patrick Behrens[5], Nils Bernhardt[5], Jonathan Correa[8], Stefan Düsterer[8], Benjamin Erk[8], Thomas Fennel[6,7], Linos Hecht4, Andrea Heilrath[5], Robert Irsig[6], Norman Iwe[6], Patrice Kolb[4], Björn Kruse[6], Bruno Langbehn[5], Bastian Manschwetus[8], Philipp Marienhagen[9], Franklin Martinez[4], Karl-Heinz Meiwes-Broer[6,7], Kevin Oldenburg[6,7], Christopher Passow[8], Christian Peltz6, Mario Sauppe[4,5], Fabian Seel[5], Rico Mayro P. Tanyag[5], Rolf Treusch[8], Anatoli Ulmer[5,10], Saida Walz[5], Michael Moseler[1,3], Thomas Möller[5], Daniela Rupp[4,11] and Bernd von Issendorff[1,12]

1. Institute of Physics, University of Freiburg, Freiburg, Germany
2. European XFEL, Schenefeld, Germany
3. Fraunhofer IWM, MikroTribologie Centrum, Freiburg, Germany
4. Laboratory for Solid State Physics, ETH Zurich, Zurich, Switzerland
5. Institut für Optik und Atomare Physik, Technische Universität Berlin, Berlin, Germany
6. Institute of Physics, University of Rostock, Rostock, Germany
7. Department Life, Light and Matter, University of Rostock, Rostock, Germany
8. Deutsches Elektronen-Synchrotron DESY, Hamburg, Germany
9. Institute of Chemistry, University of Rostock, Rostock, Germany
10. Department of Physics, University of Hamburg, Hamburg, Germany
11. Max Born Institute for Nonlinear Optics and Short Pulse Spectroscopy, Berlin, Germany
12. Freiburg Materials Research Center, Universität Freiburg, Freiburg, Germany

Probing metal alloy nanoparticles with CO

New insights into the role of the PdPt alloy nanoparticle catalysts gained with FT-IRRAS and DFT

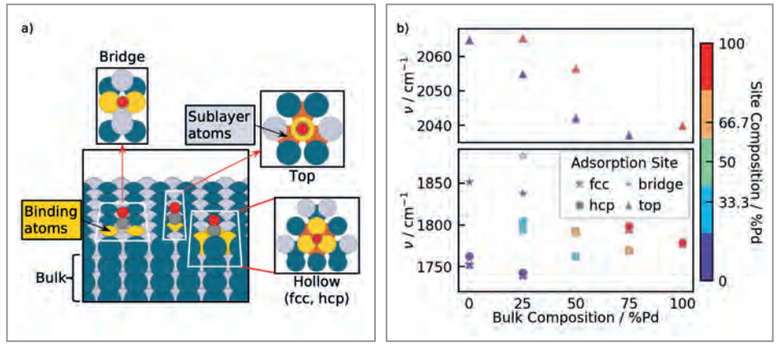

Figure 2

a) Illustration of the CO adsorption sites on the fcc(111) surface based on a bulk alloy with 50% Pd in the Pd/Pt alloy system. The binding atoms at the active site are highlighted in yellow and the subsurface layer is indicated in red. Pd and Pt are shown in blue and light gray, C and O in dark gray and red. b) CO vibrational frequencies adsorbed on different sites on (111) surfaces with varying compositions based on DFT calculations. All surfaces are assumed to have a stoichiometric termination of ordered bulk alloys.

The cleaning of exhaust gases from combustion engines remains one of the most important applications for PdPt catalysts, facilitating the conversion of harmful compounds such as carbon monoxide, hydrocarbons and nitrogen oxides into less harmful substances like carbon dioxide and water. Despite their widespread technological importance, the fundamental mechanisms, particularly the atomic-scale processes enabling the catalytic reaction and the active site of this catalyst remain unknown, especially in the context of alloy nanoparticles. Here, we present an investigation of the PdPt catalyst by adsorbing CO as a test molecule, identifying different adsorption sites for different metal ratios using Fourier transform infrared reflection absorption spectroscopy (FT-IRRAS) and density-functional theory (DFT).

Pd/Pt alloy nanoparticles (NPs) are most prominently used for emission control in applications involving CO and methane oxidation, as well as for catalysts in fuel cells [1,2]. In emission control, Pd/Pt NPs are often supported by porous Al_2O_3 due to its good thermal and mechanical stability and the high surface area [3,4]. The catalytic activity is controlled by the active surface sites of the NPs [5]. Here, we investigated the model system of PdPt alloy NPs on α-Al_2O_3(0001) single crystals by CO adsorption. The adsorption of CO molecules on metal surfaces weakens the bond between carbon and oxygen, resulting in a shift in the vibrational frequency that can be probed by FT-IRRAS [6,7]. The frequency shift reflects the chemical environments at the catalyst surface as well as the adsorption site. CO can adsorb on metal surfaces in different configurations, most of them fall into one of three categories: on-top, bridge or hollow adsorption sites. The vibrational frequency is additionally influenced by the coordination number of the adsorption site, enabling the differentiation of CO on facets and on edge sites [8,9,10].

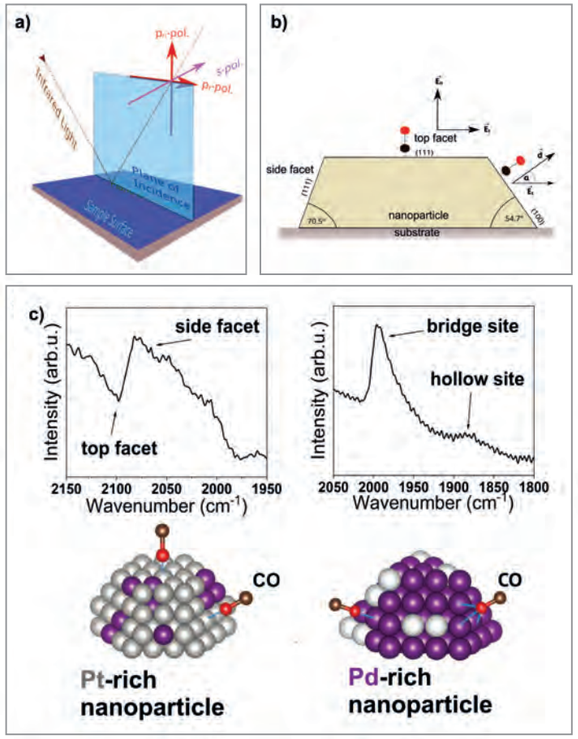

Figure 1

a) Geometry and notation for the polarised infrared beam in the FT-IRRAS experiment. b) Possible adsorption modes and the corresponding parts of the E-field of the infrared light which can excite the vibrational motion. c) Schematic representations of Pd-rich and Pt-rich particles combined with FT-IRRAS spectra corresponding to CO adsorption for such particles at saturation coverage.

Infrared spectroscopy experiments can be performed in s- or p-polarisation to excite only specifically oriented adsorbed species, see Fig. 1 a) and b). In this work, the main interest regarding light polarisation is the possibility to distinguish signals from NP side facets with a dipole moment partially parallel to the substrate surface (p_t- and s-polarisation), from signals from the top facets with a dipole moment normal to the substrate (pn-polarisation), see Fig. 1c).

At DESY NanoLab, the NPs were grown in an ultrahigh-vacuum (UHV) chamber using simultaneous Pt and Pd deposition by e-beam evaporation on α-Al_2O_3(0001) single crystals at a substrate temperature of 400–450 °C. NPs with defined compositions were prepared by adjusting the calibrated fluxes of Pd and Pt individually. The particles are about 20 nm in diameter and have heights between 3 and 9 nm. The coverage is roughly 70% with outliers going up to almost full coverage. It is expected that Pd and Pt are fully mixed in the NPs [11]. Additionally, density-functional theory (DFT) calculations were employed to explore the effect of different atom configurations surrounding the adsorption site, see Fig. 2.

Our main findings are that the adsorption sites of CO vary, depending on the NP alloy composition: On pure Pt NPs, CO exclusively adsorbs in *on-top* configuration on single Pt atoms, whereas it mainly adsorbs on bridge sites and hollow sites between two or three atoms on pure Pd NPs. On alloy NPs both adsorption modes are found simultaneously, highlighting that the surface of alloy NPs is constituted from Pd and Pt atoms. For Pt-rich particles, however, the intensity of the adsorption bands of Pd hollow and bridge sites is significantly lower than for Pd-rich particles. Moreover, adsorption of CO on the top facet was only found to appear on Pt atoms, suggesting that the Pd-containing particles feature smaller top facets. To confirm the IR band assignments, DFT calculations were performed simulating the adsorption of CO on different Pd/Pt alloy compositions, indicating that the broadening of the IR bands arises from the presence of multiple local alloy compositions at the CO adsorption which results in different vibrational wavenumbers for distinct atomic configurations. The results from this study help to better understand the active sites on Pd/Pt alloy catalysts and thus to produce and develop more effective catalysts for heterogeneous catalysis applications in emission control and energy conversion reactions. The use of polarisation-dependent infrared spectroscopy in combination with CO as a probe molecule enabled the identification of the composition-dependent adsorption on *on-top* and side facets of the NPs, highlighting that this method will be beneficial for further studies on alloy NPs under reaction conditions where CO is in feed, intermediate or product.

Author contact: Daniel Silvan Dolling, silvan.dolling@desy.de
Heshmat Noei, heshmat.noei@desy.de

References

1. A. Higareda, G. Rosas and R. Pérez, R. Esparza, 'Characterization and Electro-catalytic Features of PtPd and PdPt Bimetallic Nanoparticles for Methanol Electro–oxidation', ChemNanoMat 7, 958– 965 (2021).
2. Y. Liu, M. Chi, V. Mazumder, K.L. More, S. Soled, J.D. Henao and S. Sun, 'Composition-Controlled Synthesis of Bimetallic PdPt Nanoparticles and Their Electro-oxidation of Methanol', Chem. Mater. 18, 4199–4203 (2011).
3. A. Winkler, D. Ferri and M. Aguirre, 'The influence of chemical and thermal aging on the catalytic activity of a monolithic diesel oxidation catalyst', Appl. Catal., B 93, 177– 184 (2009).
4. A. Russell and W. S. Epling, 'Diesel Oxidation Catalysts', Catal. Rev., 53, 337–423 (2011).
5. F. Schüth, 'Heterogene Katalyse. Schlüsseltechnologie der chemischen Industrie.', Chem. Unserer Zeit, 40, 92–103 (2006).
6. R. G. Greenler and R. K. Brandt, 'The origins of multiple bands in the infrared spectra of carbon monoxide adsorbed on metal surfaces', Colloids Surf. A: Physicochem. Eng. Asp., 105, 19–26 (1995).
7. A. Schlapka, U. Käsberger, D. Menzel and P. Jakob, 'Vibrational spectroscopy of CO used as a local probe to study the surface morphology of Pt on Ru(001) in the submon olayer regime', Surf. Sci., 502–503, 129–135 (2002).
8. N. M. Martin, M. van den Bossche, H. Grönbeck, C. Hakanoglu, F. Zhang, T. Li, J. Gustafson, J. F. Weaver and E. Lundgren, 'CO Adsorption on Clean and Oxidized Pd(111)', J. Phys. Chem. C, 118, 1118–1128 (2014).
9. D. M. Haaland, 'Infrared Studies of CO Adsorbed on Pt/Al_2O_3: Evidence for CO Bonded in 3-fold Coordination', Surf. Sci., 185, 1–14 (1987).
10. H. J. Krebs and H. Lüth, 'Evidence for two different adsorption sites of CO on Pt(111) from infrared reflection spectroscopy', Appl. Phys. 14, 337– 342 (1977).
11. Z. W. Lu, B. M. Klein and A. Zunger, 'Ordering Tendencies in Pd-Pt, Rh-Pt and Ag-Au Alloys', J. Phase Equilib., 16, 36–45 (1995).

Original publication

'Probing Active Sites on Pd/Pt Alloy Nanoparticles by CO Adsorption ', ACS Nano 18, 45, 31098–31108 (2024).
DOI: 10.1021/acsnano.4c08291

Daniel Silvan Dolling[1,2], Jiachen Chen[3], Jan-Christian Schober[1,2], Marcus Creutzburg[1], Arno Jeromin[1], Vedran Vonk[1], Dmitry I. Sharapa[3], Thomas F. Keller[1,2], Philipp N. Plessow[3], Heshmat Noei[1] and Andreas Stierle[1,2]

1. Centre for X-ray and Nano Science CXNS, DESY, Hamburg, Germany
2. Fachbereich Physik, Universität Hamburg, Hamburg, Germany
3. Institute of Catalysis Research and Technology (IKFT), Karlsruhe Institute of Technology (KIT), Eggenstein-Leopoldshafen, Germany

X-ray parametric down-conversion reveals an EUV-polariton

How the search for nonlinear X-ray diffraction opened a path to access the strong-coupling regime at short wavelengths

Polaritons—hybrid states of light and matter—arise when photons couple strongly to material excitations. In doing so, they can substantially modify properties such as conductivity, magnetism and even the chemical reactivity of matter for which they are extensively studied at visible and infrared wavelengths. In contrast, polaritonic phenomena in the extreme ultraviolet (EUV) and X-ray regimes have remained largely unexplored. We showed how to detect the characteristic conversion cone of X-ray parametric down-conversion (XPDC) for the first time and demonstrated how to excite and probe EUV-polaritons using the nonlinear diffraction process of XPDC.

Parametric down-conversion (PDC) in the X-ray regime has been the subject of several challenging experiments in the past [1]. One of the major obstacles is its extremely low conversion rate, preventing the detection of the full cha-racteristic conversion cone at X-ray wavelengths. In contrast, such conversion cones have long been well-established for PDC in the optical regime [2].

At its core, XPDC can be described as a nonlinear diffraction process in which a high-energy 'pump' photon is diffracted off a crystal and thereby splits into a correlated photon pair—commonly referred to as the 'signal' and 'idler' photons. The process will occur only if its phase-matching condition is satisfied. For X-rays, this involves a reciprocal lattice vector of the crystalline sample which governs the direction of the nonlinear diffraction (Fig. 1a). As illustrated, the down-converted photons are constrained up to a rotational degree of freedom, resulting in the emission of a signal cone. In order to resolve this weak XPDC signature, we use a spherically-bent crystal analyser to filter the cone against much stronger linear background scattering (Fig. 1b). Then, the reflected cone is imaged onto a 2D pixel detector, capturing a momentum-resolved map of the pattern before it is refocused. We demonstrated the viability of this scheme on a diamond sample at the ESRF, using a monochromatised 9.79 keV pump beam. Measuring this way, we could resolve the cone of non-degenerate XPDC for the first time and directly scan for several phase-matching conditions, showing their precise alignment with theoretical predictions (Fig. 1d).

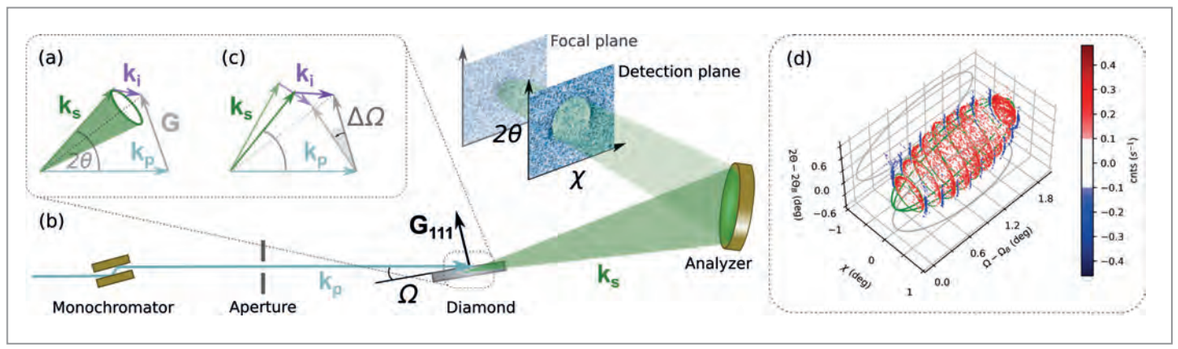

Figure 1

Schematics of XPDC and its detection: a) The phase-matching condition in diffraction geometry (k_p: pump, k_s: signal and k_i: idler) using the reciprocal lattice vector G; green shade indicates the rotationally symmetric emission cone of signal photons. b) Experimental setup. c) A range of phase-matching conditions is accessible by the sample angle ΔΩ, resulting in cones of different radii. d) Measurements of the circular XPDC pattern for eight phase-matching positions; green wire-frame indicates the theoretical prediction.

Looking closer at the measured XPDC patterns, however, revealed a surprise: There is a distinct two-fold modulation visible where a positive circular pattern on the inside is surrounded by a negative feature of count rates falling below the average background level (Fig. 2a). This observation contrasts sharply with the uniformly positive signal cones that are known from down-conversion in the optical regime and demands a new interpretation.

To explain this phenomenon, we introduced a polaritonic model of XPDC, identifying the two-fold pattern with two distinct dispersion branches of an EUV-polariton. Theoretically, we formalise this interpretation, using a minimal two-level system (TLS) model, the Hopfield coefficients [3] of which we embed into the dynamic structure factor for inelastic X-ray scattering. This simple model reproduces the measured features extremely well, as exemplified in Fig. 2b, and allows us to trace the position of the two-fold modulation directly to the avoided crossing of the underlying dispersion branches (Fig. 2d).

Moreover, we used the model to fit a momentum line-out (Fig. 2c) in an effort to quantify the light–matter coupling strength of the new EUV-polariton. This yielded a coupling of V ≈ 0.82±0.08 eV or a Rabi splitting 2V ≈ 1.64 eV which is comparable to the overall width $\hbar\Gamma \approx 1.64\pm0.22$ eV of the polaritonic excitation. Both, the closely approaching 2V ~ $\hbar\Gamma$ and the direct visibility of the avoided crossing (Fig. 2d) indicate the onset of strong coupling. Remarkably for this EUV scenario, it is observable without any enhancing cavity but just by using XPDC to launch and detect the polariton.

By extending strong-coupling physics into the EUV regime, our new finding of an EUV-polariton offers enticing prospects for future research, both on fundamental aspects of strong light–matter interaction and on practical applications of the EUV-polariton as a probe. In a visionary sense, the combination of XPDC and thus X-ray quantum optics with polaritonic hybridisation raises the potential to create non-classical states of light–matter entanglement and calls for further exploration of the EUV-polariton.

Author contact: Dietrich Krebs, dietrich.krebs@desy.de
Christina Bömer, christina.boemer@desy.de

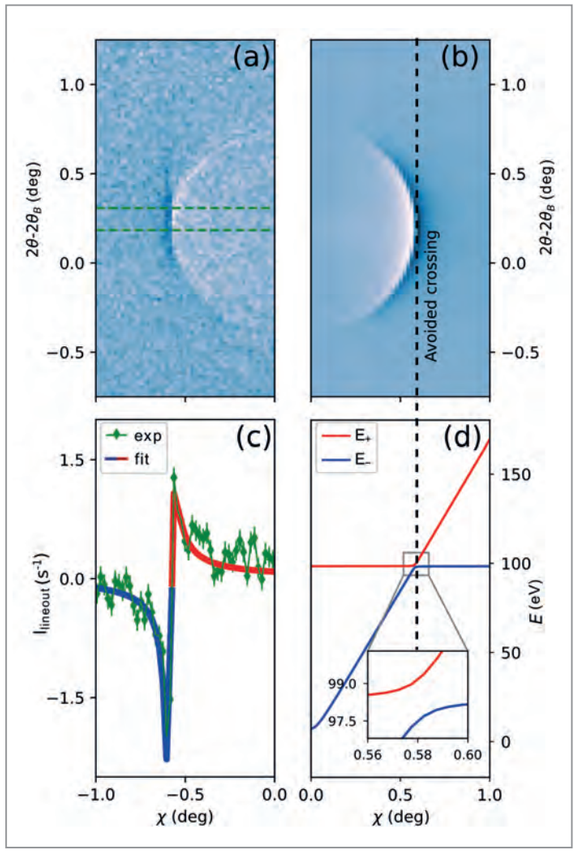

Figure 2

Polaritonic imprints revealed in XPDC cone: Comparison of a) experimental and b) simulated scattering patterns. c) Horizontal line-out of the XPDC cone (green diamonds) fitted with the TLS-model to extract the coupling strength V (red/blue line). d) Simulated polaritonic dispersion, indicating the upper (red) and lower (blue) polariton branches. Inset highlights the Rabi-splitting of 2V = 1.64 eV.

References

1. **B. Adams, P. Fernandez, W.-K. Lee, G. Materlik, D. M. Mills and D. V. Novikov, 'Parametric down conversion of X-ray photons', J. Synchrotron Radiat. 7, 81–88 (2000).**
2. **P. G. Kwiat, K. Mattle, H. Weinfurter, A. Zeilinger, A. V. Sergienko and Y. Shih, 'New high-intensity source of polarization-entangled photon pairs', Phys. Rev. Lett. 75, 4337–4341 (1995).**
3. **J. J. Hopfield, 'Theory of the contribution of excitons to the complex dielectric constant of crystals', Phys. Rev. 112, 1555–1567 (1958).**

Original publication

'X-ray parametric down-conversion reveals EUV-polariton', Nature Communications 16, 5383 (2025). DOI: 10.1038/s41467-025-60845-8

Dietrich Krebs[1,2,4], Fridtjof Kerker[2,4], Xenia Brockmüller[4], Christoph J. Sahle[5], Blanka Detlefs[5], Simo Huotari[6], Nina Rohringer[1,2,4] and Christina Bömer[1,2]

1. Deutsches Elektronen-Synchrotron DESY, Hamburg, Germany
2. The Hamburg Centre for Ultrafast Imaging CUI, Hamburg, Germany
3. Center for Free-Electron Laser Science CFEL, DESY, Hamburg, Germany
4. Department of Physics, University of Hamburg, Hamburg, Germany
5. ESRF, The European Synchrotron, Grenoble, France
6. Department of Physics, University of Helsinki, Helsinki, Finland

Breathing nanopores: deformation dynamics during water imbibition

How nanoscale capillarity and surface stress turn porous glass into an artificial tree

In plants, water rises through narrow channels against gravity, powered only by capillary forces. Nanoporous materials behave in much the same way but with capillary pressures a thousand times higher due to their tiny pore sizes. As these pores fill, the solid matrix deforms—a process that remains largely unexplored. Understanding this behaviour is relevant not only to natural systems but also to everyday technologies, from absorbent materials to simple passive microfluidic devices such as paper-based test strips where capillary forces alone move and sustain the flow of liquid.

We studied the coupled dynamics of water imbibition and mechanical deformation in a model nanoporous solid—commercial Vycor glass, a silica-based network with nanometre-wide pores. Optical imaging, gravimetry and dilatometry tracked how the porous monolith expands as water climbs through its pores.

As water entered the pores, we measured the square-root-of-time expansion of the entire monolith. When the imbibition front reached the top surface, the release of capillary tension caused a sudden extra length increase—the "Laplace expansion jump". This jump vanished when evaporation stopped the front from progressing, demonstrating that the macroscopic deformation directly reflects the nanoscale filling dynamics [1].

Two opposing nanoscale forces govern this deformation [2]:

- Laplace pressure, pulling the solid inward due to curved menisci and
- Surface-stress release (Bangham effect), expanding it as the pore walls become wetted.

Figure 1

Artificial tree analogy. Artistic rendering illustrating capillarity-driven water flow and deformation in nanoporous solids as a biomimetic counterpart to transpiration in plants. (Credit: M. Künsting TUHH/DESY)

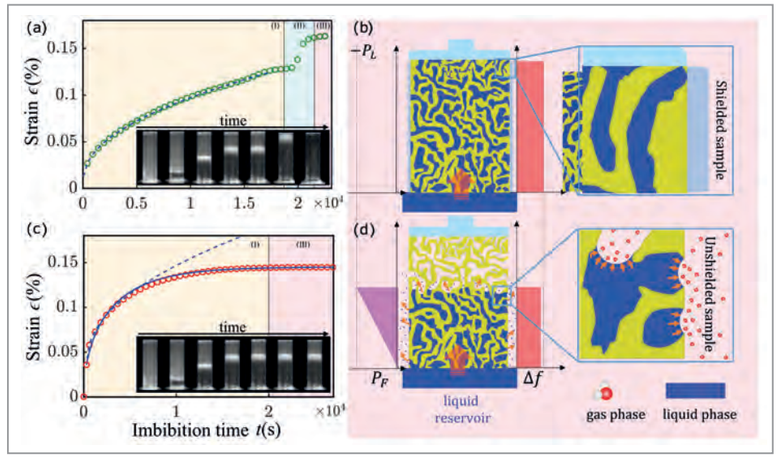

Figure 2

In situ dilatometry and optical imaging reveal how water infiltration expands a nanoporous Vycor glass monolith. When the sample is sealed (a–b), water rises freely through the pores and deformation follows a smooth square-root-of-time law. When evaporation is allowed (c–d), a dynamic balance forms between liquid uptake and evaporation, stabilising curved menisci at the advancing front. The contrast between both cases highlights how capillary flow and evaporation jointly control the mechanical "breathing" of nanoporous solids.

Figure 3

Molecular dynamics simulations show how water rising through a silica nanopore deforms the solid matrix. Snapshots illustrate the advancing meniscus over time while the imbibition length follows a square-root-of-time law. The pore walls expand laterally and longitudinally as surface stresses are released during wetting.

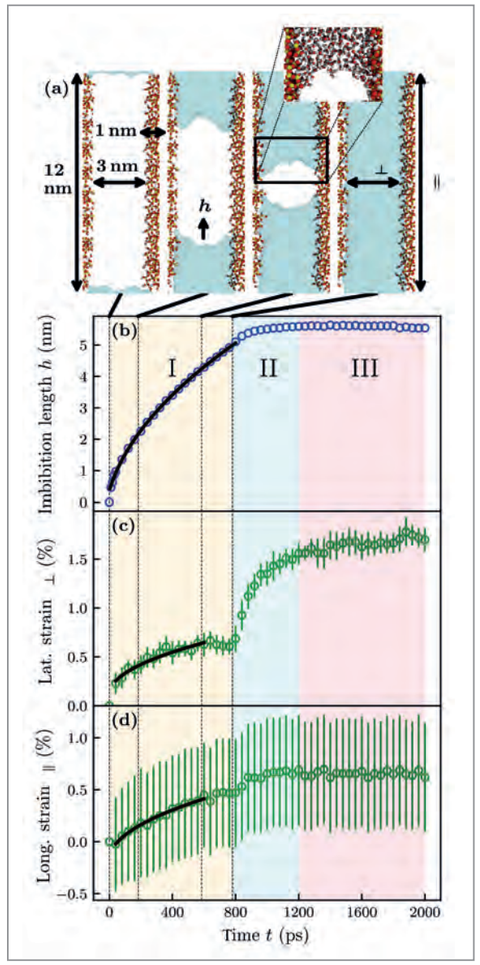

The net expansion arises because surface-stress release dominates Laplace contraction. Our quantitative model links these effects to the imbibition height and reproduces the measured strain evolution with remarkable accuracy (Fig. 2) [3].

Molecular dynamics simulations of water imbibition in single silica nanopores reveal the same three regimes—gradual expansion, abrupt jump and final plateau—at the nanoscale (Fig. 3). As menisci, the curved water–air interfaces, advance and vanish, the release of negative Laplace pressure leads to net expansion of the pore walls.

The physical picture that emerges is both simple and universal: Capillary flow creates a Laplace-pressure gradient that contracts the matrix, while wetting releases surface stress that expands it. Once the front reaches the surface, the Laplace contribution disappears and the matrix relaxes into its expanded state.

This elastocapillary coupling offers a quantitative handle on nanoscale forces. Measuring only a sample's length change can reveal surface stresses, Laplace pressures and transport parameters of confined liquids. The concept extends to liquid-infused materials such as responsive membranes, porous sensors and adaptive nanocomposites.

The analogy to natural transpiration is compelling: Just as water rises through xylem channels in plants, where evaporation and capillary tension drive flow, our experiments reproduce this phenomenon in a controlled, synthetic analogue — an "artificial tree" (Fig. 1). Such bioinspired materials could inform self-regulating structures capable of sensing, pumping or cooling without external power.

Understanding nanopore deformation opens new routes to couple mechanics and transport at the smallest scales. It bridges classical capillarity and nanomechanics, offering pathways to engineer materials that respond to their fluid environment much like living systems do — by *breathing with the flow*. The nanoporous glass–water system exemplifies a "Blue Material" within the Cluster of Excellence BlueMat in Hamburg: Water-Driven Materials—a new class of sustainable, interactive systems whose remarkable functionality emerges from their intimate interplay with water, harnessing its unique properties as a nanoscale working fluid.

Author contact: Patrick Huber, patrick.huber@tuhh.de

References

1. S. Gruener, T. Hofmann, D. Wallacher, A. V. Kityk and P. Huber, 'Capillary rise of water in hydrophilic nanopores', Phys. Rev. E 79, 067301 (2009).
2. G. Y. Gor, P. Huber and N. Bernstein, 'Adsorption-induced deformation of nanoporous materials—A review', Appl. Phys. Rev. 4, 011303 (2017).
3. J. Sanchez, L. Dammann, L. Gallardo, Z. Li, M. Fröba, R. H. Meißner, H. A. Stone and P. Huber, 'Deformation dynamics of nanopores upon water imbibition', PNAS 121, e2318386121 (2024).

Original publication

'Deformation dynamics of nanopores upon water imbibition', PNAS 121, e2318386121 (2024). DOI: 10.1073/pnas.2318386121

Juan Sanchez[1], Lars Dammann[1,2,3], Laura Gallardo[1,4], Zhuoqing Li[1,2], Michael Fröba[5], Robert H. Meißner[3,6], Howard A. Stone[7] and Patrick Huber[1,2]

1. Institute for Materials and X-ray Physics, Hamburg University of Technology, Hamburg, Germany
2. Centre for X-ray and Nano Science CXNS, DESY, Hamburg, Germany
3. Institute of Soft Matter Modeling, Hamburg University of Technology, Hamburg, Germany
4. Centre for the Study of Manuscript Cultures, University of Hamburg, Hamburg, Germany
5. Institute of Inorganic and Applied Chemistry, University of Hamburg, Hamburg, Germany
6. Institute of Surface Science, Helmholtz-Zentrum Hereon, Hamburg, Germany
7. Department of Mechanical and Aerospace Engineering, Princeton University, Princeton, USA

A cryogenic alloy with record-high strength-toughness

Staying strong when it gets cold

High strength and large tensile ductility (indicating high materials toughness, i.e. the area under the stress-strain curve) are critical prerequisites for the engineering applications of metallic structural materials, especially for those used in low-temperature environments. The strength-ductility-toughness synergy of materials is particularly important to avoid immature fracture, particularly low-temperature brittleness. This typically requires alloys not only to possess high yield strength (YS, σ_y > 1.0 GPa) but also to have a high work hardening rate (WHR, Θ) to achieve a large uniform elongation (UE, εu > 15%) and high ultimate tensile strength (UTS, σ_{UTS} > 2.0 GPa).

Currently, widely used low-temperature alloys, such as 316L stainless steel, fail to meet these requirements due to their low volume fractions of strengthening phases and low-temperature brittleness which drastically reduces the plasticity and toughness of the alloy temperatures [1,2]. Specifically, an effective route to improving the low-temperature performance of alloys, compared to traditional low-temperature steels, is the design of complex concentrated alloys, involving multiple principal elements to form iron-rich FCC complex concentrated alloys. While single-phase FCC complex concentrated alloys exhibit high plasticity/toughness, their strength is generally low. In particular, FCC complex alloys with a transformation-induced plasticity (TRIP) effect suffer from very low yield strength which makes their toughness inadequate for many applications.

To address these challenges, we were inspired by the microstructure of iron-based and nickel-based high-temperature alloys superalloys [3,4]. We proposed the use of high-volume fraction, coherently bonded $L1_2$ nano-precipitates to strengthen FCC iron-rich complex concentrated alloy (CCA) matrices (Fig. 1). To achieve low-temperature high strength with large ductility/toughness, the design concept of this alloy was to construct an ultra-high density of dual-function, coherently bonded $L1_2$ nano-precipitates within the FCC matrix. On the one hand, the $L1_2$ phase acts as a dislocation barrier, significantly enhancing yield stress. On the other hand, under sufficiently high stress, the $L1_2$ phase acts as a dislocation source, providing abundant partial dislocations to achieve high-work hardening performance, thus enabling large uniform elongation.

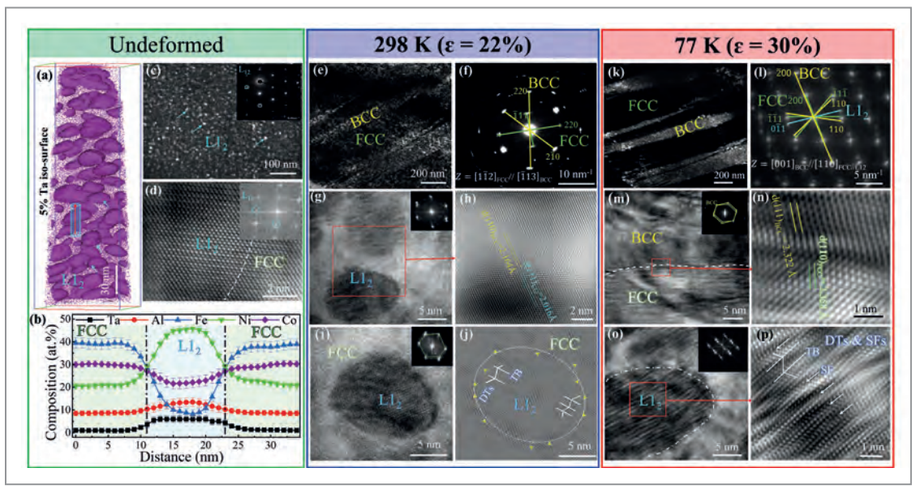

Figure 1
Microstructure of $Fe_{35}Co_{29}Ni_{24}Al_{10}Ta_2$ cryogenic alloy in the initial state, room-temperature deformation and low-temperature deformation.

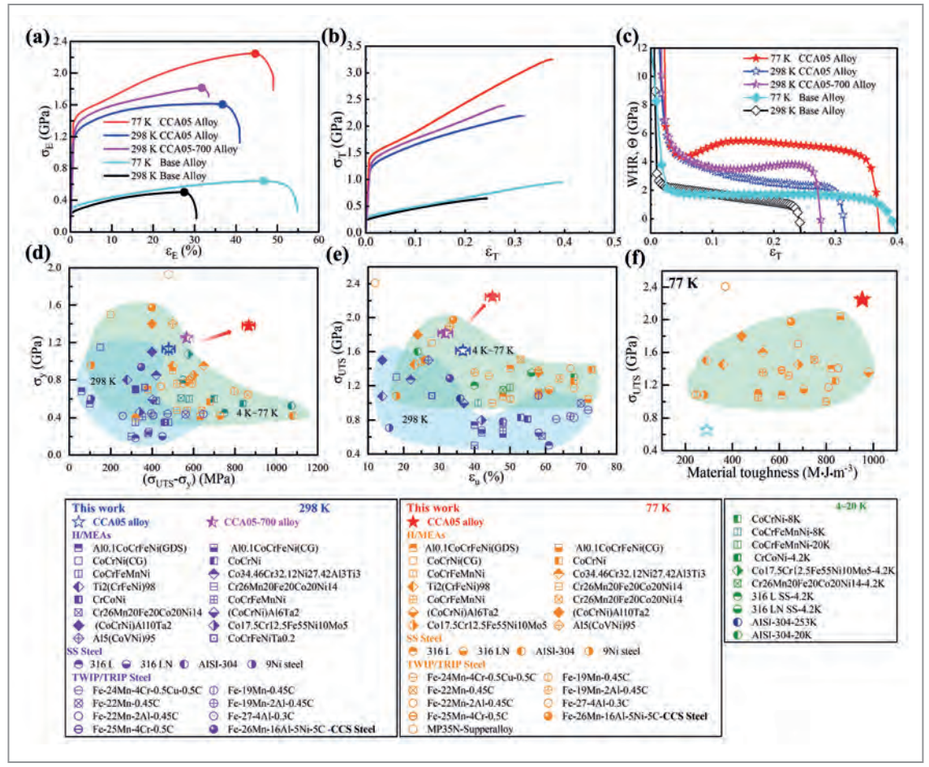

Figure 2
Performance comparison between the designed $Fe_{35}Co_{29}Ni_{24}Al_{10}Ta_2$ cryogenic alloy and currently reported high-performance alloys at room temperature/low temperature.

Particularly, the ultra-high density of $L1_2$ nanophases significantly increased the alloy's flow stress during twinning deformation, making the FCC matrix transform into a BCC phase during low-temperature (77 K) tensile tests (Fig. 1). This TRIP effect further enhanced the alloy's work hardening rate (WHR > 4 GPa). Due to the similar mobility of screw and edge dislocations in the BCC phase generated by the complex concentrated alloy phase transformation, low-temperature brittleness induced by the FCC-BCC transformation is avoided (Fig. 2). This is distinctly different from the low-temperature brittleness induced by the FCC-BCT phase transformation in conventional high-carbon martensitic alloys. Based on this strategy, the team used machine learning assisted by domain knowledge to design an alloy, resulting in the $L1_2$ precipitate-strengthened $Fe_{35}Co_{29}Ni_{24}Al_{10}Ta_2$ complex concentrated alloy.

The $L1_2$ phase in this alloy has a size of approximately 10 nm and a volume fraction of approximately 65 ± 3 vol.%, achieving unprecedented performance combinations at liquid nitrogen temperatures: YS ≈ 1.4 GPa, UTS ≈ 2.25 GPa, UE ≈ 45%, and WHR > 4 GPa (Fig. 1). The static toughness of this complex concentrated alloy is higher than all known low-temperature alloys and is expected to be applied in low-temperature fields. The alloy design strategy proposed by the team also provides new ideas for the design of other high-performance alloys.

Author contact: Yasir Sohail, yasirsohail@xjtu.edu.cn
Jinyu Zhang, jinyuzhang1002@xjtu.edu.cn

References

1. Y. Lu, Y.-H. Zhang, E. Ma and W.-Z. Han, 'Relative mobility of screw versus edge dislocations controls the ductile-to-brittle transition in metals', Proc. Natl. Acad. Sci. 118, e2110596118 (2021).
2. M. Tanaka, E. Tarleton and S. G. Roberts, 'The brittle–ductile transition in single-crystal iron', Acta Mater. 56, 5123-5129 (2008).
3. B. Geddes, H. Leon and X. Huang, 'Superalloys: alloying and performance', ASM International, (2010).
4. X. Wu et al., 'Unveiling the Re effect in Ni-based single crystal superalloys', Nat. Commun. 11, 389 (2020).

Original publication

'A complex concentrated alloy with record-high tensile strength and toughness at 77 K', Advanced Materials, 2410923 (2024).
DOI: 10.1002/adma.202410923

Yasir Sohail[1], Chongle Zhang[1], Jinyu Zhang[1], Shaohua Gao[1], Wenli Song[2,3], Bo Wang[1], Li Xuanzhe[1], Suzhi Li[1], Dezhen Xue[1], Gang Liu[1], Emad Maawad[4], Weimin Gan[5], Evan Ma[1] and Jun Sun[1]

1. State Key Laboratory for Mechanical Behavior of Materials, Xi'an Jiaotong University, Xi'an, 710049, China
2. Institute of High Energy Physics, Chinese Academy of Sciences (CAS), Beijing, China
3. Spallation Neutron Source Science Center, Dongguan, China
4. GEMS at Heinz Maier-Leibnitz Zentrum (MLZ), Helmholtz-Zentrum Hereon, Garching, Germany
5. Institute of Materials Research, Helmholtz-Zentrum Hereon, Geesthacht, Germany

Blink and you miss it: cubic on the outside, chaotic within

Dynamic nanodomains in lead halide perovskites

Halide perovskites are unusual semiconductors: They can be easily assembled via low-temperature solution processing, yet possess exceptional optoelectronic properties that make them ideal for high-performance photovoltaics, light-emitting diodes (LEDs) and X-ray detectors. While most semiconductors lose carriers to traps, perovskites are defect-tolerant and keep charges mobile. Their lattice is highly dynamic: Organic cations reorient, ions hop, lone-pair electrons and carriers couple to the lattice, forming polarons. Soft, anharmonic low-frequency modes transiently break average cubic symmetry and create nanoscale tetragonal domains that flicker on ultrafast timescales.

Lead halide perovskites (LHP) deliver striking optoelectronic performance; yet the microscopic origin of that performance has remained unclear. Our study reveals that even when crystallography reports a cubic average phase, the lattice hosts dynamic, low-symmetry tilt nanodomains (Fig. 1) whose character is set by the respective organic A-site cation. By combining single crystal X-ray diffuse scattering with inelastic neutron spectroscopy, hyperspectral photoluminescence microscopy and machine-learning assisted molecular dynamics (MD), we connect those hidden structures to strikingly different macroscopic behaviour in the two LHPs methylammonium and formamidinium lead bromide ($MAPbBr_3$ and $FAPbBr_3$).

Single-crystal X-ray diffraction measurements were performed at the PETRA III beamline P21.1 which is optimised for diffuse scattering studies. Figure 2 presents slices of the X-ray scattering function, S(q), at L = 1.5 for $MAPbBr_3$ and $FAPbBr_3$, alongside molecular dynamics (MD) simulations carried out in collaboration with the Aron Walsh group at Imperial College London. The simulated S(q) shows remarkable agreement with the experimental data (Fig. 2 a,c). Single-crystal X-ray diffraction captures both, elastically and inelastically scattered X-rays, and thus does not directly provide information about the real-space structural dynamics inferred from S(q). To isolate the quasi-elastic diffuse scattering (QEDS) contribution, we subtracted intensities originating from higher energy phonons, as shown in the left panels of Fig. 2 b,c. When extracting only the low-energy component of the MD-simulated S(q,E), the resulting S(q) closely reproduces the QEDS signal observed experimentally. These combined results reveal that the local structure comprises low-symmetry tetragonal nanodomains with lifetimes on the picosecond timescale.

The QEDS patterns of $MAPbBr_3$ and $FAPbBr_3$ exhibit distinct characteristics. In $MAPbBr_3$, rod-like 3D QEDS in reciprocal space (Fig. 3 a) indicates planar (anisotropic) local nanodomains in real space with out-of-phase tilted octahedra akin to the tetragonal *I4/mcm* symmetry (Fig. 3 b). By contrast, $FAPbBr_3$ exhibits ellipsoidal QEDS (Fig. 3 d), reflecting a more isotropic local structure in real space, with spherical nanodomains having in-phase tilted octahedra akin to the *P4/mbm* symmetry where $\xi_{\parallel} \approx 21$ Å and $\xi_{\perp} \approx 14$ Å (Fig. 3 e).

The contrasting nanodomain morphologies can be understood to originate from the difference in dynamic hydrogen bonds. The directionality of hydrogen bonds can be inferred from MD trajectories by computing spatially and temporally averaged probabilities of the electric polarisation vector orientation in the MA and FA molecules (Fig. 3 c,f, respectively). In FA, the vector shows strong preferential orientations whereas MA vectors adopt a broader range of orientations. These findings suggest that the isotropic (spherical) dynamic nanodomains in $FAPbBr_3$ arise from the robust and highly directional coupling of FA to the inorganic cage, facilitating extended out-of-plane correlation lengths.

First-principles calculations on MD snapshots show that within a nanodomain the electron and hole wavefunctions are locally depleted which raises the local bandgap and creates transient barriers to carrier motion. Barrier heights depend strongly on domain shape, being larger for the anisotropic planar domains of $MAPbBr_3$ and smaller for the more spherical domains of $FAPbBr_3$.

We performed hyperspectral photoluminescence measurements on single crystals to probe the connection between macroscopic optoelectronic properties and the dynamic nanodomains observed in these materials. $FAPbBr_3$ exhibits higher photoluminescence quantum efficiency, larger diffusion coefficients and lower Urbach energies and linewidths than $MAPbBr_3$, as its sparser and more isotropic nanodomains perturb the band edges less, thereby reducing dynamic electronic disorder. Together, these findings reveal how anharmonic local structure governs bulk optoelectronic response and point to routes for improved perovskite photovoltaics, light-emitting diodes, X-ray detectors and quantum light sources through A-site engineering.

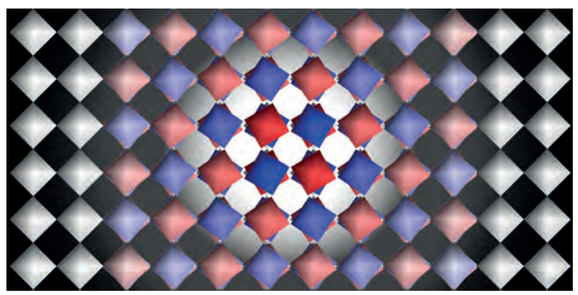

Figure 1
Visualisation of a low-symmetry tetragonal nanodomain embedded in a high-symmetry (cubic) perovskite lattice. Octahedra are coloured by the tilt angle, defined relative to the rotation axis out of the image plane; blue indicating positive, red negative and white zero tilt. The white background denotes the in-plane correlation length of the nanodomain.

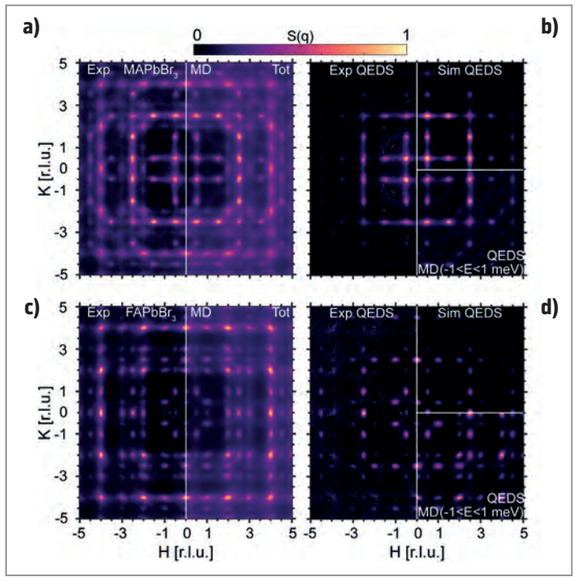

Figure 2
X-ray scattering function S(q) at the (H, K, L = 1.5) reciprocal space plane in the average cubic $Pm\bar{3}m$ phase of $MAPbBr_3$ and $FAPbBr_3$. Experimental (300 K), MD simulated patterns in a) $MAPbBr_3$ and c) $FAPbBr_3$. The figures b) for $MAPbBr_3$ and d) for $FAPbBr_3$ are divided into three quadrants: left) experimentally derived QEDS; top right) simulated QEDS obtained by fitting the experimentally derived QEDS data to a phenomenological model; bottom right) MD-simulated S(q, E) integrated over the QEDS energy window, that is, −1 meV < E < 1 meV.

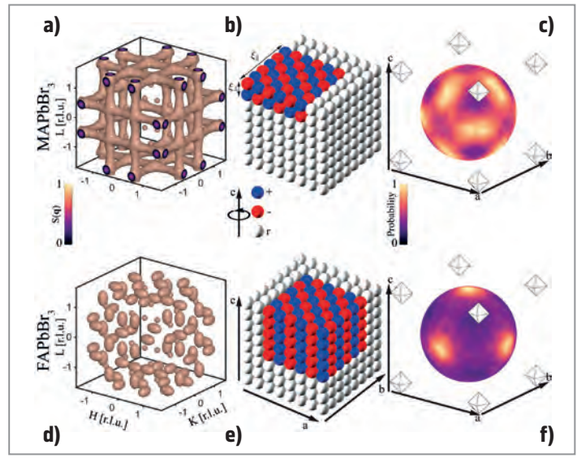

Figure 3
Isosurface representations of 3D QEDS at 300 K in a) $MAPbBr_3$ and d) $FAPbBr_3$. b) and e) Local octahedral correlations at a single snapshot in time inferred from the experimentally derived QEDS in a) $MAPbBr_3$ and d) $FAPbBr_3$. Each octahedron is represented by a sphere in which the colour represents the respective tilt angle along the c crystallographic direction, with blue corresponding to positive, red to negative and white to a random close-to-zero tilt angle. Coloured spheres for c) $MAPbBr_3$ and f) $FAPbBr_3$ depict the spatial distributions of the electric polarisation vector probability density of A-site cations, as derived from the MD trajectories.

Author contact: Milos Dubajic, milos.dubajic@hotmail.com

Original publication
'Dynamic nanodomains dictate macroscopic properties in lead halide perovskites', Nature Nanotechnology 20, 755–763 (2025). DOI: 10.1038/s41565-025-01917-0

Milos Dubajic, James R. Neilson, Johan Klarbring, Xia Liang, Stephanie A. Bird, Kirrily C. Rule, Josie E. Auckett, Thomas A. Selby, Ganbaatar Tumen-Ulzii, Yang Lu, Young-Kwang Jung, Cullen Chosy, Zimu Wei, Yorrick Boeije, Martin v. Zimmermann, Andreas Pusch, Leilei Gu, Xuguang Jia, Qiyuan Wu, Julia C. Trowbridge, Eve M. Mozur, Arianna Minelli, Nikolaj Roth, Kieran W. P. Orr, Arman Mahboubi Soufiani, Simon Kahmann, Irina Kabakova, Jianning Ding, Tom Wu, Gavin J. Conibeer, Stephen P. Bremner, Michael P. Nielsen, Aron Walsh and Samuel D. Stranks

For affiliations, please refer to the original publication.

Capturing PFAS with mechanochemical COFs

A green route to resilient frameworks for water purification

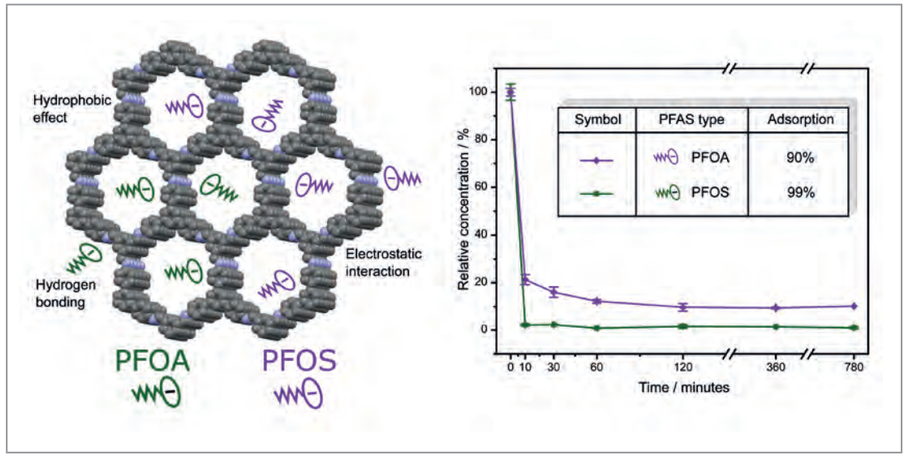

Figure 2
Illustration of the interactions between PFOA and PFOS with the TAPB–TFB COF, along with adsorption results demonstrating removal efficiencies of 90% for PFOA and 99% for PFOS. Most of the adsorption occurred within the first ten minutes, highlighting the rapid adsorption kinetics of the COF.

Per- and poly-fluoroalkyl substances (PFAS) represent one of the most persistent man-made pollutants confronting global water systems. Their stability arises from strong carbon-fluorine bonds which make them resistant to natural degradation. In our recent study published in *Small*, we demonstrate that mechanochemically synthesised covalent organic frameworks can capture and remove PFAS molecules from water. The work connects solvent-free materials synthesis with synchrotron-assisted characterisation and offers a new direction for sustainable technologies.

PFAS are widely used compounds in coatings, textiles and firefighting foams, valued for their exceptional durability yet notorious for their environmental persistence. Their accumulation in soil and water poses serious ecological and health concerns, including endocrine disruption and carcinogenic potential. Conventional purification strategies, such as activated carbon or ion-exchange resins, often fail to remove short-chain PFAS species due to their low hydrophobicity and high solubility. Developing efficient and selective sorbents from sustainable materials has therefore become a major research goal [1].

We address this challenge through a mechanochemical synthesis strategy for covalent organic frameworks (COFs). COFs are a class of crystalline porous polymers built from strong covalent bonds. Unlike conventional solvothermal syntheses that require hours of reaction time and toxic solvents, the mechanochemical route relies solely on mechanical energy and a few drops of liquid to activate bond formation. Mechanochemically synthesised COFs exhibit the same degree of crystallinity and functional tunability as their solution-synthesised counterparts but can be produced within minutes and under ambient conditions, thus saving both energy and resources [2].

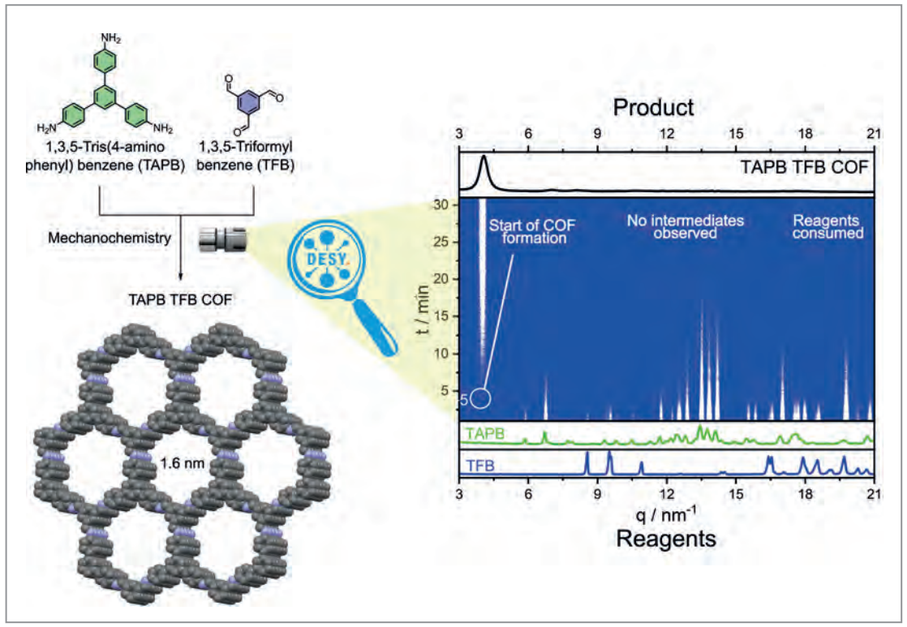

Figure 1
TAPB–TFB COF. The reaction was monitored in real time using PETRA III at DESY to elucidate the direct transformation from reactants to the final COF product without the formation of intermediates.

The mechanochemical transformation from reactants to the COF product was monitored in real time using X-ray powder diffraction at DESY PETRA III beamline P02.1.

The reaction occurred quickly, as XRD reflections of the COF product start emerging only after seven minutes of milling. In our laboratory, the reaction was completed in only 90 minutes. This is a remarkable improvement, transforming a process that normally involves multiple freeze-thaw cycles and three days of heating at high temperature into one that occurs at room temperature in just an hour and a half. The resulting COF provides an ordered array of nitrogen-rich cavities capable of electrostatic interactions with polar molecules such as PFAS.

To investigate the adsorption mechanism, the COFs were exposed to aqueous solutions of perfluorooctanoic acid (PFOA) and perfluorooctane sulfonic acid (PFOS). The COF achieved over 90% removal efficiency for both PFOS and PFOA, with most adsorption occurring within the first ten minutes. Post-adsorption characterisation using Fourier Transform Infrared Spectroscopy (FTIR), X-ray Photoelectron Spectroscopy (XPS) and Density Functional Theory (DFT) analyses revealed that the COF interacts with PFAS primarily through hydrophobic effects and electrostatic interactions between the partially protonated imine bonds and the deprotonated anionic heads of the PFAS molecules. This cooperative binding mechanism accounts for the high uptake capacity and selectivity observed in Fig. 2. Crucially, the mechanochemically synthesised COF retained its structural integrity in various environments, demonstrating its durability for practical water purification.

The synergy between mechanochemistry and synchrotron characterisation was instrumental in this discovery. High-resolution X-ray measurements at PETRA III enabled the monitoring of mechanochemical reactions in real time which is not possible in conventional laboratories.

Our findings underline that energy-efficient solid-state synthesis routes can yield next-generation materials for environmental remediation and beyond. Looking ahead, the mechanochemical methodology could be extended to functional frameworks capable of catalysis, ion capture or gas separation. Photon-based tools at PETRA III provide the means to resolve these materials' dynamic behaviour in real time, opening a new era where sustainable fabrication and advanced characterisation evolve hand in hand.

Author contact:
Maroof Arshadul Hoque, maroof-arshadul.hoque@bam.de
Biswajit Bhattacharya, biswajit.bhattacharya@bam.de
Franziska Emmerling, franziska.emmerling@bam.de
Martin Etter, martin.etter@desy.de

References

1. C. Ng, I. T. Cousins, J. C. DeWitt, J. Glüge, G. Goldenman, D. Herzke, R. Lohmann, M. Miller, S. Patton, M. Scheringer, X. Trier and Z. Wang, 'Addressing Urgent Questions for PFAS in the 21st Century', Environ. Sci. Technol. 55, 12755–12765 (2021).
2. J. Alić, M. Schlegel, F. Emmerling and T. Stolar, 'Meeting the UN Sustainable Development Goals with Mechanochemistry' Angew. Chem. Int. Ed., 63, e202414745 (2024).

Original publication
'Mechanochemically Synthesized Covalent Organic Framework Effectively Captures PFAS Contaminants', Small 21, e09275 (2025). DOI: 10.1002/smll.202509275

Maroof Arshadul Hoque[1], Thomas Sommerfeld[1], Jan Lisec[1], Prasenjit Das[1], Carsten Prinz[1], Christian Heinekamp[1,3], Tomislav Stolar[1], Martin Etter[2], David Rosenberger[1], Janine George[4], Biswajit Bhattacharya[1] and Franziska Emmerling[1,3]

1. BAM Federal Institute for Materials Research and Testing, Berlin, Germany
2. Deutsches Elektronen-Synchrotron (DESY), Hamburg, Germany
3. Department of Chemistry, Humboldt University Berlin, Berlin, Germany
4. University of Jena, Institute of Condensed Matter Theory and Optics, Jena, Germany

New Na-ion storage mechanism in layered cathode materials

Operando diffraction to explore the solvent co-intercalation reaction in Na-ion batteries

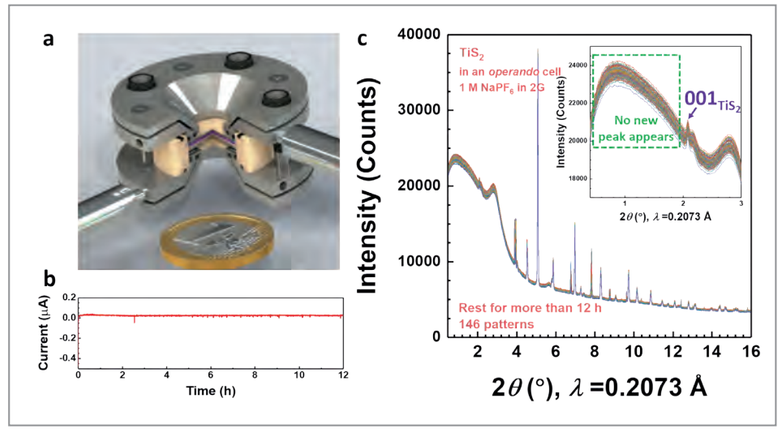

Figure 2
a) In-house designed *operando* cell. b) Recorded current in the rest state of TiS_2 in the 2G-based electrolyte assembled in the in-house designed *operando* cell. c) The corresponding *operando* synchrotron X-ray diffraction patterns. Inset: An enlarged view of the region between 0.4 and 3 degrees. No solvent co-intercalation peak occurred during the 12-hour rest period. (Adapted from original publication Sun et al.)

The performance of metal-ion batteries (metal = Li, Na, Mg etc.) relies on how metal ions and their solvent shells move into and out of electrode structures. Conventionally, only the bare ions intercalate into layered electrodes while the solvent molecules remain in the electrolyte. However, solvent co-intercalation, the simultaneous uptake of ions and solvent molecules that bypasses the stripping of solvated shells, offers a new dimension for tuning electrode properties. Combining diffraction with complementary experiments and theory, we reveal how co-intercalation occurs in layered cathodes, how it alters structure and electrochemistry and why it opens new routes for electrode design.

Understanding how ions enter and leave electrode structures is crucial for investigating the ion storage mechanism in metal-ion batteries. While the intercalation of bare ions in layered materials is well established, the process becomes far more complex when solvent molecules accompany these ions. This phenomenon, known as solvent co-intercalation, in which solvent molecules move together with metal ions during (de)intercalation into the host structure, can significantly influence the structure, the electrochemical reversibility and the long-term stability of electrodes.

To directly track these dynamics, we used *operando* synchrotron X-ray diffraction with high photon energy (~60 keV) and high time resolution at the P02.1 beamline of PETRA III [1,2]. The technique allowed us to monitor, in real time, the lattice expansion and contraction that occurs when solvated sodium ions enter and leave layered cathodes. Using the representative P2-Na_xTiS_2 material, we observed that changing the electrolyte solvent from a carbonate mixture (EC/DMC) to propylene carbonate (PC) or diglyme (2G) produced markedly different structural responses. In EC/DMC, only minor reversible lattice shifts were detected, whereas in PC or 2G a new phase emerged with the 002 reflections moving to lower angles, showing clear evidence of significant interlayer expansion (Fig. 1a). Together with other characterisation techniques such as *operando* dilatometry, we confirmed that this expansion stemmed from solvent co-intercalation, in which solvated Na ions and solvent molecules jointly enter the interlayer spacing.

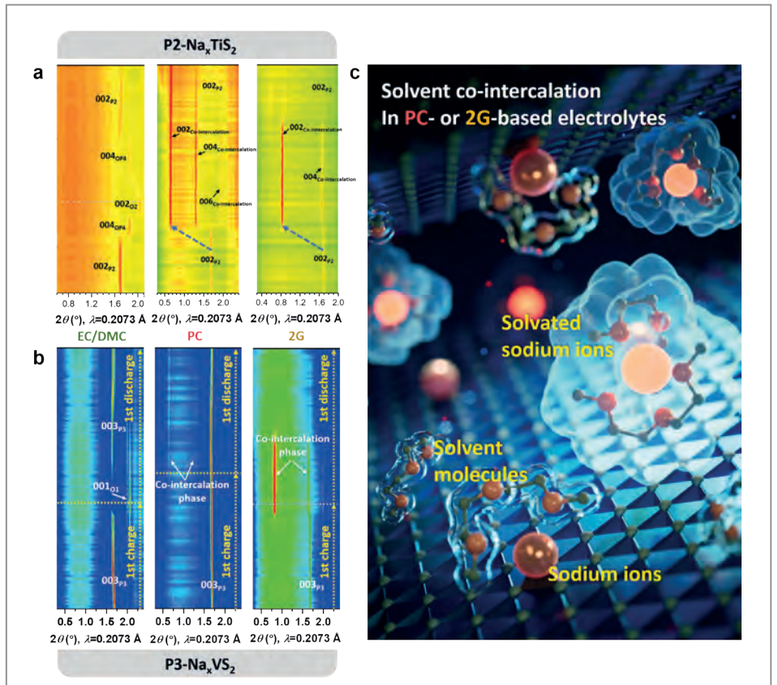

Figure 1
Operando synchrotron X-ray diffraction of a) P2-Na_xTiS_2 b) P3-Na_xVS_2 b). Changes were made to the layout. Large lattice expansion can be observed in PC- and 2G-based electrolytes due to solvent co-intercalation, while only conventional intercalation was detected when the EC/DMC-based electrolyte was used. c) Schematic illustration of solvent co-intercalation in PC- or 2G-based electrolytes in layered cathode active materials. (Adapted from original publication Sun et al.)

Extending the investigation to other layered sulfide cathodes, for instance P3-Na_xVS_2 (Fig. 1b), demonstrated that solvent co-intercalation is a general phenomenon in selected electrolyte systems. Because the solvent actively participates in the reaction, only *operando* techniques can capture its dynamics and reversibility, as *ex situ* methods risk solvent loss during sample handling. These insights establish *operando* diffraction as a powerful approach for uncovering the coupled behaviour of ions, solvents and host lattices in real working electrodes (as illustrated in Fig. 1c).

Building on extensive experimental observations, we developed theoretical guidelines to explain when and how solvent co-intercalation occurs in layered electrode materials. Two key factors govern this process: the interlayer binding energy and the interlayer free volume (the amount of free space available between the layers). *Operando* synchrotron X-ray diffraction was instrumental in testing these ideas. Using a specially designed cell (Fig. 2a), we examined whether solvent molecules could spontaneously diffuse into the layered TiS_2 structure. Even after prolonged exposure for 12 h, no solvent uptake was detected in the pristine (unsodiated) TiS_2 material, indicating that its strong interlayer attraction prevents solvent entry (Fig. 2b and c). This result supports our theoretical framework which links low interlayer binding energy and sufficient free volume to the ability of layered materials to host solvated ions.

Beyond their immediate electrochemical relevance, these discoveries highlight the broader significance of solvent co-intercalation as a new design principle for energy storage materials. In contrast to the detrimental effects of solvent co-intercalation often seen in graphite anodes, certain layered cathodes can accommodate solvated ions with minimal capacity loss and exceptionally fast kinetics. This opens up a vast chemical landscape for exploring new layered compounds and electrolyte combinations, offering exciting opportunities to engineer materials with tailored structural flexibility and ion transport properties. The work exemplifies how combining advanced *operando* techniques with theory can challenge established paradigms and inspire new directions in battery research.

Author contact: Yanan Sun, yanan.sun@helmholtz-berlin.de
Philipp Adelhelm, philipp.adelhelm@hu-berlin.de
Volodymyr Baran, volodymyr.baran@desy.de

References

1. A.-C. Dippel, H.-P. Liermann, J. T. Delitz, P. Walter, H. Schulte-Schrepping, O. Seeck and H. Franz, 'Beamline P02.1 at PETRA III for High-Resolution and High-Energy Powder Diffraction', J. Synchrotron Radiat. 22, 675–687 (2015).
2. J. Kieffer, V. Valls, N. Blanc and C. Hennig, 'New tools for calibrating diffraction setups', J. Synchrotron Radiat. 27, 558–566 (2020).

Original publication

'Solvent co-intercalation in layered cathode active materials for sodium-ion batteries', Nature Materials 24, 1441–1449 (2025).
DOI: 10.1038/s41563-025-02287-7

Yanan Sun[1,2], Gustav Åvall[1,3], Shu-Han Wu[1], Guillermo A. Ferrero[1,2], Annica Freytag[1,2], Pedro B. Groszewicz[4,5], Hui Wang[1,2], Katherine A. Mazzio[1,2], Matteo Bianchini[6], Volodymyr Baran[7], Sebastian Risse[2] and Philipp Adelhelm[1,2]

1. Institut für Chemie, Humboldt-Universität zu Berlin, Berlin, Germany
2. Joint Research Group Operando Battery Analysis (CE-GOBA), Helmholtz-Zentrum Berlin für Materialien und Energie (HZB), Berlin, Germany
3. SEEL Swedish Electric Transport Laboratory, Gothenburg, Sweden
4. SE-ASPIN, Helmholtz-Zentrum Berlin für Materialien und Energie (HZB), Berlin, Germany
5. Department of Radiation Science and Technology, Delft University of Technology, Delft, Netherlands
6. Bavarian Center for Battery Technology (BayBatt), Bayreuth, Germany
7. Deutsches Elektronen-Synchrotron (DESY), Hamburg, Germany

The kinetics of human coronavirus polyprotein processing

How polyprotein processing functions as a molecular switch

To propagate infection, viruses must replicate inside their human host. In coronavirus (CoV) infections, the host ribosomes produce polyproteins – long protein chains – that are processed into non-structural proteins (nsps). These nsps largely form the replication/transcription complex (RTC) which is critical for viral growth and represents a key therapeutic target. While processing order is crucial, its regulation and connection to RTC assembly remain poorly understood. In our study, we used native mass spectrometry (nMS) to follow the proteolytic processing reaction of four coronaviruses and quantify the kinetics and subsequent protein-protein interactions. This comparative analysis allowed us to unravel the underlying molecular regulatory mechanism of polyprotein processing.

Coronaviruses (CoVs) are RNA viruses with large genomes that rely on a sophisticated replication machinery including proofreading. During infection two long polyproteins, pp1a (nsp1-11) and pp1ab (nsp1-16), are translated and processed by autocatalytic proteases residing in the polyproteins. This processing is essential for assembling a functional RTC and must occur in a defined order [1]. However, the regulatory mechanism governing processing and the impact of processing dynamics are not well understood.

Here, we studied two key aspects: the order of polyprotein processing of the nsp7-11 region in four coronaviruses and its influence on protein complex formation of the proofreading enzyme nsp16. For this, we produced nsp7-11 of severe acute respiratory syndrome CoV (SARS-CoV), SARS-CoV-2, middle east respiratory syndrome CoV (MERS-CoV) and human CoV-229E (HCoV-229E). Furthermore, we produced the viral main protease M^{pro} of SARS-CoV-2 that is cleaving at the four cleavage sites: CS7/8, CS8/9, CS9/10 and CS10/11. We then followed the processing reaction in a time-resolved manner using nMS.

To conduct a comparative analysis of the processing reaction, we quantified this complex reaction, as it did not proceed in the same way in the different species. Therefore, we first established a method to determine rate constants *k* for each cleavage site (Fig. 1). The novelty here lies in extracting kinetic constants from a structured polyprotein. Therefore, we developed a custom Python script to automate the analysis of polyprotein processing. Time-resolved data resulted in complex nMS spectra. To depict the processing reaction from nMS data, the peaks were assigned to the corresponding species (deconvolution) and precise species intensities were extracted for plotting over time (Fig. 1a). We exploited the fact that nMS detects all species occurring in parallel to extract cleavage site kinetics [2].

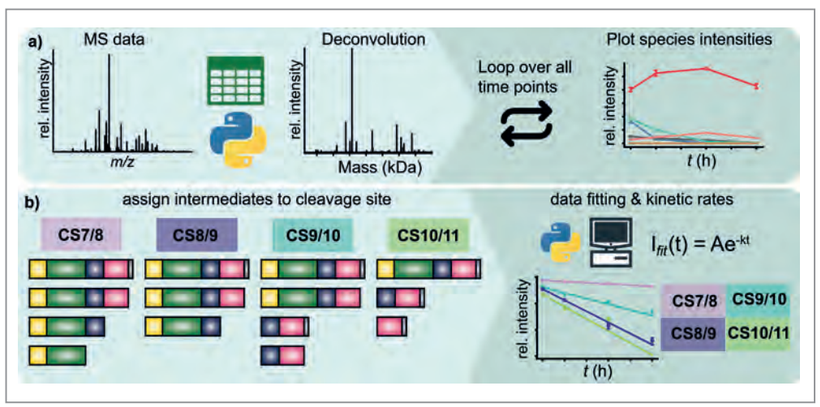

Figure 1
a) A custom Python script was developed to import MS data, deconvolute peaks and plot species intensities. b) To extract kinetic rate constants for the four cleavage sites CS7/8, CS8/9, CS9/10 and CS10/11, intermediate species were assigned to the corresponding cleavage site based on the intactness. The resulting data were fitted using the specified exponential model.

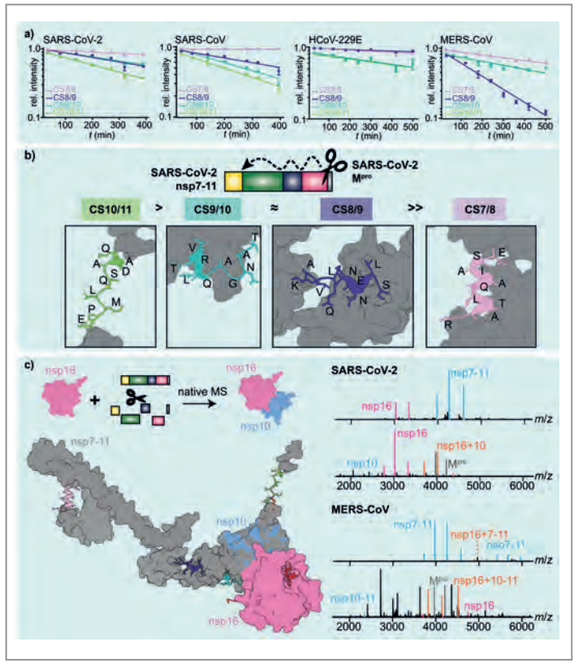

Figure 2
a) Comparative analysis of the four human CoVs - SARS-CoV-2, SARS-CoV, HCoV-229E and MERS-CoV - revealed distinctive processing patterns, suggesting that processing is not strictly evolutionarily conserved. However, certain features, such as the delayed cleavage of CS7/8, appear to be conserved. b) As all processing reactions were carried out using SARS-CoV-2 M^{pro}, species-specific effects cannot be excluded. Therefore, we propose a cleavage order only for SARS-CoV-2. In this context, M^{pro} appears to cleave preferentially from the *C*-terminus to the *N*-terminus, with CS9/10 and CS8/9 being processed at comparable rates. c) Interaction studies with the proofreading enzyme nsp16 show efficient complex formation only after processing of nsp7-11. SARS-CoV-2 nsp7-11 was probed with SARS-CoV-2 nsp16 in the presence (upper panel) and absence (lower panel) of M^{pro}; MERS-CoV nsp7-11 was probed with SARS-CoV-2 nsp16 under the same conditions.

So, we were able to simplify the complex processing reaction to first order kinetics by assigning processing species to corresponding cleavage sites based on their intactness. We then fitted the data to an exponential model and extracted kinetic rates (Fig. 1b).

Our sensitive nMS approach gave novel insights into polyprotein processing of the nsp7-11 reaction in CoVs, revealing conserved features and species-specific variations. The experimentally determined rate constants are put into perspective with a comprehensive analysis of protein sequence and structural models (Fig. 2a,b).

Conversion rates at CS7/8 in all four CoVs were substantially slowed down compared to other cleavage sites (Fig. 2a), suggesting a structural hindrance. AlphaFold 3 (AF3) models supported this observation, showing an α-helical fold at this location, which reduces the cleavage efficiency of M^{pro}. In general, the AF3 predictions confirmed the experimental data and could provide structural rationale [3].

Notably, varying rates at CS10/11 indicated that cleavage is not essential for complex formation of nsp10/16. Subsequent nMS binding experiments with SARS-CoV-2 nsp16, SARS-CoV-2 nsp10 and the nsp10-11 intermediate of MERS-CoV confirmed that cleavage at CS10/11 is not a prerequisite for nsp10/16 complex formation. Experiments with unprocessed nsp7-11 showed no efficient binding of nsp16, though superposition of nsp7-11 AF3 model and the crystal structure of nsp10/16 complex only showed minor clashes (Fig. 2c) [4]. This suggests that polyprotein processing is like a molecular switch that 'turns on' binding capabilities which then allows for complex formation and functionality.

To sum up: A key advantage of our nMS approach is its ability to extract cleavage site kinetics including protein folding. Our findings offer new mechanistic insights into CoV polyprotein processing and complex assembly which may inform future antiviral drug development strategies.

Author contact:
Kira Schamoni-Kast, kira.schamoni-kast@cssb-hamburg.de
Boris Krichel, boris.krichel@cssb-hamburg.de
Charlotte Uetrecht, charlotte.uetrecht@cssb-hamburg.de

References

1. K. Schamoni-Kast and C. Uetrecht, 'From Science to Fiction – Connecting In Vivo and In Vitro Results in Polyprotein Processing of Coronaviruses', J. Mol. Biol. 437, 169370 (2025).
2. M. Barth and C. Schmidt, 'Native mass spectrometry-A valuable tool in structural biology', J. Mass Spectrom. 55, e4578 (2020).
3. J. Abramson et al., 'Accurate structure prediction of biomolecular interactions with AlphaFold 3', Nature 630, 493–500 (2024).
4. S. Lin, H. Chen et al., 'Crystal structure of SARS-CoV-2 nsp10/nsp16 2-O-methylase and its implication on antiviral drug design', Signal Transduct. Target Ther. 5, 131 (2020).

Original publication

'The kinetics of nsp7-11 polyprotein processing and impact on complexation with nsp16 among human coronaviruses', Nature Communication 16, 8244 (2025).
DOI: /10.1038/s41467-025-61554-y

Kira Schamoni-Kast[1,2], Boris Krichel[1,2], Tomislav Damjanović[1,2], Fatema-Aqila Said[1], Thomas Kierspel[1], Sibel Toker[1] and Charlotte Uetrecht[1,2]

1. Centre for Structural Systems Biology CSSB, Deutsches Elektronen-Synchrotron DESY & Leibniz Institute of Virology (LIV) & University of Lübeck, Hamburg, Germany.
2. Institute of Chemistry and Metabolomics, University of Lübeck, Lübeck, Germany.

A flying protein in a flash

An ephemeral snapshot captures a single protein in flight

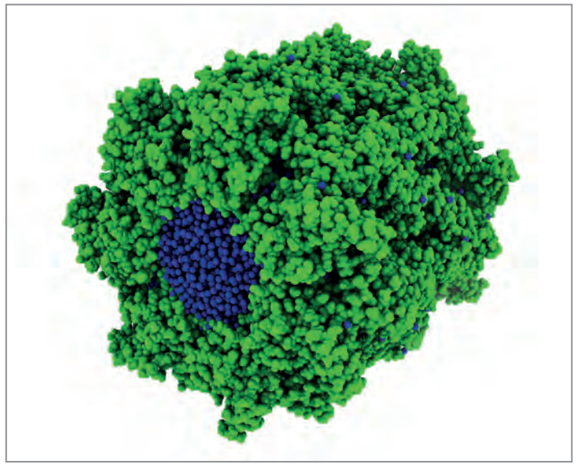

Figure 2

The most probable orientation of GroEL during X-ray diffraction. This model depicts the GroEL complex positioned as inferred from its optimal match to the observed experimental diffraction pattern. The X-ray beam is directed orthogonal to and into the plane of the figure.

Proteins are life's molecular machines. To understand them, we need to see their 3D shape. Traditionally, this requires large crystals or freezing the sample, giving only a static, averaged picture. The dream has been to capture a snapshot of a single protein to see its individual behaviour. This requires a snapshot faster than atomic motion. X-ray free-electron lasers (XFELs) promise this with their ultrashort, brilliant pulses which can in theory record a pattern from a molecule before it is destroyed. But demonstrating this for a single protein has remained an elusive goal—until now.

Our work was inspired by one of the driving forces behind the construction of X-ray free-electron lasers: the ability to perform single-particle imaging (SPI). The core concept, known as 'diffraction-before-destruction', is that an ultra-short femtosecond X-ray pulse is so brief that it can scatter off a molecule and produce a diffraction pattern before the molecule is obliterated by the pulse's immense energy [1]. While this has been successfully demonstrated on large biological objects like viruses [2], its application to the much smaller scale of a single protein has been a formidable challenge. The primary obstacle has always been the extremely low signal-to-noise ratio. The scattering from a single protein is incredibly faint and is easily lost in the background noise generated by the gas used to deliver the sample into the vacuum chamber.

In our experiment at the European XFEL's Small Quantum Systems (SQS) instrument, our team set out to finally overcome this barrier. We chose the chaperonin GroEL from *E. coli* as our target. It is a well-characterised, 800 kDa protein complex with a distinctive, non-spherical barrel shape about 14 nm in diameter, making its structural signature more recognisable than a simple sphere. Using an electrospray source, we aerosolised a solution containing GroEL, creating a fine beam of isolated protein molecules that we directed into the path of the XFEL beam [3]. For each X-ray pulse, the detector recorded the resulting pattern with the hope that sometimes the protein will intersect the X-ray pulse (Fig. 1).

The subsequent data analysis was a search for a needle in a haystack. From 84000 detector images, the vast majority contained only background noise. However, we successfully identified one very distinct pattern that clearly rose above this background. The crucial next step was to verify that this signal was, indeed, from a single GroEL molecule.

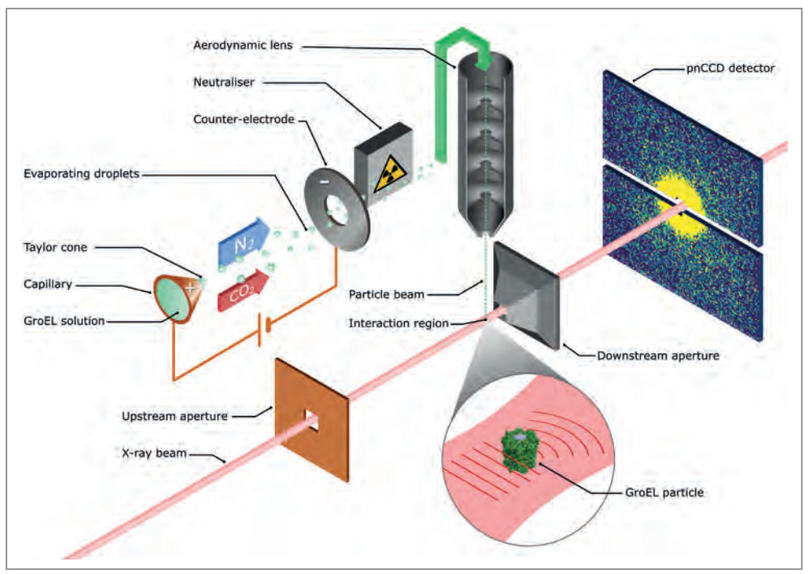

Figure 1

Overview of the experimental setup. Individual GroEL particles (~ 14 nm diameter) are aerosolised from solution using an electrospray ioniser. Following neutralisation, the particles are focused by an aerodynamic lens to form a particle beam that traverses the interaction region. Here, the beam is intersected by the XFEL pulse, and the forward-scattered diffraction signal is captured by a dual-panel pnCCD detector. (Figure is adapted from the original publication licensed under CC BY 4.0)

Our validation was a two-fold process. Firstly, we analysed the radial profile of the diffraction pattern to estimate the size of the object that was hit. This analysis yielded a dia-meter of approximately 15 nm—a good match for GroEL. Secondly, and more importantly, we analysed the pattern's shape. A simple sphere would produce a perfectly circular pattern, but the barrel-like structure of GroEL should produce anisotropy. Our simulated diffraction patterns predicted that a side-on view of the molecule would create a ring broken up into distinct speckles. Our experimental pattern displayed exactly this feature, providing a structural fingerprint that strongly corroborated its identity as GroEL.

To further refine our analysis, we compared the experimental data to a library of 4.3 million simulated patterns from different models and orientations of GroEL. This led to a fascinating insight. The best fit was not from a model of a completely 'dry' protein but rather from a model where the hollow interior of the GroEL barrel was filled with extra electron density which we modelled as water (Fig. 2). This strongly suggests that the protein retains a significant amount of its hydration shell during its flight into the beam. This residual solvent appears to be critical for preserving the protein's native-like structure in the harsh gas-phase environment.

This observation represents the proof-of-concept of ideas that had been dreamed of well over a decade. While a single pattern is not enough to reconstruct a full 3D structure, it provides the first definitive experimental evidence that single-protein diffraction is possible. It validates the core principles of the method and confirms that macromolecules can be delivered to the beam with their structural integrity intact. Our work shifts the problem from one of fundamental feasibility to one of technical optimisation. With the advent of higher repetition rate sources, better detectors, better X-ray optics and improved sample delivery methods, we are now on a clear path towards collecting the thousands of snapshots needed to create 3D reconstructions and, ultimately, molecular movies of flying proteins.

Author contact: Filipe Maia, filipe.maia@icm.uu.se

References

1. H. N. Chapman et al., 'Femtosecond diffractive imaging with a soft-X-ray free-electron laser', Nat. Phys. 2, 839–843 (2006).
2. T. Ekeberg et al., 'Three-dimensional reconstruction of the giant mimivirus particle with an x-ray free-electron laser', Phys. Rev. Lett. 114, 098102 (2015).
3. J. Bielecki et al., 'Electrospray sample injection for single-particle imaging with x-ray lasers', Sci. Adv. 5, eaav8801 (2019).

Original publication

'Observation of a single protein by ultrafast X-ray diffraction', Light: Science & Applications 13, 15 (2024).
DOI: 10.1038/s41377-023-01352-7

Malte Tomas Ekeberg, Dameli Assalauova, Johan Bielecki, Rebecca Boll, Benedikt J. Daurer, Lutz A. Eichacker, Linda E. Franken, Davide E. Galli, Luca Gelisio, Lars Gumprecht, Laura H. Gunn, Janos Hajdu, Robert Hartmann, Dirk Hasse, Alexandr Ignatenko, Jayanath Koliyadu, Olena Kulyk, Ruslan Kurta, Markus Kuster, Wolfgang Lugmayr, Jannik Lübke, Adrian P. Mancuso, Tommaso Mazza, Carl Nettelblad, Yevheniy Ovcharenko, Daniel E. Rivas, Max Rose, Amit K. Samanta, Philipp Schmidt, Egor Sobolev, Nicusor Timneanu, Sergey Usenko, Daniel Westphal, Tamme Wollweber, Lena Worbs, Paul Lourdu Xavier, Hazem Yousef, Kartik Ayyer, Henry N. Chapman, Jonas A. Sellberg, Carolin Seuring, Ivan A. Vartanyants, Jochen Küpper, Michael Meyer and Filipe R. N. C. Maia

For affiliations, please refer to the original publication.

Turning up the heat on time-resolved crystallography

Multi-dimensional serial synchrotron crystallography captures the temperature dependence of enzyme function in real time

To understand how living organisms function at the molecular level, it is crucial to decipher the role of proteins, the molecular machines that drive all processes of life. The three-dimensional structure of most proteins is determined at cryogenic temperatures where the intrinsic movements of the molecules are immobilised. However, under physiological conditions proteins are anything but static: they wiggle, breathe and bend as they catalyse reactions. Capturing these fleeting motions is the key to understanding how enzymes work, how drugs bind and how mutations alter their function. Now, scientists using the time-resolved crystallography end station T-REXX, at PETRA III beamline P14 operated by EMBL, have developed a novel method that allows them to observe the 3D structure of proteins over time and temperature, revealing previously invisible dynamics.

Our team refined an approach called 'multidimensional serial synchrotron crystallography' (5D-SSX), which combines time-resolved serial crystallography with temperature control. To achieve this, we integrated our established time-resolved SSX setup [1-3] with a newly developed environmental control box (Fig. 1). This device not only regulates temperature but also relative humidity, which is crucial for the preservation of sensitive protein crystals.

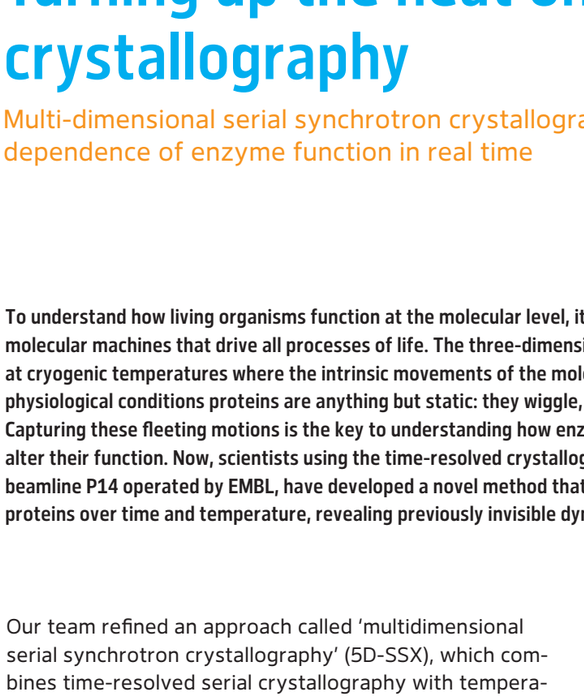

Figure 1

The experimental basis for 5D-SSX. a) Schematic of the environmental control box that enables precise control of the relative humidity and the temperature (10-70°C) surrounding the chips. The setup has approximately an A4-footprint and contains a complete fixed-target TR-SSX solution based on the HARE-chips and the LAMA-technology for *in situ* mixing reaction initiation. The setup also permits working with light-activated systems. b) A photograph of the 5D-SSX box implemented iinto the T-REXX end station at P14.
(Credit: Kinga Lubowiecka, EMBL)

The setup enables measurements from below 10 °C to above 70 °C, covering both mesophilic and thermophilic enzymes. Importantly, with this setup we aim to correlate structural changes and reaction rates with each other in the crystal.

Two aspects were crucial for these developments: firstly, access to the world's first dedicated time-resolved crystallography synchrotron end station T-REXX and secondly, the close collaboration between beamline scientists, structural biologists and instrument developers from the University of Hamburg, the Max Planck Institute for the Structure and Dynamics of Matter, the EMBL and the University Medical Centre Hamburg-Eppendorf.

The method bridges the gap between static crystal structures and the thermodynamics of biological reactions, providing new insights into how proteins behave under physiological conditions. To test our 5D-SSX approach, we applied it to two model systems: first, to a medically relevant β-lactamase – an enzyme that leads to antibiotic resistance in pathogenic bacteria – and second, to the biotechnologically important enzyme xy-lose isomerase which converts glucose to fructose and vice versa.

Figure 2

The two model systems via 5D-SSX. a) The mesophile β-lactamase CTX-M-14 catalyses the hydrolysis of β-lactam antibiotics. This mechanism displays the most common resistance mechanism against antibiotics. We studied the turnover of the clinically most prescribed antibiotic Piperacillin. The multi-temperature analysis revealed that for a given time-point different intermediates can be isolated at different temperatures. Notably, we also observed a new conformation of the hydrolysed product in the active site. b) The thermophile enzyme xylose isomerase catalyses the interconversion of glucose to fructose which proceeds via an open-chain intermediate state. By increasing the temperature for a given time-delay we could selectively enrich the previously unobserved open-chain intermediate of glucose in the active site of XI.

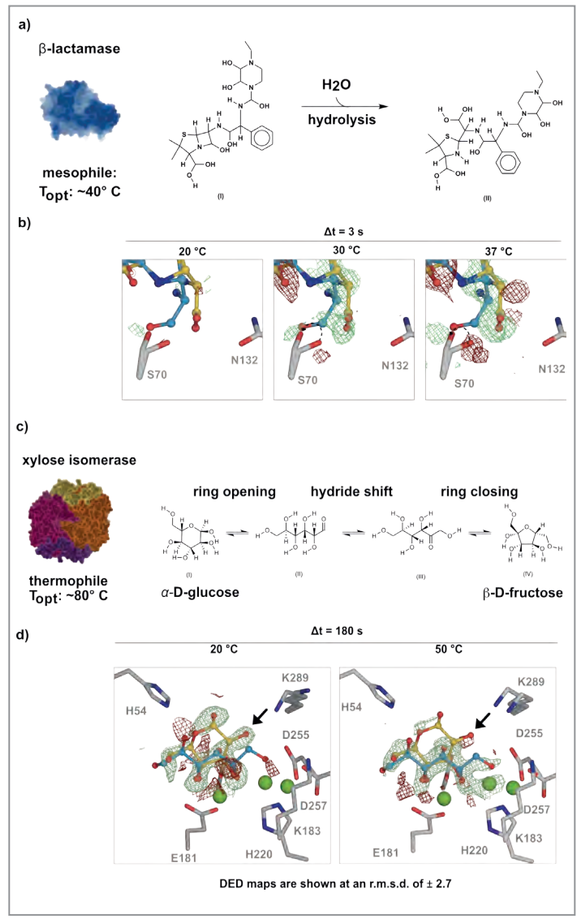

At the beginning we simply changed the temperature without triggering a reaction and observed a direct response in the conformational dynamics which can be effectively translated into structural changes for both enzymes. We then investigated how temperature affects the catalytic activity of our two model enzymes. For both enzymes, the results provided direct evidence of how temperature modulates conversion rates and revealed new catalytic intermediate structures (Fig. 2). We also found that temperature plays an important role in whether certain reaction intermediates can be detected. Simply waiting longer at a lower temperature does not make up for the effects of working at a higher temperature.

From a practical point of view, temperature modulation can therefore help us to selectively enrich important intermediates that were previously unattainable. This means that we can now generally see how catalytic mechanisms respond to temperature. Thus, 5D-SSX opens up the possibility of studying enzymes and drug targets closer to physiological conditions where temperature and dynamics play a crucial role.

Structural biology is moving beyond static snapshots toward methods that can capture how proteins change and interact over time [4-6]. We expect 5D-SSX to help bridge structural and kinetic information, providing a more complete experimental picture of how enzymes actually work in our body. This approach will help reveal distinct catalytic pathways and inform the design of improved enzymes and their inhibitors. Looking ahead, the PETRA IV upgrade will allow us to extend the method to faster processes and achieve higher temporal resolution, providing a more detailed view of biochemical reactions in real time.

Author contact:
Friedjof Tellkamp, friedjof.tellkamp@mpsd.mpg.de
Pedram Mehrabi, pedram.mehrabi@uni-hamburg.de
Eike C. Schulz, ec.schulz@uke.de

References

1. E. C. Schulz et al., 'The hit-and-return system enables efficient time-resolved serial synchrotron crystallography', Nat. Methods 15, 901–904 (2018).
2. P. Mehrabi, E. C. Schulz, M. Agthe et al., 'Liquid application method for time-resolved analyses by serial synchrotron crystallography', Nat. Methods 16, 979–982 (2019a).
3. P. Mehrabi, E. C. Schulz, R. Dsouza et al., 'Time-resolved crystallography reveals allosteric communication aligned with molecular breathing', Science 365, 1167–1170 (2019b).
4. M. A. Wilson, 'Mapping Enzyme Landscapes by Time-Resolved Crystallography with Synchrotron and X-Ray Free Electron Laser Light' Annu Rev Biophys 51, 1–20 (2021).
5. M. D. Miller and G. N. Phillips, 'Moving beyond static snapshots: Protein dynamics and the Protein Data Bank', J. Biol. Chem. 296, 100749 (2021).
6. G. Khusainov, J. Standfuss and T. Weinert, 'The time revolution in macromolecular crystallography', Struct. Dyn. 11, 020901 (2024).

Original publication

'Probing the modulation of enzyme kinetics by multi-temperature, time-resolved serial crystallography', Nature Communication 16, 6553 (2025). DOI: https://doi.org/10.1038/s41467-025-61631-2

E. C. Schulz[1,2,3,6], A. Prester[1], D. von Stetten[4], G. Gore[1], C.E. Hatton[3], K. Bartels[1], J. P. Leimkohl[2], H. Schikora[2], H. M. Ginn[5], F. Tellkamp[2] and P. Mehrabi[2,3]

1. University Medical Center Hamburg-Eppendorf UKE, Hamburg, Germany
2. Max-Planck-Institute for the Structure and Dynamics of Matter, Hamburg, Germany
3. Institute for Nanostructure and Solid State Physics, University of Hamburg, Hamburg, Germany
4. European Molecular Biology Laboratory EMBL, Hamburg, Germany
5. Deutsches Elektronen Synchrotron DESY, Hamburg, Germany

‘Sharkitecture’: a nanoscale peek into a shark’s skeleton

Visualising the structure and deformation of mineralised cartilage

Nature builds remarkable skeletal materials by combining minerals with biopolymers such as collagen – a process known as biomineralisation. This strategy allows organisms like sea urchins, lobsters and even humans to develop mechanically robust skeletons that provide structural support. Sharks have evolved for more than 450 million years, developing skeletons not from bone but from a tough, mineralised form of cartilage. These cartilaginous fish are extraordinarily fast swimmers: their vertebral spines act like natural springs, storing and releasing energy with each tailbeat [1], allowing them to gracefully cross the oceans.

Researchers from Florida Atlantic University collaborated with scientists from the Helmholtz Centre Hereon at DESY in Hamburg and the U.S. National Oceanic and Atmospheric Administration (NOAA) to elucidate the internal structure of Blacktip shark vertebrae (*Carcharhinus limbatus*) in unprecedented detail. Blacktip sharks are medium-sized sharks known for their distinctive, black-tipped fins (Fig. 1a). The fast-swimming predators are common in warm coastal waters around the world. The high spatial resolution at the nanotomography branch of the PETRA III imaging beamline P05 [2] operated by Hereon enabled us to visualise nano-structural features and minute deformations of mineralised cartilage in the sharks’ vertebral column. Our study pioneered complementary nanoscale imaging modes, *in situ* mechanical testing and deep learning data analysis strategies that have rarely been applied to biological materials.

At the macroscale, the shark vertebral column is built from cylindrical disks called centra. Each centrum consists of the alternating mineralised *intermediale* (M) and unmineralised sections, and the hourglass-shaped hyper-mineralised *corpus calcareum* (CC) (Fig. 1a) [3]. The two mineral-containing regions within the shark’s mineralised cartilage, the CC and the M, differ substantially in their internal microstructure [4]. The CC is made from dense mineralised plates connected by short, diagonal struts (Fig. 1b) while M resembles the interconnected mineral network found in spongy bone (Fig. 1c). In both regions, mineralised plates are arranged in a hierarchical structure that helps the skeleton withstand strain from multiple directions – a critical adaptation for sharks which perform complex bending motions during swimming. At the nanoscale, the trabecular mineral network in the M is made from tiny needle-like bioapatite crystals (Fig. 2a,b) – the same mineral found in human bones. These nanocrystals are arranged in swirling patterns. Using X-ray nano-tomography, we discovered that fibres in the M wrap around the lacunar spaces where chondrocyte cells are located. In the highly mineralised CC, bioapatite minerals are incorporated within highly aligned strands of collagen fibres, supporting and reinforcing the organic matrix (Fig. 2c,d). This sophisticated arrangement of soft fibres and hard minerals makes shark cartilage stiff and tough but also flexible. The layered mineral honeycomb structure is optimised to prevent cracks from spreading, while being mechanically robust and lightweight.

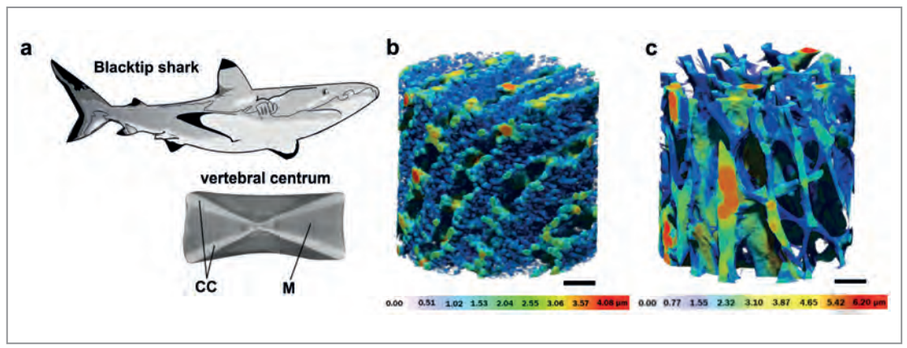

Figure 1
a) Blacktip sharks are characterised by their black-tipped fins. The vertebral column of sharks consists of vertebral centra which contain the hypermineralised corpus calcareum (CC) and mineralised intermediale (M). The 3D volumes of the CC (b) and M (c) translate the wall thickness into a colour. Scalebars equal 10 µm.

In some of the experiments at PETRA III, we combined X-ray nanotomography with *in situ* nanoindentation to quantify how tiny blocks of shark vertebrae deform under mechanical stress (Fig. 3a, b). After a single indentation cycle, we detected minute deformations of less than a micrometre – roughly hundred times smaller than a hair’s breadth. Interestingly, permanent fractures in the CC occurred only after a second loading cycle and were contained within the densely mineralised plane towards the thick, interconnecting rods (Fig. 3c), highlighting the material’s built-in toughness and failure resistance. With little permanent deformation detected, we concluded that the soft collagen tissue is crucial for absorbing energy. In the wild, shark vertebrae need to undergo millions of bending cycles during the animal’s lifetime without taking advantage of any known repair mechanism.

Taken together, our work contributes to a better biomechanical model of the ‘sharkitecture’ that can inspire the design of fracture-resistant fibre composites for structural engineering. The intricate fibre-reinforced structure of shark cartilage offers a compelling model for high-performance, resilient design which holds promise for developing functional materials from medical implants to impact-resistant gear. While cartilage in the human body is unmineralised in a healthy state, conditions like osteoarthritis can lead to pathological calcifications similar to the ones in shark cartilage. An in-depth study of shark vertebrae can inform the diagnosis and treatment of bone and joint diseases using advanced tissue engineering approaches.

Author contact: Vivian Merk, vmerk@fau.edu

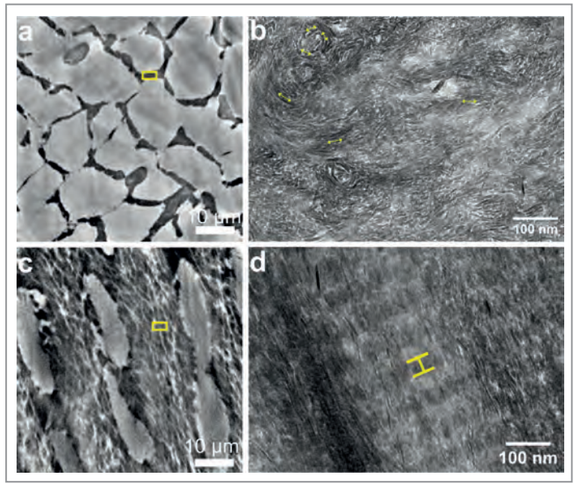

Figure 2
Representative nanoCT slices (a,c) and transmission electron micrographs (b,d) of mineralised portions of the CC (a,b) and the M (c,d) of Blacktip shark. Yellow boxes in (c,d) indicate the type of region from which TEM images were acquired. Arrows in b) highlight orientations of rod-like bioapatite crystals. d-spacing of mineralised collagen fiber bundles highlighted in d).

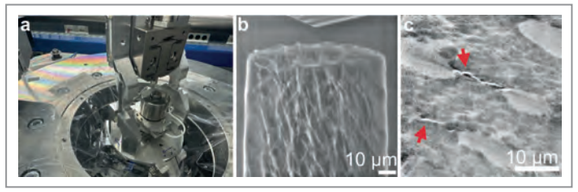

Figure 3
a) Nanoindentation at P05 with 0.1 µm diamond Berkovich tip. b) Nanoindenter approaching the sample during *in situ* experiment. c) Fractures observed at interplanar connections of CC after second indentation.

References

1. M. E. Porter, R. H. Ewoldt and J. H. Long Jr, ‘Automatic control: the vertebral column of dogfish sharks behaves as a continuously variable transmission with smoothly shifting functions’, J. Exp. Biol. 219, 2908-2919 (2016).
2. E. Longo, L. Sancey, S. Flenner, A. Kubec, A. Bonnin C, David, M, Müller and I. Greving, ‘X-ray Zernike phase contrast tomography: 3D ROI visualization of mm-sized mice organ tissues down to sub-cellular components’, Biomedical Optics Express 11, 5506–5517 (2020).
3. W. G. Ridewood and E. G. MacBride, ‘VIII.—On the calcification of the vertebral centra sharks and rays’, Phil. Trans. R. Soc. B, 210, 372-381 (1921).
4. D. Raja Somu, M. Fuentes, L. Lou, A. Agarwal, M. Porter and V. Merk, ‘Revealing Chemistry-Structure-Function Relationships in Shark Vertebrae across Length Scales’, Acta Biomater. 189, 377–387 (2024).

Original publication

‘A Nanoscale View of the Structure and Deformation Mechanism of Mineralized Shark Vertebral Cartilage’, ACS Nano 19, 14410–14421 (2025). DOI: 10.1021/acsnano.5c02004

Dawn Raja Somu[1], Steven Soini[1], Ani Briggs[1], Kritika Singh[2], Imke Greving[2], Marianne Porter[3], Michelle Passerotti[4] and Vivian Merk[1]

1. Department of Chemistry and Biochemistry, Department of Ocean and Mechanical Engineering, Florida Atlantic University, Boca Raton, USA
2. Institute of Materials Physics, Helmholtz-Zentrum Hereon, Geesthacht, Germany
3. Department of Biological Sciences, Florida Atlantic University, Boca Raton, USA
4. NOAA Fisheries, U.S. Department of Commerce, Narragansett, USA

Imaging pre-aligned proteins

Paving the way for atomic-resolution molecular movies: computational breakthrough in laser alignment of proteins

Determining the three-dimensional structure of individual proteins remains a central challenge in modern science. X-ray lasers offer a powerful tool for this purpose, yet the random orientation of molecules hinders data interpretation. This computational study shows that standard laser pulses can align nanoparticles and proteins in space. By tuning parameters such as temperature and laser intensity, strong alignment can be achieved, enabling atomic-resolution imaging and real-time observation of biomolecular dynamics.

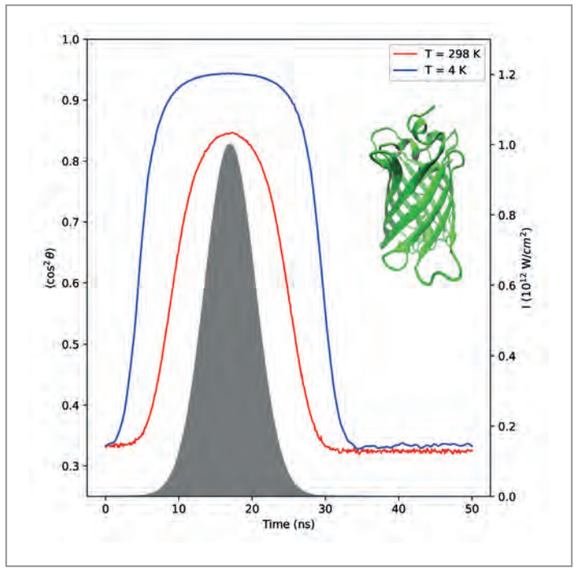

Figure 2
Degree of alignment of the green fluorescent protein, depicted in the inset, at 298 K (red) and 4 K (blue) using a 10^{12} W/cm^2 pulse intensity (shaded area in grey). The protein has a cylindrical shape with a base diameter of 2.5 nm and a length of 5.3 nm.

The dream of imaging proteins in action has long been hindered by a practical problem: how to recover the three-dimensional orientation of individual molecules from the two-dimensional snapshots captured by ultrafast X-ray lasers. A solution, proposed years ago, is to use a laser pulse to align the molecules just before the X-ray pulse arrives (Fig. 1). But whether this was feasible for large, isolated biomolecules remained an open question, in part because the computational modelling required was prohibitively expensive.

In our work, we report comprehensive simulations demonstrating that laser-induced alignment of proteins and nanoparticles is not only possible, but also achievable with standard laser technology. Our work provides a quantitative roadmap for experiments and reveals that the vast majority of proteins have the right physical properties to be strongly aligned, paving the way for atomic-resolution single-particle imaging.

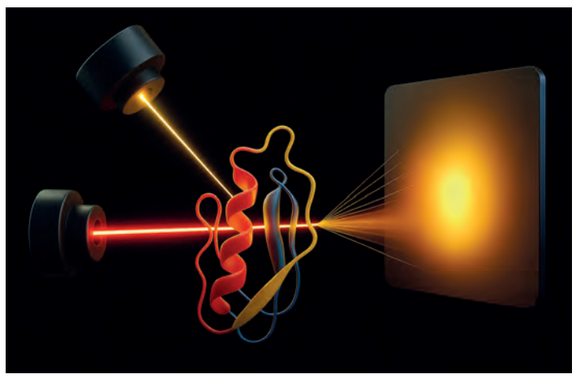

Figure 1
Single-particle X-ray diffractive imaging of laser-aligned proteins.

X-ray free-electron lasers (XFELs) can capture diffraction patterns from single molecules using the 'diffraction-before-destruction' principle. However, in standard single-particle imaging, the molecules are randomly oriented, and computationally determining each molecule's orientation from its diffraction pattern is a major bottleneck. This is especially true for weakly scattering proteins, where the signal is low. If molecules could be pre-aligned, their identical diffraction patterns could be averaged, dramatically boosting the signal and simplifying the path to high-resolution 3D structures.

We tackled the immense computational challenge by treating the nanoparticles and proteins as rigid bodies. We calculated the key property for alignment – the polarisability tensor – for various targets, from gold nanorods to over 150000 proteins from the Protein Data Bank. We then simulated the rotational dynamics of 20000 particles for each scenario, using our newly developed open-source software package, CMIclassirot, to obtain statistically robust results.

Our findings reveal several key principles for achieving strong alignment. First, the regime of alignment – whether it is temporary or permanent – depends on the particle's size and temperature. Large, cold nanorods have slow rotational periods and exhibit permanent alignment after the laser pulse is turned off, whereas small, warm particles only align during the pulse. Crucially, cooling a sample to cryogenic temperatures (4 K) can push even small particles into the desirable alignment.

Second, the molecule's shape, quantified by its polarisability anisotropy α_r, is paramount. Alignment increases sharply with anisotropy for α_r values between 1.2 and 2.5. Our most significant finding here is that an analysis of the protein database showed that 96% of proteins have an $\alpha_r > 1.2$, meaning the vast majority are inherently anisotropic enough to be aligned.

Finally, we identify temperature as the most powerful experimental lever. Cryogenic cooling dramatically enhances alignment, allowing for very strong alignment even with relatively weak laser pulses. For instance, we demonstrated that a model nanorod requires the highest laser intensity (10^{12} W/cm^2) to reach good alignment at room temperature, but at 4 K, the same alignment was achieved with a pulse twenty times weaker.

To bridge the gap from model systems to real-world applications, we simulated the alignment of green fluorescent protein (GFP) (Fig. 2). At room temperature and high intensity, GFP achieved moderate alignment. However, at 4 K, a much weaker pulse achieved a similar level, and with a high-intensity pulse at 4 K, GFP reached a very strong alignment $< \cos^2\theta = 0.94 >$, exceeding the threshold considered sufficient for resolving secondary structures.

Our study also thoughtfully addresses the critical concern of laser-induced damage. We argue that the risk of exciting damaging vibrations is negligible, as the narrow bandwidth of a nanosecond laser pulse does not overlap with the lowest-frequency modes of proteins. We also show that ionisation is unlikely at the moderate field strengths required, especially for cold samples, as ionisation is a local event and does not scale inversely with the large, global polarisability of the protein.

This computational work provides a clear and optimistic path forward. We have demonstrated that the vision of using laser alignment for single-particle imaging is within reach, transforming it from a theoretical concept into a practical experimental strategy. By combining cryogenic sample preparation – a technology we are already developing – with standard laser systems, we can now realistically aim to achieve the high-degree alignment needed to finally unlock atomic-resolution structures, and ultimately, molecular movies, from single biomolecules.

Author contact: Muhamed Amin, muhamed.amin@cfel.de
Amit Samanta, amit.samanta@cfel.de
Jochen Küpper, jochen.kuepper@cfel.de

References

1. L. Zecca et al., 'The Role of Iron and Copper Molecules in the Neuronal Vulnerability of Locus Coeruleus and Substantia Nigra during Aging', Proc. Natl. Acad. Sci. U.S.A. 101, 9843–48 (2004).
2. N. Weiskopf, L. J. Edwards, G. Helms, S. Mohammadi and E. Kirilina. 'Quantitative Magnetic Resonance Imaging of Brain Anatomy and in Vivo Histology', Nat. Rev. Phys. 1–19 (2021).
3. I. Friedrich et al., 'Cell Specific Quantitative Iron Mapping on Brain Slices by Immuno-MPIXE in Healthy Elderly and Parkinson's Disease', Acta Neuropath. Commun. 9, 47 (2021).

Original publication

'Laser-Induced Alignment of Nanoparticles and Macromolecules for Coherent-Diffractive-Imaging Application', Journal of the American Chemical Society 147, 7445–7451 (2025).
DOI: 10.1021/jacs.4c15679

Muhamed Amin[1,2,3], Jean-Michel Hartmann[4], Amit Samanta[1,5] and Jochen Küpper [1,5]

1. Center for Free-Electron Laser Science CFEL, DESY, Hamburg, Germany
2. Laboratory of Computational Biology, National Heart, Lung and Blood Institute, National Institutes of Health, Bethesda, Maryland, United States
3. Department of Sciences, University College Groningen, University of Groningen, Groningen, Netherlands
4. Laboratoire de Météorologie Dynamique/IPSL, CNRS, Ecole Polytechnique, Institut Polytechnique de Paris, Sorbonne Université, Ecole Normale Supérieure, Université PSL, Palaiseau, France
5. The Hamburg Centre for Ultrafast Imaging CUI, University of Hamburg, Hamburg, Germany

From milliseconds to nanoseconds — from frames to events

A two-dimensional X-ray detector captures nanosecond dynamics

Most modern state-of-the-art X-ray detectors are based on hybrid pixel array technology. It consists of two elements: a semiconductor sensor layer which transforms absorbed photon energy into a current and an application-specific integrated circuit (ASIC) which analyses the signal and converts it to photon counts. This hybrid approach allows both flexibility and sophisticated functionality. Various sensor materials can be chosen for optimal quantum efficiency at a given photon energy. In addition, ASICs can be designed for single photon counting, charge integration or event detection modes. The latter approach, initially conceived for particle tracking, now makes its way to synchrotrons.

The high brightness of modern synchrotron radiation X-ray sources in combination with large-area pixel detectors offers a powerful tool to study the structure, kinetics and dynamics of materials from micron down to Ångström length scales. Although synchrotron science has seen remarkable progress in the last years, the study of microsecond and nanosecond processes remains rare. The culprit is the limited detector frame rate that does not allow access to such short timescales; the data rates required for it are simply too high even for the fastest data transfer links. To overcome this bottleneck, we exploited an event-driven mode implemented in a prototype detector TEMPUS [1] built at DESY. In event-driven mode (Fig. 1), when a pixel is hit by a photon, a detector sends a data packet with information about the hit: a timestamp recording when the hit occurred (Time of Arrival, ToA); the length of the signal pulse which is proportional to the energy (Time over Threshold, ToT) and a pixel index. The TEMPUS detector is based on the Timepix4 [2] readout chip developed by the 'Medipix4 Collaboration' led by CERN. The chip offers sub-nanosecond timestamp accuracy and a bandwidth that supports 1.28 billion hits per second for a single chip containing 448 × 512 pixels of 55 µm size.

The data packets acquired in an experiment can be interpreted as a series of two-dimensional frames with down to nanosecond time intervals or as a collection of time traces for each pixel, making this detector outstanding for fast time-resolved measurements. We have shown that the event-driven mode can be used in X-ray Photon Correlation Spectroscopy (XPCS) to measure diffusion of colloids with nanosecond time resolution. In XPCS, one quantifies temporal speckle intensity fluctuations due to the particles' motion by calculating intensity autocorrelation functions using a multi-speckle method [3]. Usually, the speckle size matches the pixel size to maximise the signal-to-noise ratio (Fig. 2, top). Under these conditions, the shortest accessible time is not limited by the frame rate, as in 'normal detectors', but by the pixel dead time – typically hundreds of nanoseconds. This was demonstrated in an experiment with a gold colloidal solution (Fig. 3a). However, when the speckle size covers two or more neighbouring pixels, their timestamps reflect the intensity fluctuation of a single speckle, since pixels operate independently. Thus, by calculating the intensity cross-correlation function (Fig. 2, bottom) between neighbouring pixels, we could remove the limitation given by the pixel dead time and reach timescales down to approximately 10 ns for the first time, albeit with reduced contrast. Experimental results with the gold colloidal solution are shown in Fig. 3b.

Event-driven readout, perfectly suited for XPCS, allows bridging the gap between the spin echo technique and XPCS, opening new possibilities for studies of ns-µs dynamics with fourth generation synchrotron sources. In addition, one might also envisage using event detection mode operation for time-resolved measurements in powder diffraction, scattering and imaging applications, allowing unprecedented time resolution.

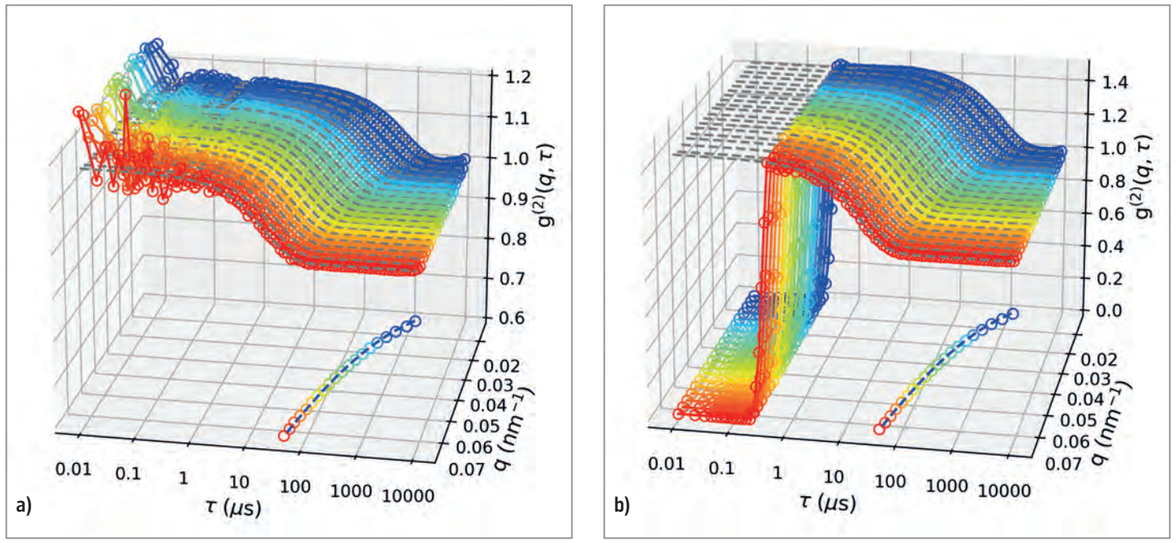

Figure 3

Calculated correlation functions with 10 ns time bins. a) The autocorrelation function obtained for 20 iso-q regions from a gold colloidal solution. The shortest accessible time is ~450 ns, which is much faster than of any available commercial detectors. The extracted relaxation times τ (open symbols) agree with the free Brownian diffusion D model (dashed line) $\tau = 1/Dq^2$

b) The cross-correlation function for the same 20 iso-q regions extends to 10 ns and provides identical results as the autocorrelation function despite lower contrast.

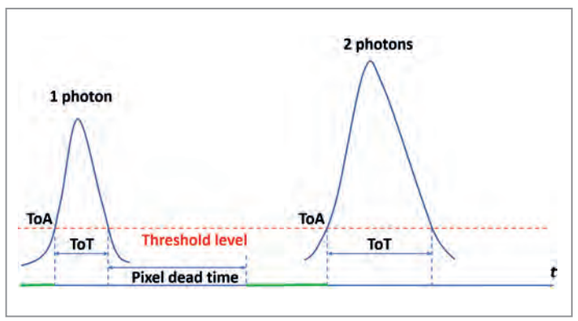

Figure 1

Event-based photon detection mode. For an individual pixel, a Time of Arrival is recorded when a signal rises above a predefined threshold. Time over Threshold measures the duration of the pulse and is proportional to the energy deposited (i.e. the number of photons when using monochromatic beam). The shortest time spacing between successive photon detections is given by the sum of ToT and pixel dead time.

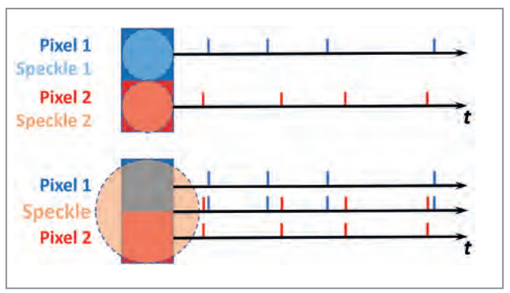

Figure 2

Top: The maximum SNR in XPCS is obtained when the speckle size matches the pixel size. The shortest time of the calculated autocorrelation function is limited by the pixel dead time. Bottom: When a speckle size is twice the pixel size or greater, the neighbouring pixels probe the same fluctuations, and their ToA can be merged to calculate the cross-correlation function. Here, the shortest accessible time is given by the time interval between X-ray pulses.

Author contact: Yuriy Chushkin, chushkin@esrf.fr
Jonathan Correa, jonathan.correa@desy.de
Marco Cammarata, marco.cammarata@esrf.fr

References

1. J. Correa et al., 'TEMPUS, a Timepix4-based system for the event based detection of X-rays', J. Synchrotron Rad. 31, 1209-1216 (2024).
2. X. Llopart et al., 'Timepix4, a large area pixel detector readout chip which can be tiled on 4 sides providing sub-200 ps timestamp binning', JINST 17, C01044 (2022).
3. S.B. Dierker et al., 'X-Ray Photon Correlation Spectroscopy Study of Brownian Motion of Gold Colloids in Glycerol', Phys. Rev. Lett. 75, 449–452 (1995).

Original publication

'Achieving nanosecond time resolution with a two-dimensional X-ray detector', Journal of Synchrotron Radiation 32, 1220–1227 (2025). DOI: 10.1107/S1600577525006599

Yuriy Chushkin[1], Jonathan Correa[2,3], Alexandr Ignatenko[1], David Pennicard[2,3], Sabine Lange[2,3], Sergei Fridman[2,3], Sebastian Karl[5], Björn Senfftleben[6], Felix Lehmkühler[2,7], Fabian Westermeier[2], Heinz Graafsma[2,3] and Marco Cammarata[1]

1. ESRF – The European Synchrotron, Grenoble, France
2. Deutsches Elektronen-Synchrotron DESY, Hamburg, Germany
3. Center for Free-Electron Laser Science CFEL, DESY, Hamburg, Germany
4. Friedrich Schiller University Jena, Jena, Germany
5. University of Erlangen-Nuremberg, Erlangen, Germany
6. European XFEL GmbH, Schenefeld, Germany
7. The Hamburg Centre for Ultrafast Imaging, Hamburg, Germany

Observation of orbital quantum vortices

3D dichroism imaging in soft X-ray angle-resolved photoemission spectroscopy reveals orbital momentum-space quantum vortices

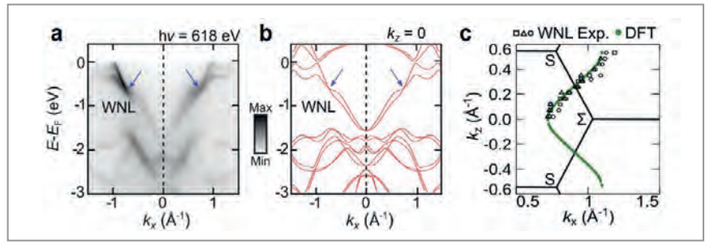

Figure 2

SX-ARPES data (a) and density functional theory band structure calculation (b) taken on TaAs. The arrows indicate the two-fold degenerate crossing points corresponding to the almost movable Weyl nodal line (WNL) which undulates to the full 3D Brillouin zone (c). All figures are adapted from the original publication (see article title and DOI below) under the Creative Commons Attribution 4.0 International license.

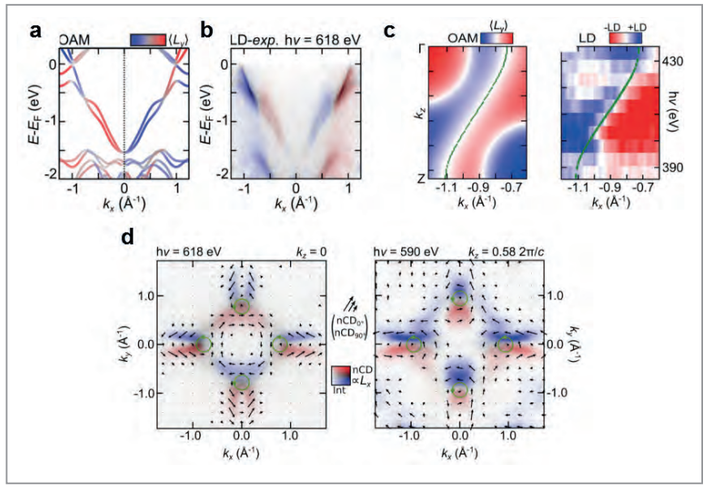

Figure 3

Sign switch of the OAM as obtained from a) density functional theory calculation and b) linear dichroism (LD) SX-ARPES. c) In full 3D momentum space, the sign change is directly at the almost movable Weyl nodal line. d) Around the nodal line, the OAM forms a vortex texture which is reconstructed from circular dichroism (CD) SX-ARPES measurements. Because of the four-fold crystal symmetry, there are four nodal lines and four vortex windings indicated by the green circles. All figures are adapted from the original publication. (All figures adapted from the original publication; CC BY 4.0).

Vortices are ubiquitous in nature, with familiar examples like tornadoes or whirls in turbulent fluids. Moreover, in the quantum realm, the formation of vortices is central to disparate key phenomena of quantum matter physics, such as flux quantisation in type-II superconductors. In contrast to, e.g. tornadoes, which can simply dissipate by slowing down the rotation speed, quantum vortices are particularly stable. This robustness traces back to the geometrical concept of topology characterising the winding properties of the underlying vector field configuration. Interestingly, the wave nature of electrons in crystalline solids, expressed by wave numbers (or momenta) *k*, may also allow for the formation of quantised vortex textures. Those may not appear in real- but rather momentum-, i.e. *k*-space. Here, the authors have proven the existence of momentum-space vortices for the first time (Fig. 1).

Topological defects (also called topological solitons) are stable textures which cannot be removed by adiabatic changes of their supporting structure. In the context of condensed matter physics, the latter can be either the crystal lattice, with the topological defect being described in conventional real space, or the electronic band structure. In this case, one finds a characteristic winding of pseudospin around Dirac- or Weyl-type band degeneracies in topological quantum materials. One of the most prominent examples is the monopole texture around chiral fermion excitations in topological semimetals. In recent studies, it has been shown that this chirality reflects itself in an important quantum degree of freedom, the orbital angular momentum (OAM) of the electronic states [1]. Recent experimental advances, in turn, have proven that such chiral OAM textures can be probed by soft X-ray angle-resolved photoemission spectroscopy (SX-ARPES) in combination with dichroism. In particular, dichroism SX-ARPES experiments of two pilot studies were carried out at the ASPHERE end station, located at beamline P04 of the PETRA III storage ring [1,2].

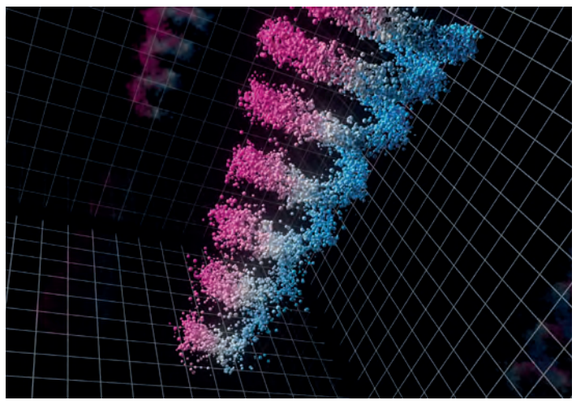

Figure 1

Schematic 'quantum tornadoes' in momentum space.

In the present work, the authors have now focused on the question whether topological quantum materials can also host other types of quantum textures beyond monopoles. In particular, the focus was on the search for higher-dimensional objects, i.e. momentum-space quantum vortices. In fact, theoretical studies have predicted that these form in so-called nodal line semimetals in which the band degeneracies do not appear as zero-dimensional points but rather one-dimensional lines in momentum space [3]. However, these inspiring model considerations were based on simplified two-band models, and a direct proof in realistic materials has remained elusive.

This has now been achieved by an international research team with scientists from the Würzburg-Dresden Cluster of Excellence ctd.qmat, the NTNU Trondheim and CAU Kiel as well as groups from China, Italy and the USA being directly involved. The team has investigated a topological semimetal TaAs. This compound belongs to a family of non-centrosymmetric materials, predominantly known as a paradigmatic class of Weyl semimetals [1]. In this work, the authors could experimentally establish another (new) type of topological excitation called almost movable Weyl nodal lines. These have been predicted by theory to appear in materials belonging to this space group [4] but their existence has not been verified experimentally so far. Using high-resolution SX-ARPES (again carried out at the ASPHERE setup), the authors could identify a crossing point in the TaAs valence bands to form a line degeneracy which undulates through 3D *k*-space and has the exact characteristic of the theoretically predicted feature (Fig. 2).

The key finding of this study is the decisive modulation of the eigenstates exactly at the crossing point (Fig. 3). Again, OAM is found to play a pivotal role. That is, a combination of crystal- and time-reversal symmetries enforce the OAM to change sign at the nodal line. This sign change, in turn, is directly reflected in the dichroic SX-ARPES measurements. A more precise symmetry analysis proves that in every horizontal slice through the nodal line, the OAM has to form a vortex-like winding texture, i.e. in total a 'quantum tornado' in momentum space (Fig. 1). These vortices can be reconstructed from experimental k_x-k_y circular dichroism maps with photon-energy-dependent measurements allowing for k_z-sensitive dichroic 3D imaging.

This work does not only unveil a hitherto completely unobserved topological quantum texture, i.e. momentum space orbital vortex lines; moreover, it establishes 3D dichroism imaging in SX-ARPES as an approach to uncover orbital textures in 3D quantum materials. Such textures (like the orbital vortex lines observed in the present study) may, in turn, be relevant in the research on orbitronic applications, aiming to make use of the OAM as an information carrying quantum degree of freedom.

Author contact: Maximilian Ünzelmann, maximilian.uenzelmann@uni-wuerzburg.de

References

1. M. Ünzelmann et al., 'Momentum-space signatures of Berry flux monopoles in the Weyl semimetal TaAs', Nat. Commun., 12, 3650 (2021)
2. Stefanie Suzanne Brinkman et al., 'Chirality-Driven Orbital Angular Momentum and Circular Dichroism in CoSi', Phys. Rev. Lett. 132, 196402 (2024)
3. Lih-King Lim et al., 'Pseudospin Vortex Ring with a Nodal Line in Three Dimensions', Phys. Rev. Lett. 118, 016401 (2017)
4. M. M. Hirschmann et al., 'Symmetry-enforced band crossings in tetragonal materials: Dirac and Weyl degeneracies on points, lines, and planes', Phys. Rev. Mater. 5, 054202 (2021)

Original publication

'Imaging Orbital Vortex Lines in Three-Dimensional Momentum Space' Physical Review X 15, 011032 (2025).
DOI: 10.1103/PhysRevX.15.011032

Malte T. Figgemeier, M. Ünzelmann, P. Eck, J. Schusser, L. Crippa, N. Neu, B. Geldiyev, P. Kagerer, J. Buck, M. Kalläne, M. Hoesch, K. Rossnagel, T. Siegrist, L.-K. Lim, R. Moessner, G. Sangiovanni, D. Di Sante, F. Reinert and H. Bentmann

For affiliation, please refer to original publication.

Elucidating the structure of liquid carbon

European XFEL enables an unprecedented glance into the peculiar liquid state of carbon

Although carbon is one of the most common and chemically stable elements in nature, remarkably little is known about its liquid phase. At normal pressures, carbon transitions directly from solid to vapour; pressure is required to form a liquid. Under such extreme conditions, its melting temperature becomes extraordinarily high, making it impossible to statically contain liquid carbon for experimental studies using any conventional material. Therefore, dynamic experiments transiently creating liquid carbon are needed to overcome this limitation. Laser-driven shock compression combined with *in situ* probing by X-ray pulses from the European XFEL has now provided unique insights into the structure and melting properties of liquid carbon.

Our international team of 123 scientists from more than ten different countries transiently produced liquid carbon by driving strong shock compression waves into solid carbon samples using the pulsed high-energy laser DiPOLE 100-X at the High Energy Density-Helmholtz International Beamline for Extreme Fields (HED-HIBEF) instrument of EuXFEL (Fig. 1). In this way, pressures exceeding 1 Mbar (100 GPa) were achieved and the compression waves simultaneously heated the samples to ~7000 K, forming liquid carbon for a few nanoseconds. *In situ* snapshots of the structure were obtained by diffraction of ultrabright X-ray pulses of the European XFEL with a duration of 25 fs. When we subjected the samples to lower pressures and temperatures, we found compressed diamond. At intermediate pressures, a coexistence state of diamond and liquid carbon was created. Using these observations, we mapped the melting line of diamond and determined its volume change and latent heat at melting.

We found liquid carbon to be a complex fluid with a tetrahedral structure similar to that of water (Fig. 2a). The structure has a coordination number around four, meaning that each central carbon atom has an average of four nearest neighbours. This is in contrast to simpler liquids which usually have higher coordination numbers [1]. Moreover, we found that the melting temperature of carbon is about 6700 K at a pressure of 1.2 Mbar (120 GPa).

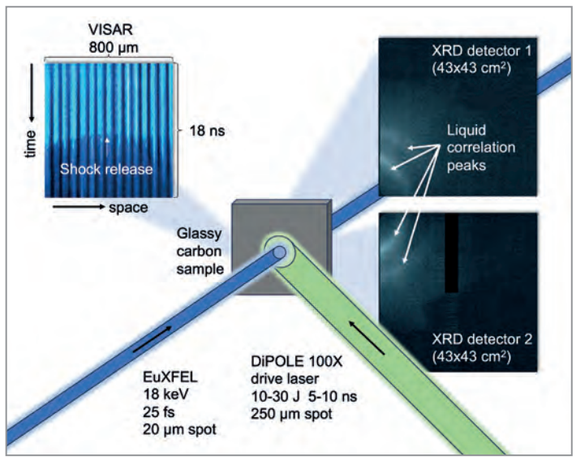

Figure 1

Schematic of the experimental setup at the HED-HIBEF instrument at European XFEL. The DiPOLE 100X drive laser creates a shock wave that simultaneously compresses and heats the glassy carbon samples. The structure is then probed *in situ* by an XFEL pulse, while an optical velocity interferometer system for any reflector (VISAR) captures the shock dynamics (image from original publication (CC-BY 4.0)).

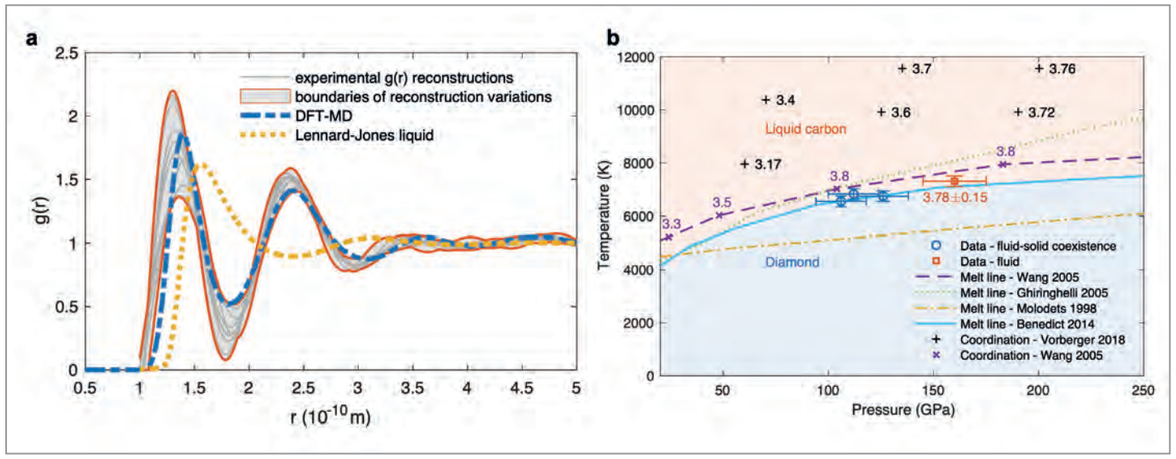

Figure 2

a) Experimentally determined pair correlation function of liquid carbon compared with simple (Lennard-Jones liquid) and sophisticated (DFT-MD) models.

b) Our experimental data of the melting transition and the first coordination number of liquid carbon in comparison to different theoretical predictions.

(Images from original publication (CC BY 4.0))

Our measurements support the liquid carbon structure predicted by elaborate density functional theory with molecular dynamics (DFT-MD) simulations [2] and disagree with simpler models which have been used to describe, e.g. planetary interiors and inertial confinement fusion concepts. Moreover, only the sophisticated simulations agree with the experimentally inferred melting temperature. These insights will help to clarify the role of carbon in the interior structure and evolution of icy giant planets such as Uranus, Neptune and carbon-rich exoplanets. Moreover, our findings will inform the choice of ablator materials that accelerate the fusion fuel during inertial fusion implosions and the synthesis of certain carbon materials, such as the long-sought but only predicted superhard and tough eight-atom body-centred cubic (BC8) structure of carbon.

These measurements were enabled by the integrated dynamic-compression and X-ray-diagnostics capability assembled through HIBEF. Crucial elements for the presented study included the DiPOLE 100-X laser driver, and a precision interaction chamber optimised for diffraction from dynamically compressed samples using VAREX area detectors. The diffraction setup contributed by DESY to the HIBEF instrumentation provided the geometry, detectors and alignment/optical infrastructure needed to capture high-quality, single-pulse diffraction patterns from the transient liquid state during the few-nanosecond time window of the shock [3].

Author contact: Dominik Kraus, dominik.kraus@uni-rostock.de
Hanns-Peter Liermann, hanns-peter.liermann@desy.de
Cornelius Strohm, cornelius.strohm@desy.de

References

1. C. J. Hull et al., 'The liquid state of carbon', Chem. Phys. Lett. 749, 137341 (2020).
2. J. Vorberger et al., 'The structure in warm dense carbon', High Energy Density Phys. 35, 100737 (2020).
3. M. G. Gorman et al., 'Shock compression experiments using the DiPOLE 100-X laser on the high energy density instrument at the European x-ray free electron laser: Quantitative structural analysis of liquid Sn', J. Appl. Phys. 135, 165902 (2024).

Original publication

'The structure of liquid carbon elucidated by in situ X-ray diffraction', Nature 642, 351-355 (2025).
DOI: 10.1038/s41586-025-09035-6

D. Kraus, J. Rips, M. Schörner, M. G. Stevenson, J. Vorberger, D. Ranjan, J. Lütgert, B. Heuser, J. H. Eggert, H.-P. Liermann, I. I. Oleynik, S. Pandolfi, R. Redmer, A. Sollier, C. Strohm, T. J. Volz, B. Albertazzi, S. J. Ali, L. Antonelli, C. Bähtz, O. B. Ball, S. Banerjee, A. B. Belonoshko, C. A. Bolme, V. Bouffetier, R. Briggs, K. Buakor, T. Butcher, V. Cerantola, J. Chantel, A. L. Coleman, J. Collier, G. W. Collins, A. J. Comley, T. E. Cowan, G. Cristoforetti, H. Cynn, A. Descamps, A. Di Cicco, S. Di Dio Cafiso, F. Dorchies, M. J. Duff, A. Dwivedi, C. Edwards, D. Errandonea, S. Galitskiy, E. Galtier,H. Ginestet, L. Gizzi, A. Gleason, S. Göde, J. M. Gonzalez, M. G. Gorman, M. Harmand, N. J. Hartley, P. G. Heighway, C. Hernandez-Gomez, A. Higginbotham, H. Höppner, R. J. Husband, T. M. Hutchinson, H. Hwang, D. A. Keen, J. Kim, P. Koester, Z. Konôpková, A. Krygier, L. Labate, A. Laso Garcia, A. E. Lazicki, Y. Lee, P. Mason, M. Masruri, B. Massani, E. E. McBride, J. D. McHardy, D. McGonegle, C. McGuire, R. S. McWilliams, S. Merkel, G. Morard, B. Nagler, M. Nakatsutsumi, K. Nguyen-Cong, A.-M. Norton, N. Ozaki, C. Otzen, D. J. Peake, A. Pelka, K. A. Pereira, J. P. Phillips, C. Prescher, T. R. Preston, L. Randolph, A. Ravasio, D. Santamaria-Perez, D. J. Savage, M. Schölmerich, J.-P. Schwinkendorf, S. Singh, J. Smith, R. F. Smith, J. Spear, C. Spindloe, T.-A. Suer, M. Tang, M. Toncian, T. Toncian, S. J. Tracy, A. Trapananti, C. E. Vennari, T. Vinci, M. Tyldesley, S. C. Vogel, J. P. S. Walsh, J. S. Wark, J. T. Willman, L. Wollenweber, U. Zastrau, E. Brambrink, K. Appel and M. I. McMahon

For affiliations, please refer to the original publication.

Innovations for health: when molecular spectroscopy meets lasers and photonics

Spectral fingerprinting of aqueous glucose

The International Diabetes Federation reports that one in nine adults worldwide lives with diabetes, and nearly half remain undiagnosed. Continuous glucose monitoring is therefore vital, yet current methods—based on blood samples or test strips—are invasive and imprecise. Infrared vibrational spectroscopy has recently emerged as a promising alternative [1], exploiting the rich molecular information within the mid-infrared (Mid-IR) fingerprint region, where each molecule exhibits a unique spectral signature (Fig. 1).

Detecting these subtle vibrations, however, is far from straightforward. Water, the main constituent of biological fluids, strongly absorbs infrared light, effectively drowning out weaker molecular signals. Conventional FTIR spectroscopy can detect glucose only at concentrations above around 50 mM [2], whereas normal blood glucose typically lies between 4 and 11 mM. To overcome this gap, we turned to a powerful nonlinear optical method called vibrational sum-frequency generation (VSFG).

Figure 1
Artistic view of spectral fingerprinting of glucose molecule.
(Credit: Tim Laarmann, DESY)

In VSFG spectroscopy, two beams of light—one visible and one infrared—are interacting with a sample at the same time. When the infrared beam resonates with a particular molecular vibration and the visible beam interacts with that vibrating molecule, the process generates a new beam at the sum of their frequencies. Because the VSFG process can only occur in regions where centrosymmetry is broken, so it is inherently interface-sensitive. Moreover, VSFG's selectivity brings two major advantages for glucose sensing: it minimises the IR absorption by water and enhances the signal from molecules located at interfaces. An additional benefit is that the emitted VSFG lies in the visible range, which can be efficiently detected using standard silicon-based detectors.

To observe glucose-VSFG, a light source capable of delivering ultrashort Mid-IR pulses at high average power was essential. Together with Class 5 Photonics GmbH, a company founded in 2014 as a spin-off from DESY and the Helmholtz-Institute Jena, our team developed a state-of-the-art Mid-IR optical parametric chirped-pulse amplification (OPCPA) system. Building upon years of research and development into nonlinear optical materials, we created a new laser architecture known as the ´White Dwarf HE DFG prototype´ [3, 4]. At its core lies the $LiGaS_2$ crystal, a material with exceptional optical properties that enables the efficient conversion of 1 µm pump light directly into broadband Mid-IR pulses. The system generates pulses centred at 9 µm with a duration of only 114 fs, an average power of 245 mW, and a pulse energy of 1.2 µJ at a high repetition rate of 200 kHz (Fig. 2).

Using this advanced laser source, we measured the VSFG spectra of glucose solutions from 10 to 1000 mM. As shown in Fig. 3, all spectra exhibit a distinct resonance at 1035 cm^{-1}, corresponding to the C–O stretching vibration of glucose molecules. To ensure that this signal indeed arises from glucose, we compared the results with a reference measurement of pure water (shown in grey). The absence of any significant spectral feature in the water trace confirms that the observed VSFG peak originates solely from the glucose molecules. Furthermore, the intensity of the 1035 cm^{-1} band scales proportionally with glucose concentration, following a clear quantitative relationship. To the best of our knowledge, this work represents the first observation of glucose VSFG signals between 1000 and 1200 cm^{-1} in aqueous environment.

The significance of this research extends far beyond the detection of glucose alone. Our work complements pioneering efforts by Ferenc Krausz, the 2023 Nobel Laureate in Physics, whose team achieved field-resolved infrared spectroscopy of native blood serum [5]. These techniques could lead to the development of a new generation of all-optical, non-invasive and label-free diagnostic tools, opening avenues for early disease detection, real-time medical monitoring, and personalised healthcare.

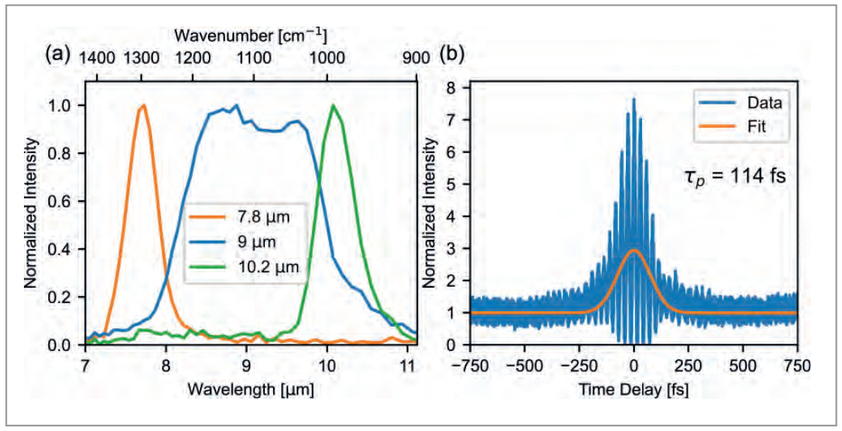

Figure 2
a) Wavelength-tunable Mid-IR pulse spectra at 7.8 µm, 9 µm, and 10.2 µm central wavelength. b) The second-order interferometric autocorrelation trace (blue data points) of the broadband, 9 µm Mid-IR pulse fitted with a Gaussian function (orange line) reveals a pulse duration 114 fs.

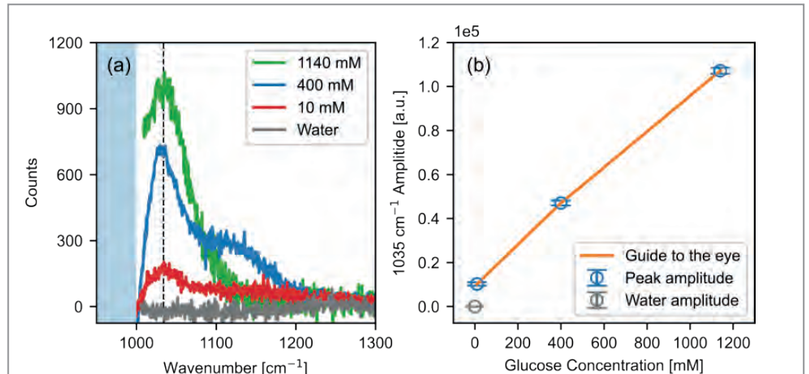

Figure 3
a) Recorded VSFG spectra from aqueous glucose for different concentrations (1140, 400, and 10 mM). The spectral range < 1000 cm^{-1} affected by background signal from the visible pump is indicated in blue and the pure water solvent spectrum is shown in gray. b) The Lorentzian amplitude of the 1035 cm^{-1} C-O stretch vibration is given as a function of glucose concentrations. The solid line is a guide to the eye.

Author contact: Cheng Luo, cheng.luo@desy.de
Tim Laarmann, tim.laarmann@desy.de
Mahesh Namboodiri, mahesh.namboodiri@desy.de

References

1. M. Huber et al., 'Infrared molecular fingerprinting of blood-based liquid biopsies for the detection of cancer', eLife 10, 68758 (2021).
2. J.-J. Max and C. Chapados, 'Glucose and fructose hydrates in aqueous solution by IR spectroscopy', J. Phys. Chem. A 111, 2679–2689 (2007).
3. M. Namboodiri et al., 'Optical properties of Li-based nonlinear crystals for high power mid-IR OPCPA pumped at 1 µm under realistic operational conditions', Opt. Mater. Express 11, 231-239 (2021).
4. M. Namboodiri et al., 'Versatile few-cycle high-energy MID-IR OPCPA for nonlinear optics, spectroscopy and imaging', Opt. Continuum 1, 1157–1164 (2022).
5. I. Pupeza et al., 'Field-resolved infrared spectroscopy of biological systems', Nature 577, 52–59 (2020).

Original publication

'Spectral fingerprinting of aqueous glucose with ultra-broadband vibrational sum-frequency generation spectroscopy at bio-relevant low concentration', Optics Express 33, 6080–6091 (2025).
DOI: 10.1364/OE.544862

Malte Cheng Luo[1,2], Mahesh Namboodiri[1], Michael Schulz[3], Robert Riedel[3], Mark James Prandolini[3,4] and Tim Laarmann[1,2]

1. Deutsches Elektronen-Synchrotron DESY, Hamburg, Germany
2. The Hamburg Centre for Ultrafast Imaging CUI, of Hamburg, Hamburg, Germany
3. Class 5 Photonics GmbH, Hamburg, Germany
4. Institute of Experimental Physics, University of Hamburg, Hamburg, Germany

Towards watching ultrafast spin transfer

Full polarisation control opens new opportunities at FLASH

Understanding the dynamical behaviour of electrons in multi-element magnetic materials is fundamental for future applications such as energy-efficient magnetic storage or spintronic devices. X-rays with circular polarisation can probe the laser-induced manipulation of the electronic structure and thus provide deep insights into the coupling between electrons, spins and the atomic lattice. At the free-electron laser FLASH, the new third harmonic afterburner undulator generates ultra-short X-ray pulses with variable polarisation. We presented the first time-resolved X-ray magnetic circular dichroism experiments at FLASH2 on FeNi and CoPt alloys using the new beamline FL23.

The continuous transformation in the digital age leads to an ever-increasing demand for data storage, requiring higher storage densities and energy-efficient technologies for data processing. Magnetic materials that are interesting for such applications consist of a combination of one or more transition metal ferromagnets (Co, Fe and Ni) with heavier elements such as platinum (Pt) or magnetic rare earth elements. A very fast and efficient way of manipulating magnetic order involves ultrashort laser pulses. While laser-induced magnetisation changes typically occur on time scales of 100 femtoseconds (fs) or longer, the researchers in this field have recently started to understand that electronic processes on time scales of only a few fs play a crucial role as well by transferring spin between different elements. For the spectroscopic investigation of these processes, ultra-short soft X-ray pulses with circularly polarisation and variable energy are needed. After the last FLASH2020+ upgrade of the free-electron laser (FEL) FLASH, such studies have finally become possible.

To probe ultrafast spin transfer processes, circularly polarised soft X-ray pulses are tuned to electronic transitions from localised core levels to valence states of the different elemental species. Time-resolved X-ray magnetic circular dichroism (XMCD) allows for the determination of the spin-resolved electronic structure and its changes for each element based on the difference in absorption for opposite helicities of the X-rays.

To make this possible, the third-harmonic helical afterburner undulator at FLASH2 has recently been installed as part of the FLASH2020+ upgrade; it enables full polarisation control up to a photon energy of 930 eV [1]. We used this new capability to perform XMCD measurements on FeNi and CoPt alloys at the $L_{2,3}$-edges of the important 3d-transition metals Co, Fe and Ni in the MUSIX end station [2] at the new monochromator beamline FL23 [3]. In this beamline (Fig. 1), a split beam normalisation scheme with a transmission grating is implemented to normalise FEL intensity fluctuations [4]. A Kirkpatrick-Baez active optics system (KAOS2) is used to focus the beam onto the FeNi or CoPt sample which is then transmitted and detected with a photodiode. A new pump laser system for the FL23 beamline was developed to enable ultrafast excitations at a wavelength of 1030 nm. In MUSIX, an in-vacuum electromagnet allows for switching the magnetisation state of the sample. The resulting change in absorption can be seen in the left inset of Fig. 1, while the magnetic hysteresis curve is shown in the right inset. With this setup, static X-ray absorption spectroscopy (XAS) and XMCD spectra on CoPt and FeNi alloys are measured as a first benchmark. Fig. 2a,b shows the difference in X-ray absorption across the Fe $L_{2,3}$- and Ni L_3-edge when the magnetisation direction is flipped. Fig. 2c,d shows the corresponding XMCD signal. By comparing with reference spectra measured at the PM3 beamline at the synchrotron radiation source BESSY II in Berlin (Germany) , degrees of circular polarisation close to 100% at FLASH2 could be confirmed.

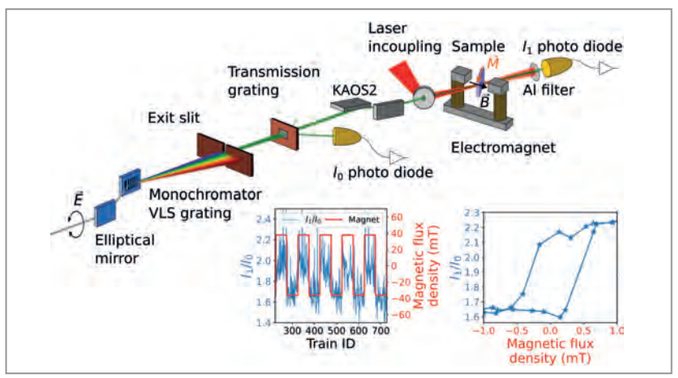

Figure 1
Experimental setup used for the XMCD measurements at FL23. See text for more details.

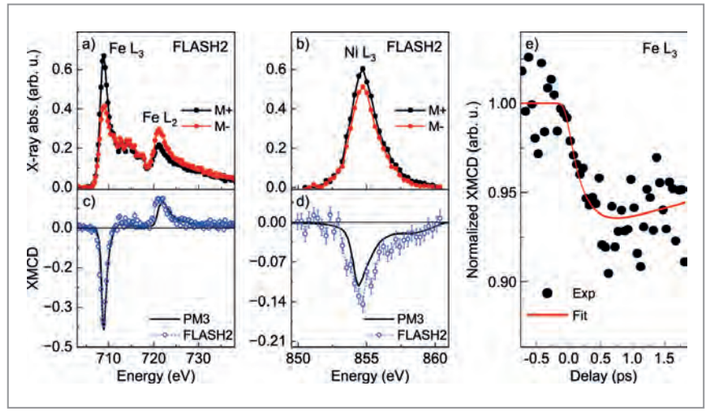

Figure 2
a-d) Static XAS and XMCD at the Fe L_{23} and Ni L_3-edges recorded at the FL23 beamline at FLASH2 with circularly polarised X-ray pulses. XMCD reference spectra were taken from the same samples at the PM3 beamline of BESSY II. e) Normalised transient demagnetisation dynamics in the FeNi alloy measured at the Fe L_3 absorption resonance. The solid red line represents an exponential fit with Gaussian convolution.

The feasibility of time-resolved XMCD studies is demonstrated for the FeNi sample at the Fe L_3 absorption edge (Fig. 2e). The temporal resolution of the ultrafast reduction of the XMCD signal is ~270 fs, mostly limited by the pulse elongation due to the use of a single X-ray monochromator. In a second study by our collaboration, an investigation on the electronic and spin dynamics in a $Co_{50}Pt_{50}$ alloy was performed [5].

In the future, the temporal resolution at FL23 can be improved significantly using its pulse-length preserving double monochromator design. Moreover, a dedicated end station for the investigation of magnetic systems, named SPINFLASH, with a superconducting magnet system, is currently being set up. These improvements will allow the investigation of spin transfer mechanisms with unprecedented precision and open new avenues for a wide range of studies on magnetic and chiral materials.

Author contact:
Simon Marotzke, simon.marotzke@desy.de
Niko Pontius, pontius@helmholtz-berlin.de
Martin Beye, martin.beye@fysik.su.se
Nele Thielemann-Kühn, nele.thielemann@helmholtz-berlin.de

References

1. M. Tischer, H. Bienert, K. Götze, P. Neumann, T. Ramm, A. Schöps, P. Talkovski, S. Telawane and P. Vagin, 'Construction and commissioning of an APPLE-III afterburner undulator as a prototype for radiators in the new seeding line of FLASH2020+', J. Phys. Conf. Ser. 3010, 012045 (2025).
2. M. Beye, R. Y. Engel, J. O. Schunck, S. Dziarzhytski, G. Brenner and P. S. Miedema, 'Non-linear soft x-ray methods on solids with MUSIX—the multi-dimensional spectroscopy and inelastic x-ray scattering endstation', J. Phys. Condens. Matter 31, 014003 (2018).
3. L. Poletto, F. Frassetto, G. Brenner, M. Kuhlmann and E. Plönjes, 'Double-grating monochromatic beamline with ultrafast response for FLASH2 at DESY', J. Synchrotron Rad. 25, 131 (2018).
4. G. Brenner, S. Dziarzhytski, P. S. Miedema, B. Rösner, C. David and M. Beye, 'Normalized single-shot x-ray absorption spectroscopy at a free-electron laser', Opt. Lett. 44, 2157 (2019).
5. M. Pavelka, S. Marotzke, R.-P.Wang, M. F. Elhanoty, G. Brenner, S. Dziarzhytski, S. Jana, W. D. Engel, C. v. Korff Schmising, D. Gupta, I. Vaskivskyi, T. Amrhein, N. Thielemann-Kühn, M. Weinelt, R. Knut, G. Cirmi, J. Rönsch-Schulenberg, E. Schneidmiller, C. Schüßler-Langeheine, M. Beye, N. Pontius, O. Grånäs and H. A. Dürr, 'Femtosecond charge and spin dynamics in a $Co_{50}Pt_{50}$ alloy', Struct. Dyn. 12, 024303 (2025).

Original publication

'First experiments with ultrashort, circularly polarized soft x-ray pulses at FLASH2', Structural Dynamics 12, 034301 (2025).
DOI: 10.1063/4.0000298

Simon Marotzke[1,2], Deeksha Gupta[3], Ru-Pan Wang[1], Martin Pavelka[4], Siarhei Dziarzhytski[1], Clemens von Korff Schmising[5], Somnath Jana[5], Nele Thielemann-Kühn[6], Tim Amrhein[6], Martin Weinelt[6], Igor Vaskivskyi[7], Ronny Knut[4], Dieter Engel[5], Markus Braune[1], Markus Ilchen[1,8,9], Sara Savio[8,10], Thorsten Otto[1,8], Kai Tiedtke[1], Vincent Scheppe[3,6], Juliane Rönsch-Schulenberg[1], Evgeny Schneidmiller[1], Skirmantas Alisauskas[1], Ayhan Tajalli[1], Giovanni Cirmi[1], Hüseyin Cankaya[1], Pavel Vagin[1], Kathrin Götze[1], Christian Schüßler-Langeheine[3], Hermann A. Dürr[4], Martin Beye[1,11], Günther Brenner[1] and Niko Pontius[3]

1. Deutsches Elektronen-Synchrotron DESY, Hamburg, Germany
2. Institut für Experimentelle und Angewandte Physik, Christian-Albrechts-Universität zu Kiel, Kiel, Germany
3. Helmholtz-Zentrum Berlin für Materialien und Energie, Berlin, Germany
4. Department of Physics and Astronomy, Uppsala University, Uppsala, Sweden
5. Max Born Institute for Nonlinear Optics and Short Pulse Spectroscopy, Berlin, Germany
6. Freie Universität Berlin, Fachbereich Physik, Berlin, Germany
7. J. Stefan Institute, Ljubljana, Slovenia
8. University of Hamburg, Hamburg, Germany
9. Center for Free-Electron Laser Science CFEL, DESY, Hamburg, Germany
10. Technische Universität Dortmund, Dortmund, Germany
11. Stockholm University, Stockholm, Sweden

Power unleashed on a chip

Large-mode-area integrated photonics for high-power, low-noise light generation

Integrated photonics enables dramatic reductions in the size, weight, and power consumption of optical systems, offering disruptive potential in space, medical, and communication technologies. Yet, after decades of research, the field has lacked a truly integrated, low-noise, high-power light source, relying instead on bulky benchtop lasers that limit scalability and deployment. Our work introduces the large-mode-area (LMA) technology to integrated photonics, achieving watt-level output power from a miniature chip: a performance previously unattainable with on-chip devices, paving the way toward compact, mass-producible photonic systems capable of replacing traditional benchtop sources.

High-power optical systems traditionally scale with physical volume — the larger the system, the greater its ability to store and extract energy. This scaling, however, runs directly counter to the compact nature of integrated photonic chips, which are designed for miniaturisation in a planar geometry (Fig. 1). In such systems, increasing energy extraction by simply increasing volume is not straightforward. Our research addresses this challenge by leveraging two inherent aspects of integrated photonics: its large planar surface area and the long optical path length in tightly-guided circuits to create an effectively large optical interaction volume within a chip-scale footprint.

This concept forms the foundation of our new large-mode-area (LMA) integrated photonics approach, which we have demonstrated for the first time. In this system, a light signal that is to be amplified is launched into a narrow silicon nitride (SiN) waveguide coated with a carefully controlled layer of aluminium oxide (Al_2O_3). This layer is doped with thulium ions (Tm^{3+}), which act as a temporary storage to transfer energy from the pump light to the signal light for amplification. The SiN waveguide is routed through many "LMA" regions. Initially, the optical mode is small and tightly confined within the SiN core. As it propagates, it encounters a specially designed taper that gradually narrows the waveguide width along its length (Fig. 2). This adiabatic taper allows the guided light to expand smoothly beyond the SiN region, enlarging its mode area and causing it to "float" through the doped Al_2O_3 layer above, while still remaining weakly coupled to the SiN structure beneath it — much like a hot-air balloon that drifts freely but remains tethered to its basket. This is the LMA region, where energy conversion from the optical pump to the signal takes place. Because the optical mode is now much larger, it can interact with many more ions simultaneously than conventional waveguides allow, enabling much greater energy extraction — analogous to how a large snowplow can clear more snow at once than a small shovel.

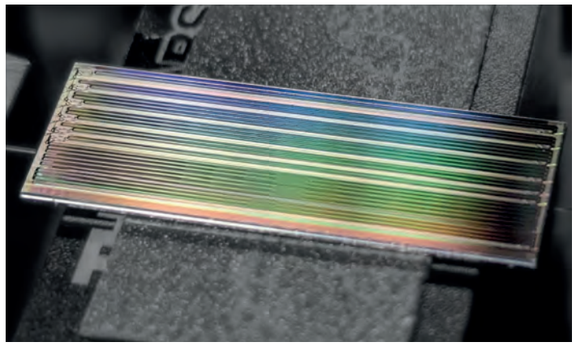

Figure 1

Photo of our silicon photonic chip containing many LMA amplifiers. Each chip is ~ 1x2 cm² in size and has space for up to 50 amplifier devices which can be combined with other photonic structures.

With this approach, we have achieved optical output power 10–20 times higher than the best reported values in over three decades of integrated photonics research (Fig. 3), and 4–5 times higher than telecom grade benchtop fiber amplifiers. One might expect such a power increase to require a proportionally large device, but our entire amplifier fits within a footprint of just 4.5 mm² — a remarkable demonstration of both scalability and compactness. Moreover, our LMA waveguide exhibits significant advantages over traditional LMA fibers: it supports only the fundamental mode, ensuring excellent beam quality, while offering an ultra-small footprint, which is unattainable with fibre-based systems.

This development represents a paradigm shift in integrated photonics. It opens a path toward on-chip, high-power, low-noise light sources and amplifiers that could transform multiple application domains. In space photonics, these integrated amplifiers can support lightweight optical systems for planetary exploration and deep-space communications. Furthermore, using the LMA approach as a component of high-energy, chip-scale femtosecond lasers opens up applications in low-noise microwave generation, high-speed sampling, and timing distribution in large-scale facilities. Looking ahead, the same architecture can be extended to other rare-earth ions, such as erbium, which may allow this platform to replace conventional erbium-doped fibre amplifiers (EDFA) in many applications. Such integrated amplifiers could serve not only as boosters for long-haul communication links but also as active components within fully integrated photonic circuits: combining amplification, switching, and multiplexing on a single silicon chip. The result is a compact, efficient, and versatile photonic system that brings the long-promised scalability of integrated photonics into practical reality.

Author contact:
Jan Lorenzen, jan.lorenzen@desy.de
Neetesh Singh, neetesh.singh@desy.de

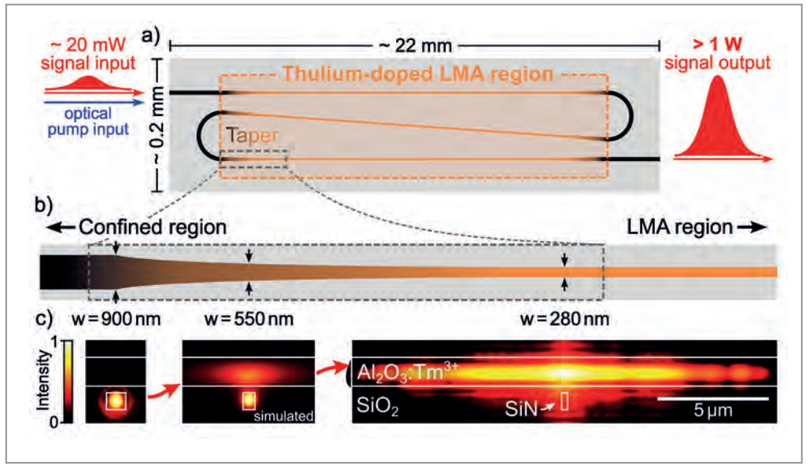

Figure 2

Schematic of the on-chip amplifier design. a) Top-down view of a 6-cm-long amplifier waveguide. The black lines indicate sections where the light is fully confined in the SiN waveguide, while orange lines indicate LMA sections, where the light is almost entirely in the Al_2O_3 gain film. b) Zoomed-in view of the waveguide taper which slowly narrows down the SiN width (w) to create a smooth transition of the optical mode between the different sections. c) Measured images of the optical mode in the confined and LMA sections. The middle image in the transition region is simulated.

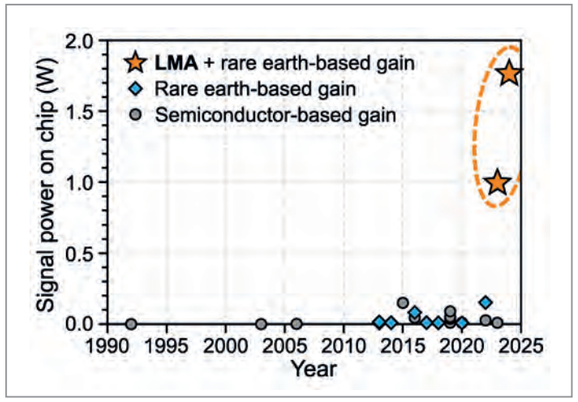

Figure 3

Comparison of the signal power level achieved on chip-scale photonic-integrated platforms with different types of gain media. Our LMA waveguide design paired with the rare earth doping (thulium) enabled an improvement of the power levels by an order of magnitude. The full list of compared references can be found in [1].

Reference

1. **N. Singh et al., 'Sub-2W tunable laser based on silicon photonics power amplifier', LSA 14.1, 18 (2025).**

Original publication

'Watt-class silicon photonics-based optical high-power amplifier', Nature Photonics 19, 307-314 (2025).
DOI: 10.1038/s41566-024-01587-9

Neetesh Singh[1], Jan Lorenzen[1], Kai Wang[2], Mahmoud A. Gaafar[1], Milan Sinobad[1], Henry Francis[3], Marvin Edelmann[1], Michael Geiselmann[3]

1. Center for Free-Electron Laser Science CFEL, DESY, Hamburg, Germany
2. Integrated Optical Systems, MESA+ Institute for Nanotechnology, University of Twente, Enschede, Netherlands
3. LIGENTEC SA, Ecublens, Switzerland

Focusing to 50 nm out of the box

Compact, aberration-corrected diamond optics promise sharper X-ray nanoimaging

Diamond refractive lenses promise crisp X-ray nanoimages at today's brightest light sources, but subtle shape errors from fabrication can blur the focus. We introduce the compact lens cube: tightly stacked diamond lens plates with built-in refractive phase plates that neutralise residual aberrations across a wide photon-energy range. Demonstrated at DESY's PETRA III, the approach delivers 50 nm focal spots near the diffraction limit with high transmission and simple integration, enabling plug-and-play nanoimaging for general users at synchrotron radiation sources and XFELs.

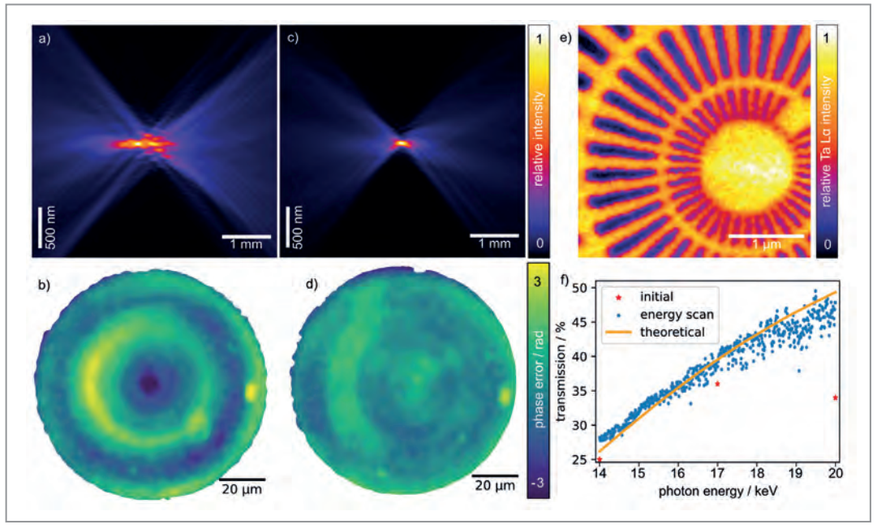

Figure 2
Performance of the combined LCs at 14 keV, as well as the transmission rate of the combined LCs over a photon energy range. a) Beam profile along the optical axis without phase plates. b) Wavefront error at the exit of the lens stack without phase plates. c) Corrected beam profile. d) Corrected wavefront. e) A 2D X-ray fluorescence image obtained by measuring Ta Lα emission from a Siemens star test sample. f) Measured and theoretical transmission of the combined LCs from 14 keV to 20 keV. Blue points are results of energy scan measurements while red stars refer to the results of initial measurements at 14, 17 and 20 keV.

Thanks to its high transmission, radiation hardness, thermal conductivity and fabrication flexibility, diamond is well suited for hard-X-ray optics [1,2]. However, lenses made by femtosecond laser ablation, just like beryllium compound refractive lenses (CRLs) [3], often retain shape imperfections that distort the wavefront and enlarge focal spots. We address this issue with our compact lens cube (LC) design: a precisely aligned stack of bi-concave, two-dimensionally focusing diamond lens plates that incorporates a thin corrective phase plate (Fig. 1a). The result is high-resolution focusing for general science users, eliminating the need for external correction optics and cumbersome alignment.

Each diamond lens has a circular aperture of at least 120 µm and a bi-concave parabolic profile with a 25 µm radius of curvature, fabricated by femtosecond laser ablation. Sixty lenses were produced and characterised in sets of ten using at-wavelength ptychography to reconstruct the complex wavefield and quantify wavefront errors [4,5]. For each set of ten lenses, a dedicated corrective phase plate was then designed from the measured wavefront to compensate its specific cumulative shape deviations. These phase plates were fabricated on thinned diamond membranes and inserted after every ten lenses, preserving optical thinness and transmission.

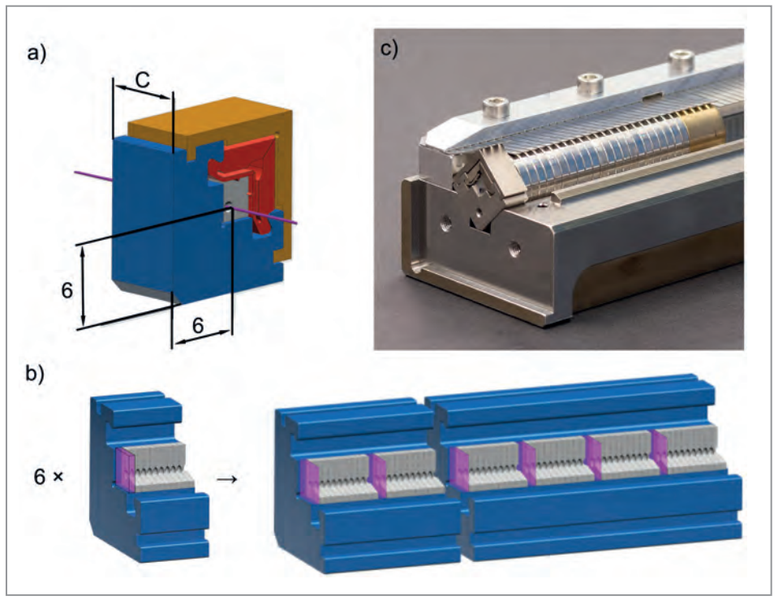

Figure 1
Concept of the aberration-corrected diamond LC. a) Sketch of a single LC. b) Six LCs, each with 10 lenses, are characterised individually. The lenses are recombined into two LCs, consisting of 20 and 40 lenses, respectively. Thin refractive phase plates are inserted after every 10 lenses. c) A CRL holder containing a LC with 10 diamond lenses followed by 22 beryllium CRLs with equivalent focal power showing their relative size.

We then configured the lenses into two LCs (Fig. 1b), with 20 and 40 lenses in each LC, respectively. Their performance was evaluated at the PtyNAMi microscope of beamline P06 at PETRA III [6], using the two lens cubes in series. Without correction, the lenses produced pronounced aberrations, visible as tails and secondary foci in the beam profile as well as wavefront distortion (Fig. 2a,b). The Strehl ratio, which quantifies the sharpness of the focus relative to an ideal lens, was below 0.4. With the integrated phase plates, however, the wavefront error dropped considerably across 14–20 keV. Previous aberration features vanished (Fig. 2c,d) and the Strehl ratio improved to 0.69 at 14 keV, 0.75 at 17 keV and 0.83 at 20 keV. The measured focal spot size of $52 \times 51\ nm^2$ reached the diffraction limit, resolving 50 nm Siemens-star features (Fig. 2e). Transmission through the combined LCs matched theory across the 14–20 keV energy range (Fig. 2f), confirming high throughput and stability for routine operation.

Two features make the LC appealing. The first one is intrinsic alignment: each lens and phase plate is fabricated and positioned with a common reference, ensuring their centres align within 5 µm, so stacking does not compound misalignments. The second one is bandwidth flexibility: distributed phase correction works over a wide photon energy range rather than a single tuned energy. Physically, the LC fits standard CRL holders and short working-distance setups, offering a smaller footprint than equivalent Be CRLs (Fig. 1c).

In practice, this enables plug-and-play nanofocusing at modern light sources: radiation-hard, compact and corrected optics ready for general user beamlines. The LC concept demonstrates, for the first time, 50 nm level focusing with diamond refractive optics, paving the way for robust nanoimaging and scanning microscopy at 4th-generation synchrotron sources and XFELs.

Author contact: Wenxin Wang, w.wang@desy.de

References

1. C. G. Schroer, M. Kuhlmann, U. T. Hunger, T. F. Günzler, O. Kurapova, S. Feste, F. Frehse, B. Lengeler, M. Drakopoulos, A. Somogyi, A. S. Simionovici, A. Snigirev, I. Snigireva, C. Schug and W. H. Schröder, 'Nanofocusing parabolic refractive x-ray lenses', Appl. Phys. Lett. 82, 1485–1487 (2003).
2. S. Terentyev, V. Blank, S. Polyakov, S. Zholudev, A. Snigirev, M. Polikarpov, T. Kolodziej, J. Qian, H. Zhou and Y. Shvyd'ko, 'Parabolic single-crystal diamond lenses for coherent x-ray imaging', Appl. Phys. Lett. 107, 111108 (2015).
3. R. Celestre, S. Antipov, E. Gomez, T. Zinn, R. Barrett and Thomas Roth, 'Polished diamond X-ray lenses', J. Synchrotron Radiat. 29, 629–643 (2022).
4. F. Seiboth, A. Schropp, M. Scholz, F. Wittwer, C. Rödel, M. Wünsche, T. Ullsperger, S. Nolte, J. Rahomäki, K. Parfeniukas, S. Giakoumidis, U. Vogt, U. Wagner, C. Rau, U. Boesenberg, J. Garrevoet, G. Falkenberg, E. C. Galtier, H. Ja Lee, B. Nagler and C. G. Schroer, 'Perfect X-ray focusing via fitting corrective glasses to aberrated optics', Nat. Commun. 8, 14623 (2017).
5. F. Seiboth, F. Wittwer, M. Scholz, M. Kahnt, M. Seyrich, A. Schropp, U. Wagner, C. Rau, J. Garrevoet, G. Falkenberg and C. G. Schroer, 'Nanofocusing with aberration-corrected rotationally parabolic refractive X-ray lenses', J. Synchrotron Radiat. 25, 108–115 (2018).
6. A. Schropp, R. Döhrmann, S. Botta, D. Brückner, M. Kahnt, M. Lyubomirskiy, C. Ossig, M. Scholz, M. Seyrich, M. E. Stuckelberger, P. Wiljes, F. Wittwer, J. Garrevoet, G. Falkenberg, Y. Fam, T. L. Sheppard, J.-D. Grunwaldtd and C. G. Schroer, 'PtyNAMi: ptychographic nano-analytical microscope', J. Appl. Crystallogr. 53, 957–971 (2020).

Original publication

'Diamond X-ray lens cubes with integrated aberration compensation', Optics Express 33 (11), 22349–22359 (2025). DOI: 10.1364/OE.562556.

Wenxin Wang[1,2], Ralph Döhrmann[1], Stephan Botta[1], Anders Madsen[2], Christian G. Schroer[1,3,4] and Frank Seiboth[1]

1. Center for X-Ray and Nano Science CXNS, DESY, Hamburg, Germany
2. European XFEL, Schenefeld, Germany
3. Department Physik, Universität Hamburg, Hamburg, Germany
4. Helmholtz Imaging, DESY, Hamburg, Germany

Lightning-fast data processing

Real-time analysis pipeline for X-ray crystallography

Every day the beamlines at PETRA III generate terabytes of raw data, with associated large costs for data storage and computing. As beamlines become more automated and detectors run at ever-higher frame rates, faster ways to process the deluge of data are essential. One type of experiment, serial crystallography, is particularly known for producing large amounts of data. In a collaborative project involving colleagues from DESY Photon Science, IT and CFEL, we established a way to process data from serial crystallography experiments streamed directly from the detector, keeping up with the rate of data production and without any need to store the data on disk in between.

Serial X-ray crystallography is an experimental technique in which millions of small crystals are exposed one-by-one to the X-ray beam, recording the resulting diffraction patterns on a two-dimensional detector. Each exposure gives only partial information about the crystal structure, but the images can be analysed to calculate the orientation of each crystal and piece together the entire three-dimensional scattering pattern. From the combined information, the structure of the material can be reconstructed. Serial crystallography is mostly used to examine protein crystals [1], but other types of material are also amenable to the technique.

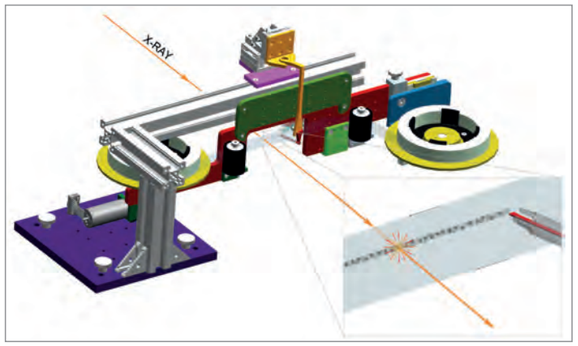

Figure 1

Design diagram showing components of the CFEL tape drive system used for serial crystallography at P11.

When carrying out an experiment, it is essential that the scientists have rapid feedback on the data they measure. With this information, scientists can adjust the experimental parameters, such as the alignment of the X-ray beam with the sample. The feedback is usually provided by processing a small fraction of the data while the experiment is still going on, or by using a simplified analysis method to get results as fast as possible.

At DESY's synchrotron light source PETRA III, serial crystallography experiments can be carried out at several beamlines. Among them is the macromolecular crystallography beamline P11, where a 'tape drive' system developed at CFEL [2] is used to convey the crystals into the path of the X-ray beam (Fig. 1). At P11, we built a system in which in BE: the data are streamed between the various data processing modules over network links. This was done using ASAP::O, a middleware system developed in the DESY IT department and designed to handle vast amounts of photon science data [3]. The overall flow diagram is shown in Fig. 2 and consists of building blocks which can be re-used for different types of experiments.

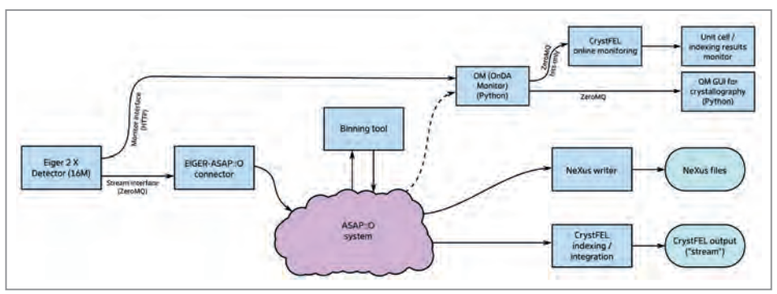

Figure 2

Flow diagram of the real-time processing system for serial crystallography, showing modular building blocks which combine to make a complete processing pipeline. The individual building blocks can be re-used for different types of experiments at other beamlines.

The data processing methods needed for serial crystallography data have previously been considered as compute-intensive, requiring high-performance computing systems with clusters of powerful computers. For instance, at LCLS in the USA, data are transferred the nearby supercomputing centre NERSC [4]. We set out to make data processing as efficient as possible by measuring the time taken by different parts of the processing (Fig. 3). We found several bottlenecks, and by fixing them we were able to speed up the processing software by over 50 times. This made it fast enough to keep up with the data stream, even with the detector reading out at its maximum frame rate of 133 frames per second and while using very small amounts of computing hardware: only one computer from DESY's 'Maxwell' cluster.

Traditionally, data are acquired during the experiment, stored on disk for some time and processed weeks or months later. A crucial characteristic of the real-time processing system is that data storage on disk occurs only at the end of the pipeline instead of disk storage being central to the processing workflow. This gives us the flexibility to decide on the best way to store the data, storing only the most useful data and perhaps in a compressed or reduced form. This leads to a very large cost saving while still following the requirements of scientific integrity.

In the future, we plan to investigate ways to make the processing even faster. Since the original paper was published, we have been able to bring the processing speed up to 2000 frames per second, still while using only one compute node. The next generation of detectors, aimed at fourth-generation synchrotron light sources such as PETRA IV, can produce frames at tens or hundreds of thousands of frames per second. Based on these results, by using multiple computers in parallel, we expect to be able to handle these extreme data rates.

Author contact: Thomas White, thomas.white@desy.de
Martin Gasthuber, martin.gasthuber@desy.de

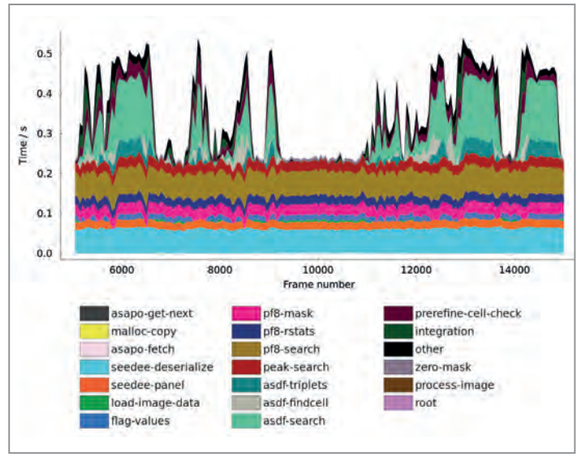

Figure 3

Graph of average processing times for various stages of data processing. The different colours represent the time taken by various subroutines within CrystFEL, the names of which are shown in the key. The 'rainbow' appearance of the graph indicates that the different stages take approximately equal time. Graphs such as this were used to find bottlenecks where one part of the process dominated the total time.

References

1. Dominik Oberthür, 'Microcrystals in structural biology: small samples, big insights', IUCrJ 12, 259–264 (2025).
2. Kara A. Zielinski, Andreas Prester, Hina Andaleeb, Soi Bui, Oleksandr Yefanov, Lucrezia Catapano, Alessandra Henkel, Max O. Wiedorn, Olga Lorbeer, Eva Crosas, Jan Meyer, Valerio Mariani, Martin Domaracky, Thomas A. White, Holger Fleckenstein, Iosifina Sarrou, Nadine Werner, Christian Betzel, Holger Rohde, Martin Aepfelbacher, Henry N. Chapman, Markus Perbandt, Roberto A. Steinerd and Dominik Oberthuer, 'Rapid and efficient room-temperature serial synchrotron crystallography using the CFEL TapeDrive', IUCrJ 9, 778–791 (2022).
3. ASAP::O website: https://asapo.pages.desy.de/asapo/
4. Johannes P. Blaschke, Aaron S. Brewster, Daniel W. Paley, Derek Mendez, Asmit Bhowmick, Nicholas K. Sauter, Wilko Kröger, Murali Shankar, Bjoern Enders and Deborah Bard, 'Real-time XFEL data analysis at SLAC and NERSC: A trial run of nascent exascale experimental data analysis', Concurrency Computat. Pract. Exper. 36, e8019 (2024).

Original publication

'Real-time data processing for serial crystallography experiments', IUCrJ, 12, 97–108 (2025).
DOI: 10.1107/s2052252524011837

Thomas White[1,2], Tim Schoof[1], Sergey Yakubov[1], Aleksandra Tolstikova[1], Philipp Middendorf[3], Mikhail Karnevskiy[1], Valerio Mariani[4], Alessandra Henkel[3], Bjarne Klopprogge[3,5], Juergen Hannappel[1], Dominik Oberthuer[3], Ivan De Gennaro Aquino[3], Dmitry Egorov[3], Anna Munke[3], Janina Sprenger[3], Guillaume Pompidor[1], Helena Taberman[1], Andrey Gruzinov[1], Jan Meyer[1], Johanna Hakanpää[1] and Martin Gasthuber[1]

1. Deutsches Elektronen-Synchrotron DESY, Hamburg, Germany
2. Center for Data and Computing in Natural Science CDCS, DESY, Hamburg, Germany
3. Center for Free-Electron Laser Science CFEL, DESY, Hamburg, Germany
4. Linac Coherent Light Source, SLAC National Accelerator Laboratory, Menlo Park, USA
5. The Hamburg Centre for Imaging CUI, Hamburg, Germany

Light Sources and User Infrastructures

FLASH – after the second large FLASH2020+ upgrade

FLASH1 turned into an externally seeded free-electron laser

FLASH had stopped operation for the second installation period of the FLASH2020+ upgrades in June 2024. Since then, within 14 months the whole FLASH team went for a complete makeover of the FLASH1 free-electron laser (FEL) branch with external seeding at high repetition rate as a new key feature. For this, about 120 m of accelerator tunnel were completely cleared and refurbished before being equipped with state-of-the-art installations, such as new APPLE III-type undulators with variable gap and full polarisation control and a new photon transport beamline with pulse-resolved photon diagnostics tailored to seeded FEL pulses. This new photon beamline FL10 in the FLASH1 tunnel (Fig. 1) now includes two mirrors, like beamline FL20 in the FLASH2 tunnel. On one hand, these mirrors allow to steer the FEL beam ideally into the FLASH experimental hall 'Albert Einstein' and on the other hand they – for FL10 – generate a horizontal beam offset of 40 cm.

Similar to FLASH2, the offset is part of the radiation protection concept. This means, that now the beam distribution area (BDA) at the beginning of the experimental hall, which previously served as a radiation protection area, is fully accessible during FEL beam delivery. The part of FL10 which crosses the PETRA III storage ring tunnel is again used as a gas attenuator. However, at the BDA side a new differential pumping concept is used which has been conceived and realised inhouse. It allows to maintain higher pressure differences within the available length, and hence yields a stronger attenuation of the FEL pulses, if demanded.

A central component in this upgrade is the inhouse developed seed laser system that delivers two seed beams at MHz repetition rate (during a bunch train). Here, the first beam called 'seed1' operates at fixed wavelength of 343 nm and a pulse duration of 500 fs while 'seed2' delivers tuneable pulses at wavelength between 294 and 317 nm at 50 fs pulse duration. These two seed lasers enable to cover a broad FEL wavelength range from 60 nm down to 4 nm to be delivered to users, employing the methods of high-gain harmonic generation (HGHG) or echo-enabled harmonic generation (EEHG). In addition, the THz and the soft X-ray FEL generation were separated to enable independent THz operation.

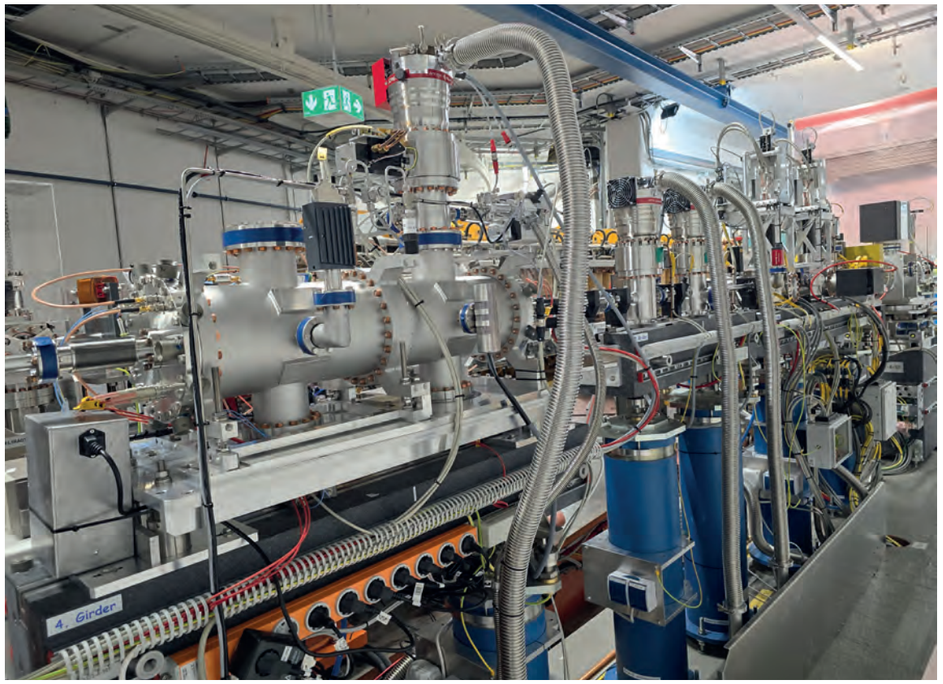

Figure 1
View of the new photon beamline FL10 at the end of the FLASH1 tunnel. The granite girder in the foreground holds the vacuum chamber of the new X-ray gas monitor detectors (XGMD), the inhouse-developed state-of-the-art FEL intensity and beam position monitors. In the upper right, the second mirror chamber of the pair of offset-mirrors is visible (for more details, see text). (Credit: DESY)

Figure 2
View into the full FLASH1 tunnel a few days before the restart on 4 August 2025. Over a length of about 120 m, the new electron beamline, undulators, laser and photon beamlines and all the related infrastructure, such as AC, cooling water, electricity and IT-networks were installed. (Credit: DESY)

The schedule for this extensive FLASH2020+ upgrade was met thanks to a strong team effort during the extensive hardware installations (Fig. 2). The vacuum system was closed and machine operation restarted on 4 August 2025. Keeping his date has been of highest importance to ensure the FLASH2 user programme start early November 2025. This worked out, even though some extra challenges delayed the initial planning, such as water leaking through the tunnel roof during heavy rain, demanding an extensive resealing of the concrete tubbing parts of the tunnel. However, the high number of tunnel installations that, due to such unforeseen obstacles, piled up towards the shutdown end did not leave enough time for all the originally planned commissioning of the new components without beam. Hence, that was organised in an interleaved manner with ramping up the FLASH accelerator and in particular the FLASH2 FEL branch. Getting the latter up to full performance again was most important to keep the goal of delivering at least 1000 hours of beam for FEL user experiments at FLASH2 for the remainder of 2025.

Since the FLASH2 FEL branch remained nearly unchanged during the upgrade shutdown, it was successfully brought back into operation quite rapidly. Just three weeks after the FLASH accelerator restarted, FLASH2 achieved its usual excellent beam parameters for the SASE (self-amplified spontaneous emission) FEL pulses (Fig. 3).

The operating team in the accelerator control room ('BKR') could then start to work with the scientists at the beamlines and instruments in the FLASH2 experimental hall 'Kai Siegbahn' to prepare and optimise the FEL parameters for the first six experiments from 3 November until just before Christmas 2025.
The new round of user experiments at FLASH2 was kicked off by a team of researchers led by the scientists Weiyu Zhang (from the group of Robert Moshammer) and Thomas Pfeifer, both from the Max Planck Institute for Nuclear Physics in Heidelberg (Fig. 4).

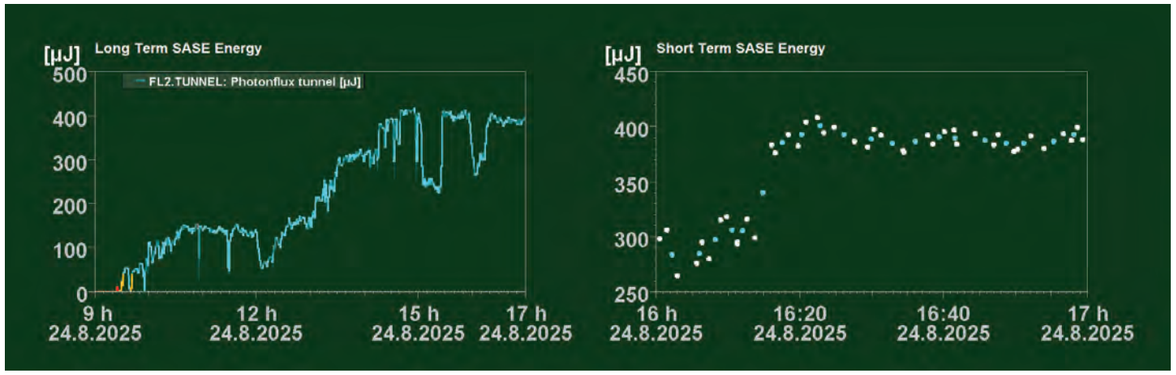

Figure 3

Excerpt from the FLASH machine logbook dated 25 August 2025. It shows the measured (long and short term) energy of the first SASE pulses at FLASH2 after the shutdown, increasing over time during the optimisation process carried out by the accelerator experts. (Credit: DESY)

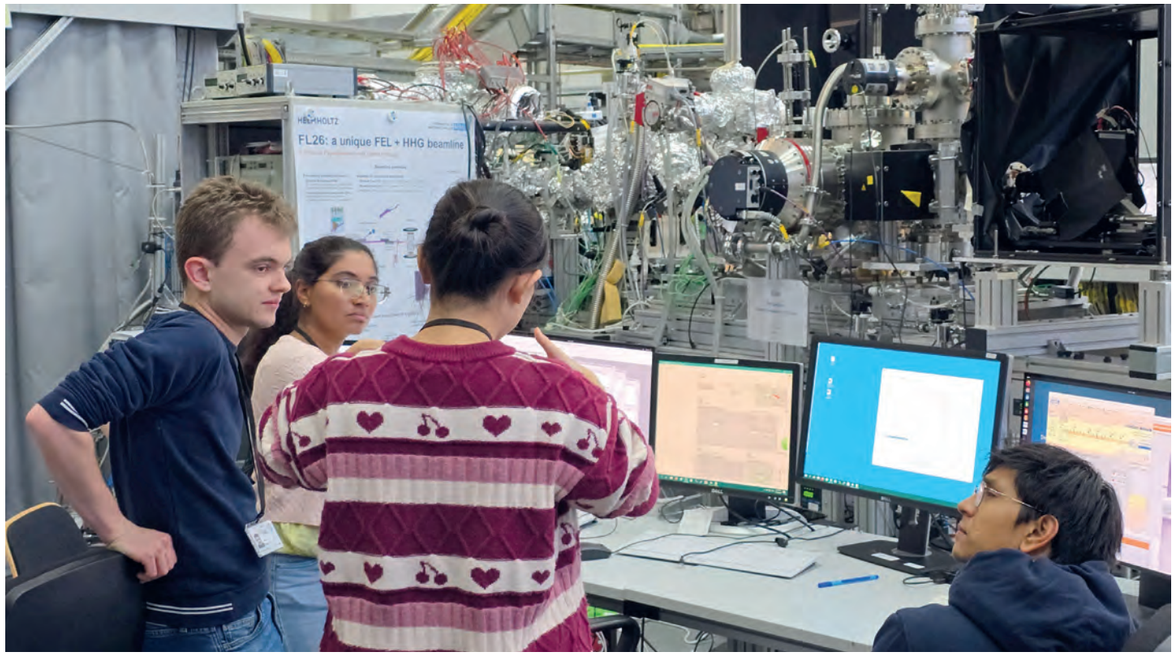

Figure 4

Weiyu Zhang (middle) discusses the planning of the upcoming experiment at FLASH2 with members of her team. (Credit: DESY)

At the Reaction Microscope (REMI) end station at beamline FL26, the user group studied the distortions of small molecules based on the Jahn-Teller effect after excitation by the XUV FEL beam. The team used Coulomb explosion imaging (CEI) with a second FEL probe pulse to investigate the molecular geometry changes happening in fractions of a picosecond. The Jahn-Teller effect has implications in many areas of chemistry, as molecules can achieve more energetically favourable states through these geometric distortions. The experiment by Weiyu Zhang, Thomas Pfeifer and colleagues aims to provide deeper insights into the complex coupling of electrons and nuclear degrees of freedom in molecules.

In parallel to the new user campaign, the completely renewed FLASH1 FEL branch, equipped with high repetition rate external seeding, is gradually being commissioned. End of August, 24 days after the machine has been restarted, the first electron beam was transported to the electron dump. Meanwhile, the seed laser and the timing systems have been tested, and it is planned that first seeded photons will be generated before the end of 2025. This will be a startup at rather long wavelengths well above 60 nm owing to the low electron beam energy of 470 MeV as required by the parallel FLASH2 user experiment.

Over the course of time, when machine conditions are suitable, the commissioning of higher harmonics and thus shorter wavelengths will be pursued. To push towards the shortest wavelength around 4 nm, three additional Apple-III undulators will be added to the FLASH1 beamline as soon as possible but in a three weeks shutdown around Easter 2026 at the latest. This break will also enable final installations of potentially missing hardware and its commissioning, as well as short term upgrades that are already in preparation. We expect the full undulator chain, then consisting of three planar and six APPLE-III type radiators, to be fully operational by the second half of 2026.

As mentioned in the last Annual Report, the first experiments after the FLASH1 commissioning and before starting the normal peer-reviewed access mode will be community-driven experiments. In January 2024, we asked the FLASH user community to develop the "Community Proposals" (CPs) for these experiments in a process that is open to any interested members of the science community. The CPs have a certain level of public visibility, the process includes sharing them with our Photon Science Committee (PSC) and the members of the Proposal Review Panel (PRP), and it also includes information about them in workshops and at meetings. A CP is intended to demonstrate the value of the special parameters of the new FLASH1 FEL for a specific scientific direction and to be open to all interested participants. We held several workshops for the atomic and molecular physics (AMO), materials science, chemistry and biology communities to organise and streamline their proposals.

The AMO and materials science CPs, received in autumn 2025, are optimally tailored to the parameters of the seeded FLASH1 FEL. In the AMO field, the longitudinal coherence plays a major role, whereas materials science concentrates on the radical improvements in bandwidth and stability for time-resolved photoelectron spectroscopy (PES). The submitted CPs were highly rated by the PSC and will now be carried out in close coordination with the commissioning of FLASH1 during the first three quarters of 2026. Up to four additional CPs in the field of chemistry and biology are expected for the PSC meeting in April 2026. Since these user communities will be conducting experiments at shorter wavelengths that will only be available somewhat later (relying on the availability of the abovementioned Apple III-undulators), these were postponed in the CP process.

Having finished the experiments of the Community Proposals, FLASH1 will, presumably in early 2027, also go into standard user operation with regular calls for proposals and the usual PRP review.

The next call for FLASH proposals, opened at the end of 2025 and with a deadline on 1 March 2026, relates to beamtimes at the end of 2026 and in the first half of 2027. Although most experiments during this period will be FLASH2 experiments, it is planned to already provide a few slots during this period for new 'regular' user proposals for the seeded FLASH1.

Contact (FLASH and FLASH2020+):
Rolf Treusch, rolf.treusch@desy.de
Markus Gühr, markus.guehr@desy.de
Lucas Schaper, Lucas.schaper@desy.de

Along with our recent FLASH2020+ upgrade, the FLASH1 beamlines have been renamed following the FLASH2 scheme (see also FLASH beamline table in the 'Facts and Numbers' chapter):

BL3 has been decommissioned and **will soon be** replaced by the new beamline **FL11**.

FL11 will be optimised towards higher FEL energies and equipped with a state-of-the-art bendable KB system, similar to FL24 and FL23. It will provide improved conditions for pump-probe experiments using the complementary accelerator-generated THz radiation and/or the new FLASH1 pump-probe laser.

BL1 with the permanent CAMP instrument for AMO physics is now renamed to **FL12**.

PG0 with its diagnostics port is now **FL13**.

PG2, the plane grating monochromator beamline with its open port turns into **FL14**.

PG1 with the TRIXS instrument behind the monochromator is now **FL15**.

PETRA III

User operation and new beamlines

Figure 1
View into the PETRA III experimental hall 'Paul P. Ewald' which hosts five beamlines. (Credit: DESY)

In the year 2025 about 3740 individual users, including mail-in and remote access, performed experiments at the PETRA III beamlines. In total, 25 beamlines, including those operated by EMBL and Hereon, are operational and open for users. Two run periods of PETRA III were scheduled in 2025 for user operation. The first period was from 4 March to 21 July 2025, while the second period was from 25 August 2025 to 12 December 2025. During the first run period, 2549 hours and during the second period 2034 hours of user beamtime were provided, resulting in a total of 4583 hours of X-ray user beamtime at PETRA III in 2025. Due to organisational reasons related to the prolonged shutdown planned in 2026 (see 'PETRA III – machine operation' section below) beamtimes allocated to successful proposals submitted in 2025 will also be scheduled from 9 January to 16 February 2026.

Upon regular calls for proposals, users submitted 1259 proposals in 2025, thereof 3 'Block Allocation Group' (BAG) proposals and 19 'Long Term Proposals' (LTP). For the generic rolling access 159 proposals have been submitted (details see below). In addition, 136 proposals, including 74 BAG proposals, have been collected for the EMBL beamlines P12-P14 at PETRA III. Beamtime was also provided for five proposals submitted to NFFA and eight proposals submitted to ReMade@ARI, both EU-funded programs.

PETRA III – machine operation

In 2025, the overall availability of the PETRA III storage ring for synchrotron radiation users was at a very good level of 98.5%. Some technical faults caused the loss of a total of 72 hours of user beamtime. The cooling water infrastructure was the major source of faults in 2025: Three back-to-back incidents involving punctured water hoses occurred during weeks 20, 23 and 24. The reason for the defective water hoses was accelerated aging due to higher water temperature. This effect was caused by sextupoles of the 'Superconducting Undulator' (SCU) type that operate at a higher current resulting in a higher water temperature. The leaks were found only close to the SCU locations and all hoses affected were replaced during the summer shutdown. Samples from other locations are in good condition.

A broken water filter incident occurred during week 27 in 2025. The broken filter distributed resin particles throughout the copper water circuit. Almost 529 dirt traps installed in the tunnel, as well as the power supplies connected to the copper water circuit, had to be cleaned before the machine could operate again. The water filter was replaced, and a root cause analysis revealed that the mesh holding the particles inside the filter had detached. These important aspects will be considered for the dirt trap concept for PETRA IV.

In week 37 a radiation-damaged temperature sensor caused repeated beam dumps. Apart from that, a few other failures were also related to power interruptions which were mainly caused by glitches in the external electricity grid. Since the electrical infrastructure at DESY cannot compensate for sudden power drops of a few percent, as is possible with batteries or flywheels for example, power glitches almost always result in a beam dump. Depending on the respective equipment failures, the PETRA III storage ring usually recovers within 15-45 minutes from a beam loss caused by a power glitch. Despite these failures, the planned value of over 98% was achieved.

As usual, PETRA III beamtime was offered with two different bunch filling modes: a 'time-resolved' mode with 40 bunches and a 'multi-bunch' mode with 480 bunches, with about equal time shares. This distribution of both bunch modes has proven to be the optimal scenario for providing the maximum number of 'timing mode' shifts, while minimising radioactive activation of ring components and radiation damage to undulators. However, the P02 undulator was impaired by radiation damage to the undulator magnets. This degradation resulted in reduced flux and resolution in the energy space of the X-ray beam after the monochromator which affected the *in situ* measurements at beamline P02. The undulator was repaired and successfully reinstalled in October 2025 and the beamline regained its full flux.
An extended seven-month operational shutdown is scheduled for PETRA III from September 2026 until beginning of April 2027. The major tasks during this shutdown include installing new 110KV distribution units, refurbishing the pre-accelerator (PIA) and interlock system in the injector chain, realigning the wiggler sections and rerouting cables in the northern section of the PETRA III accelerator in preparation for PETRA IV. Furthermore, this period will be dedicated to essential maintenance and testing of the new laser-plasma injector.

PETRA III – New access, cooperation and automation

Generic rolling access

At PETRA III, a concept for a new access model, 'Generic Rolling Access', has been formulated that allows proposals to be submitted, reviewed and scheduled on a continuous basis [1]. This model is applicable to any beamline, irrespective of the number of experimental methods it provides. The allocation of user beamtime under this testing phase of the rolling access started in September 2024. The participating beamlines are

- P08: High-resolution diffraction beamline
- P11: High-throughput macromolecular crystallography beamline
- P22: Hard X-ray photoelectron spectroscopy beamline
- P23: *In situ* diffraction and imaging beamline
- P24: Chemical crystallography beamline

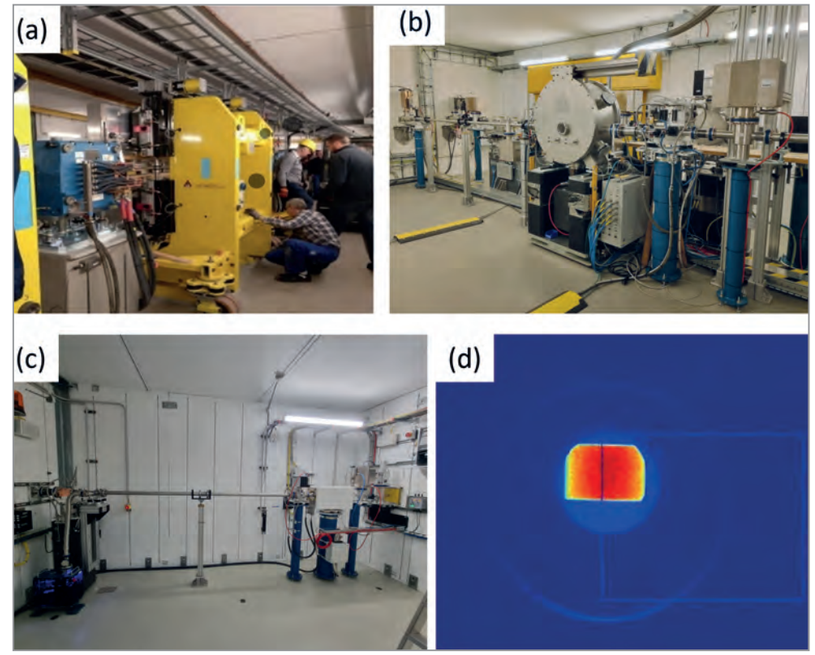

Figure 2
a) The 2-metre U32 undulator (yellow) installed for the PETRA III beamline P25. b) The optics hutch of the P25 beamline, showing the installed double-crystal monochromator (DCM) in the middle. c) The experimental hutch which provides both white and monochromatic beam test stations. d) The first beam was observed in the P25 experimental optics hutch on 12 November 2025. (Credit: DESY)

The associated preparation and characterisation laboratories are incorporated in internal reviews and scheduling on a rolling basis to support users of these five PETRA III beamlines.

The new access model significantly reduces the minimal waiting time between proposal submission and experiment execution as compared to the bi-annual call-based access. The average minimum waiting time is around six months for bi-annual call-based access, which is too long for users in industry and academia who have urgent needs, whereas for some users six months waiting time is perfect to prepare the experiment. Under the generic rolling access model, it has been observed that urgent requests can be accommodated as well as long-term user requests. Initial data shows that the average minimum time from proposal submission to the earliest possible experimental time has been reduced to two months for academic proposals including the time for review and scheduling. This could only be achieved with significant support from the proposal review panel members. If the average additional waiting time between the conceptualisation of an idea and a call deadline for proposals is considered, the generic rolling access reduced the minimum waiting time by a factor of approximately four. In March 2026, an independent external evaluation of the new access scheme will be carried out to identify benefits and shortcomings of the new access mode as basis for future developments.

Strategic cooperation between Fraunhofer Institute and DESY

On 25 February 2025, Fraunhofer and DESY signed a cooperation agreement with the aim of consolidating expertise, infrastructure and knowledge resources to facilitate a more rapid translation of research findings into industrial applications. At the heart of the agreement is a customised access model providing Fraunhofer projects with priority scientific and commercial access to beamtime at PETRA III for payment. This access is exclusively for the Fraunhofer research community and promises guaranteed access to beamtime at the PETRA III beamlines. This cooperation will enable to answer complex technical questions – quickly, precisely and in a way that is relevant to industry with the aim of accelerating practical applications.

ROCK-IT

Three years ago, the Helmholtz ROCK-IT ('Remote, Operando, Controlled, Knowledge-driven and IT-based') initiative was started to develop an automation procedure for X-ray absorption fine structure (XAFS) applications, particularly at the PETRA III beamline P65. By 2025, the ROCK-IT initiative had made significant progress in advancing automation, improving user experience and enhancing data management at this beamline. In October 2025, a complex *operando* experiment including a gas flow control (17-hour CO_2 methanation) experiment was successfully performed here, demonstrating the automated system's end-to-end capabilities. User interfaces and access control were improved through in-person interviews with users that informed the implementation of authentication and authorisation in a Daiquiri prototype and the adoption of a Bluesky–Daiquiri connector via QueueServer. The Daiquiri prototype provides a graphical, web-based user interface for controlling experiments remotely at the beamline P65. Remote control is possible through automation such as Tango-ROS integration for robot-assisted sample handling and improved sample cell design. Key progress in hardware and software integration includes developing a Tango server and an Ophyd device representing the mass spectrometer; establishing connections between SciLog/SciCat and the control system to enhance data logging and cataloging; and introducing new ASAP::O workers, a pipeline manager, a web-based real-time visualisation tool and a Docker container to simplify pipeline deployment across institutes.

PETRA III – two new beamlines

The PETRA III measurement portfolio is currently expanded to include two new beamlines – P25 in the PETRA III experimental hall 'Ada Yonath' and P63 in the PETRA III experimental hall 'Paul Peter Ewald'.

The PETRA III beamline P25 is being developed as part of an internal cooperation project at DESY, primarily funded by the DESY Innovation and Technology Transfer (ITT) group. Funding is also provided by the DESY Innovation Facility (DIF). Construction of the optics test hutch (for white beam operation), the experimental hutch and the control hutch was completed in 2024. In 2025, the vacuum system in the experimental and optics hutches with the cryo-cooled DCM (Fig. 2b) were installed and precisely aligned and are currently brought into commission. Major installations have occurred in the main experimental hutch, with the delivery and installation of granite tables for the beam conditioning optics and the imaging table of the scanning microprobe end station. The diffractometer for the powder diffraction end station is under construction, robots for sample delivery and detector placement are installed and 'Mythen' strip detectors are under test. Significant progress has been made to integrate and test the 'BeamLine Instrumentation Support Software' (BLISS) control system at the beamline. The experimental hutch is being equipped with three different instruments: A fully automated powder diffraction station that is planned to serve many industrial clients via a 'mail-in' service, whereby samples are sent to DESY, and the beamline staff carry out the experiments supported by robot-assisted automation. Furthermore, an element-specific X-ray fluorescence microscopy and imaging station is available, mainly for biomedical applications. The third instrument is a high energy X-ray fluorescence imaging station operated in collaboration with the University Medical Center Hamburg-Eppendorf (UKE) and others. The beamline will also be used to test technical advancements, e.g. in X-ray optics, within the framework of the PETRA IV project. The most significant milestone achieved at beamline P25 this year was successful beam steering by the DESY machine group, along with the group for beamline technology, to achieve 'first light' in the experimental Optics Hutch 1 on 12 November 2025 (Fig. 2d). Further fine-tuning of the canted Sector 3, shared by P24 and P25, is being performed. Radiation safety tests have been completed, and the commissioning of the first beamline is ongoing.

The PETRA III 'OperandoCat' beamline P63 is being developed in cooperation with partners from the Fritz Haber Institute in Berlin and the Institute for Chemical Energy Conversion in Mühlheim, both from the Max Planck Society (MPG) in Germany. Beamline P63 is dedicated to combined X-ray absorption spectroscopy (XAS) and small-angle scattering (SAXS) studies, as well as powder diffraction. It will complement the XAS capabilities available at the high-demand XAS beamlines P64 and P65, as well as the SAXS experiments at the beamlines P62 and P03. The experimental hutch was installed in 2025 (Fig. 3), enabling the setup and necessary technical infrastructure to be installed in 2026. The P63 beamline hutches will be constructed in such a way that they can remain unmodified when PETRA IV is commissioned. The upcoming schedule includes installing the undulator in the PETRA III tunnel in February 2026, followed by installing the control hutch and sample preparation laboratory in March 2026. The monochromator and interlock systems will be installed in July 2026. The undulator will then be implemented in the accelerator in August 2026 and shortly after the first beam is expected to reach the experimental hutch.

PETRA III – new techniques and methods

The PETRA III Extreme Conditions Beamline P02.2 uses X-ray diffraction (XRD) as the primary diagnostic tool to probe the structural and physical properties of materials under high-pressure and -temperature conditions which are comparable to e.g. those of planetary interiors. This is achieved using diamond anvil cells (DACs). The facility supports research in geoscience, materials science and chemistry, enabling *in situ* studies of phase transitions, melting behaviour, deformation mechanisms and kinetics. In 2025, the beamline expanded its capabilities to include X-ray phase contrast imaging (XPCI) combined with simultaneous XRD. This advancement allows for the real-time investigation of hierarchical structures of materials from macro to microscopic scales under static (10^{-3} s^{-1}) and dynamic (10^{-2} s^{-1}) strain rate regimes. Using imaging and diffraction together provides unprecedented insights into melting, recrystallisation, phase segregation and deformation at high temperatures. These developments allow for the exploration of strain-rate-dependent phenomena relevant to the modeling of dynamic processes in planetary interiors such as convection and seismicity. Users can study opaque and transparent materials, particularly focusing on melting, kinetics and viscosity. For transparent materials, the beamline offers a multimodal imaging setup that combines XPCI and optical imaging with simultaneous XRD, further strengthening its capabilities. This combination of techniques is unique within the DAC community, significantly broadening the scientific reach of the beamline.

Figure 3

Installed large experimental hutch of the PETRA III beamline P63 in the experimental hall 'Paul Peter Ewald'. (Credit: DESY)

The PETRA III beamline P11 for high-throughput macromolecular crystallography (MX) has been equipped with ISPyB (Information System for Protein Crystallography Beamlines) and MXCuBE (Macromolecular Crystallography Customised Beamline Environment) as the default software since the beginning of the user run in 2025. The MXCuBE project is a large international collaboration that combines the graphical user interface developments of MX beamlines at numerous European and worldwide MX synchrotron beamlines. While MXCuBE can be used as a standalone software, integrating it with ISPyB, a laboratory information management system (LIMS), allows for the import of sample information, tracking of metadata and display of data collection results. ISPyB can also be used to manage sample shipments and track the location and status of sample containers. MXCuBE has many built-in features that users value such as the ability to queue data collections and transition to unattended data collections. MXCuBE can be used remotely or locally as a Qt version. The interface to ISPyB is EXI (Extended ISPyB Interface) which is available to users registered for remote experiments at P11 via the DOOR user portal. To date, more than 200 industrial and academic experiments have made use of this system at P11.

Contact: Hans-Christian Wille, hans.christian.wille@desy.de
Oliver Seeck, oliver.seeck@desy.de
Arka Bikash Dey, arka.bikash.dey@desy.de

References

1. A. Dey et al., Synchrotron Radiat. News, 38, 20–25 (2025).

PETRA IV – The ultimate 4D-X-Ray microscope

PETRA IV is on the national prioritisation short list for large-scale scientific infrastructures

PETRA IV is the planned ultra-low-emittance upgrade of the existing PETRA III storage ring. DESY's flagship project will deliver the brightest synchrotron light source in the world. Academic and industrial users will benefit from the enormous increase in coherent X-ray photon flux, new cutting-edge beamlines, novel experimental possibilities, and the new business model in preparation for the facility. It will provide easy on-demand access, extended services and support for non-expert synchrotron radiation users, especially for the processing and analysis of their data. PETRA IV is a cornerstone of the Science City Hamburg Bahrenfeld and a central element of DESY's vision of a data and information driven solution ecosystem for academia and industry.

The PETRA IV project reached several important milestones in 2025 and starts to get ready for project execution:

The Preparation Project started
The PETRA IV preparation project started with all work packages in January 2025. It aims to achieve readiness for the execution of the PETRA IV project at the beginning of 2027. Key deliverables are to be achieved in seven work package groups.

For the civil construction programme, the planning for the area PETRA IV North-West started including the new experimental hall PETRA West (PXW (Fig. 1 and Fig. 2)) accommodating 17 new beamline sectors, the new RF hall North, two supply buildings, all connecting tunnel sections, and two laboratories and office buildings.

The first demonstrator girder (Fig. 3) has been completed within the prototyping programme and its response to external vibrations is currently being tested. A cell of the lattice consists of four girders all individually optimised for the magnets and equipment they accommodate.

The prototyping programme for a novel injector based on a laser-plasma-accelerator (LPA) has been expanded. The existing LUX facility has been turned around in its accommodating tunnel to be able to inject 300 MeV electron bunches into the DESY II booster synchrotron. The goal is to demonstrate the feasibility of an LPA injector for user operation starting in March 2026.

The conceptual design of the new undulators and frontends, as part of the preparation project, is progressing as well. Parallel to this prototyping programme, effort is being made to transform the user operation of PETRA from a call-based beamtime proposal system (2 calls per year) to a rolling access proposal scheme with the possibility to submit proposals for comprehensive projects mainly on specific topics , not only single beamtimes. The new access scheme is currently being tested at five beamlines at PETRA III to gain experience with the new approach. The first results are promising and the new access scheme will be scientifically reviewed in March 2026 after the first pilot phase of two years.

Transformation is a goal not only for accelerator technology, business model and user operation, but also for administrative processes, e.g. digitising procurement and recruitment processes, digitising and harmonising safety assessments for components and trades, as well as improving digital forms in general. A key element for this transformation of digital processes is the application of artificial

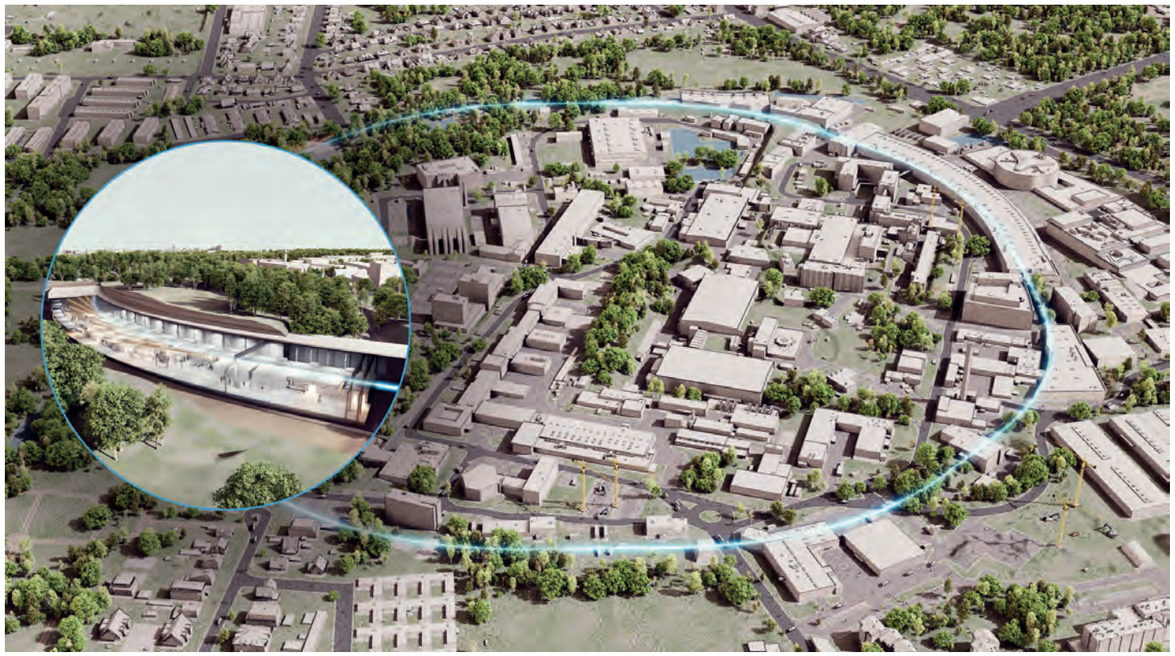

Figure 1
Artistic view of the planned DESY campus with PETRA IV. Inset: zoom into the new experimental hall PETRA West (Credit: DESY, Science Communication Lab)

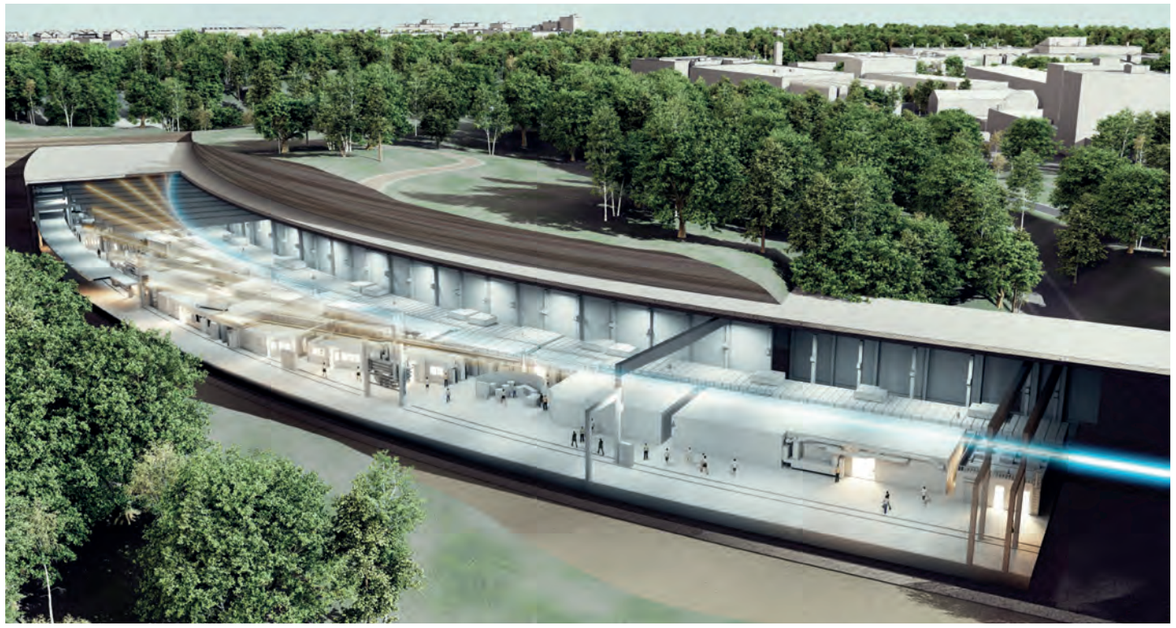

Figure 2
Artistic view of the planned underground experimental hall PETRA West (PXW) with direct look on the so-called sector 0 providing additional services to users from academia and industry. (Credit: DESY, Science Communication Lab)

intelligence to the workflow to further improve the user experience in digitised processes.

The Beamline CDRs have been finalised and reviewed
The conceptual designs for the first 31 beamlines for both phase I (19 beamlines in the existing experimental halls planned to go in operation in 2032) and phase II (12 beamlines in the new hall PXW planned to go in operation until the end of 2035) have been finalised. The phase I beamline conceptual designs reports (CDRs) have been reviewed by the members of the Technical Advisory Committee (TAC) in their autumn meeting in September 2025 at DESY and their feedback is currently being integrated. The CDRs for the phase II beamlines are prepared for review at the TAC meeting in spring 2026. PETRA IV is designed for a total of 36 beamlines and one additional beamline for diagnostic purposes.

One change in the process was the harmonisation of the beamline numbering with the numbering of the sectors of the PETRA IV electron storage ring (Fig. 4).

The project was selected as one of nine large-scale scientific infrastructures of national importance
In 2024, the German federal government issued a call for the submission of concepts for new large-scale scientific infrastructures. The PETRA IV project team successfully submitted its short concept ("Kurzkonzept") in October 2024, which was subsequently evaluated by expert panels under the auspices of the German Scientific Council (WR) in three different subcategories: Scientific excellence, innovation and technology transfer, and costs and risks including sustainability.

On 8 July 2025, Dorothee Bär, Minister of Federal Ministry for Research, Technology and Space (BMFTR), announced the selected projects including PETRA IV.

The Engineering Design Report is complete
Subsequently, the German Scientific Council was charged by the BMFTR to review all prioritised projects in preparation for a decision for funding. The review included an update of the existing material provided with the short concept as well as the submission of a comprehensive project description collected in the 'Engineering Design Report' (EDR) of PETRA IV. The version for the evaluation was completed in November 2025 and will be finalised for publication in spring 2026 describing the status of the project in fourth quarter of 2025 including all beamline CDRs.

The project has been evaluated by the German Scientific Council
The evaluation of the PETRA IV project by the review panel of the WR took place on 2 and 3 December 2026. In dedicated sessions with representatives of the user community, DESY's Foundation Council, and with the PETRA IV project team and the DESY management/board of directors, the status and the scope of the project were reviewed in detail. The evaluation also included a guided tour visiting experimental stations in the PETRA III experimental hall 'Max von Laue', the new LPA prototype injector system for DESY II, the PETRA IV prototype programme, a group of representatives from the different science centres on the DESY campus, the innovation and start-up ecosystem on the DESY campus, the computing centre of DESY, and an information point on the various construction projects on the DESY campus. The tour demonstrated the enthusiasm and the dedication of the project team as well as the DESY staff, which was also reflected in the concluding remarks of the review panel at the end of the visit.

With the project review complete, the project team is preparing all necessary steps for a possible project execution starting in 2027.

Contact: Harald Reichert, harald.reichert@desy.de
Riccardo Bartolini, riccardo.bartolini@desy.de
Karolin Baev, karolin.baev@desy.de
Selina Storm, selina.storm@desy.de
Kai Bagschik, kai.bagschik@desy.de
Stephan Klumpp, stephan.klumpp@desy.de

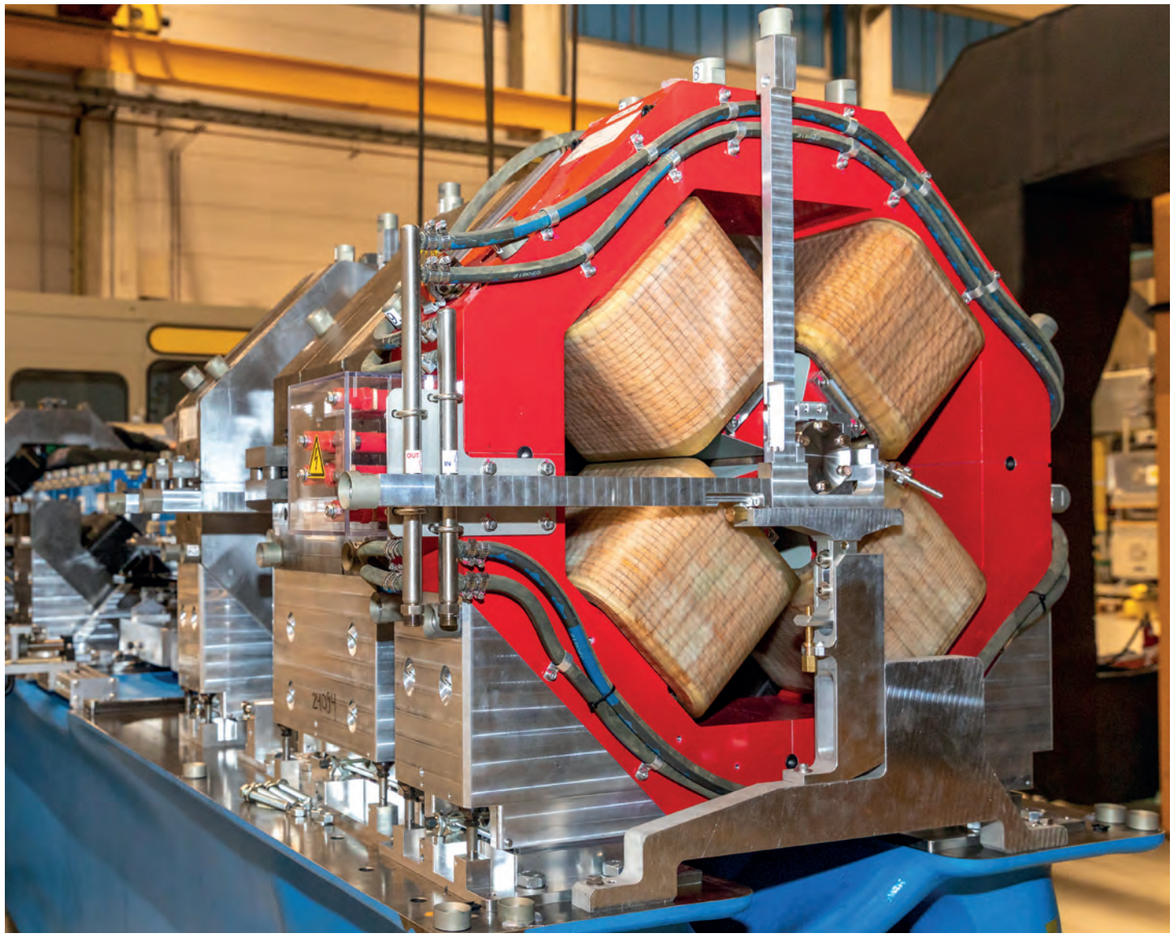

Figure 3
Fully assembled demonstrator girder (blue) with magnets (red) for the PETRA IV storage ring. (Credit: DESY)

Figure 4
Map of the planned PETRA IV beamlines in the three existing (right) and one new (left) experimental halls. (Credit: DESY)

The European Molecular Biology Laboratory Hamburg Unit

Research and infrastructures for applications in the life sciences

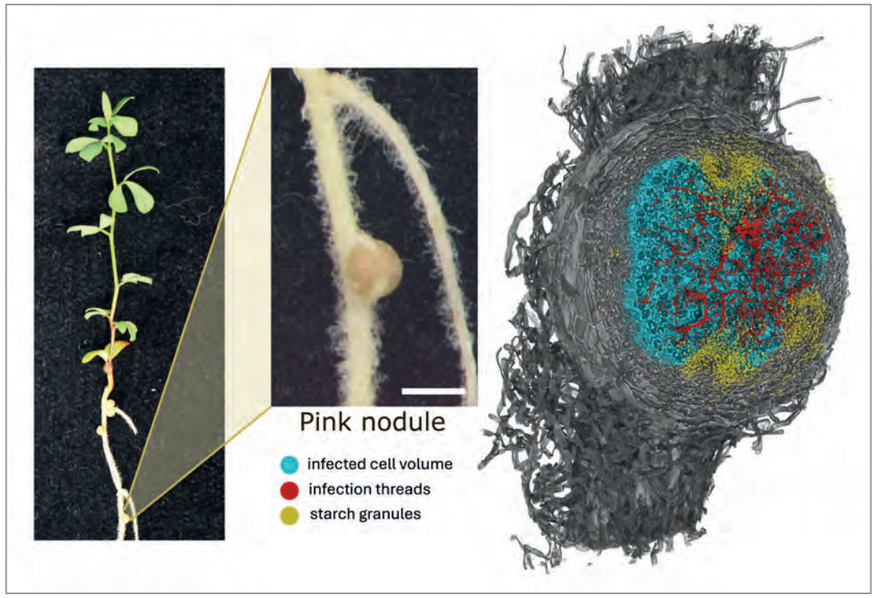

Figure 2
Photo of a Lotus japonicus plant root nodule (left). 3D rendering of HiTT data of a similar nodule with segmentation. The infected volume is shown in cyan, bacterial infection threads in red and starch granules in yellow (right). (Credit: Jonas Albers and Liz Duke/EMBL Hamburg, in collaboration with Emma Birkeskov and Jens Stougaard/ University of Aarhus)

The European Molecular Biology Laboratory (EMBL) unit in Hamburg provides access to three beamlines at PETRA III and a Sample Preparation and Characterisation (SPC) Facility for users from academia and industry as well as training. EMBL Hamburg carries out research with a focus on infection biology using structural biology and imaging tools at various scales. In 2025, EMBL Hamburg served 582 individual users at its facilities. External access to EMBL's facilities is supported by several European consortia: INSTRUCT, HALRIC, MOSBRI.

EMBL's Sample Preparation and Characterisation (SPC) Facility provides a high-throughput pipeline for optimising and characterising biological samples, tailored for structural and biophysical studies. Our state-of-the-art crystallography and biophysics platforms have supported 118 unique users (1 January to 17 October 2025), offering them the advantage of accessing the latest technologies and expert staff, all in one location.

Our eSPC data analysis platform continues to expand, with the recent addition of the KinGenie module (Beta version) for assessing binding kinetics, performing global fitting of association and dissociation kinetics curves and estimating binding rates. In the latest reporting period, we recorded up to 6041 visits from around the world. Please visit spc.embl-hamburg.de for more information.

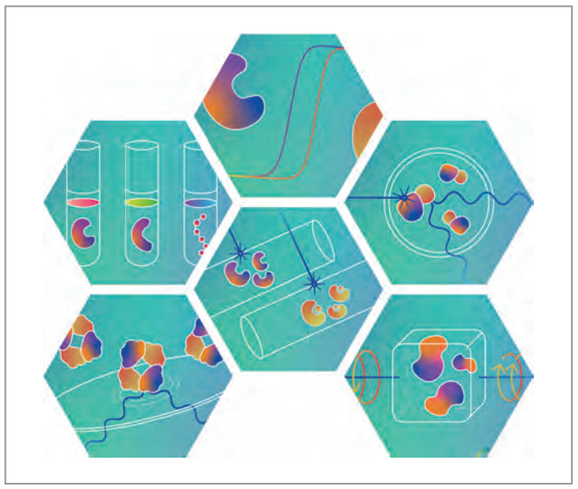

Figure 1
The eSPC platform provides easy to use software for the understanding of biophysical experiments. (Credit: Silvia Burastero)

Beamline P12 for biological small-angle X-ray scattering (BioSAXS)
is specialised in studying biological macromolecules and biocomposites in solution, offering detailed insights into their structure and behaviour. This includes time-resolved studies of molecular dynamics and screening of environmental conditions, such as pH, salt or ligand concentration providing deeper insights into their functional mechanisms. In 2025, EMBL Hamburg provided SAXS services to 178 unique users.

Recent developments have enabled in-vacuum microfluidic measurements, combining the benefits of reduced background scattering with highly efficient sample usage. Initial results demonstrate that high-quality SAXS data can be obtained from very limited sample volumes under vacuum conditions [1]. Several user groups are now actively using this platform to develop microfluidic devices for rapid mixing studies. This emerging capability broadens the scope of experiments possible at P12, particularly for investigating fast structural transitions in biological systems under near-native conditions.

Beamlines P13 and P14 for macromolecular crystallography (MX)
continue providing unique atomic-resolution structural information to a broad range of interdisciplinary studies, in academic (e.g [2]) as well as in an industrial setting [3] and served 286 unique users in 2025. While P13 is fully focused on high-throughput MX, P14 in 2025 has shared about 50% its capacity with T-REXX time-resolved serial crystallography and HiTT imaging experiments. Along with the standard high-throughput MX, P14 supports unique applications requiring microbeams as e.g. for *in vivo* and *in situ* serial crystallography [4], and high-energy photon applications combined with advanced data collection techniques [5] for ultra-high resolution studies in chemical enzymology.

The T-REXX end station of the P14 beamline is dedicated to time-resolved serial macromolecular crystallography (TR-SSX) and has been in operation since 2018, now using ca. 20% of the available P14 beamtime. T-REXX offers, as standard to users, a temperature- and humidity-controlled sample chamber for fixed-target SSX (for more details please refer to the Science Highlight section of this report). Very recently, we have demonstrated anaerobic (< 50 ppm oxygen) fixed-target data collection, still with full temperature and humidity control. We have also commissioned, and taken into first user experiments, an electric-field crystallography setup, inspired by pioneering work at APS. This setup combines a pulsed electric-field with multiplexing data collection approaches to allow fast (sub-ms) time-resolved structural studies of electric field perturbations of macromolecular structure.

Development of the T-REXX end station is carried out jointly by the T-REXX collaboration which, includes the Schneider Group at EMBL, the Tellkamp Group at the Max Planck Institute for Structure and Dynamics of Matter and the Pearson, Mehrabi and Schulz groups at the University of Hamburg.

X-ray Imaging at P14 beamline
X-ray imaging continues to be developed as a user service on EMBL Beamline P14, which provided services to 58 unique users in 2025. Techniques have been developed to extend the field of view beyond ~1.3 mm × 1.3 mm alongside automatic and rapid stitching of data volumes. A wide variety of biological samples are imaged from plants through to human tissues. Fig. 2 shows an image from a project funded by the Novo Nordisk Foundation led by University of Aarhus in collaboration with Danish Technical University and EMBL Hamburg investigating the symbiotic bacterial infection of plant root nodules.

EMBL Hamburg's 50th anniversary
This year marks the 50th anniversary of the establishment of EMBL Hamburg, following the signing of the agreement between EMBL and DESY on 21 April 1975. Since then, the site has built a strong legacy of excellence and innovation in structural and infection biology.

Contact:
Dorota Badowska, dorota.badowska@embl-hamburg.de
Thomas R. Schneider, thomas.schneider@embl-hamburg.de

References

1. C.E. Blanchet et al., J. Phys. Conf. Ser., 3010 012145 (2025).
2. D. Sabonis et al., Nature 642, 467–473 (2025).
3. C. Weller et al., Science 389, eads0239 (2025).
4. R. Schönherr et al., Nat. Commun. 15, 1709 (2024).
5. J. P. Rivas-Fernández, M. Vuillemin, B. Pilgaard et al., Nat. Commun. 16, 2670 (2025).

The GEMS branch at PETRA III – beamlines and instruments operated by Hereon

Diffraction and imaging techniques optimised for the needs of materials research

Helmholtz-Zentrum Hereon operates the German Engineering Materials Science Centre (GEMS). The experimental stations of GEMS at PETRA III are being continuously developed and upgraded for engineering materials and biomaterials science users from institutions in Germany, Europe and around the world. The design and specifications of the successor beamlines at PETRA IV are currently being developed in order to meet future user demands for cutting-edge instrumentation optimised for materials science.

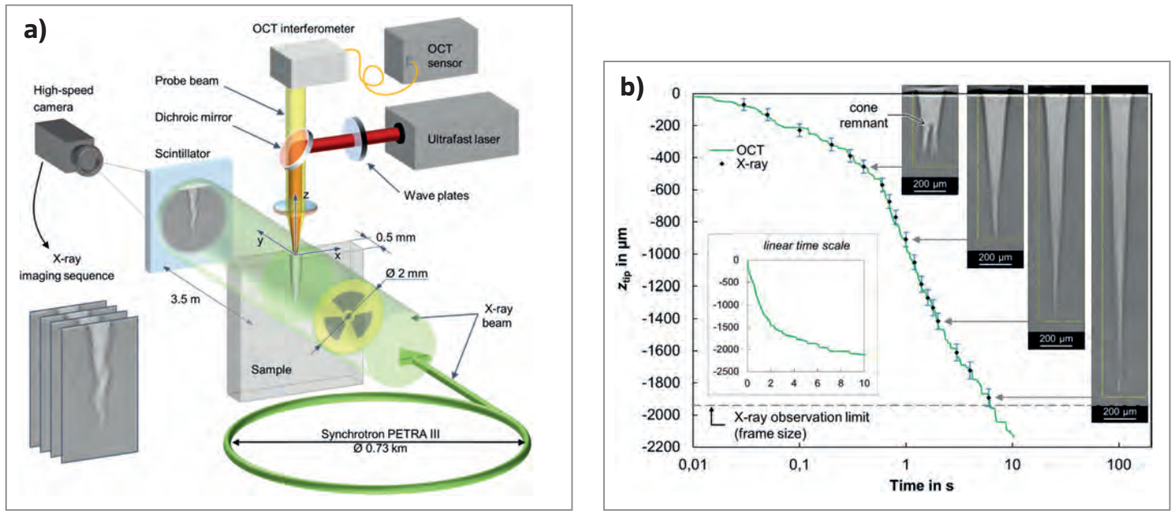

Figure 2

a) Setup for the X-ray imaging of the laser drilling process at beamline P07. b) Successful validation of the optical coherence tomography (OCT) method to determine the laser drilling depth. Process parameters E_p = 250 µJ, f_{rep} = 50 kHz, circular polarisation, d_{helix} = 96 µm, circle scanning frequency f_{helix} = 1.3 kHz. The dashed gray line represents the X-ray observation limit of the depth in this experimental setup given by the image height of the high-speed camera. Image from [8].

Diffraction

In spring 2025, the new sample environment for *in situ* laser powder bed fusion (LPBF) or selective laser melting (SLM) experiments, internally called FlexiSLM, was tested at P07B for the first time (Fig. 1). It is a commercial Aconity Midi machine, slightly modified for use in the X-ray beam. With this machine, metal powder printing is carried out under near-industrial conditions. Hundreds of layers can be built while the forming structure is monitored using high-energy X-ray diffraction (photon energy > 70 keV), small-angle X-ray scattering or X-ray radiography. The research with FlexiSLM is a cooperation of GEMS with the group of Florian Pyczak in the Hereon Institute of Materials Physics and Ronald Schnitzer, the Chair of Physical Metallurgy in the Department of Materials Science of the Montanuniversität Leoben. The dilatometer at P07 was again requested by many proposers, being the workhorse of P07 [1,2]. Also, residual stress analysis with the conical slits was often requested [3].

At the engineering materials station P61A of the white-beam beamline P61, the sample environment 'Minimelt' for additive manufacturing by powder bed fusion with an electron beam produced first results. The Minimelt is operated by a consortium led by KTH Stockholm (G. Lindwall) with participation of FAU Erlangen (C. Körner) and Hereon. The high-speed radiography system at P61A, used with moderate image rates of up to 6 kHz, yielded unique results on the powder consolidation and melt pool dynamics in a CMSX-4 Ni-based alloy [4]. Recently, an image rate of 50 kHz was achieved with this system.

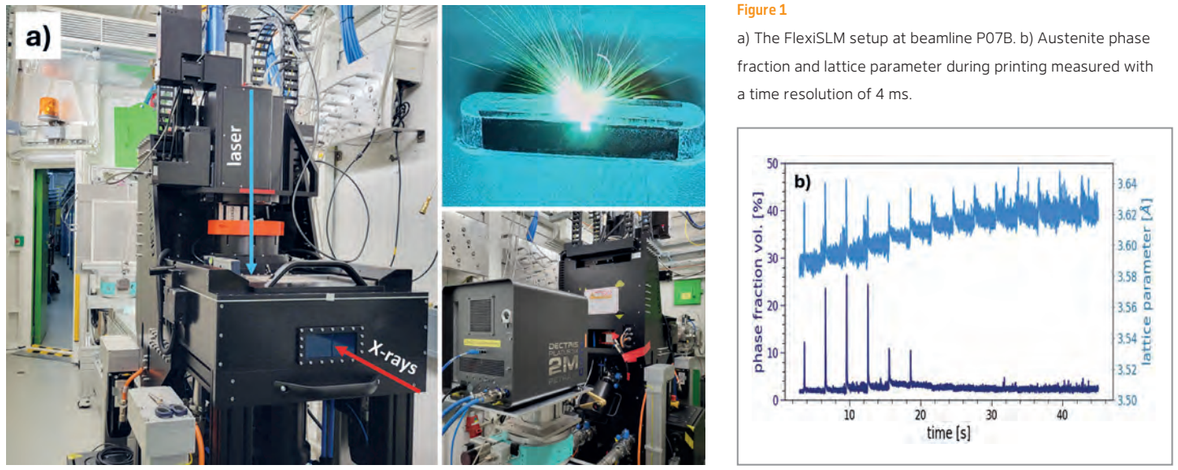

Figure 1

a) The FlexiSLM setup at beamline P07B. b) Austenite phase fraction and lattice parameter during printing measured with a time resolution of 4 ms.

Imaging

Our X-ray imaging branch operates instruments at beamlines P03, P05 and P07. Designed specifically to allow *in situ* and *operando* studies with full-field and scanning imaging techniques, these setups are highly valued in materials science but are also widely applied in life science research. Our users appreciate the unique combination of high X-ray energies, the broad range of spatial resolutions, generous space for complex sample environments and advanced phase-contrast methods.

In the process of the continuous scientific quality assurance, beamlines at PETRA III are regularly reviewed by independent review panels. In 2025, our Imaging Beamline P05 (IBL) has been evaluated, as well as the Micro- and Nanofocus X-ray Scattering Beamline P03 (MINAXS) where Hereon operates the Nanofocus Endstation; one of its two experimental hutches. For both beamlines the evaluation committees certified that the instruments are very competitive internationally and that their performance is reflected by the high publication output levels. Specifically for P05, the review panel emphasised that maintaining its excellent performance and high impact requires ensuring that the capabilities are not significantly diminished at its successor beamline of PETRA IV. To achieve this, the beam size for microtomography (µCT) should be at least on the order of 5 mm × 5 mm, a critical size for many *in situ* / *operando* studies.

The ability to apply *in situ* / *operando* methods is of high relevance in many fields of research, as demonstrated by these recent examples from our user and in-house research: Scanning nanodiffraction at P03 was key to observing the local crystallisation inside the polymer electrolyte of lithium metal batteries [5] at *operando* conditions, a process critical in the adverse formation of dendrites. Microtomography at P05 was used to investigate the applicability of glutamate as a bio-compatible electrolyte additive for sustainable high-performance magnesium-air batteries [6], an inhouse research project in the Hereon Institute of Surface Science. The nanotomography instrument of P05 has enabled a nanoscale view of the structure and deformation mechanism of mineralised shark vertebral cartilage [7]. For more details on this particular research example, please refer to the Research Highlight section of this report. Lastly, the combination of high X-ray energy and a high time resolution was essential for the verification of optical methods as suitable tools to monitor the process of laser drilling in metals [8], as shown in Fig. 2.

Contact: Christina Krywka, christina.krywka@hereon.de
Peter Staron, peter.staron@hereon.de
Martin Müller, martin.mueller@hereon.de

References

1. S. Henninger et al., Materialia 39, 102343 (2025).
2. J. Agirre et al., Intern. J. Material Forming 18, 33 (2025).
3. R. Laurence et al., Strain 61, e70005 (2025).
4. N. Semjatov et al., Additive Manufacturing 110, 104943 (2025).
5. F.A.C. Apfelbeck et al., Nat. Commun. 16, 8958 (2025).
6. Y. Wu et al., Energy Storage Materials 80, 104365 (2025).
7. D.R. Somu et al., ACS Nano 19, 14410 (2025).
8. M. Buser et al., Lasers Manuf. Mater. Process. 12, 257 (2025).

DESY NanoLab

Invigorating the interconnected approach in nanoscience

The DESY NanoLab offers on-site methods for nanoscience that complement techniques and experiments at the DESY light sources and the European XFEL, including nanocharacterisation, nanostructuring and nanosynthesis techniques for investigating atomic scale structure, chemical composition and magnetism.

For internal and external users, the DESY NanoLab is providing high-level user support in its microscopy, spectroscopy, laser and sample preparation labs at the Centre for X-ray and Nanoscience (CXNS) as well as the Scanning Auger Electron microscopy lab, X-ray labs and the electrochemistry lab (Fig. 2) in adjoining buildings (see table in the Facts and Number section of this report). Access is also offered to e-beam lithography in cooperation with the Centre for Hybrid Nanostructures (CHyN) of the University of Hamburg. A further specific offer for users is the 'nanotransfer protocol' that assists in the relocalisation of preselected microscopic regions of interest during experiments using focused PETRA III X-rays.

Several research highlights emphasise the interconnected research, the huge variety of studied topics and wide diversity of analysing techniques offered at the DESY NanoLab. In 2025, collaborative research at the DESY NanoLab has been successful in improving the atomic-scale understanding of catalytic processes, of gaining a deeper insight into more complex and multifunctional adsorption processes of larger biomolecules or promoting the study of magnetic nanoparticle processes to name but a few.

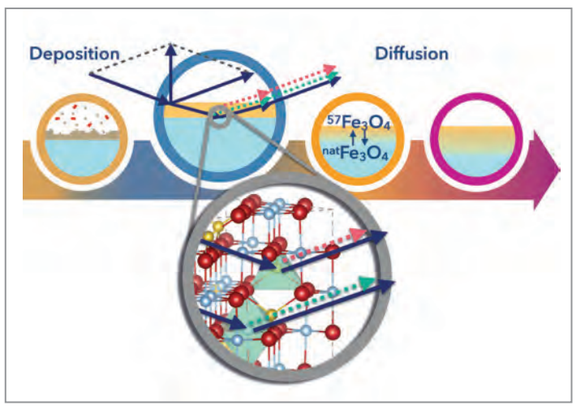

Figure 1
An isotopically labelled magnetite thin-film was prepared and temperature-induced cation transport was site-selectively observed by nuclear forward scattering. (Credit: S. Tober, DESY)

For catalysis research, platinum-rhodium nanoparticles underwent a combination of microscopic analyses at the DESY NanoLab and spectro-microscopy at BESSY II in Berlin which gave new insights into the chemical behaviour of rhodium platinum nanocatalysts under oxidising and reducing conditions. Mixing platinum particles with the element rhodium can further increase efficiency. The location of the two elements plays an important role in this process. So-called core-shell nanoparticles with a platinum core and an extremely thin rhodium shell can help to understand how the elements are optimally distributed in a future catalyst with an extended lifetime [1].

A new study of the DESY NanoLab in collaboration with the Materials Science Department & Center of Nanomedicine of the University of Milano-Bicocca (Italy) reveals surprising bonding of the amino acid cysteine. The scientists elucidated how the amino acid cysteine binds to oxide surfaces, using a unique combination of techniques available at the DESY NanoLab: X-ray photoelectron spectroscopy (XPS), Fourier-Transform infrared reflection absorption spectroscopy (FT-IRRAS) and scanning tunneling microscopy (STM), complemented by theoretical quantum mechanical calculations in Milan. The result is a very detailed picture of cysteine–oxide interface. These findings could open new paths to better biosensor materials, like medical tests, targeted drug delivery systems, smart biomedical coatings and systems enhancing solar disinfection technologies [2].

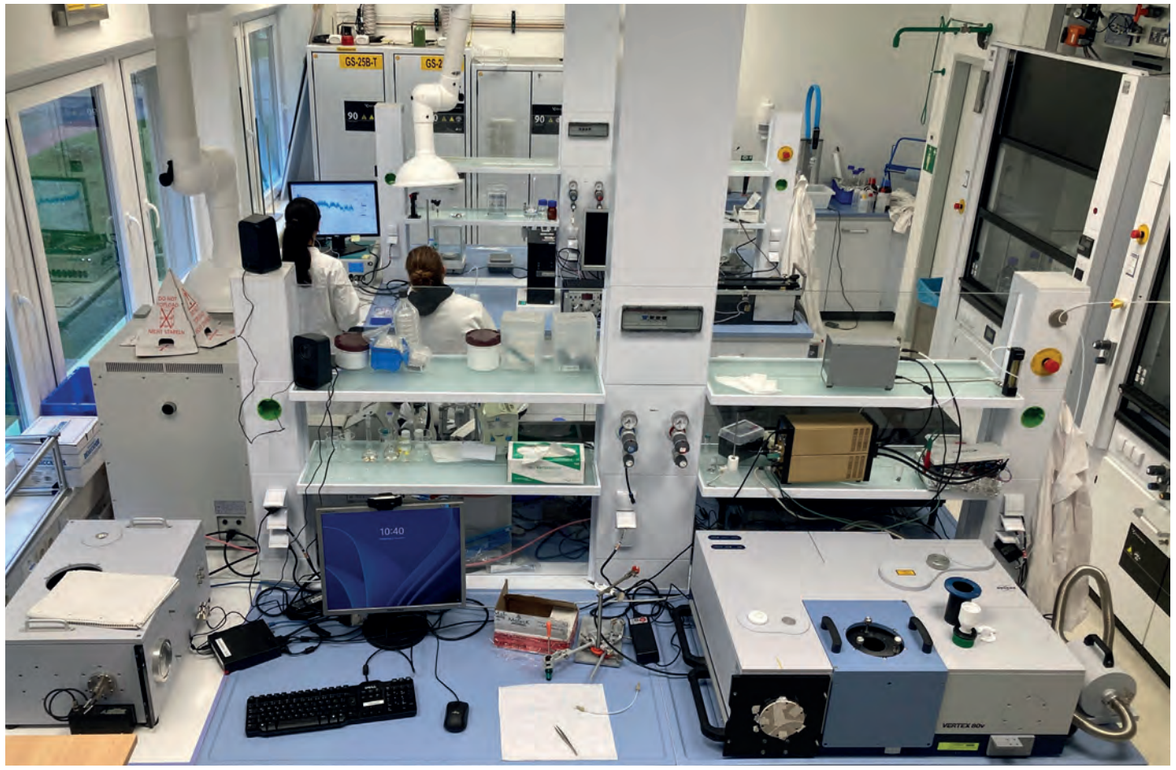

Figure 2
DESY NanoLab electrochemistry laboratory. (Credit: Katharina Röper, DESY)

Another recent publication has uncovered the special way in which iron diffuses in the near-surface region of magnetite. By using specially designed thin-films of this iron-oxide, containing the isotope ^{57}Fe, hopping of iron atoms through the crystal lattice was studied by nuclear forward scattering carried out at the PETRA III beamline P01. The outcome of this study provides new insights into the stability of magnetite when used in various applications such as magnetic nanoparticles. Until now, iron diffusion in the different oxides was studied mostly in the bulk of the materials at elevated temperatures. Now, for the first time, the diffusion mechanism has been elucidated in the near-surface region at relatively low temperatures (Fig. 1). These aspects are very important for understanding the stability of magnetite when used as nanoparticles for various magnetic applications when size plays a role [3].

This combined research and new levels of analysis lead to a better understanding on the nanoscale level. It paves the way for improving and developing materials – ranging from smarter biomedical coating and self-cleaning surfaces to air purifiers, better catalysts and even new environmental processes. Metallic nanoparticles can facilitate chemical conversions, whether for environmental protection, industrial synthesis or the production of (sustainable) fuels from CO_2 and hydrogen. Magnetite nanoparticles have emerged as a very promising material in medicine, either for drug delivery, imaging or cancer therapy by hyperthermia.

Detailed insight into further research activities at DESY NanoLab is provided in the Science Highlights section of this report.

Contact: Andreas Stierle, andreas.stierle@desy.de

References

1. J. Dwivedi, L. J. Bachmann, A. Jeromin, S. Kulkarni, H. Noei, L. C. Tănase, A. Tiwari, L. de Souza Caldas, T. Schmidt, B. Roldan Cuenya, A. Stierle and T. F. Keller, 'Spectro-Microscopy of Individual Pt–Rh Core–Shell Nanoparticles during Competing Oxidation and Alloying', ACS Nano 19, 28516–28529 (2025).
2. M. Blanco Garcia, D. Perilli, C. Daldossi, A. Ugolotti, M. Giordano, D.S. Dolling, M. Wagstaffe, M. Kohantorabi, A. Stierle, C. Di Valentin and H. Noei, 'Unraveling the Role of the Multifunctional Groups in the Adsorption of L-Cysteine on Rutile TiO_2(110)', J. Am. Chem. Soc. 147, 40158–40170 (2025).
3. S. Tober, J.-C. Schober, M. Creutzburg, E. E. Beck, G. Dalla Lana Semione, S. Chung, L. Jacobse, B. Arndt, A. Vlad, R. Steinbrügge, H.-C. Wille, I. Sergueev, H. Noei, K. Schlage, O. Leupold, V. Vonk and A. Stierle, 'Site-resolved near-surface cation diffusion in magnetite', Phys. Rev. Lett. 134, 236203 (2025).

DESY Photon Science at the European XFEL

User consortia

DESY is not only responsible for the operation of the European XFEL linear accelerator but also plays an important role as a user. Moreover, DESY scientists are developing lasers and detectors for usage at the European XFEL (EuXFEL) and are involved in several user consortia including the three largest ones:

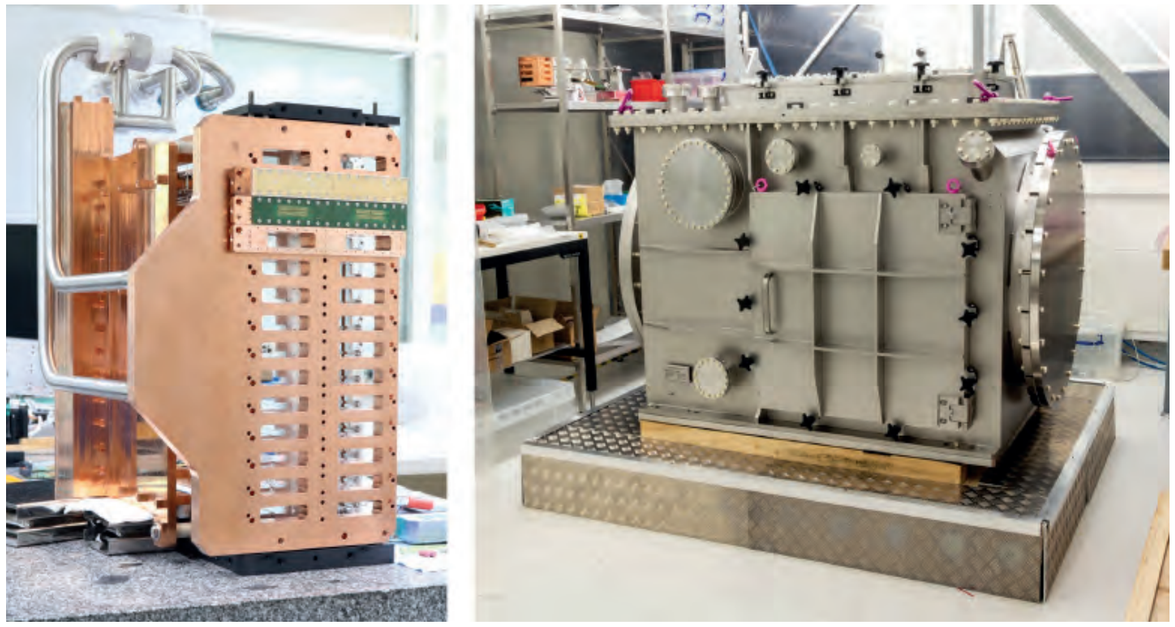

Figure 1

Left figure: The 'Adaptive Gain Integrating Pixel detector' (4M-AGIPD) and the corresponding vacuum chamber (right figure), that were developed by the DESY Photon Science detector group, here under assembly in preparation for installation at the SPB/SFX Instrument of the European XFEL. (Credit: DESY)

Serial Femtosecond Crystallography (SFX)
The International SFX User Consortium helped to establish the method of serial femtosecond crystallography at the European XFEL and works with the "Single Particles, Clusters, and Biomolecules and Serial Femtosecond Crystallography" (SPB/SFX) instrument to provide instrumentation and develop methodology for macromolecular structure determination using intense XFEL pulses.

The megahertz pulse trains of the European XFEL pose the challenge of moving protein microcrystals fast enough to expose a fresh crystal on each pulse. Fast liquid jets were developed but much protein is consumed during the time between pulse trains where measurements are not possible. In the last year, the feasibility of a more efficient approach was demonstrated. Instead of moving the crystals across the beam path, the beam was scanned across a membrane supporting the crystals. An X-ray spinning mirror sweeps the XFEL pulse train vertically as the membrane is stepped horizontally. This promises to enable time-resolved structures with much less material which has hampered the study of some molecular systems - a publication is in preparation.

Early in 2026 the consortium will install an 'Adaptive Gain Integrating Pixel detector' (4M-AGIPD) detector (Fig. 1) that was developed and built in the DESY Photon Science detector group of Heinz Graafsma. This has 4 million pixels, 4 times the current 1M detector and will record up to 3520 frames per second at a rate of 48 Gbytes/second. The detector operates in vacuum and must be cooled to dissipate 3.5 kW of power created by more than 896 detector modules and associated electronics. The entire mass, including the vacuum chamber, is almost 3 tonnes. This will extend the unit cell dimensions of macromolecular crystals that can be measured at high resolution at the SPB/SFX instrument which is currently limited by the pixel count of the detector.

Helmholtz International Beamline for Extreme Fields (HIBEF)
The HIBEF consortium contributes drivers and experimental platforms for the study of matter under extreme conditions of temperature, pressure and external electromagnetic fields at the High Energy Density instrument (HED) of European XFEL. The installations are operated in cooperation between HED and HIBEF open to EuXFEL users.

This year, Talbot imaging was first implemented in combination with the ReLAX laser as a driver and also commissioned with the DiPOLE 100X laser system. The latter is of interest for future fusion research. DiPOLE was again used in a series of user campaigns. Here its unique high repetition rate in combination with rapid target delivery has enabled spectroscopy experiments with eV and meV energy resolution. The diffraction platform for Diamond anvil cells saw continued demand for research on thermal conductivity, chemical reactions and planetary ices.

HIBEF Priority Access beamtime was again dedicated to the realisation of strategic goals such as the observation of relativistic transparency as well as to expand the DiPOLE user community.

Since June 2025 EuXFEL has entered the "long installation and maintenance period" for the accelerator until March 2026. This is also used to improve the experimental platforms and install the HIBEF AGIPD 1M detector which is currently under final assembly at the HED instrument.

The excellent research at HIBEF in various fields is reflected in the highlights listed below.

Heisenberg Resonant Inelastic X-ray Scattering (hRIXS)
The hRIXS consortium includes partners from Germany, Switzerland, Finland, France, Sweden, Italy and the UK. The project is coordinated by Potsdam University in close collaboration with DESY and European XFEL.

Contact:
SFX: Henry Chapman, CFEL/DESY, henry.chapman@desy.de
HIBEF: Thomas Cowan, HZDR, t.cowan@hzdr.de
hRIXS: Alexander Föhlisch, Potsdam University and HZB, alexander.foehlisch@helmholtz-berlin.de

References

1. D. Kraus et al., The structure of liquid carbon elucidated by in situ X-ray diffraction', Nature 642, 351 (2025)
2. M. Frost et al., 'Synthesis of Gold Hydride at High Pressure and High Temperature', Angew. Chem. Int. Ed., 64, e202505811 (2025)
3. YH. Lee et al., 'Multiple freezing–melting pathways of high-density ice through ice XXI phase at room temperature', Nat. Mater. (2025)

Campus and Cooperations

Campus overview

Research centres and cooperations

The research and cooperation landscape at DESY Photon Science includes local, national and international partners with a number of research centres as nuclei for cooperation. All benefit from the excellent scientific environment and research facilities on the Research Campus Bahrenfeld. The image below highlights the light sources, the four research centres in which DESY Photon Science is involved as well as the outstations of EMBL and HEREON and the research centres of the Universität Hamburg. Some major cooperative activities with universities and the interdisciplinary research platforms on campus are reported on within this chapter.

German universities are also closely involved in developments at PETRA III and FLASH, for example through collaborative research projects funded via the BMFTR programme ErUM-Pro. Major developments related to PETRA III, FLASH and European XFEL are described in the chapter 'Light Sources and User Infrastructures'.

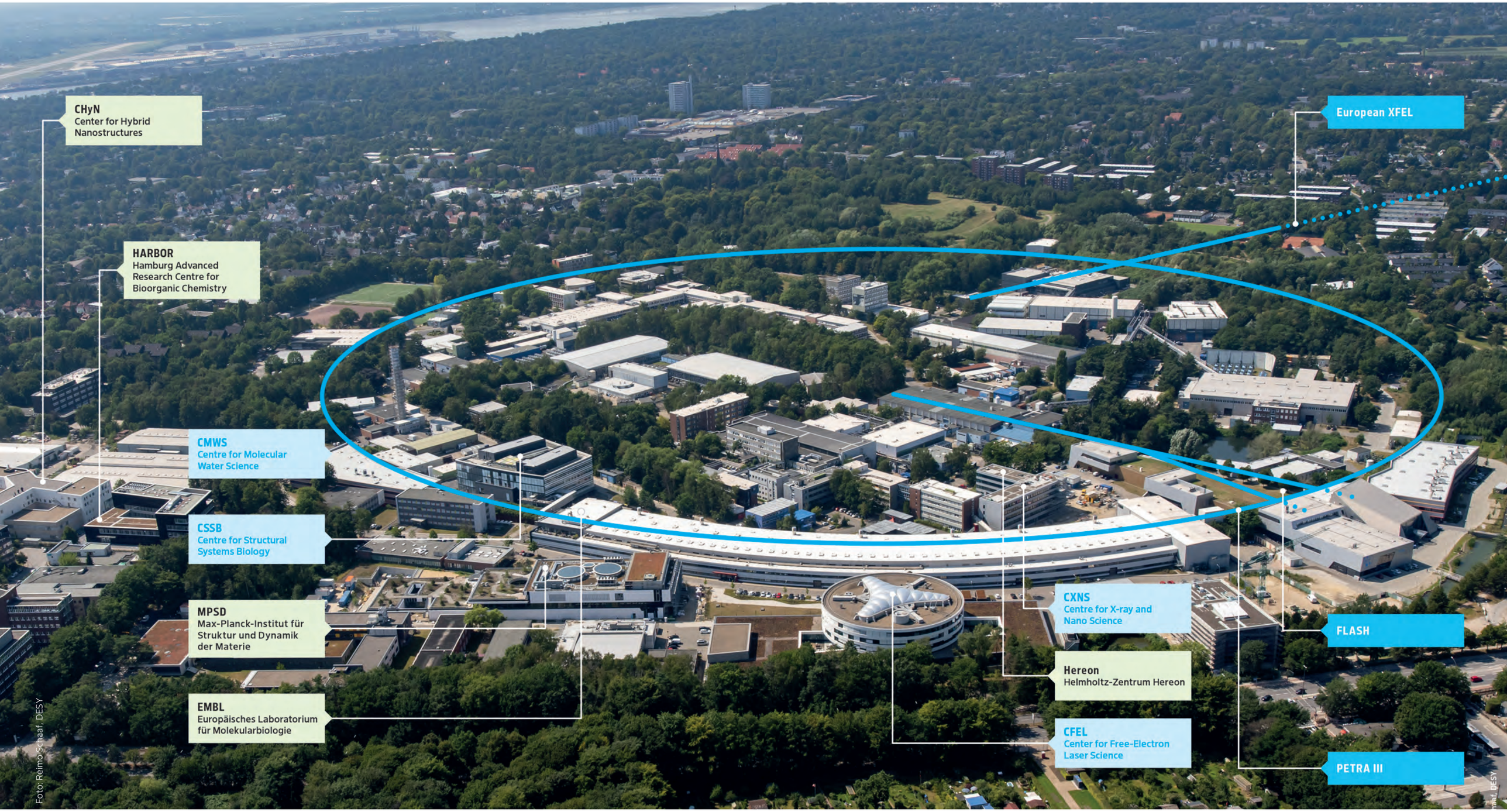

Foto: Reimo Schaaf, DESY

Cooperation in research and education

Overview

Graduate Schools

- **PIER Helmholtz Graduate School (PHGS)**

PHGS is a joint programme of DESY and Universität Hamburg (UHH). In 2025, about 300 PhD students were members of the PHGS. They benefit from an outstanding research environment focused on particle and astroparticle physics, nanoscience, photon science, infection and structural biology as well as accelerators and theoretical physics and from the 'PIER emerging topic' artefact profiling.
In addition to numerous skills trainings and language courses, PHGS offers career guidance, a buddy programme and travel awards.

The annual PIER Graduate Week offers stimulating lectures and workshops in the PIER research fields. This year's event from 6-10 October was attended by 100 doctoral researchers. The program featured two in-depth lecture series on state-of-the-art methods in Optical and X-ray Techniques in Photon Science by Prof. Henning Moritz and Dr. Michael Martins (UHH) and on principles and best practices of Scientific Software Development by Prof. Jörn Behrens (UHH). A further highlight was the Industry Talk and Company Speed Dating with Thermo Fisher Scientific.

PHGS graduates participating in the PIER PhD reception on 17 July at DESY. (Credit: PHGS, K. Winkler)

During the 2025 PIER PhD reception on 17 July, more than 90 doctoral researchers, supervisors, staff, friends and families met to welcome all new doctoral researchers and to honour this year's 52 graduates.
graduateschool.pier-hamburg.de

- **The Helmholtz-Lund International Graduate School (HELIOS)**

Launched in October 2020, HELIOS focuses on advancing instrumentation in particle physics, molecular physics, nanobiology and ultrafast photon science. A key objective of the programme is to prepare young scientists for the next generation of research instrumentation. The project is a collaboration between the University of Hamburg, Lund University, the City of Hamburg and DESY. At present, twenty-one doctoral candidates are enrolled in HELIOS, and thirteen have successfully completed their PhDs.

In 2025, the training programme centred on electronics and imaging technologies and methodologies. Highlights included a workshop on signal processing and a tutorial on velocity map imaging led by Marc Vrakking from the Max Born Institute in Berlin. In addition, HELIOS offered a range of soft skills courses during the training weeks, e.g. on AI-assisted time- and self-management and scientific writing.

On 7 November, the HELIOS Day 2025 took place at the LINXS Institute of Advanced Neutron and X-Ray Science in Lund, bringing together senior scientists and PhD students for a full day of knowledge exchange, discussion and networking. Selected doctoral researchers presented their latest research results, and a poster session provided an opportunity for all doctoral candidates to showcase their work and engage in lively discussions with peers and senior scientists.
heliosgraduateschool.org

Participants of the Signal Processing workshop. (Credit: HELIOS, S. Tille)

- **Data Science in Hamburg – Helmholtz Graduate School for the Structure of Matter (DASHH)**

DASHH is one of six Helmholtz Information & Data Science (HIDS) Schools. It is a joint interdisciplinary project of DESY and eight partner institutions (UHH, TUHH, HSU, HAW, Hereon, HZI, MPSD, EuXFEL). An increase of DESY base funding helped to extend DASHH until 2029.

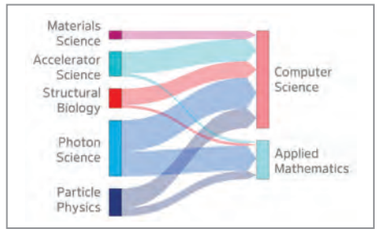

Interdisciplinarity of DASHH projects. (Credit: DASHH)

All PhD projects are jointly supervised by scientists from computer science/mathematics and the fields of photon science, particle physics, accelerator science, structural biology or materials science. So far, 45 PhD projects have been supported by DASHH. As of November 2025, 19 PhD projects have been completed. Another 210 applications were received in 2025 – seven out of the thirteen positions will be in DESY Photon Science. One highlight in 2025 was DASHH alumnus Ke Li winning one of the two VFFD[1] PhD awards for her work at the interface of mixed reality, computer and accelerator science.

The DASHH curriculum enables all PhD students to acquire the required expertise, strengthen their soft skills and broaden their scientific horizon. PhD Seminars, a Data Science Colloquium and PhD get-togethers accomplish the courses. Doctoral researchers from all partner institutions can benefit from the various offers through associated memberships.

[1] Association of the Friends and Sponsors of DESY

dashh.org

Strategic networks

- **LEAPS**

The 'League of European Accelerator-based Photon Sources' LEAPS further consolidated as Europe's strategic network for accelerator-based photon sources. The 2025 Joint Technology Roadmap defined six technological fields (photon sources, diagnostics, X-ray optics, sample environments, detectors and data/IT) guiding future collective investment and innovation. LEAPS was recognised by the OECD as a best-practice example for coordinated governance and strategy in research infrastructures. LEAPS strengthened its science-diplomacy role through Light for Ukraine and the MAVKA beamline project at SOLARIS.

- **PIER PLUS**

PIER PLUS is coordinated by University of Hamburg and acts as the Hamburg metropolitan region's scientific platform. Aims are to strengthen Hamburg as a scientific center and to promote collaboration in the fields: Science City Hamburg Bahrenfeld, Health and Infection, Climate and Coast, Conflict and Coordination, Climate-friendly Mobility and New Materials. In June 2025 the Medical Center Hamburg-Eppendorf joined as 23rd partner to strengthen the network.

Clusters of Excellence with the University of Hamburg

- **'CUI: Advanced Imaging of Matter'**

Many of the DESY Photon Science leading scientists are strongly involved in CUI, with Francesca Calegari and Henry Chapman acting as two of the three spokespersons. CUI has been extended for another seven years after the 2024 call for proposals of the German government's Excellence Initiative. It brings together 25 PIs from UHH, DESY, MPSD and EuXFEL to investigate the dynamics of matter on different time and length scales. CUI recognises the importance of education and diversity (e.g. through the dynaMENT mentoring programme) and fosters the creation of an international and multicultural environment for excellent research.

- **'Understanding Written Artefacts'**

Christian Schroer, leading scientist at DESY Photon Science, is principal investigator and co-spokesperson of the cluster of excellence 'Understanding written Artefacts' that was extended for another seven years in the frame of German government's Excellence Initiative this year. His team has developed a portable tomography scanner to read ancient closed cuneiform texts directly in museums, such as the Louvre in Paris and museums in Turkiye.

Joint laboratories

- In the 'Helmholtz International Laboratory on Reliability, Repetition, Results at the most advanced X-ray Sources' HIR3X, DESY, European XFEL and the US National Accelerator Laboratory SLAC in California have joined forces to develop techniques and procedures that enable the reliable application of X-ray lasers. After three years of successful joint research activities the project ended in 2025.

- DESY is partner of the Helmholtz Institute Jena, an outstation of the GSI Helmholtz Center for Heavy Ion Research on the campus of the Friedrich Schiller University of Jena. The institute is mainly focused on applied and fundamental research at the borderline of high-power lasers and particle accelerator facilities.

- The Ruprecht Haensel Laboratory is a joint research facility of Christians-Albrecht-Universität zu Kiel (CAU) and DESY and combines state-of-the-art instruments and methods of nano-research, makes new developments available to international cooperation partners and ensures that teaching in the field of nanoscience and surface physics is strengthened in a research-oriented manner.

Collaborative research

- Tracking the active site in heterogeneous catalysis for emission control (SFB 1441), coordinated by Karlsruhe Institute of Technology
- Tailor-made multi-scale materials systems (SFB 986), coordinated by Technische Universität Hamburg (TUHH)
- Atomic scale control of energy conversion (SFB 1073), coordinated by Georg-August-Universität Göttingen
- Quantum Cooperativity of Light and Matter (TRR 306), coordinated by FAU Erlangen-Nürnberg
- Center for Integrated Multiscale Materials Systems (CIMMS), coordinated by TUHH
- Center for Data and Computing in Natural Sciences (CDCS), coordinated by University of Hamburg
- Extreme Light for sensing and driving molecular CHirality (SFB 1319), coordinated by Universität Kassel
- DAta for PHoton and Neutron for a National Research Data Infrastructure (DAPHNE4NFDI), coordinated by DESY
- Basic Services for a German National Research Data Infrastructure (Base4NFDI), coordinated by Technische Universität Dresden
- Sustainability-driven nano- and materials science and technology with synchrotron radiation, cooperation with TU Bergakademie Freiberg.
- X-ray analyses on the PETRA III synchrotron radiation source and their evaluation, cooperation with DESY, Hereon, EMBL and Fraunhofer-Gesellschaft
- Regulation of bacterial physiology and infections, coordinated by University Maryland, University Santa Cruz and University Dartmouth

Center for Free-Electron Laser Science CFEL

Three institutions working together successfully

An international research team around Tomke Glier and Michael Rübhausen from the University of Hamburg at CFEL has developed a groundbreaking experimental method to directly and selectively observe the Higgs mode in superconductors [1]. This represents a major step forward, as many fundamental questions about superconductivity, particularly high-temperature superconductivity, which persists even at relatively high temperatures, remain unresolved.

The team developed Non-Equilibrium Anti-Stokes Raman Scattering (NEARS) (Fig. 1). The method involves initiating a controlled 'soft quench' of the so-called Mexican hat potential, which leads to the targeted excitation of metastable Higgs states. NEARS opens up a systematic approach for analysing amplitude modes across a wide range of quantum condensates — from superconductors with competing orders to transiently induced superconducting states or interface superconductors.

DESY researchers around Neetesh Singh from Franz Kärtner's Ultrafast Optics and X-rays Group at CFEL have developed a millimetre-sized high-power amplifier with an output power of more than one watt on silicon-based optical microchips [2]. This output power is many times higher than what has previously been achievable on this tiny scale and enables the use of high-power on-chip amplifiers in the field of integrated photonics instead of external amplifiers. This could make it much easier and cheaper to operate miniaturised devices and sensors, such as those increasingly used in medical surgery, remote sensing by laser and telecommunications, as well as in optical circuits for future accelerator systems and X-ray sources. For details see the Science Highlight section of this report.

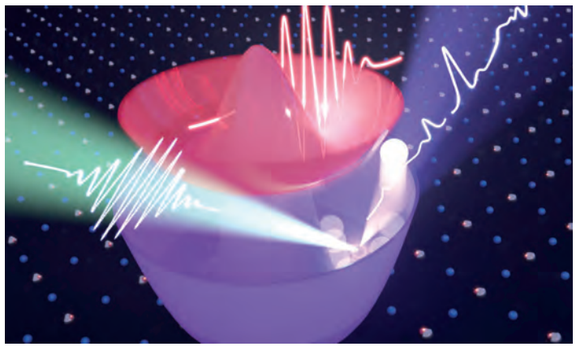

Figure 1

A NEARS measurement on the superconductor characterises its Higgs mode like a fingerprint. To do this, the Higgs mode is excited into oscillation by a quench pulse (red). These oscillations can then be fully characterised in different symmetry channels via anti-Stokes Raman scattering (blue). (Credit: T. Glier, UHH)

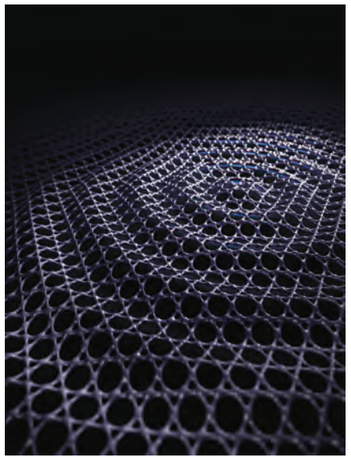

Figure 2

Illustration of long-range electron coherence. (Credit: C. Guo, MPSD)

Physicists at the Max Planck Institute for the Structure and Dynamics of Matter at CFEL around Chunyu Guo and Philip Moll — as part of an international research collaboration — have discovered many-body interference in Kagome crystals, a striking new form of quantum behaviour. In star-shaped Kagome crystals — named after a traditional Japanese bamboo-basket woven pattern — electrons that usually act like a noisy crowd suddenly synchronise, forming a collective 'song' that evolves with the crystal's shape (Fig. 2). Their findings reveal that geometry itself can tune quantum coherence, opening new possibilities to develop materials where form defines function.

Contact: Ralf Köhn, ralf.koehn@cfel.de

References

1. T. Glier et al., Nat. Comm. 16, 7027 (2025).
2. N. Singh et al., Nat. Photonics 19, 307-314 (2025).
3. C. Guo et al., Nature 647, 68-73 (2025).

CFEL Partner Institutions

- Deutsches Elektronen-Synchrotron DESY
- Max Planck Institute for the Structure and Dynamics of Matter (MPSD)
- University of Hamburg (UHH)

www.cfel.de

Centre for Structural Systems Biology CSSB

Together we investigate the molecular mechanisms of infections

CSSB is a growing hub for molecular infection research and is looking forward to welcoming its 10th partner, the Universität zu Lübeck (UzL), at the beginning of 2026.

Over 130 participants from 14 different countries participated in the 4th CSSB International Symposium entitled 'Mechanisms of Infection – From Structure to Translation' in May. Together with the University of Hamburg, two CSSB core facilities were positively evaluated by external review panels in July.

Appointments

Maria Rosenthal, currently a junior group leader at the BNITM, will soon join the CSSB as a group leader. She received a professorship funded through the 'Leibniz Programme for Women Professors'. Her team focuses on integrative structural virology and structure-based drug development, seeking new approaches to treat bunyavirus infections. Jens Bosse, CSSB group leader for 'Quantitative Virology', has been appointed to a W2 professorship at Hannover Medical School (MHH) with the title 'Structural Biology of Infections'.

Research highlights

This past year, our scientists revealed key insights into the cellular process of clathrin-mediated endocytosis [1], examined the molecular interactions taking place during the initial steps of Human Papillomavirus infection [2], discovered a novel family of bacterial enzymes [3], uncovered a promising vulnerability in Pseudomonas aeruginosa [4], generated a mini-antibody that neutralises a protein essential for herpes virus infection [5] and discovered new insights into the order of polyprotein processing in corona viruses (Fig. 1) [6].

Our scientists are also involved in the development of new tools and technologies for the infection and structural biology community such as a structure prediction database covering the proteomes of all human herpes viruses [7], a new approach named MAP-X which revealed the global landscape of protein–protein interactions that govern the biology of the malaria parasite [8] and a proof-of-principle study demonstrating the gas-phase activation and dissociation of biomolecules in particular proteins and their complexes using X-rays provided by PETRA III and FLASH [9].

Awards

Holger Sondermann recently received the 'Plenary Lecturer of the Pan American Association for Biochemistry and Molecular Biology (PABMB)' award at SAIB 2025 in Argentina.

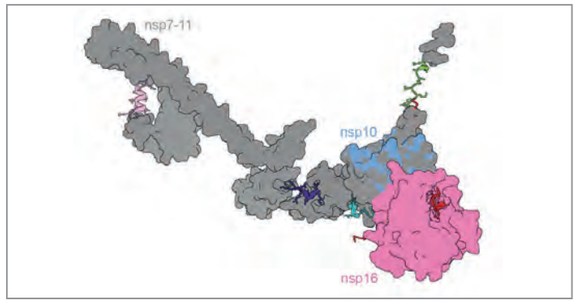

Figure 1

Comparing polyprotein processing in four human coronaviruses revealed distinct and common features like delayed cutting between nsp7 and nsp8 [6]. (Credit: K. Schamoni-Kast)

Gabriele Diana, PhD student in Maya Topf's group, received the Italian Crystallographic Association (AIC) award 'Fiorenzo Mazzi' for the best crystallographic thesis 2025.

Contact:
Holger Sondermann, holger.sondermann@cssb-hamburg.de

References

1. L. Defelipe et al., Nat. Commun. 15, 9655 (2024).
2. Y. Feng et al., Nat. Commun. 15, 10076 (2024).
3. S. Mortensen et al., Nucleic Acids Res. 53, gkae1235 (2025).
4. J. Lormand et al., mBio 16, e00872-25 (2025).
5. B. Vollmer et al., Nature 646, 433–441 (2025).
6. K. Schamoni-Kast et al., Nat. Commun. 16, 8244 (2025).
7. T.K. Soh et al., Nat. Commun. 15, 10230 (2024).
8. S. Pazicky et al., Nat Microbiol. 10, 3229–3244 (2025).
9. J.C.K. Kung et al., Phys. Chem. Chem. Phys. 27, 13234-13242 (2025).

CSSB Partner Institutions

- Bernhard Nocht Institute for Tropical Medicine (BNITM)
- Deutsches Elektronen-Synchrotron DESY
- European Molecular Biology Laboratory (EMBL)
- Forschungszentrum Jülich (FZJ)
- Hannover Medical School (MHH)
- Leibniz Institute of Virology (LIV)
- Helmholtz Centre for Infection Research (HZI)
- Research Center Borstel (FZB)
- Universität zu Lübeck (UzL)
- University of Hamburg (UHH)
- University Medical Center Hamburg-Eppendorf (UKE)

CSSB Stakeholders

- Federal Republic of Germany
- Free and Hanseatic City of Hamburg
- Federal State of Lower Saxony
- Federal State of Schleswig-Holstein

www.cssb-hamburg.de

Centre for X-ray and Nano Science CXNS

Embracing the possibilities – research in materials science and nanoscience in a multi-institutional centre

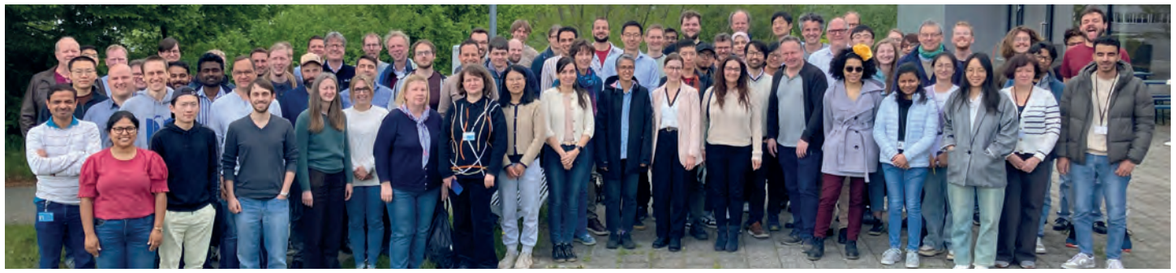

Figure 1

NanoMat Science Day 2025 at DESY (Credit: K. Röper, DESY)

The CXNS is a centre of collaborative research on the nano level. Its highly specialised unique lab infrastructure offers high spec multivariant methods of analysis for inhouse and external researchers. Its core research fields include corrosion, materials science, quantum research as well as catalysis, hydrogen and medical research.

In May 2025, the annual NanoMat Science Day took place at DESY with around 100 participants (Fig. 1). It is an event for advancing inter-institutional exchange and cooperation especially for young scientists in the CXNS core research fields. This year's focus was on research within the Helmholtz research topic 'from matter to materials and life' (MML): complex, functional and quantum materials.

The labs at the CXNS never cease to develop and improve. With the installation of a new femtosecond laser system, the Laser JointLab, a cooperation of IKZ and DESY NanoLab, has added a unique measuring station for time-resolved optical spectroscopy to its portfolio. This unique setup is particularly suited for studying high-frequency acoustic waves and thermal properties in crystalline solids and nanostructures. Thanks to the new laser system it has already been possible to detect acoustic eigenmodes with frequencies of up to 50 GHz. A second setup for studying surface sound waves is under construction [1].

A highlight of CXNS current research activities has been the approval of the cluster of excellence 'BlueMat: Water-Driven Materials' where the CXNS scientists Vasily Artemov, Imke Greving, Patrick Huber, Melanie Schnell, Andreas Stierle and Berit Zeller-Plumhoff are leading projects as principal investigators.

One important publication out of this collaboration, published in 'Nano Energy', presents a novel way for converting mechanical energy into electricity – by harnessing water confined in nanometre-sized pores of silicon as the active working fluid. The developed system, known as an Intrusion–Extrusion Triboelectric Nanogenerator (IE-TENG), uses pressure to repeatedly force water into and out of nanoscale pores (Fig. 2). During this process, charge generation occurs at the interface between the solid and the liquid. This is a type of friction electricity that often occurs in everyday life. An example that everyone is familiar with: walking across a PVC carpet with shoes on. Electrons transfer from one body to another, accumulating a charge that is suddenly discharged when a third body, e.g. a door handle, is touched [2].

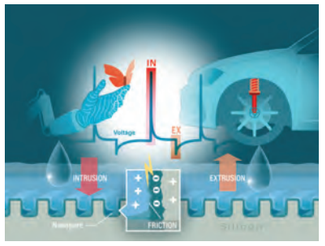

Figure 2

Converting mechanical energy into electricity – generated in silicon pores through friction using only pressure and water. (Credit: TU Hamburg/DESY, M. Künsting)

Contact: Andreas Stierle, andreas.stierle@desy.de

References

1. https://www.ikz-berlin.de/en/public-relations/news/article/femtosecond-laser-system-at-the-ikz-desy-jointlab-goes-into-operation
2. L. Bartolomé et al., Nano Energy 146, 111488 (2025).

CXNS Partner Institutions

- Helmholtz-Zentrum Hereon, German Engineering Materials Science Centre (GEMS)
- Christian-Albrechts-Universität zu Kiel (CAU), Ruprecht-Haensel-Laboratory
- Deutsches Elektronen-Synchrotron DESY
- Technical University Hamburg (TUHH), Center for Integrated Multiscale Material Systems (CIMMS)
- Leibniz-Institut für Kristallzüchtung (IKZ Berlin)

photon-science.desy.de/research/centres_for_research/cxns

Centre for Molecular Water Science CMWS

Achieving a detailed molecular understanding of water

The CMWS continues to unite leading experts to uncover molecular structures, phenomena and dynamic processes of water and at water interfaces across relevant timescales for energy, health and environmental technologies. Its research is structured into five pillars, coordinated by DESY using a combined theoretical and multimodal experimental approach. Central to the CMWS agenda is access to photon science methods at DESY and European XFEL, as well as complementary techniques at DESY, other Helmholtz facilities and partner institutions.

CMWS network and strategic developments

During the last year CMWS has grown to 49 partner institutions from 14 countries, reinforcing its standing as an internationally coordinated research hub. A major milestone is the successful application as cluster of excellence 'BlueMat – Water-Driven Materials', which will formally start in January 2026, aiming to translate molecular water insights into innovative material concepts. 2025 has been the final year of the CMWS Science Programme, jointly funded by DESY and CMWS partners, with PhD and postdoctoral projects in alignment with the CMWS White Paper [1].

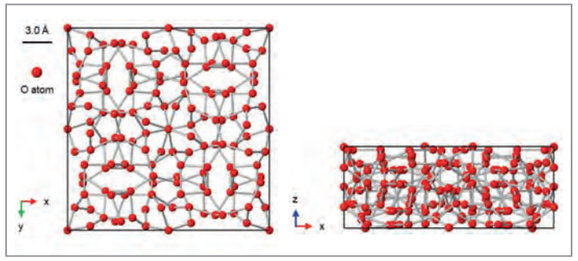

Figure 1

Structure of ice XXI [3].

Advancing water research

This year's research achievements include the discovery of novel deformation dynamics of water in nanoporous media and demonstrated energy generation through confinement-induced friction in nanoscale systems [2]. Details are featured in the Highlight Section of this report.

CMWS researchers were part of a combined PETRA III and European XFEL study on water under compression at room temperature which revealed unexpected complexity in the crystallisation process [3]. This study was part of the topical call on molecular water science at European XFEL. Experiments identified multiple freezing–melting pathways, demonstrating that ice formation under moderate pressure is significantly more intricate than previously assumed. Notably, a previously unknown metastable ice phase (ice XXI) was observed (Fig. 1), acting as a structural link between high-density and very-high-density water during rapid compression. These findings substantially refine current understanding of the water phase diagram and have far-reaching implications for modelling planetary interiors, transient metastable ice formation and improving predictive water models. A special issue on 'Water: Molecular Origins of its Anomalies' has been published as a collection of 58 articles with multiple contributions from CMWS researchers, presenting advances in various disciplines [4].

Figure 2

Delegates during CMWS inauguration ceremony. (Credit M. Mayer, DESY)

Events and activities

The CMWS Water DAYS in February 2025 showcased research highlights from all scientific pillars and celebrated the official inauguration ceremony of the CMWS (Fig. 2). In September, the second CMWS Graduate Workshop was hosted by TU Bergakademie Freiberg and covered topics from fundamental properties of water to applied research on the quality of mining water and energy storage. The bi-weekly CMWS seminar series continued to provide a platform for knowledge exchange and introducing students to CMWS research areas through lectures by network and external experts. In addition, several outreach activities targeting the general public were organised, including evening events within the *Hamburger Horizonte* format featuring science pitches of CMWS scientists and an accompanying exhibition on molecular water science.

Contact: Claudia Goy, claudia.goy@desy.de

References

1. G. Gruebel et al. (eds.), DESY, 127 pp. (2021). DOI: 10.3204/PUBDB-2021-01859
2. J. Sanchez et al., PNAS (2024) 121,38, e2318386121.
3. Y. Lee et al., Nat. Mater., (2025).
4. Goy et al., J. Chem. Phys. 163, 110401 (2025).

www.cmws-hamburg.de

Facts and Numbers

FLASH

PETRA III

FLASH

Experimental halls, machine and photon parameters

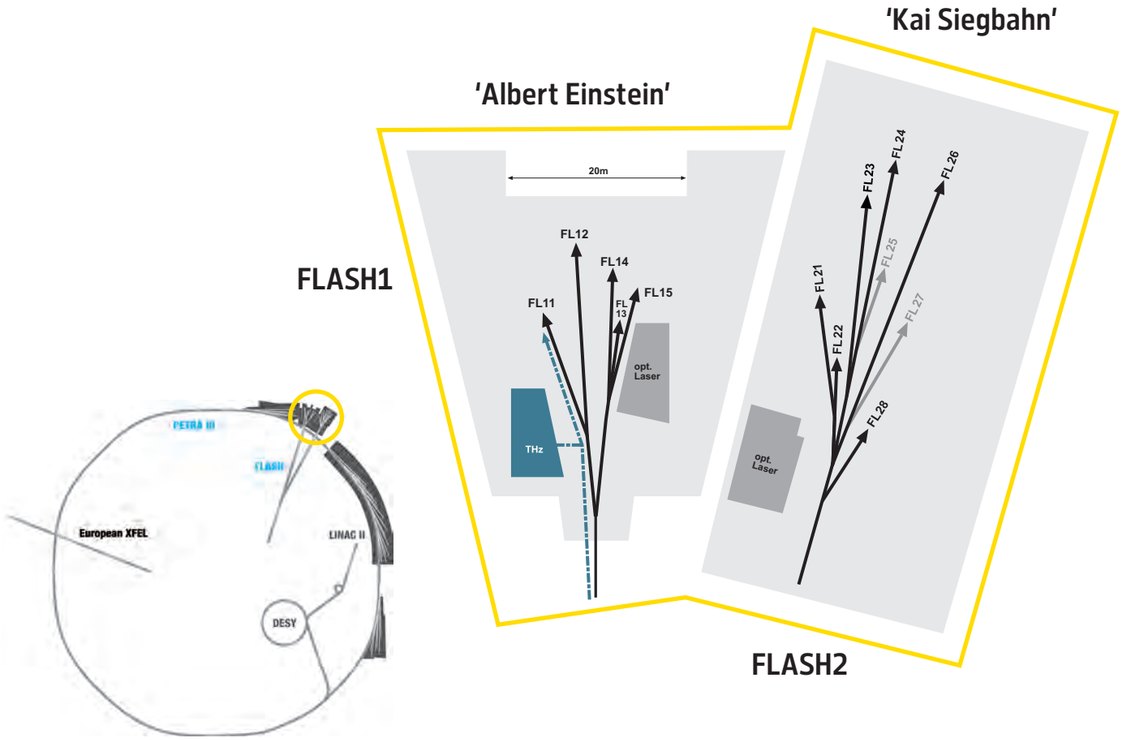

FLASH — machine parameters

Electron energy range	0.35–1.35 GeV (standard operation at 0.75, 0.92 and 1.35 GeV)
Normalised emittance at 0.4 nC (rms)	0.5 mm mrad
Energy spread	200 keV
Electron bunch charge	0.01–1.2 nC
Peak current	2.5 kA
Electron bunches per second (shared between FL1 and FL2)	15000

FLASH — photon parameters

	FLASH1 seeded expected parameters from 2026 on	FLASH2 SASE	FLASH1 THz
Photon energy	20.6–310 eV	14–390 (–890*) eV	0.015–0.124 eV
Min FWHM bandwidth	0.05%	0.5%	10%
Max pulse energy	< 20 uJ	1000 uJ	50 uJ -150 uJ (wavelength dependent)
Pulse energy fluctuation	≤ 10%	10–100%	10%
Typical pulse duration	11–40 fs	5–200 fs	300-3000 fs
Polarisation	variable	horizontal (*variable) * when using FLASH2 afterburner	horizontal

FLASH

Beamlines and laser systems

FLASH1 experimental hall ´Albert Einstein´

Along with our recent FLASH2020+ upgrade, the FLASH1 beamlines have been renamed following the FLASH2-Scheme: BL3 is currently upgraded and named FL11, BL1 with the CAMP end station is now FL12, PG2 is FL14, PG1 with the TRIXS end station is FL15 and the diagnostics port at PG0 is renamed to FL13.

FL11	**under construction, future capabilities from late 2026/2027** non-monochromatic FEL photons, wavelength range: 2–60 nm fundamental plus 3. harmonic Kirkpatrick-Baez (KB) focusing optics with variable foci down to < 10 µm (FWHM)/unfocussed beam size ≈ 5–10 mm (FWHM, depending on wavelength)
	optional pump–probe experiments using the **new** FLASH1 optical laser system for FL11 and FL12
	optional pump–probe experiments using THz radiation: Double pulse scheme with tunable undulator source and broadband dipole source synchronised to X-ray pulses, new parameters to be confirmed in 2027
	about 3 × 4 m platform for user-provided end station
FL12	non-monochromatic FEL photons Kirkpatrick-Baez (KB) focusing optics, FEL focal spot of ≈ 7 µm × 8 µm (FWHM)
	split-and-delay unit for XUV pump–XUV probe experiments *TU Berlin* (multilayer-mirrors for 13.57 nm, -30 ps to +650 ps delay)
	permanent end station: multipurpose CAMP chamber with pnCCD detectors, electron and ion spectrometers and collinear incoupling optics for optical laser
FL13	Diagnostics port at 0 order of monochromator beamlines – not available for user experiments
FL14	high resolution plane grating XUV monochromator (SX 700 type, < 10^{-4} bandwidth, carbon coated optics): - variable combination of photon flux and resolution (from high flux to high resolution) - controlled temporal-spectral properties at moderate resolution for pump–probe experiments - high photon flux with harmonic filtering 50 µm focus
	XUV beam splitter with variable time delay (±6 ps) for time resolved studies
	optional pump–probe experiments using FLASH1 optical laser system for FL14 and FL15
	about 3 × 4 m platform for user-provided end station
FL15	uses the same monochromator as FL14 Kirkpatrick-Baez (KB) refocusing optics, FEL focal spot down to 5 µm FWHM (vertically, monochromator exit slit size dependent)
	permanent end station: - XUV-Raman spectrometer TRIXS for high-resolution and time-resolved RIXS measurements on solid samples (20–400 K, resolving power ≈ 1700, time resolution 170–300 fs FWHM) optional pump–probe experiments (RIXS; XAS and reflectivity with angular resolution) using the FLASH1 optical laser system for FL14 and FL15

FLASH1 optical / NIR laser system for pump–probe experiments for beamlines **FL11 and FL12**

The FLASH1 pump–probe laser for FL11 (former BL3) has been decommissioned in 2024. A new laser system is expected to be available from the last quarter of 2026. Expected parameters are:	
central wavelength	1030 nm
spectral bandwidth (@-10dB)	< 50 nm
intra-burst repetition rate	200 kHz
number of pulses per burst	80 (burst 800 µs flat)
pulse duration	> 70 fs (FWHM (compressed to 1.1 × bandwidth limit), >3000 fs FWHM (uncompressed)
timing jitter to FEL	≈ 30 fs rms (≈ 15 fs rms with Laser Arrival Monitor [LAM])
pulse energy	0–0.5 mJ (at interface with experimental chamber)
polarisation	Linear (s or p)
focus size (1/e^2 diameter)	> 50 µm (1/e^2)
peak intensity	> 10^{15} W/cm²
time delay to FEL	-80 ps to +80 ps, larger delays optional
energy stability	< 10% pulse-to-pulse peak (3% rms)
Harmonic generation conversion to 515nm (20% of fundamental)/ 343nm (3% of fundamental)/ 257nm (2% of fundamental)	

FLASH1 optical / NIR laser system for pump–probe experiments for beamlines **FL14 and FL15**

central wavelength	1030 nm
spectral bandwidth	30 to 50 nm (pre-set for experiment)
intra-burst repetition rate	Up to 1 MHz
number of pulses per burst	1–800
pulse duration	90 fs up to 2 ps chirped (FWHM)
timing jitter to FEL	< 50 fs rms (no drift compensation)
pulse energy	0–30 µJ (at interaction point at 1030 nm)
polarisation	Linear (s or p)
peak intensity	> 10^{14} W/cm²
time delay to FEL	-80 ps to +80 ps, larger delays optional
energy stability	< 10% pulse-to-pulse peak (3% rms)

Harmonic generation conversion to (SHG) 515 nm, (THG) 343 nm or (FHG) 257 nm central wavelength is available with conversion efficiencies of > 50% SHG, > 10% THG, > 6% FHG.

FLASH2 experimental hall 'Kai Siegbahn'

FL21	diagnostics beamline – not available for user experiments	
FL23	pulse-length preserving double grating monochromator beamline wavelength range: 2–20 nm fundamental plus 3. harmonic High transmission option (single grating) & high temporal resolution option (double grating) (effective) pulse duration <50 fs FWHM Kirkpatrick-Baez (KB) focusing optics with variable foci down to < 10 µm (FWHM)/unfocussed beam size ≈ 5–10 mm (FWHM, depending on wavelength)	
	optional pump–probe experiments using FLASH2 optical laser system	
	grazing incidence split-and-delay unit with -5/+18 ps time delay	*Univ. Münster*
	about 3 × 4 m platform for user-provided end station	
FL24	non-monochromatic FEL photons wavelength range: 0.8–90 nm fundamental plus harmonics Kirkpatrick-Baez (KB) focusing optics with variable foci down to < 10 µm (FWHM)/unfocussed beam size ≈ 5–10 mm (FWHM, depending on wavelength)	
	optional pump–probe experiments using FLASH2 optical laser system	
	grazing incidence split-and-delay unit with -5/+18 ps time delay	*Univ. Münster*
	about 3 × 4 m platform for user-provided end station	
FL26	non-monochromatic FEL photons wavelength range: 6–90 nm fundamental	
	optional pump–probe experiments using FLASH2 optical laser system	
	Laser-based high harmonic generation VUV source for VUV-XUV pump–probe experiments with up to 50 eV VUV photon energy	*Univ. Hannover*
	permanent end station: - reaction microscope (REMI) for time-resolved AMO spectroscopy - grazing incidence split-and-delay unit and refocusing optics: FEL focal spot < 10 µm × 10 µm (FWHM, depending on wavelength) - ± 2.7 ps time delay range, 1 fs precision - grating spectrometer for online spectral distribution monitoring and for transient absorption spectroscopy	*MPI-K Heidelberg*

FLASH2 optical / NIR laser system for pump–probe experiments for beamline **FL23 and FL26**

central wavelength	1030 nm
spectral bandwidth (@-10dB)	< 50 nm
intra-burst repetition rate	100 kHz
number of pulses per burst	80 (burst 800 µs flat)
pulse duration	> 70 fs (FWHM (compressed to 1.1 × bandwidth limit), >3000 fs FWHM (uncompressed)
timing jitter to FEL	≈ 30 fs rms (≈ 15 fs rms with Laser Arrival Monitor [LAM])
pulse energy	0–1 mJ (at interface with experimental chamber)
polarisation	Linear (s or p)
focus size (1/e² diameter)	> 50 µm (1/e²)
peak intensity	> 10^{15} W/cm²
time delay to FEL	-80 ps to +80 ps, larger delays optional
energy stability	< 10% pulse-to-pulse peak (3% rms)

Harmonic generation conversion to 515nm (20% of fundamental)/ 343nm (3% of fundamental)/ 257nm (2% of fundamental), Only available in FL23.

FLASH2 optical / NIR laser system for pump–probe experiments for beamline **FL24**

central wavelength	700 to 900 nm (tunable, pre-set for experiment)
spectral bandwidth	30 to 140 nm (pre-set for experiment)
intra-burst repetition rate	100 kHz
number of pulses per burst	1–77
pulse duration	15–65 fs FWHM (compressed to 1.1 × bandwidth limit), ≈1000 fs FWHM (uncompressed)
timing jitter to FEL	≈ 30 fs rms (≈ 15 fs rms with Laser Arrival Monitor [LAM])
pulse energy	0–120 µJ (at interaction region)
polarisation	Linear (s or p)
focus size (1/e² diameter)	> 50 µm (1/e²)
peak intensity	10^{13} W/cm² (@50 µm)
time delay to FEL	-80 ps to +80 ps, larger delays optional
energy stability	< 10% pulse-to-pulse peak (3% rms)

Harmonic generation conversion to 400 nm (SHG) and 266 nm (THG) central wavelength is available with conversion efficiencies of > 10% SHG, > 3% THG, pulse durations are increasing.

All FLASH beamlines provide online photon diagnostics for intensity, wavelength and beam position, fast shutter, aperture and filter sets.

FLASH beamtime statistics 2025

FLASH
Operation period 2025

	User beamtime	Machine studies and user experiment preparation	Maintenance	Commissioning	Shutdown
FLASH (Linac)					
1 Jan – 24 Nov	528 h	512 h	26 h	1646 h	5167 h
planned for 25 Nov–31 Dec	528 h	93 h	0 h	0 h	260 h
FLASH1					
1 Jan – 24 Nov	0 h				
planned for 25 Nov– 31Dec	0 h				
FLASH2					
1 Jan – 24 Nov	528 h				
planned for 25 Nov– 31Dec	528 h				

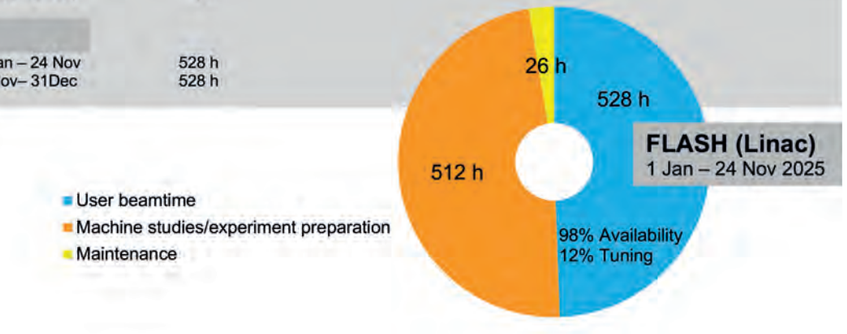

Please note that the machine operation after the second FLASH2020+ upgrade shutdown was resumed on 4 August 2025. User beamtime started on 3 November.

PETRA III

Experimental halls and machine parameters

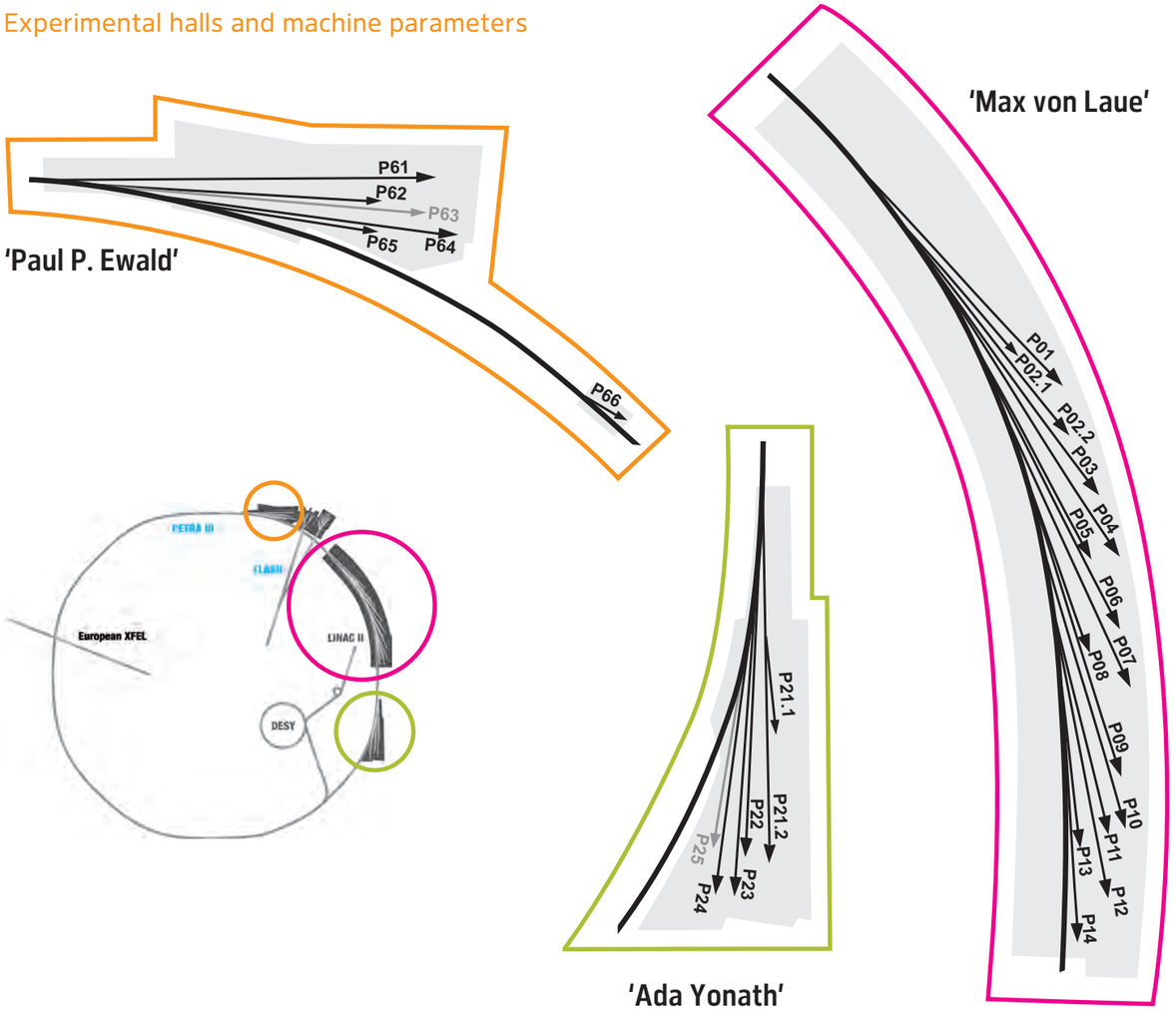

PETRA III – machine parameters

Electron energy	6.08 GeV
Circumference of the storage ring	2304 m
Number of bunches	40 (timing mode) 480 (continuous mode)
Bunch separation	192 ns (timing mode) 16 ns (continuous mode)
Electron beam current	100 mA (timing mode) 120 mA (continuous mode)
Horizontal electron beam emittance	1.3 nmrad
Vertical electron beam emittance	0.01 nmrad
Electron beam energy spread (rms)	0.1%
Horizontal × vertical beam size (rms) at 5 m undulator (high β section) and 10 keV photon energy	161 µm × 5.2 µm
Horizontal × vertical beam size (rms) at 5 m undulator (low β section) and 10 keV photon energy	42 µm × 5.7 µm

PETRA III

Beamlines

PETRA III experimental hall ´Max von Laue´

Beamline and instruments		Operated by
R — option for remote user operation M — option for mail-in service ***rolling*** — submission of proposals at any time under the generic rolling access scheme		
P01	High Resolution Dynamics 10 m U36 | 2.5–80 keV	DESY
	Nuclear resonant scattering	DESY
	Synchrotron Mössbauer Source-based spectroscopy	DESY
	Resonant inelastic X-ray scattering	DESY | MPI
	X-ray Raman scattering	DESY | MPI
P02.1	Powder Diffraction and Total Scattering 2 m U23 | 60 keV	DESY
M	Standard and *in situ* powder diffraction	DESY
M	Standard and *in situ* total scattering	DESY
P02.2	Extreme Conditions 2 m U23 | 25.6 keV, 42.7 keV	DESY
R	Laser heating experiment for X-ray diffraction and imaging in diamond anvil cells (DACs)	DESY
R	General purpose experiment for X-ray diffraction and imaging in DACs	DESY
P03	Micro- and Nanofocus X-ray Scattering (SAXS/WAXS/GISAXS/GIWAXS/USAXS) 2 m U29 | 12–20 keV	DESY
	Grazing incidence and transmission micro-beam small and wide-angle scattering	DESY
	Nano-beam scattering and diffraction	DESY | Hereon | collaborators
P04	Variable Polarisation Soft X-rays 5 m UE65 | 250–2800 eV	DESY
	UHV diffractometer and soft X-ray spectrometer	DESY | collaborators
	Photon-ion spectrometer (PIPE)	DESY | collaborators
	Ultra-high resolution angular resolved photoelectron spectroscopy (solids & liquids)	DESY | collaborators
	Soft X-ray absorption holographic imaging instrument	DESY | collaborators
P05	Micro- and Nanoimaging 2 m U29 | 8–50 keV	Hereon
M	Microtomography	Hereon
	Nanotomography	Hereon
P06	Hard X-ray Micro- and Nanoprobe 2 m U32 | 5–45 keV	DESY
	Microprobe	DESY
	Nanoprobe	DESY
P07	High Energy X-ray Materials Science 4 m IVU21 | 50–200 keV	Hereon
	Diffraction tomography, Surface diffraction, grazing incidence total scattering	DESY
	Heavy-load diffractometer	Hereon
	Grain mapper	Hereon
	High energy tomography	Hereon
P08 ***rolling***	High Resolution Diffraction 2 m U29 | 5.4–29.4 keV	DESY
M	X-ray diffraction and scattering from solid surfaces and thin films	DESY
	X-ray scattering from Langmuir monolayers	DESY | collaborators
	X-ray reflectivity from liquid/vapor and liquid/liquid interfaces	DESY
P09	Resonant Diffraction / HiPhaX 2 m U32 | 2.7–24 keV / 16 keV	DESY
	Resonant X-ray diffraction at low temperatures (2 K < T < 750 K)	DESY
	Resonant X-ray diffraction in high B-fields (2 K < T < 300 K; B < 14 T, B ⊥ Q)	DESY
	Resonant X-ray diffraction at high pressure (4 K < T < 300 K; p < 30 GPa)	DESY
	High-throughput Pharmaceutical X-ray screening (HiPhaX)	DESY
P10	Coherence Applications 5 m U32 | 4–20 keV	DESY
	X-ray photon correlation spectroscopy (SAXS/USAXS/WAXS geometry) (5–15 keV)	DESY
	Bragg coherent diffraction imaging (5–13 keV)	DESY
	GINIX — Nanofocusing setup (8 and 13.8 keV)	DESY | collaborators
P11 ***rolling***	High-throughput Macromolecular Crystallography 2 m U32 | 2.4–30 keV	DESY
R, M	Macromolecular crystallography (6–26 keV)	DESY | HZI | Univ. Lübeck
M	Serial crystallography (6–26 keV)	DESY

PETRA III

Beamlines

PETRA III experimental hall 'Max von Laue'

Beamline and instruments		Operated by
R — option for remote user operation M — option for mail-in service ***rolling*** — submission of proposals only under the generic rolling access scheme		
P12	Bio SAXS 2 m U29 | 4–20 keV	EMBL
R	Small-angle and wide-angle X-ray scattering	EMBL
	Time-resolved X-ray scattering	EMBL
	Anomalous small-angle X-ray scattering	EMBL
P13	Macromolecular Crystallography 2 m U29 | 4.5–17.5 keV	EMBL
R	Macromolecular crystallography	EMBL
P14	Macromolecular Crystallography and Imaging 2 m U29 | 6–32 keV	EMBL
R	Macromolecular crystallography (7–27 keV)	EMBL
R	Serial crystallography (7–18 keV)	EMBL
	High throughput microtomography (6–32 keV)	EMBL
	Time-resolved serial crystallography (12.7 keV)	EMBL | U Hamburg

PETRA III experimental hall 'Ada Yonath'

Beamline and instruments		Operated by
R — option for remote user operation M — option for mail-in service ***rolling*** — submission of proposals only under the generic rolling access scheme		
P21.1	High-Energy Diffraction for Physics and Chemistry at the Swedish Beamline side branch: 2 m U29 | 54 keV, 88 keV, 102 keV	DESY | Swedish host: Center for X-rays in Swedish Materials Science (CeXS)
	Single crystal diffuse scattering and 3d-ΔPDF	DESY
	Total scattering (transmission and grazing incidence)	DESY
P21.2	Swedish Materials Science Beamline 4 m IVU21 | 40–150 keV	DESY | Swedish host: Center for X-rays in Swedish Materials Science (CeXS)
	Wide-angle scattering (bulk and surface, grain resolved and averaged)	DESY
	Small-angle-scattering (bulk and surface)	DESY
	Imaging (CT and radiography)	DESY
P22 ***rolling***	Hard X-ray Photoelectron Spectroscopy 2 m U33 | 2.4–15 keV	DESY
R	Hard X-ray photoelectron spectrometer (HAXPES)	DESY
	Ambient pressure XPS (POLARIS)	DESY | collaborators
	Hard X-ray photoemission electron microscope (HAXPEEM)	DESY | collaborators
R	Hard X-Ray momentum microscope (HarMoMic)	DESY
P23 ***rolling***	*In-situ* X-ray Diffraction and Imaging beamline 2 m U32 | 5–35 keV	DESY
	XRD and secondary processes, *in situ* and complex environments	DESY
	Hierarchical X-ray imaging	KIT | DESY
P24 ***rolling***	Chemical Crystallography 2 m U29 | 8 keV, 15–44 keV	DESY
	Single crystal diffraction in complex sample environments	DESY
	Small molecule crystallography	DESY
P25	Beamline for applied Biomedical Imaging, Powder Diffraction and Innovation 2m U32 | 8–60 keV	DESY - ITT Commissioning in 2025 | Operation planned for 2026
	X-ray fluorescence imaging (milliprobe) (XFI)	DESY |U Hamburg
	Scanning X-ray microscopy (SXRM)	DESY
	High throughput powder diffraction (15–35 keV)	DESY
	PETRA IV test station (white beam)	DESY

PETRA III

Beamlines

PETRA III experimental hall 'Paul P. Ewald'

Beamline and instruments		Operated by
R — option for remote user operation M — option for mail-in service ***rolling*** — submission of proposals only under the generic rolling access scheme		
P61	High Energy Wiggler Beamline 10 × 4 m damping wigglers | white beam btw. 30–250 keV	DESY
	High energy engineering materials science	Hereon
	Large volume press — extreme conditions	DESY
P62	SAXSMAT Beamline P62 2 m U32 | 3.5–35 keV	DESY
	Anomalous small-angle X-ray scattering	DESY
	SAXS tensor tomography	DESY
P63	OperandoCat | 4–44 keV	DESY | MPI Start of operation: not yet defined
	Operando XAFS/XES & XRD/SAXS	
P64	Advanced X-ray Absorption Spectroscopy 2 m U33 | 4–44 keV	DESY
	Ex-situ and *in-situ* XAFS	DESY
	High-resolution X-ray emission spectroscopy (non-resonant and resonant)	DESY
	Sub-second XAS with QEXAFS monochromator	DESY
P65	Applied X-ray Absorption Spectroscopy 41 cm U33 | 4–44 keV	DESY
	Ex situ and *in situ* XAFS of bulk samples	DESY
P66	Superlumi *(between PETRA III halls 'Paul P. Ewald' and 'Max von Laue')* Bending magnet | 4–40 eV	DESY
	Time-resolved luminescence spectroscopy	DESY

PETRA III beamtime statistics 2025

PETRA III
Operation period 2025

	User beamtime	Machine studies and test runs	Maintenance	Shutdown
1 Jan – 31 Dec	4656	1513 h	90 h	2501 h

User run periods:
4 Mar – 21 July
25. Aug – 12 Dec

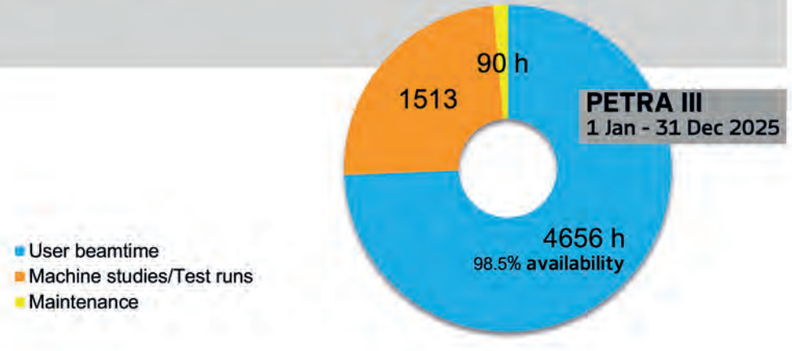

DESY NanoLab

Instruments

Instruments	Operated by
Sample preparation (CXNS, ground floor, laboratory 006a and 006b)	DESY
2 UHV sample preparation chambers	DESY
Low energy electron diffraction	DESY
Zn evaporation chamber	DESY
Auger electron spectroscopy	DESY
UHV multi flange tunnel chamber	DESY
Surface spectroscopy (CXNS, ground floor, laboratory 006a and 006b)	DESY
UHV Infrared reflection absorption spectroscopy (IRRAS)	DESY
X-ray photoelectron spectroscopy (XPS)	DESY
Ultraviolet photoelectron spectroscopy (UPS)	DESY
X-ray diffraction (building 25, laboratory 023)	DESY
UFO chamber, 2 mini reactors, 2 gas mixer	DESY
2 *in situ* UHV chambers	DESY
Reflectometer	DESY
2 six-circle diffractometers	DESY
Microscopy and nanomanipulation (CXNS, ground floor, laboratories 001-004, 006a PETRA III experimental hall 'Max von Laue', 47c, laboratory L096)	DESY
Scanning Auger microscope (SAM)	DESY
Dual-beam focused ion beam (FIB-SEM)	DESY | Univ. Bayreuth
High-resolution scanning electron microscope (HR-SEM)	DESY
Versatile high-resolution atomic force microscope (AFM)	DESY
UHV scanning tunnelling / atomic force microscope (UHV-STM/AFM)	DESY
Optical polarisation microscope	DESY
Surface optical reflectance microscope (SOR)	DESY
Sputter coater	DESY
Physical and magnetic sample characterisation (CXNS, ground floor, laboratories 014 and 015)	DESY
Superconducting magnet	DESY
Sample cryostat	DESY
Vibrating sample magnetometer	DESY
AC susceptibility	DESY
AC and DC resistivity and Hall effect	DESY
AC calorimetry	DESY
Thermal transport	DESY
Magnetic microscopy	DESY
Electrocatalysis and electrochemistry (building 25b, laboratory 027)	DESY
Rotating disc electrode surface X-ray diffraction setup	DESY
Combined infrared X-ray diffraction setup	DESY | FAU Erlangen-Nürnberg
Hanging meniscus cell, flow cell	DESY
Langmuir trough	DESY | CAU Kiel

Acknowledgement
We would like to acknowledge all contributions to the development and operation of FLASH and PETRA III beamlines and instruments provided within the framework of 'Verbundforschung/ErUM-Pro' of the Federal Ministry of Research, Technology and Space (BMFTR), and as part of the collaboration 'India@DESY' with the Department of Science and Technology (Government of India).

Committees 2025

Photon Science Committee PSC — advises the DESY Photon Science management

Stefan Eisebitt (Chair)	MBI and Technische Universität Berlin, DE
Michael Krisch (Vice Chair)	ESRF, Grenoble, FR
Serena DeBeer	MPI-CEC, Mülheim an der Ruhr, DE
Kristina Djinovic-Carugo	Universität Wien, AT and EMBL Grenoble, FR
Jan-Dierk Grunwaldt	Karlsruher Institut für Technologie, Karlsruhe, DE
Mark Heron	Diamond Light Source Ltd, Didcot, UK
Simo Huotari	University of Helsinki, FI
Oxana Klementieva	Lund University, SE
Sarah Köster	Georg-August-Universität Göttingen, DE
Jan Lüning	Helmholtz-Zentrum Berlin, DE
Thomas Pfeifer	MPI for Nuclear Physics, Heidelberg, DE
Daniela Rupp	Eidgenössische Technische Hochschule Zürich, CH
Thomas Schröder	Humboldt-Universität zu Berlin and IKZ, Berlin, DE
Stefan Vogt	Argonne National Laboratory, Lemont, US
Christina Boemer (PSC Secretary)	DESY, Hamburg, DE

Laser Advisory Committee LAC — advises DESY and European XFEL

Thomas Dekorsy (Chair)	Deutsches Zentrum für Luft- und Raumfahrt e.V., Stuttgart, DE
Jake Bromage	University of Rochester, US
Miltcho Danailov	Elettra-Sincrotrone, Trieste, IT
Joseph Robinson	SLAC National Accelerator Laboratory, US
Clara Saraceno	Ruhr-Universität Bochum, DE
Emma Springate	STFC Rutherford Appleton Laboratory, US
Caterina Vozzi	Politecnico di Milano, IT
Jörg Hallmann (LAC Secretary)	European XFEL, Schenefeld, DE
Katharina Kucza (LAC Secretary)	DESY, Hamburg, DE

DESY Photon Science User Committee DPS-UC — represents the DESY Photon Science user community

Peter Müller-Buschbaum (Chair)	Technische Universität München, DE
Natalia Dubrovinskaia	Universität Bayreuth, DE
Hermann Duerr	Uppsala Universitet, SE
Julia Herzen	Technische Universität München, DE
Gregor Witte	Ludwig-Maximilians-Universität München, DE

Komitee Forschung mit Synchrotronstrahlung KFS — represents the German SR and FEL user community

Christian Gutt (Chair)	Universität Siegen, DE
Birgit Kanngießer (Vice Chair)	Technische Universität Berlin, DE
Taisia Gorkhover	Universität Hamburg, DE
Jan-Dierk Grunwaldt	Karlsruher Institut für Technologie, Karlsruhe, DE
Bernd Hinrichsen	BASF SE, Ludwigshafen, DE
Dorota Kozej	Universität Hamburg, DE
Martina Müller	Universität Konstanz, DE
Bridget Murphy	Christian-Albrechts-Universität zu Kiel, DE
Andrea Thorn	Universität Hamburg, DE

The European Synchrotron and FEL User Organisation ESUO (Executive Board)

Cormac McGuinness (ESUO President)	Trinity College Dublin, IE
Carla Bittencourt	Université de Mons, BE
Wojciech Gawelda	Universidad Autónoma de Madrid, ES
Tom P. Hase	University of Warwick, UK
Rainer Lechner	Montanuniversität Leoben, AT
Derek Logan	Lund University, SE
Bridget Murphy	Christian-Albrechts-Universität zu Kiel, DE
Moniek Tromp	Rijksuniversiteit Groningen, NL

For national delegates please see: www.esuo.eu/user-representation/user-delegates-representatives/

Project Review Panels 2025

Bulk and surface diffraction	Rolling access — P08 | P23 | P24
Volodymyr Bon	Technische Universität Dresden, DE
Wuge Briscoe	University of Bristol, UK
Diane Dickie	University of Virginia, Charlottesville, US
Michal Dusek	Czech Academy of Sciences, Prague, CZ
Jan Ingo Flege	Brandenburgische Tech. Univ. Cottbus-Senftenberg, DE
Joerg Grenzer	Helmholtz-Zentrum Dresden-Rossendorf, DE
Yvonne Grunder	University of Liverpool, UK
Richard Harvey	Universität Wien, AT
Alexander Hinderhofer	Universität Tübingen, DE
Vladimir Kaganer	Paul-Drude-Institut für Festkörperelektronik, Berlin, DE
Bärbel Krause	Karlsruher Institut für Technologie, Karlsruhe, DE
SoHyun Park	Ludwig-Maximilians-Universität München, DE
Paul Raithby	University of Bath, Bath, UK
Carsten Richter	Leibniz-Institut für Kristallzüchtung, Berlin, DE
Aleksandr Virovets	Goethe-Universität Frankfurt am Main, Frankfurt, DE
Florian Bertram, Dimitri Novikov, Martin Tolkiehn (PRP Secretaries)	DESY, Hamburg, DE

Coherent applications	P10
Giacomo Baldi	Università di Trento, IT
Martin Bech	Lunds Universitet, SE
Marina Eckermann	Universität Bern
Johannes Möller	European XFEL, Schenefeld, DE
Michael Paulus	Universität Dortmund, DE
Ullrich Pietsch	Universität Siegen, DE
Foivos Perakis	Stockholm University
Barbara Ruzicka	Institute for Complex Systems, Roma, IT
Dina Sheyfer	Argonne National Laboratory, Lemont, US
Olivier Thomas	Aix-Marseille Université, Marseille, FR
Fabian Westermeier (PRP Secretary)	DESY, Hamburg, DE

EXAFS	P64 | P65
Giannantonio Cibin	Diamond Light Source, Didcot, UK
Nina Genz	University of Utrecht, Utrecht, NL
Giorgia Greco	Università di Roma 'La Sapienza', Roma, IT
Konstantin Klementiev	MAX IV Laboratory, Lund, SE
Dirk Lützenkirchen-Hecht	Bergische Universität Wuppertal
Katherine Mazzio	Helmholtz-Zentrum Berlin, Berlin, DE
Dooshaye Moonshiram	Materials Science Institute of Madrid, ES
Roland Schoch	Universität Paderborn, DE
Janis Timoshenko	Fritz-Haber-Institut der Max-Planck-Gesellschaft, Berlin, DE
Case van Genuchten	Geological Survey of Denmark and Greenland, København, DK
Aleksandr Kalinko, Edmund Welter (PRP Secretaries)	DESY, Hamburg, DE

Extreme conditions	P02.2 | P61 LVP
Eglantine Boulard	Sorbonne Université, Paris, FR
Martin Bremholm	Aarhus University, DK
Silvie Demouchy	Blaise Pascal University, Aubiere Cedex, FR
Lars Ehm	Stony Brook University, Stony Brook, US
Holger Kohlmann	Universität Leipzig, DE
Zuzana Konopkova	European XFEL, Schenefeld, DE
Sergey Lobanov	Helmholtz-Zentrum Potsdam, GFZ, Potsdam, DE
Paolo Lotti	Università degli Studi di Milano Statale, Milano, IT
Hauke Marquardt	University of Oxford, UK
Sergey Medvedev	MPI für Chemische Physik fester Stoffe, Dresden, DE
Bjoern Winkler	Goethe-Universität Frankfurt am Main, DE
Hanns-Peter Liermann, Robert Farla (PRP Secretaries)	DESY, Hamburg, DE

HAXPES	Rolling access — P22
Sara Blomberg	Lunds Universitet, SE
Francesco Borgatti	CNR, Istituto per la Studio dei Materiali Nanostrutturati, Bologna, IT
Felix Gunkel	Forschungszentrum Jülich GmbH, Jülich, DE
Maria Hahlin	Uppsala Universitet, Uppsala, SE
Andreas Lindblad	Uppsala Universitet, Uppsala, SE
Martina Müller	Universität Konstanz, DE
Slavomir Nemsak	Forschungszentrum Jülich GmbH, DE
Christoph Rameshan	Montanuniversität Leoben, AT
Anna Regoutz	University College London, GB
Frederik Schiller	Centro de Fisica de Materiales, Donostia-San Sebastian, ES
Michael Sing	Universität Würzburg, DE
Yasumasa Takagi	Japan Synchrotron Radiation Research Institute, Hyogo, JP
Christoph Schlueter (PRP Secretary)	DESY, Hamburg, DE

High energy diffraction	P07 (DESY) | P21.1 | P21.2
Frauke Alves	Georg-August-Universität, Göttingen, DE
Elizabeth Blackburn	Lunds Universitet, SE
Olaf Borkiewicz	Argonne National Laboratory, Lemont, US
Peter Broekmann	Universität Bern, CH
Per-Anders Carlsson	Chalmers University of Technology
Magnus Colliander	Chalmers Tekniska Högskola, Gothenborg, SE
Margit Fabian	Centre for Energy Research, MTA, Budapest, HU
Julia Herzen	Technische Universität München, Garching, DE
Nina Lock	Aarhus University, DK
Edvin Lundgren	Lunds Universitet, SE
Lindsay Richard Merte	Malmö University, SE
Matt Miller	Cornell University, Ithaca, US
Thomas Niendorf	Universität Kassel, DE
Wolfgang Pantleon	Technical University of Denmark, Kongens Lyngby, DK
Giuditta Perversi	Maastricht University, NL
Tobias Ritschel	Technische Universität Dresden, DE
Florian Spieckermann	Montanuniversität Leoben
Ashok Sreekumar Menon	University of Warwick
Larissa Veiga	Diamond Light Source, Didcot, UK
Daniel Weber	Chalmers Tekniska Högskola, Gothenborg, SE
Fan Yang	German Aerospace Center
Ann-Christin Dippel, Martin von Zimmermann, Ulrich Lienert (PRP Secretaries)	DESY, Hamburg, DE

Project Review Panels 2025

Imaging — P05 | P06

Ulrike Boesenberg	European XFEL, Schenefeld, DE
Asuncion Carmona	Centre d'Etudes Nucléaires de Bordeaux Gradignan, FR
Fabien Chauveau	Lyon Neuroscience Research Center, Bron, FR
David Fenning	University of California, San Diego, US
Manuel Gonzalez-Guerrero	Universidad Politecnica de Madrid
Stephan Handschuh	Veterinärmedizinische Universität Wien, AU
Michael Heethoff	Technische Universität Darmstadt, DE
Sebastian Kalbfleisch	MAX IV Laboratory, Lund, SE
Andrew Kiss	Brookhaven National Laboratory, Upton, US
Ute Kraemer	Ruhr-Universität Bochum, DE
Florian Meirer	University of Utrecht, NL
Guillermo Requena	Rheinisch-Westfälische Technische Hochschule (RWTH) Aachen, DE
Thomas Sheppard	Technische Universität Wien
Roberto Terzano	Università degli studi di Bari, IT
Jürgen Thieme	Georg-August Universität Göttingen, DE
Nathalie Verbruggen	Université libre de Bruxelles, BE
Ulrich Vogt	Royal Institute of Technology, Stockholm, SE
Benjamin Wipfler	Zool. Forschungsmuseum Alexander Koenig, Bonn, DE
Fabian Wilde; Gerald Falkenberg (PRP Secretaries)	Helmholtz-Zentrum Hereon, Geesthacht; DESY, Hamburg, DE

Inelastic, magnetic and resonant scattering — P01 | P09

Lucia Amidani	Helmholtz-Zentrum Dresden-Rossendorf (HZDR)
Manuel Angst	Forschungszentrum Jülich GmbH, DE
Alessandro Barla	CNR, Istituto di Struttura della Materia (sede di Trieste), IT
Ilya Kupenko	European Synchrotron Radiation Facility, Grenoble, FR
Kristina Kvashnina	Helmholtz-Zentrum Dresden-Rossendorf, DE
Lars Lauterbach	Rheinisch-Westfälische Technische Hochschule, Aachen, DE
Daniel Merkel	Wigner Research Centre for Physics, Budapest, HU
Matteo Minola	Max-Planck-Institut für Festkörperforschung, Stuttgart, DE
Joachim von Zanthier	Friedrich-Alexander-Universität Erlangen-Nürnberg, DE
Jonathan White	Paul Scherrer Institut, Villigen, CH
Ilya Sergeev, Sonia Francoual (PRP Secretaries)	DESY, Hamburg, DE

Materials science (Hereon) — P07 (Hereon) | P61 (Hereon)

Jeremy Epp	Leibniz-IWT, Bremen, DE
Guillaume Geandier	Institut Jean Lamour, Nancy, FR
Julia Herzen	Technische Universität München, DE
Christian Krempaszky	Technische Universität München, DE
Greta Lindwall	KTH Royal Institute of Technology, Stockholm, SE
Karen Pantleon	Technical University of Denmark, Kongens Lyngby, DK
Georg Schulz	Universität Basel, CH
Carsten Siemers	Technische Universität Braunschweig, DE
Petra Spoerk-Erdely	Graz University of Technology, AT
Dieter Lott (PRP Secretary)	Helmholtz-Zentrum Hereon, Geesthacht, DE

Powder diffraction — P02.1

Jozef Bednarcik	P.J. Safarik University, Košice, SK
Robert Dinnebier	MPI für Festkörperforschung, Stuttgart, DE
Bernd Hinrichsen	BASF SE, Ludwigshafen, DE
Manuel Hinterstein	Karlsruher Institut für Technologie (KIT), Karlsruhe, DE
Kirsten Marie Jensen	Københavns Universitet, København, DK
Gregor Kieslich	Technische Universität München, Garching, DE
Michael Knapp	Karlsruher Institut für Technologie, Karlsruhe, DE
Daria Mikhailova	Leibniz-Institut f. Festkörper- und Werkstoffforschung Dresden, DE
Claudia Weidenthaler	MPI für Kohlenforschung, Mülheim a.d. Ruhr, DE
Irmgard Weissensteiner	Montanuniversität Leoben, AU
Martin Etter (PRP Secretary)	DESY, Hamburg, DE

SAXS/WAXS/GISAXS — P03 | P62

Jens Wenzel Andreasen	Danmarks Tekniske Universit, Roskilde, DK
Sabrina Disch	Universität Duisburg-Essen, DE
Marios Georgiadis	Stanford University, US
Ajay Gupta	University of Petroleum and Energy Studies, Dehradun, IN
Eva Herzig	Universität Bayreuth, DE
Tobias Kraus	Leibniz-Institut für Neue Materialien, Saarbrücken, DE
Rainer T. Lechner	Montanuniversität Leoben, AT
Eva Malmstroem	KTH Royal Institute of Technology, Stockholm, SE
Simone Mascotto	Universität Koblenz, DE
Peter Šiffalovič	Institute of Physics, Bratislava, SK
Sarathlal Koyiloth Vayalil, Sylvio Haas (PRP Secretaries)	DESY, Hamburg, DE

Soft X-ray and VUV — P04 | P66

Vladimir Babin	Czech Academy of Sciences, Institute of Physics
Paola Bolognesi	CNR-ISM, Istituto di Struttura della Materia, Roma, IT
Sergey Borisenko	Leibniz-Institut für Festkörper- und Werkstoffforschung, Dresden, DE
Felix Buettner	Universität Augsburg, DE
Francesca Cova	University of Milano – Bicocca
Raimund Feifel	Göteborgs Universitet, SE
Jochen Geck	Technische Universität Dresden, DE
Nils Huse	Universität Hamburg, DE
Andrei Kanaev	Université Paris Nord
Timo Kuschel	Universität Bielefeld, DE
Aleksandr Luštšik	University of Tartu, EE
Ján Minár	University of West Bohemia, Plzni, CZ
Anatoli Popov	University of Latvia
Yasmine Sassa	Chalmers Tekniska Högskola, Gothenborg, SE
Anna Vedda	Università di Milano-Bicocca, Milano, IT
Moritz Hoesch, Aleksei Kotlov (PRP Secretaries)	DESY, Hamburg, DE

Soft X-ray FEL experiments — FLASH

Thomas Allison	State University New York
Majed Chergui	École Polytechnique Fédérale de Lausanne, CH
Hermann Dürr	Uppsala Universitet, Uppsala, SE
Irene Groot	Universiteit Leiden, NL
Marion Harmand	Sorbonne Université, Paris, FR
Michael Meyer	European XFEL, Schenefeld, DE
Kevin Prince	Elettra-Sincrotrone Trieste, IT
Christian Schüssler-Langeheine	Helmholtz-Zentrum Berlin, DE
Marc Simon	Sorbonne Université, Paris, FR
Julia Stähler	Humboldt-Universität zu Berlin, DE
Elke Plönjes-Palm, Rolf Treusch (PRP Secretaries)	DESY, Hamburg, DE

PEC EMBL Life Science beamlines P12-P14 | PRP Macromolecular Crystallography at P11 (rolling access) and P09 HiPhaX

Pau Bernadó	CBS/CNRS, Montpellier, FR
Gwyndaf Evans	Diamond Light Source, Didcot, GB
Robert Fischetti	Argonne National Laboratory, US
Sebastian Glatt	Jagiellonian University Krakow, PL
Gergely Katona	University of Gothenburg, SE
Annette E. Langkilde	University of Copenhagen, DK
Andrea Mattevi	University of Pavia, IT
Javier Pérez	Synchrotron SOLEIL, Saint-Aubin, FR
Teresa Santos-Silva	Universidade NOVA de Lisboa, PT
Zehra Sayers	Sabanci University, Istanbul, TR
Thomas Lykke-Møller Sørensen	Aarhus University, DK
Norbert Sträter	Universität Leipzig, DE
Giedrė Tamulaitienė	Vilnius University, LT
Giuliana Tromba	Elettra-Sincrotrone Trieste, IT
Maria A. Vanoni	Università degli Studi di Milano, IT
Mark J. van Raaij	Centro Nacional de Biotecnologia, Madrid, ES
Gregor Witte	Ludwig-Maximilians-Universität München, DE
Christian Schroer (DESY observer)	DESY, Hamburg, DE

Photographs and Graphics

Jonas Albers, EMBL
Emma Birkeskov, University of Aarhus
Silvia Burastero, EMBL
Francesca Calegari, DESY
CFEL
CMWS
Maurizio Contran, Politechnico Milano
DASHH
DESY
Liz Duke, EMBL
EMBL
European XFEL
C. Guo, MPSD
T. Glier, UHH
Helmholtz-Zentrum Hereon
Diana von Ilsemann, DESY
Elisabeth Fröhlich, DESY
Piotr Kędzierski
M. Künsting, TUHH
Tim Laarmann, DESY
Kinga Lubowiecka, EMBL
Jörg Müller, DESY
Heiner Müller-Elsner, DESY
Marta Mayer, DESY
MPG
Daniel Reinhardt, DESY
Katharina Roeper, DESY
Science Communication Lab, DESY
Reimo Schaf, DESY
K. Schamoni-Kast, CSSB
Jens Stougaard, University of Aarhus
S. Tille, HELIOS
Steffen Tober, DESY
Rolf Treusch, DESY
TU Hamburg
University of Hamburg
K. B. Warmbein, DESY
Winkler, PHGS
T. Wüstefeld, EuXFEL

Acknowledgement
We would like to thank all authors and all who have contributed to the realisation of this Annual Report.

Imprint

Publishing and Contact:
Deutsches Elektronen-Synchrotron DESY
A Research Centre of the Helmholtz Association

Hamburg location:
Notkestr. 85, 22607 Hamburg, Germany
Tel.: +49 40 8998-0, Fax: +49 40 8998-3282
desyinfo@desy.de

Zeuthen location:
Platanenallee 6, 15738 Zeuthen, Germany
Tel.: +49 33762 7-70, Fax: +49 33762 7-7413

Photon Science at DESY
Tel.: +49 40 8998-2304, Fax: +49 40 8998-4141
photon-science@desy.de
photon-science.desy.de

www.desy.de

ISBN 978-3-945931-59-2
DOI 10.3204/PUBDB-2025-04704

Online version:
photon-science.desy.de/annual_report

Realisation:
Wiebke Laasch, Daniela Unger

Editing:
Sadia Bari, Krishnayan Basuroy, Lars Bocklage, Benjamin Erk, Hermann Franz, Claudia Goy, Tobias Herr, Ismar Kiseljakovic, Dmytro Kutnyakhov, Wiebke Laasch, Britta Niemann, Heshmat Noei, David Pennicard, Christoph Schlueter, Markus Scholz, Sang-Kil Son, Sebastian Trippel, Daniela Unger

Layout: Sabine Kuhls-Dawideit, Büro für Grafik und Design, Halstenbek

Printing and image processing: EHS Druck GmbH, Schenefeld

Copy deadline: December 2025

HELMHOLTZ

Deutsches Elektronen-Synchrotron DESY
A Research Centre of the Helmholtz Association

Helmholtz contributes to solving major challenges facing society, science and the economy through top-level scientific achievements in six research fields: Energy, Earth and Environment, Health, Information, Matter as well as Aeronautics, Space and Transport. With 47500 employees at 18 research centres and an annual budget of more than 6 billion euro, Helmholtz is Germany's largest scientific organisation. Its work is rooted in the tradition of the great natural scientist Hermann von Helmholtz (1821–1894).

www.helmholtz.de